the electronic structure of embedded transition metal atoms

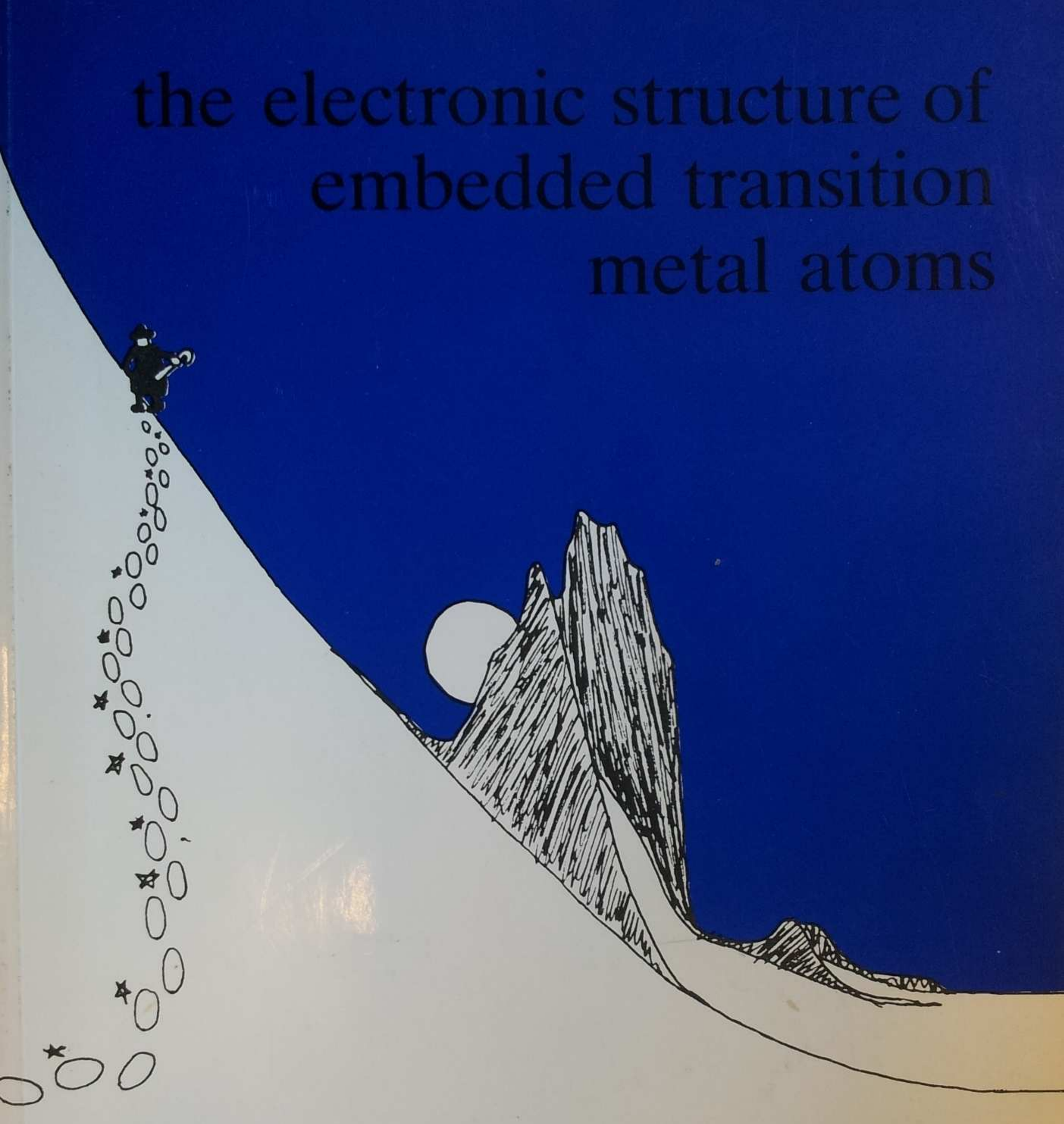

Dick van der Marel

the electronic structure of embedded transition metal atoms

RIJKSUNIVERSITEIT TE GRONINGEN

the electronic structure of embedded transition metal atoms

Proefschrift

ter verkrijging van het doctoraat
in de wiskunde en natuurwetenschappen
aan de Rijksuniversiteit te Groningen
op gezag van de
Rector Magnificus Dr. E. Bleumink
in het openbaar te verdedigen op
vrijdag 1 november 1985
des namiddags te 2.45 uur precies

door

Dirk van der Marel
geboren te Hardenberg

PROMOTOR: Prof. Dr. G.A. Sawatzky

druk: Stichting drukkerij C. Regenboog, Groningen

cover: "Mountaineering on a moonlit AgPd spectrum" (p.77 of this thesis).

This investigation was supported by the Netherlands Foundation for Chemical Research (SON) with financial aid from the Netherlands Organization for the Advancement of Pure Research (ZWO).

aan Rosemarie

STELLINGEN

1. De bewering van Williams et al., dat in hun local density band structuur berekeningen aan NiO polaronische afscherming effectief wordt meegenomen is nogal boud gezien het feit, dat in hun formalisme het rooster niet beweegt.
   A.R. Williams, J. Kübler en K. Tekura, Phys. Rev. Lett. 54, 2728 (1985).

2. Ten onrecht wijzen Veal en Paulikas de pieken in het Mn 3s XPS spectrum van MnF_2 toe aan een d^6 eindtoestandsconfiguratie.
   B.W. Veal en A.P. Paulikas, Phys. Rev. Lett. 51, 1995 (1983).

3. De gap rond het Fermi niveau die Lavagna et al. vinden in hun uitdrukking voor de indirecte exchange interacties is een artefact veroorzaakt door het blindelings gebruiken van Brillouin-Wigner storingstheorie.
   M. Lavagna en M. Cyrot, Solid State Commun. 55, 555 (1985).

4. De bewering, dat dezelfde mechanismen die de Coulomb integraal U afschermen tevens de intra atomaire exchange integralen afschermen, is niet juist.
   P.W. Anderson, Phys. Rev. 124, p.44 (1961).

5. In hun analyze van de nikkel LVV Auger spectra verwaarlozen Fuggle et al. de aanwezigheid van valentiegaten in de grondtoestand. Dit leidt tot een verkeerde bepaling van de Coulomb interactie.
   J.C. Fuggle, P. Bennet, F.U. Hillebrecht, A. Lenselink and G.A. Sawatzky, Phys. Rev. Lett. 49, 1787 (1982).

6. Het feit, dat $\langle|\Psi(0)|^2\rangle_{E_F}$ gegeven wordt door de Knight shift (K) gedeeld door de Pauli susceptibiliteit (χ_p) en niet door de richtingscoëfficient in een K tegen χ_p plot, betekent, dat de verandering van electronische golffunctie bij E_F als functie van temperatuur veel geleidelijker gaat, dan door Bottyan et al. wordt gesuggereerd.
   L. Bottyan, R. Dupree and W. Freyland, J. Phys. F 13, L173 (1983).

7. Gezien de grote belangstelling van industriële zijde voor "surface science" is de spelling "service science" wellicht even-zeer op zijn plaats.

8. Met betrekking tot chemisch en radioactief afval is het vanuit milieutechnisch oogpunt raadzaam om niet alleen actie te voeren tegen bepaalde stortingslocaties, maar ook ten gunste van goede alternatieve oplossingen.

9. De bewering, dat men een "deformatie dipool" naar keuze op het anion of het kation kan plaatsen in berekeningen aan elastische eigenschappen van ionische kristallen is alleen juist als deze ionen op een punt van gelijke symmetrie zitten.
John R. Hardy and A.M. Karo, "The Lattice Dynamics and Statics of Alkali Halide Crystals", p.63 tot 98, Plenum 1979.

Stellingen behorende bij het proefschrift van D. v.d. Marel,
Groningen, 1985.

CONTENTS

CHAPTER I

GENERAL INTRODUCTION

1.1. Introduction

When transition metal atoms are brought together to form a solid or when they are embedded in a host material, something fascinating can happen. A magnetic alloy may be formed even though the component elements are non-magnetic in their elemental form. A tiny fraction of magnetic moments dissolved in a host may increase the residual resistivity to virtually infinite or destroy superconductivity, but also superconducting compounds can be formed. Other examples of peculiar transition metal alloys and compounds are spin-glasses, Mott-Hubbard insulators, materials showing a temperature or pressure induced volume-collapse and "heavy-fermion" systems.

Less than half of these properties are really understood and the usual way in which new properties are established is: first the experimental discovery, then the theoretical explanation. The experimental approach can be twofold: one can subject the materials to all kinds of external conditions and measure their response. One can also attempt to look directly into the machinery of electronic structure with the various available spectroscopies thus obtaining direct information on the electronic properties in terms of excited states of one or more electrons and/or holes. These results can then be used as input-parameters of a theory of the physical and chemical properties, or the theory can be improved, so that it describes the electronic structure in agreement with experiment.

In this thesis, we follow the second experimental approach. The spectroscopies used here are Photo-electron Spectroscopy using Ultraviolet radiation (UPS) and X-rays (XPS), Auger Electron Spectroscopy (AES) and Bremsstrahlung Isochromat Spectroscopy (BIS).

In Photo-electron Spectroscopy a sample is irradiated with monochromatic light,

which excites electrons from occupied into unoccupied states. If these unoccupied states are above the vacuum level, the excited electron can escape from the solid. The intensity of the electron-flux emerging from the surface is monitored as a function of their kinetic energy [1]. In the smaller laboratories, one uses ultraviolet light or X-ray sources which operate at a fixed photon energy. One can also use a synchrotron radiation source which opens the possibility of employing the photon energy as an extra variable. The observed intensity is, from Fermi's Golden Rule:

$$W_{IF} = \frac{2\pi}{\hbar} |\langle I(N)|H^{int}|F(N)\rangle|^2 \delta(E_F - E_I - \hbar\omega) \tag{1.1}$$

where $|I(N)\rangle$ and $|F(N)\rangle$ are the N-electron initial- and final states (N is the number of electrons in the solid) and

$$H^{int} = \sum_{i=1}^{N} \frac{e}{mc} \vec{A}\cdot\vec{P}_i \tag{1.2}$$

$\vec{P}_i$ is the momentum operator of electron i and $\vec{A}$ is the photon vector field. In the sudden approximation one neglects the post-collisional interactions of the photoelectron with the system left behind, which is reasonable if the time spent near the site where the photoelectron is created is much shorter than the post-collisional interaction decay time. In this limit the N particle final state can be decoupled in an N-1 particle final state of the system left behind and an independent photoelectron state of energy E_k. The photoelectron current is then proportional to

$$W_{Ik} \propto \sum_f |\langle I(N)|\sum_\nu (\Psi_\nu^\dagger m_{k\nu} \Psi_k)|k, f(N-1)\rangle|^2 \delta(E_f + E_k - E_I - \hbar\omega) \tag{1.3}$$

where Ψ_k annihilates an electron in state $|k\rangle$, $\Psi_\nu^\dagger$ creates an electron in state $|\nu\rangle$ and $m_{k\nu}$ is the matrix element. It is easy to show that this expression can be written in the form

$$W_{Ik} \propto \sum_{\mu\nu} \{m_{k\nu} m_{k\nu}^* \, Im \langle I(N)|\Psi_\mu^\dagger \frac{1}{E_I + \hbar\omega - E_k - H - i0^+} \Psi_\nu |I(N)\rangle\} \tag{1.4}$$

which makes clear, that the photoelectron spectrum is the one-hole-greens function, (apart from matrix element effects), which is related to the occupied density of states. At finite temperatures $|I(N)>$ is thermally distributed above the system ground state.

In inverse photoemission a beam of electrons is aimed at the sample. Part of the incoming electrons decay radiatively to the unoccupied states. The term Bremsstrahlung Isochromat Spectroscopy is used if the photon-flux is monitored at fixed wavelength by leading the light through a monochromator. A spectrum is taken as a function of incident electron energy [2]. The intensity is given by the reverse expression of Eq. (1.4):

$$W_{kI} \propto \sum_{\mu\nu} \{M_{k\mu} M^*_{k\nu} \; Im<I(N)|\Psi_\nu \frac{-1}{E_I+\hbar\omega-E_k-H+i0^+} \Psi^\dagger_\mu|I(N)>\} \qquad (1.5)$$

This expression contains the one-electron Green's function, which is related to the unoccupied density of states.

The Fourier-transform of the single-particle causal Green's function in many-body theory is:

$$G^\nu_\mu(\omega) = <|\Psi^\dagger_\nu \frac{1}{\omega-H-i0^+} \Psi_\mu|> + <|\Psi_\mu \frac{1}{\omega-H+i0^+} \Psi^\dagger_\nu|> \qquad (1.6)$$

where the matrix elements are thermal averages. Comparison with the expressions (1.4) and (1.5) for the photoemission spectrum and the BIS spectrum shows that the combination of both spectroscopies is precisely the Lehman spectral representation of the single particle Green's function (in many-body field-theory) convoluted with the optical matrix elements.

In Auger Electron Spectroscopy the interaction Hamiltonian is the Coulomb interaction acting between electrons. The initial state is now a state containing a core hole, which can be prepared with a photoemission process. Due to the Coulomb interaction this state couples to a continuum consisting of final states with two holes and one electron. One measures the flux of these electrons as a function of their kinetic energy [3]. The intensity is proportional to:

$$W_{if} = \frac{2\pi}{\hbar} |\langle i_c(N-1)|A_{kc}|f(N-1)\rangle|^2 \ \delta(E_f - E_i)$$

$$A_{kc} = \sum_{\mu\nu} \left(V_{kc\mu\nu} \ \Psi_k^\dagger \Psi_c^\dagger \Psi_\mu \Psi_\nu + H.C. \right)$$

$$|i_c(N-1)\rangle = \Psi_c |I(N)\rangle \qquad (1.7)$$

Using the sudden approximation and a decoupling of the Auger electron state $|k\rangle$ and the final states $|f(N-2)\rangle$ similar to what we did in obtaining Eq. (1.4) we have:

$$W_{ck} \propto \sum_{\mu\nu} \sum_{\mu'\nu'} \left\{ V_{kc\mu\nu} \ V^*_{kc\mu'\nu'} \ \mathrm{Im}\langle I(N)|\Psi_\mu^\dagger \Psi_\nu^\dagger \frac{1}{E_c - E_k - H - i0^+} \Psi_{\nu'} \Psi_{\mu'}|I(N)\rangle \right\} \qquad (1.8)$$

which is the two-hole Green's function multiplied with matrix elements. The one core-hole initial state energy E_c is normally given by a distribution of energies due to the finite lifetime of the core hole. The prepared state can also contain more than one hole, if the Auger process has been preceded by another Auger process. In that case, the final state will contain three or more holes.

The combination of these techniques gives us information about one-particle properties, Coulomb interactions, exchange interactions and screening. We will use this information to calculate elastic scattering cross-sections for resistivity determinations, magnetic moments, coupling constants between local moments and an expression for a hypothetical pairing mechanism between conduction electrons.

1.2. Scope

In Chapter II a survey is given of the d and f transition metal electronic structure, using some new BIS data of the iron row elements dissolved in gold and existing data collected from the literature. We discuss the importance of screening of Coulomb interactions and show that this can result in a negative U^{eff} under certain conditions.

In Chapter III a theory is presented for the UPS spectra and electronic structure of embedded transition metal atoms having essentially full (or half-

filled) d-shells. It forms the basis of the discussions in Chapters V and VI. In Chapter IV we present and discuss BIS data of pure Cu, Ag and Au and obtain accurate values of the critical point energies. Comparison to KKR bandstructure calculations reveals that the final state electrons have an energy dependent lifetime.

In Chapter V we present UPS data of Pd and Pt embedded in Cu, Ag and Au, and give an extensive discussion of the electronic structure using the theory of Chapter III. We calculate values for the elastic d-scattering cross-sections and discuss the influence of lattice relaxation on the local density of states.

In Chapter VI we present UPS, XPS, AES and BIS data of Mn diluted in Ag and Cu, demonstrating directly the exchange-split virtual bound state of the Mn atom. Section VI.1 is a reprinted letter, and there we summarize the main ideas that are worked out in detail in section VI.2. We show that the host-impurity s-d coupling is quite strong, which is paradoxal in view of the low Kondo temperatures found in these alloys. In section VI.3 we use some of the ideas of section VI.2 to show that, apart from the RKKY interaction, also indirect charge transfer processes and particle pair production processes play an important role in the indirect coupling of the Mn moments.

In Chapter VII we use the information of Chapter II and unitary transformation techniques to show that triplet-pairing between conduction electrons can occur in systems containing centers of localized states with strongly screened Coulomb interactions.

Parts of this thesis have been published:

Chapter IV : D. van der Marel, G.A. Sawatzky, R. Zeller, F.U. Hillebrecht and J.C. Fuggle, Solid State Commun. 50, 47 (1984).

Chapter V : D. van der Marel, J.A. Julianus and G.A. Sawatzky, Phys. Rev. B, scheduled for October 15th (1985).

Appendix of Chapter V : D. van der Marel, G.A. Sawatzky and J.A. Julianus, J. Phys. F 14, 281 (1984).

Chapter VI, section 1 : D. van der Marel, G.A. Sawatzky and F.U. Hillebrecht, Phys. Rev. Lett. 53, 206 (1984).

Chapter VI, section 2 : D. van der Marel, C. Westra, G.A. Sawatzky and F.U. Hillebrecht, Phys. Rev. B 31, 1936 (1985).

Chapter VII : D. van der Marel and G.A. Sawatzky, Solid State Commun. 55, 937 (1985).

References

1. The equipment used for the UPS experiments presented in this thesis is described in detail in: A. Bosch, Ph.D. thesis, Laboratory of Physical Chemistry, Groningen, the Netherlands (1982).
2. The BIS experiments presented in this thesis were performed on the instrument described in: F.U. Hillebrecht, Ph.D. thesis, Universität zu Köln, W. Germany (1983).
3. A description of the ESCA spectrometer used for AES analysis is given in: E. Antonides, Ph.D. thesis, Laboratory of Physical Chemistry, Groningen, the Netherlands (1977).

CHAPTER II

DO LOCALIZED ELECTRONS REPEL EACH OTHER IN D AND F TRANSITION METALS?

We discuss for the d and f transition metals the competition between atomic like electrostatic coulomb- and exchange interactions and loss of atomic characteristics in the solid through screening of f and d charge fluctuations and hybridization. We show that some of the light actinides can exhibit negative U^{eff} behaviour dependent on their valence in the solid. We argue that some d transition metals may belong to the same group if properly alloyed.

2.1. Introduction

During the last two decennia it has become more and more customary among solid state physicists to assume that the one particle band picture is the correct starting point for studying the electronic structure of 3d, 4d and 5d transition metals. The physics of the rare earth metals, on the other hand, is normally started from the atomistic point of view, treating the f-shells as a partly filled core shell. Rare earth compounds exhibiting physical properties corresponding to non-integer occupation of the f-shell are considered as exceptions and indicated as mixed valence compounds. The field of actinide intermetallic compounds is rapidly growing and there is no consensus yet on how to treat the 5f shells of these elements.

In this chapter we want to discuss and compare the d and f transition metals, with special emphasis on the atomistic description of their electronic structure in the solid. As the scope of this chapter is quite general, it is not realistic to attempt to give a complete review of the literature in this field. Instead, we refer the reader to some review articles [1-9].

In Fig. 2.1 we have plotted the atomic volumes for the elements in their common crystal phase [10,11,12] as a function of their position in the periodic

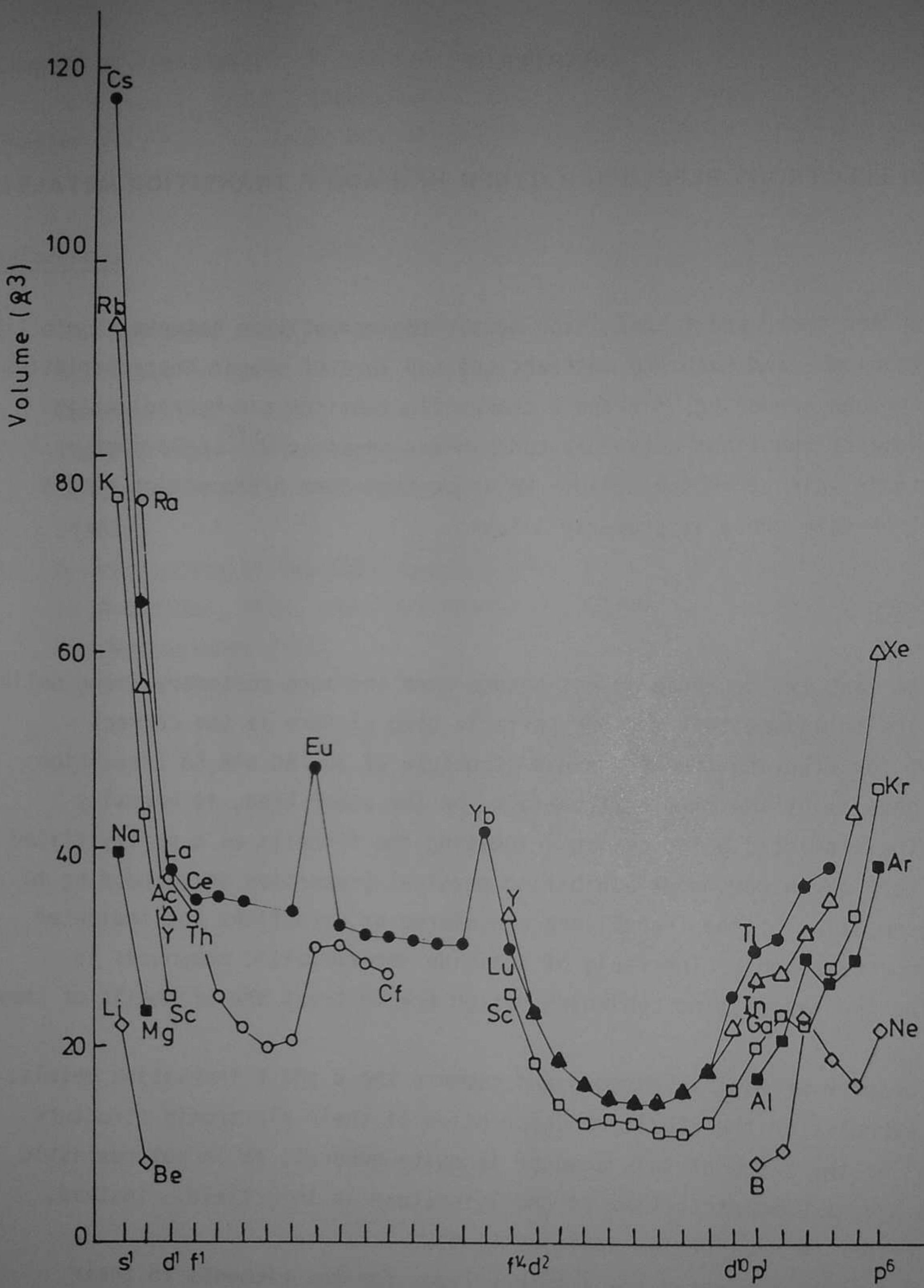

Fig. 2.1. Wigner-Seitz volumes of the elements as a function of their position in the periodic system.

table. The configurations at the horizontal axis must not be taken too literally, as in the solid many different configurations may contribute to the ground state. There are some very clear trends in this plot, that show the systematics of metallic bond formation. The sharp drop in atomic size when moving from the alkali metals to the earth alkali metals is mainly due to the decreased radius of the s orbitals in the field of the larger core potentials. The trend of increasing size on going to the 3A group elements and beyond is caused by the gradual filling of the p bands. The fourth row is intersected by the filling of the 3d band. One might expect the same thing to happen as with the filling of the sp states. A decrease in size at the left side of the row due to a decreasing d orbital radius as a function of atomic number Z, followed by an increase due to the filling of the antibonding bands. From Fig. 2.1 it is clear that there is an additional effect: the atomic size stays constant between Cr and Ni. This reflects a crucial feature of the 3d wave functions, namely that their size is small compared to the interatomic distances, so that the hybridization energy of the d states becomes relatively unimportant. What happens is that on increasing the core charge, the d levels are gradually filled, which screenes the core charge very efficiently from the s and p states. A different way of saying this is: the charge fluctuations in the open d shells are very small in comparison to those of the s and p shells. This implies, that the corresponding hybridization energies are small and the d bands are narrow. We note from Fig. 2.1 that a similar trend occurs in the 4d and 5d series, except that the flat part is missing and the sizes are bigger. The latter is a consequence of the larger (gas phase) valence s and p radii.

A similar screening effect as we mentioned in connection with the iron row also occurs in the lanthanides, with irregularities for Eu and Yb. In the rare earths, the f electrons are even more strongly localized and are usually considered as open shell core states. In their elemental metallic state the lanthanides are trivalent, with exceptions for Eu and Yb which are divalent. As a consequence, the valence electrons of Eu and Yb move in a core potential that has one positive elementary charge less than the other lanthanides, causing the larger radius of the s and d shells.

The situation in the actinide series is very intriguing. First there is a drop in size between Th and Pa, similar to what we see happen at the beginning of

the transition metal series, followed by a short plateau between U and Pu. Then there is a sudden increase in size between α-Pu and Am. Also there is a dramatic (17%) volume increase between the room temperature α phase of Pu and the high temperature δ, ε and γ phases which reminds of the volume collapses in Ce [13] and Sm compounds [14,15]. The heavy actinides Am, Cm, Bk and Cf are all trivalent. The valence of the lighter actinides is of more mixed character and some authors believe that the volume change between α-Pu and γ-Pu, and between α-Pu and Am is a Mott-Hubbard transition involving localization of the f electrons [16,17,18]. A similar argument has been used for Ce [19]. On the other hand, Allen and Martin [20] argued that the collapsed phase of Ce is in fact a Kondo state with $T_K = 766(K)$, whereas the room temperature γ phase has a Kondo temperature of 55 (K). This mechanism could very well be responsible for the actinide volume collapses as well.

To illustrate the size effect further, we plot in Fig. 2 the f and d "volume" to Wigner-Seitz volume ratio $(r_l/r_{ws})^3$, where the r_l (l = d or f) values were tabulated $\sqrt{\langle r^2 \rangle}$ Hartree-Fock values for the elements except the actinides [21]. For uranium we used published relativistic Dirac-Slater values for $\sqrt{\langle r_f^2 \rangle}$ [22]. For the other actinides we used published $\langle r \rangle$ expectation values [23,18] scaled with a factor 1.04 in order to fit the uranium $\langle r \rangle$ expectation value to the Dirac-Slater result of Ref. 22. The Wigner-Seitz radii are obtained from Fig. 2.1. We see in Fig. 2.2 that all values are smaller than one, indicating that on the average the d and f clouds lie inside the Wigner-Seitz cell. Although this is no direct measure of the hybridization, it is clear that elements with similar $(r_l/r_{ws})^3$ values have comparable bandwidths. Quite clearly, Am, Cm, Bk and Cf are more confined than the 3d elements up to nickel and more or less comparable to the lanthanides. From the spatial point of view, the lighter actinides belong to the same class as Mn, Fe, Co and Ni. The lighter 3d-transition metals are in the same way comparable to Au, Pd, Rh and Pt.

So far we have been discussing the pure elements only. Fig. 2.2 gives a rough indication of the size effect on hybridization of d and f states at neighboring sites and of the valence band-f(or d) hybridization. Alloying strongly reduces the direct f-f or d-d hybridization and influences the s-d or s-f hybridization in either way depending on the structural details of the lattice.

Apart from the size effect, the energies of the f and d electrons and their

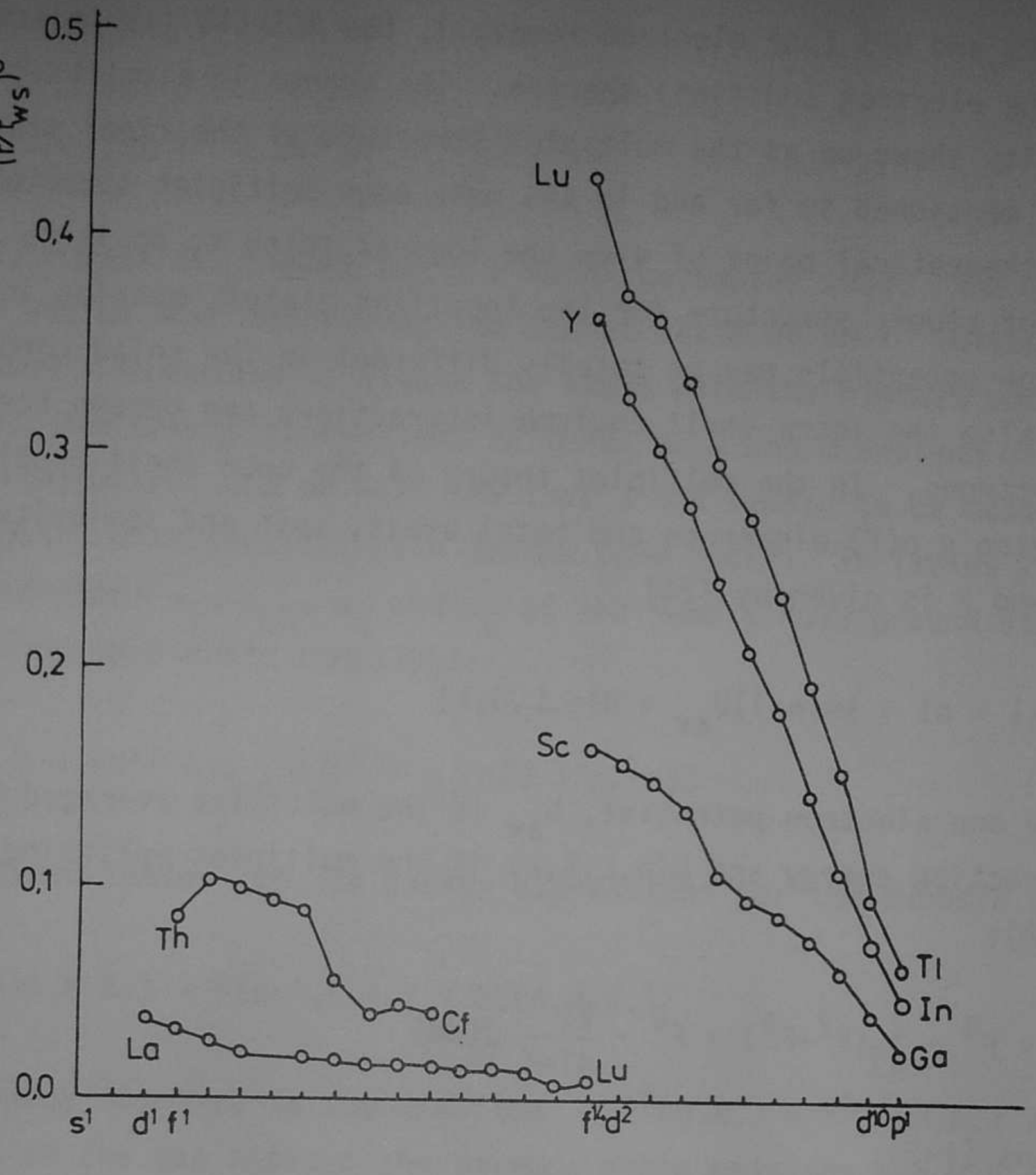

Fig. 2.2. Ratio of l shell "volume" to Wigner-Seitz volume of the 3d, 4d and 5d elements (l=2) and 4f and 5f elements (l=3) as a function of their position in the periodic system.

mutual interactions are extremely important for the understanding of the physical properties of these elements, and their compounds. The important question to be answered there is: what are the energies involved in adding (removing) one or more electrons to (from) an atom in a given state and what are the energies involved in changing the electronic configuration within the d(f) shell without changing its polarity?

From the experimental point of view, these questions correspond to:

what are the XPS and UPS (one electron removal), the AES CVV (two electron removal) and the BIS (one electron addition) spectra. The change in electronic configuration at equal polarity shows up as the multiplet structure of the final states in the spectroscopies mentioned so far and in XAS near edge multiplet structures.

From the theoretical point of view the logical thing to do is to look at the Slater theory of atomic structure for the localized states, bearing in mind that the one electron potentials may be totally different in the solid compared to the gas phase and also the intra-shell coulomb interactions can become screened by the conduction electrons. In the multiplet theory of the open shell problem the energy of a state having n d(f) electrons and total orbit, spin and seniority quantum numbers L, S and λ is given by [24]

$$E(n,L,S,\lambda) = nI + \tfrac{1}{2}n(n-1)U_{av} + U(n,L,S,\lambda) \qquad (2.1)$$

where I is the one electron potential, U_{av} is the multiplet averaged Coulomb-exchange interaction energy and $U(n,L,S,\lambda)$ is the multiplet splitting. For d electrons (l=2):

$$U_{av}(dd) = F^0 - \frac{2}{63}(F^2+F^4) = F^0 - \frac{21}{4l+1}\,J(dd) \qquad (2.2)$$

For f electrons (l=3):

$$U_{av}(ff) = F^0 - \frac{2}{27885}\,(286\,F^2 + 195\,F^4 + 250\,F^6) = F^0 - \frac{21}{4l+1}\,J(ff) \qquad (2.3)$$

For later use it is convenient to introduce the exchange interactions J(dd) and J(ff) here, describing the intrashell exchange attraction between parallel spins:

$$J(dd) = \frac{1}{14}(F^2+F^4) \qquad (2.4)$$

$$J(ff) = \frac{1}{6435}\,(286\,F^2 + 195\,F^4 + 250\,F^6) \qquad (2.5)$$

and the additional parameters describing the angular part of the multiplet splitting:

$$C(dd) = \frac{1}{14}\left(\frac{9}{7}F^2 - \frac{5}{7}F^4\right) \tag{2.6}$$

$$C(ff) = \frac{1}{6435}\left(286\,F^2 + \frac{780}{11}F^4 - \frac{1750}{11}F^6\right) \tag{2.7}$$

Note that C(ff) equals $6E_3$, where E_3 is a Racah parameter [25]. The J's and C's are especially useful when describing the lowest state of an 1^n multiplet. According to Hund's Rules this is always the state with the highest possible spin quantum number. The energy expressions in terms of J and C instead of F^2, F^4 (and F^6) are very transparent, and we will see that J has simply to be multiplied with the number of pairs with parallel spin in the same shell. In Tables 2.1 and 2.2 we give the prefactors α_I, α_{F0}, α_J and α_C of the Hund's Rule ground state expressions (neglecting spin orbit coupling):

$$E(n,H.R.) = \alpha_I(n)I + \alpha_{F0}(n)F^0 + \alpha_J(n)J + \alpha_C(n)C \tag{2.8}$$

Also given in these tables are the energy expressions for the Hubbard gap:

$$U^{eff} = E(n+1,H.R.) + E(n-1,H.R.) - 2E(n,H.R.) \tag{2.9}$$

which is the energy involved in the reaction $2\,f^n(H.R.) \rightarrow f^{n+1}(H.R.) + f^{n-1}(H.R.)$ and corresponds to the gap between the valence photo emission and BIS spectra of the d or f states. For d and f states the C's are about half the J's and the latter vary from 0.8 eV to 1.4 eV for Sc to Cu and from 0.9 eV to 1.4 eV for La to Yb. We can see from Tables 1 and 2 that the Hubbard gap for the half filled shell is always 1·J larger than for the other occupation numbers, apart from contributions from the C's. This amounts to six to eight eV for the 3d and 4f elements. Now the parameters in Tables 2.1 and 2.2 describe the situation in an atom with an open d or f shell without any other charges in the system. Even in the case of gas phase atoms there are valence electrons that interact among themselves and with the open d or f shell. This leads to further multiplet splitting of the states and to extra configuration interactions. In the solid this situation is extremely complicated due to the virtually infinite number of particles involved. A potentially successful approach to this problem is to make a formal separation between the highly

Table 2.1. Parameters determining the energies of the Hund's Rule ground states in LS coupling for all d occupations and the expression for the d-d gap for those occupations.

state	α_I	α_{F^0}	α_J	α_C	U^{eff}
$d^0(^1S)$	0	0	0	0	
$d^1(^2D)$	1	0	0	0	F^0-J-C
$d^2(^3F)$	2	1	-1	-1	F^0-J+C
$d^3(^4F)$	3	3	-3	-1	F^0-J+C
$d^4(^5D)$	4	6	-6	0	F^0-J-C
$d^5(^6S)$	5	10	-10	0	F^0+4J
$d^6(^5D)$	6	15	-10	0	F^0-J-C
$d^7(^4F)$	7	21	-11	-1	F^0-J+C
$d^8(^3F)$	8	28	-13	-1	F^0-J+C
$d^9(^2D)$	9	36	-16	0	F^0-J-C
$d^{10}(^1S)$	10	45	-20	0	

correlated f and d states and the valence electrons (which include the 5d and 6d states in case of the lanthanides and the actinides) that fall into wide bands due to strong hybridization. The latter can then be treated in terms of local density theory, whereas the former are treated as a quasi-atomic open shell system, always allowing the conduction states to relax to each new polarity state of the d or f "cores". Herbst et al. have done such calculations for the lanthanides and the actinides [26,27,28,29]. Dederichs et al. used a very promising and potentially powerful ab initio formalism to treat Ce [30].

Herring [4] introduced a simple method to estimate the effect of screening on U^{eff} by replacing the reaction of Eq. 2.9 with $2d^n s \rightarrow d^{n+1} + d^{n-1}s^2$ and similar expressions for the f shell systems. The philosophy is, that in a metallic

Table 2.2. Parameters determining the energies of the Hund's Rule ground states in LS coupling for all f occupations and the expression for the f-f gap.

state	α_I	α_{F0}	α_J	α_C	U^{eff}
$F^0(^1S)$	0	0	0	0	
$F^1(^2F)$	1	0	0	0	F^0-J-3/2C
$F^2(^3H)$	2	1	-1	-3/2	F^0-J-1/2C
$F^3(^4I)$	3	3	-3	-7/2	F^0-J+2C
$F^4(^5I)$	4	6	-6	-7/2	F^0-J+2C
$F^5(^6H)$	5	10	-10	-3/2	F^0-J-1/2C
$F^6(^7F)$	6	15	-15	0	F^0-J-3/2C
$F^7(^8S)$	7	21	-21	0	F^0+6J
$F^8(^7F)$	8	28	-21	0	F^0-J-3/2C
$F^9(^6H)$	9	36	-22	-3/2	F^0-J-1/2C
$F^{10}(^5I)$	10	45	-24	-7/2	F^0-J+2C
$F^{11}(^4I)$	11	55	-27	-7/2	F^0-J+2C
$F^{12}(^3H)$	12	66	-31	-3/2	F^0-J-1/2C
$F^{13}(^2F)$	13	78	-36	0	F^0-J-3/2C
$F^{14}(^1S)$	14	91	-42	0	

system the screening of a localized electron or hole is always such, that charge neutrality is maintained [31]. The assumption is, that this happens at the impurity site, which is not exact, but quite reasonable for many cases (see, for example, chapter 5). The energies involved in the fully screened reaction can now be obtained from the gas phase optical data involving the transitions $d^n s \rightarrow d^{n-1} s^2$

and $d^n s \rightarrow d^{n+1}$, always taking the Hund's Rule ground states of each d occupation. The charge neutrality argument also shows that F^2, F^4 and F^6, or in other words, J and C, must be quite insensitive to placing the atom in a solid, as the splittings within a given d^n multiplet do not involve a different polarity state of the atom.

2.2. The Lanthanides

The most clear cut examples to discuss are certainly the lanthanide elements. From Mann's tables [32] we obtained the following values for F^0, F^2, F^4 and F^6 as a function of atomic number:

$$\begin{aligned} F^0(Z) &= 23.8 + 0.93\ (Z-57)\ (eV) \\ F^2(Z) &= 11.2 + 0.44\ (Z-57)\ (eV) \\ F^4(Z) &= \ 7.0 + 0.29\ (Z-57)\ (eV) \\ F^6(Z) &= \ 5.0 + 0.20\ (Z-57)\ (eV) \end{aligned} \tag{2.10}$$

Using Eqs. (2.6) and (2.7)

$$\begin{aligned} J &= 0.90 + 0.0362\ (Z-57)\ (eV) \\ C &= 0.45 + 0.0178\ (Z-57)\ (eV) \end{aligned} \tag{2.11}$$

From Ref. 9 we quote the empirical (optical) values for the trivalent configurations (Again using Eqs. (2.6) and (2.7)):

$$\begin{aligned} J &= 0.69 + 0.0299\ (Z-57)\ (eV) \\ C &= 0.31 + 0.0135\ (Z-57)\ (eV) \end{aligned} \tag{2.12}$$

which are about 25% reduced from the calculated values. We want to interpolate values for the lowest Hund's Rule states relative to the ground state of the pure metals and compare those with the valence band photoemission and BIS data of Lang et al. [33,34]. We will do this by assuming a linear dependence of I and F^0 on Z

using Eq. (2.12) for J and C and neglecting spin orbit splitting. The best parametrization that we obtained was:

$$I = 5.4 - 7.071\ (Z-57)\ (eV)$$
$$F^0 = 6.68 - 0.0333\ (Z-57)\ (eV) \qquad (2.13)$$

In Fig. 2.3 we plotted the energies of the monovalent, divalent, trivalent and tetravalent Hund's Rule ground states of the lanthanides using Eqs. (2.12) and (2.13) and Table 2.2. Curve II has precisely the same trend as the calculated energy differences between $f^n d^1 s^2$ and $f^{n+1} s^2$ gas phase states of Nugent and van der Sluis [35]. Several trends are quite clear in Fig. 2.3: Eu and Tb are divalent, Sm is close to becoming divalent and is therefore a likely candidate for mixed valence behaviour. If anything, Ce will become tetravalent. Good candidates to do mixed valent chemistry on are therefore Sm, Eu, Tm, Yb and Ce. This is in good agreement with experimental observation [6].

In Fig. 2.4 we give the energy positions of the BIS and XPS Hund's Rule levels of Lang et al. [33] together with the interpolation values using Eq. (2.12) and (2.13), taking the ground states from Fig. 2.3. We see that the 25 experimental peak positions are surprisingly well reproduced in the 4 parameter fit.
In cerium Lang et al. observed a state very close to E_F. This feature has been explained convincingly by Günnarsson and Schönhammer [36] using a $\frac{1}{N_f}$ expansion. They showed that hybridization of the f shell with the valence bands results in a self-energy shift of the photoemission features. The input parameter for the f^0-f^1 separation ε_f and the f^2-f^1 separation $\varepsilon_f + U^{eff}$ that they used in fitting their theory to the experimental spectra (this is different from the calculated peak positions) are also indicated in Fig. 2.3 and close to our interpolation values.

Finally we compare in Table 2.3 the U^{eff} from Lang et al. with the values from our interpolation and with the values obtained from optical data [37], using the method outlined in the introduction as far as the necessary data were available. From the table we see, that both the interpolation method and the optical data predict the observed U^{eff} within a few tenths of an eV. From experiment the optical data underestimate U^{eff} ca. 0.25 eV on the average. This is a bit surprising, as one would expect a better screening in the solid than in the gas phase due to the

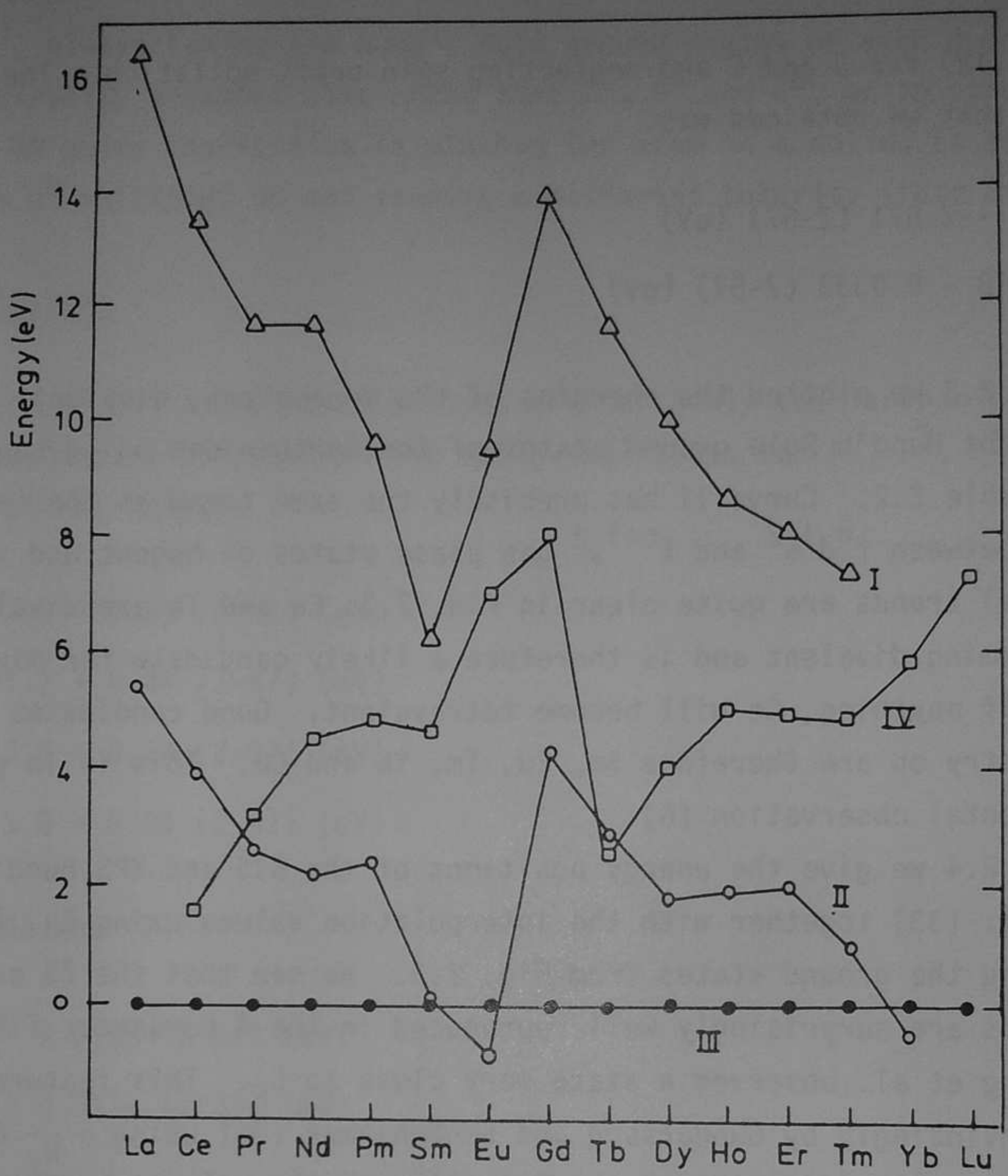

Fig. 2.3. Energies of the Hund's Rule ground states relative to the trivalent state (III) of the monovalent (I), divalent (II) and tetravalent (IV) configurations of the rare earths.

compression of the valence orbitals in the solid, as has been argued by Herring [4].

2.3. The iron series

Compared to the lanthanides, the situation in the 3d transition metals is much

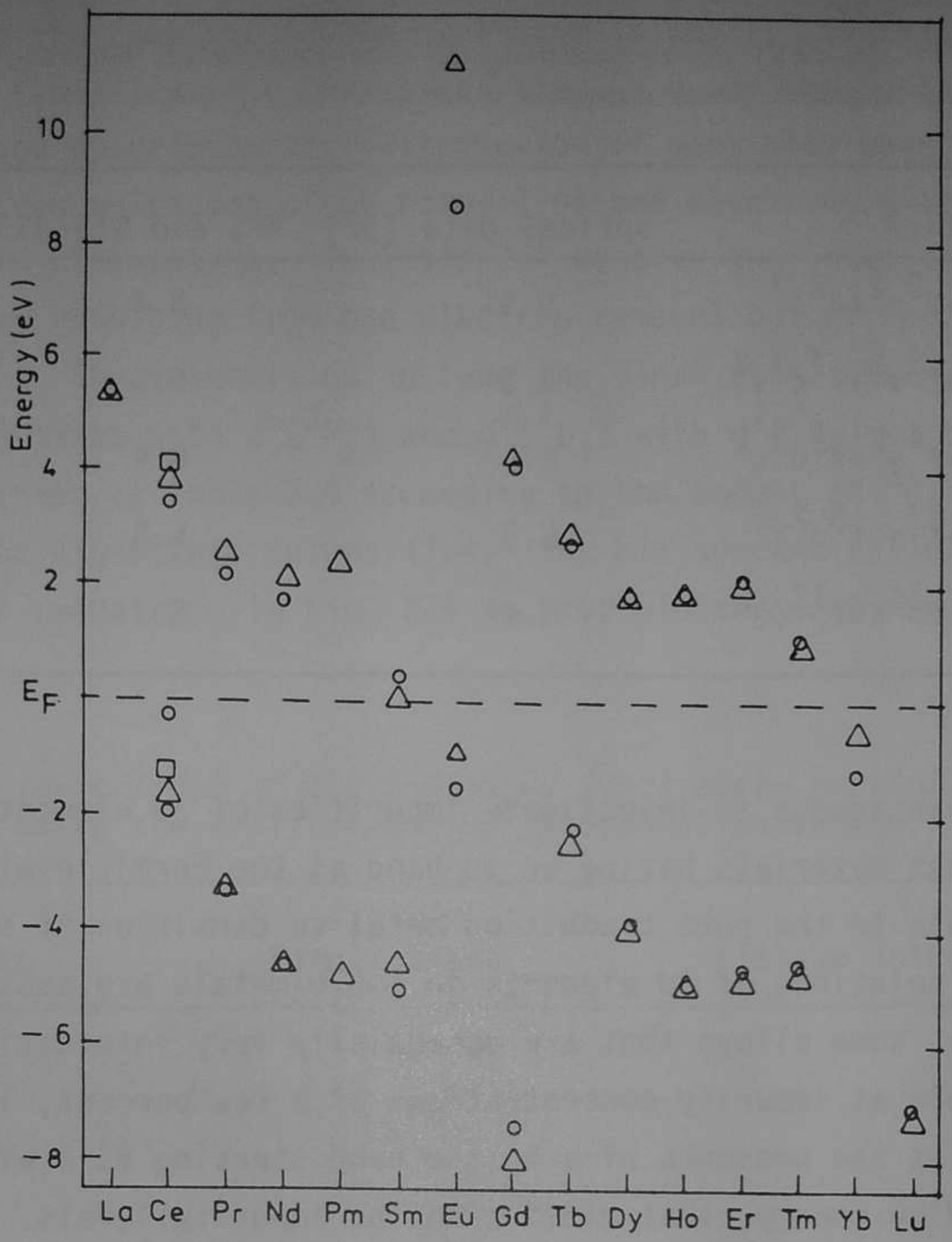

Fig. 2.4. BIS and XPS binding energies of the f-states closest to E_F.
Open circles: Experimental work of Lang et al. [33].
Triangles: Our interpolation values.
Squares: Günarsson and Schönhammer [36].

more complicated, due to the fact that the 3d states (I) are more extended than the f states (II) have smaller Coulomb interactions. Consequently the interpretation of the XPS and BIS spectra is expectedly complicated by the occurrence of satellite phenomena due to non-integer occupation of the d shells. Nickel has become a famous example of a system exhibiting satellite behaviour [38,39,40,41]. In view of the more extended nature of the 3d orbitals, leading to a d-band of several

Table 2.3. U^{eff} in (eV) corresponding to the indicated reaction and element from various sources

Element	reaction	optical data [37]	XPS and BIS [33]	interpolation
Ce	$2(f^1ds^2) \rightarrow f^2s^2+d^2s^2$	5.1	5.4	5.5
Pr	$2(f^2ds^2) \rightarrow f^3s^2+f^1d^2s^2$	5.3	5.5	5.8
Nd	$2(f^3ds^2) \rightarrow f^4s^2+f^2d^2s^2$	6.0	6.4	6.7
Sm	$2(f^6s^2) \rightarrow f^7s+f^5d^2s$	6.5	5.5	4.7
Tm	$2(f^{13}s^2) \rightarrow f^{14}s+f^{12}ds^2$	5.4	5.7	5.8

eV wide, it is advantageous to investigate impurities of 3d elements in a metallic host. The best host materials having an sp band at the Fermi level with a density of states comparable to the pure transition metal sp densities of states are Cu, Ag and Au. Solid solutions of 3d elements in noble metals are substitutional if existing. However, some alloys that are potentially very interesting are thermodynamically unstable at impurity concentrations of a few percent, like AgNi. A serious problem is the presence of a host d band starting at 2 eV (Cu and Ag) and 4 eV (Ag) binding energy, that mixes with the impurity levels. This mixing is interesting in itself and is treated in Chapter 3 of this thesis, but it also masks the many-body effects that we are interested in. It seems to be a manifestation of Murphey's Laws that AgNi, where the host d band lies deepest, does not exist.

The peaks observed in BIS fall in the region of unoccupied sp bands and are for that reason expected to be clearly visible. Nevertheless, even in the sp bands large steps occur in the density of states whenever a band crosses the Brillouin zône bounderies (Chapter 4 of this thesis [42]). This also partly masks the impurity peaks and one has to rely on subtraction methods in order to get clear impurity spectra.

Before turning to the BIS spectra we will draw a plot of what we expect to find in (inverse) photo emission of an open shell d impurity in a flat continuüm.

Suppose first that the coupling to the continuum is small. In that case the spectra are determined by (quasi)-atomic characteristics, i.e. by the coëfficients of fractional parentage describing the distribution of many body wave function character over the n-1 electron multiplet after removal of one electron, given an initial n electron state in LS coupling. In Table 2.4 we give the intensities of the various final states resulting from one electron removal out of the d^n Hund's Rule ground states [24]. The intensities include the final state degeneracies. The states $d^6(^3P_1)$ mixes with $d^6(^3P_2)$ and $d^7(^2D_1)$ with $d^7(^2D_2)$ so that one must add up the intensities of Table 2.4 according to the amount of $^3P_1$ and $^3P_2$ character in order to get the eigenstate intensities. The BIS spectra follow immediately from particle-hole symmetry. In Fig. 2.5 we have plotted combined XPS and BIS

Table 2.4. Intensities of the indicated final state multiplets using the coëfficients of fractional parentage.

Initial state	Final states	Relative intensities
$d^1(^2D)$	^1S	
$d^2(^3F)$	^2D	
$d^3(^4F)$	$^3F, ^3P$	28:3
$d4(^5D)$	$^4F, ^4P$	49:9
$d5(^6S)$	^5D	
$d^6(^5D)$	$^6S, ^4G, ^4F, ^4D, ^4P$	6:9:7:5:3
$d^7(^4F)$	$^5D, ^3H, ^3G, ^3F_1, ^3F_2, ^3D, ^3P_1, ^3P_2$	175:110:90:56:14:15:14:16
$d^8(^3F)$	$^4F, ^4P, ^2H, ^2G, ^2F, ^2D_1, ^2D_2, ^2P$	224:56:110:90:14:35:15:16
$d^9(^2D)$	$^3F, ^3P, ^1G, ^1D, ^1S$	21:9:9:5:1
$d^{10}(^1S)$	^2D	

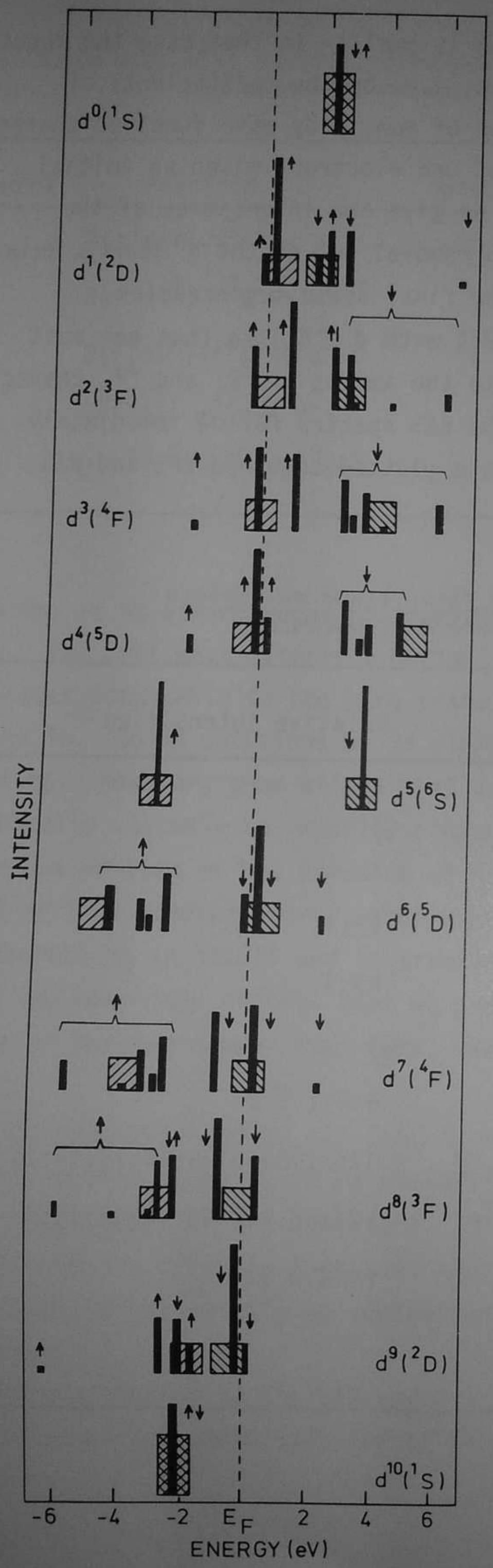

Fig. 2.5. Plot of the valence XPS and BIS peak positions of an open d shell for various occupations. We used F^0=2.0 (eV), F^2=9.8 (eV) and F^4=6.1(eV). The hatched blocks correspond to the Hartree Fock one particle energies, assuming the same parameters and a rectangular band.

spectra of an atom having zero to ten d electrons in the Hund's Rule ground state, taking F^0 = 2 eV, J = 1.14 eV and C = 0.59 eV. We indicated the multiplets with lower (higher) spin quantum number than the ground state with an up (down) arrow.

A quite different picture of the exchange split states corresponds to the Hartree Fock formalism of magnetic moment formation [43], related to, but different from the local density approximation [44]. In the Hartree Fock approach one assumes a finite width of the majority and minority spin states and takes for the exchange splitting of both bands $(n_\uparrow - n_\downarrow)J$, where $n_\uparrow$ and $n_\downarrow$ are the number of up and down d electrons per atom. The energy distributions of majority and minority spin states are then written as $B(\varepsilon - \varepsilon_{\sigma m})$, where $\varepsilon_{\sigma m} = I + \sum_{m'} U n_{\sigma m'} + \sum_{m' \neq m} (U-J) n_{\sigma m'}$, and B(x) is the band shape (often Lorentzian). The ground state is found by solving the two coupled self-consistent equations

$$\int^{E_F} B(x-\varepsilon_\sigma)dx = n_\sigma \qquad (2.14)$$

and looking for the state of lowest energy if more than one solution exists. This leads to the Anderson criterion of magnetic moment formation

$$(U+4J)\rho_d(E_F) > 1 \qquad (2.15)$$

Although this model does not tell you much about the UPS and XPS spectra, people quite often seem to believe, that a plot of these one particle states may provide the electron removal or addition spectra. To point out the differences with the atomistic point of view we have also plotted the majority (left) and minority (right) bands in Hartree Fock theory, taking rectangular bands of 1 eV wide and $E_\uparrow - E_\downarrow = \frac{1}{5}(U+4J)(n_\uparrow - n_\downarrow)$. We see that there are significant differences between both approaches, except for the d^0, d^5 and d^{10} configurations where both give exactly the same result. Fig. 2.5 also tells us, that d^0, d^5 and d^{10} are stable against charge fluctuations, d^2, d^3, d^7 and d^8 are much less stable and d^1, d^4, d^6 and d^9 are unstable if F^0 is smaller than J+C.

In Fig. 2.6 we show BIS spectra of Sc, Ti, V, Cr, Mn and Fe diluted in gold. The experimental details are the same as in Chapter 6. In Fig. 2.7 we show the differences with the pure Au spectra, which were obtained by scaling the intensities

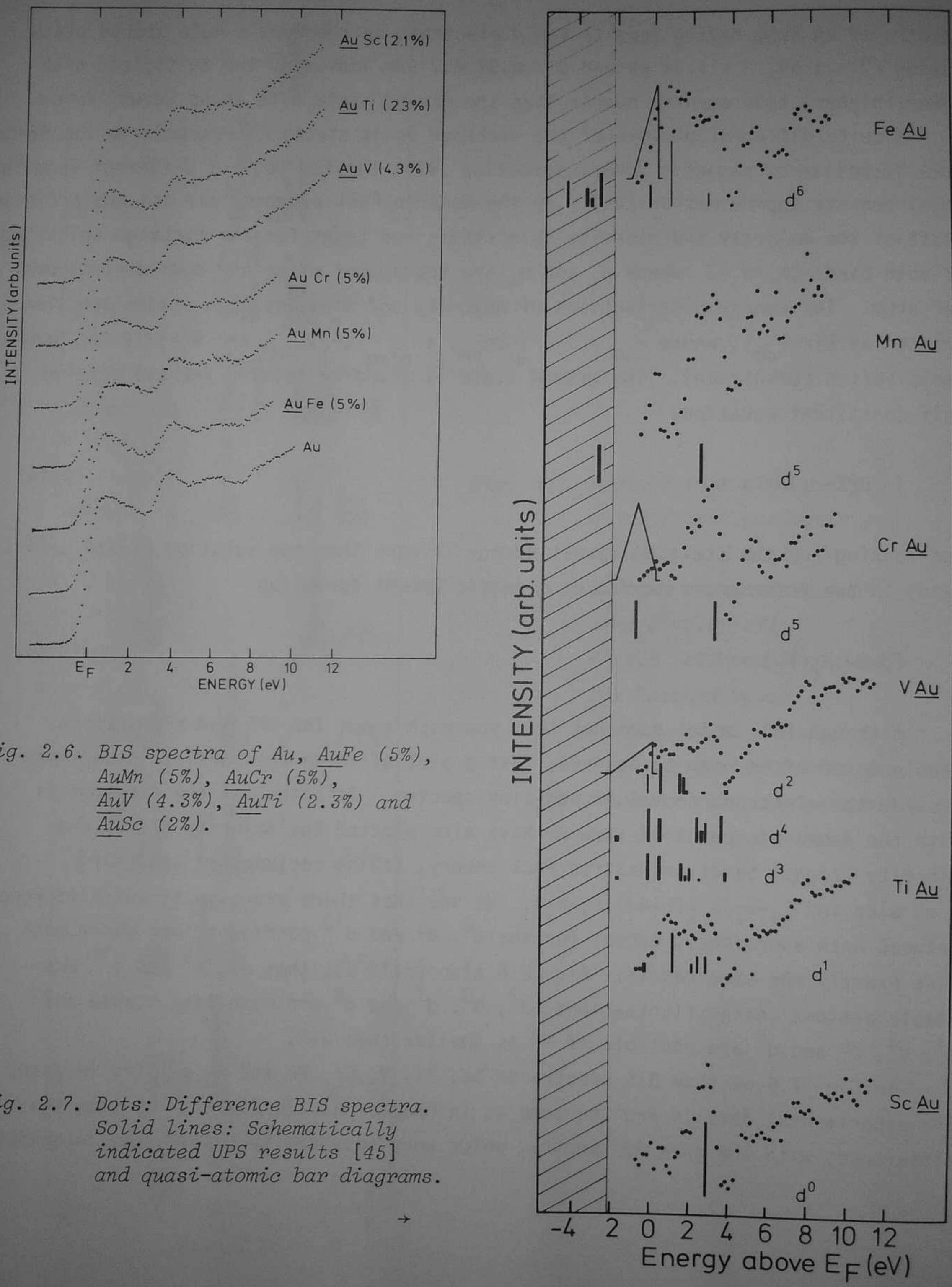

Fig. 2.6. BIS spectra of Au, AuFe (5%), AuMn (5%), AuCr (5%), AuV (4.3%), AuTi (2.3%) and AuSc (2%).

Fig. 2.7. Dots: Difference BIS spectra. Solid lines: Schematically indicated UPS results [45] and quasi-atomic bar diagrams.

→

at 4.5 eV and subtracting. This procedure is not completely unambiguous. The reader will notice, that there is a negative dip at about 4 eV in all difference spectra, which appears at the same place as the step in the pure gold spectrum. Possibly the dip is a non-Lorentzian lineshape due to a very energy dependent self-energy near the step in the gold continuum. It is difficult to separate such intrinsic effects from anomalies due to improper alignment of the spectra before subtracting them. We optimized the alignment of the spectra at the Fermi edge. Any malalignments will result in a positive or negative dip near E_F. We could not avoid this to occur in the MnAu difference spectrum, which we consider as unreliable for that reason. In all difference spectra there is a fairly high inelastic background, probably due to the extra energy loss paths introduced by the impurity atoms. We also schematically indicated the AuFe, AuCr and AuV UPS results from Andrews et al. [45]. The hatched area is the region where the gold 5d band masks the possible structures in that particular energy region. This problem has been overcome recently with synchrotron radiation, giving nice results on the whole 3d series in gold, but the results were not analyzed when writing this chapter [46].

Without looking at the details of the structures in Fig. 2.7, we can already see that there is a 4 à 5 (eV) gap for CrAu, whereas there is a pile up of states near E_F for FeAu, VAu and TiAu. ScAu exhibits a clear split off state some 3 eV above E_F. The MnAu spectrum is a bit ambiguous. However there is certainly no peak near E_F in the UPS spectrum [45,46] although a dilution induced narrowing of the Au 5d band is quite clear. It is very likely that the situation is similar to CuMn, where the Mn majority peak is absorbed in the Cu 3d band (Chapter 6 of this thesis [47]).

In order to be able to compare the spectra with quasi-atomic theory we have to know the Slater integrals F^2 and F^4, or J and C. In Table 2.5 we give the multiplet splittings of the doubly ionized and neutral 3d elements in the gas phase, from Moore's tables [48], together with the values of these splittings based on Mann's tables [32]. The F^2 to F^4 ratio was kept at Mann's values and F^2 and F^4 or J and C were fitted to the experimental values using Eqs. (2.4) and (2.6). We see from Table 2.5 that the multiplet splitting is reduced with 6 to 8% due to the presence of the 4s electrons in Cr to Cu and ~ 20% for Sc to V. The neutral atom values of J and C were used to generate the bar diagrams under the FeAu, VAu

Table 2.5. Gas phase atomic data of the indicated multiplet splittings and the resulting J's and C's for the neutral atoms and the doubly ionized atoms. All values in (eV).

element	observed splitting	value using Mann's tables [32]	Experimental neutral atom value [48] $3d^n4s^2$	J^{0+}_{exp}	C^{0+}_{exp}	Experimental doubly ionized atom value [48]	J^{2+}_{exp}	C^{2+}_{exp}
Ti	^3P-^3F	1.55	1.03	0.59	0.31	1.29	0.74	0.39
V	^4P-^4F	1.71	1.16	0.67	0.35	1.40	0.81	0.42
Cr	^5D-^3H	2.03	1.98	0.92	0.48	2.12	0.98	0.51
Mn	^6S-^4G	3.80	3.13	0.94	0.50	3.33	1.00	0.53
Fe	^5D-^3H	2.68	2.31	1.07	0.55	2.46	1.14	0.59
Co	^4P-^4F	2.28	1.63	0.95	0.49	1.81	1.05	0.54
Ni	^3P-^3F	2.40	1.82	1.05	0.55	1.96	1.13	0.59

and Ti<u>Au</u> difference spectra in Fig. 2.7.

Although the doubly peaked structure in the Fe<u>Au</u> spectrum seems to be reproduced quite well, we have to be careful with concluding that this settles that Fe is in a d^6 state: In the first place, a d^7 configuration would also result in a final state doublet; secondly, the peak at 3.5 eV has too much intensity relative to the main line. An alternative explanation might be, that the ground state is of mixed d^5, d^6 and d^7 character, resulting in a spectrum consisting of a mixture of main and satellite lines. The same could be true for vanadium, where neither of the three initial state configurations d^2, d^3 and d^4 reproduces the observed final state structure. Titanium seems to fit quite well assuming a d^1 ground state. On the other hand, the BIS spectrum could again be a main line near E_F and a d^2 satellite at higher energies (symmetrical to Ni).

It is hard to determine F^0 from the combined UPS and BIS spectra, although one can see from the pile up of intensity near E_F in <u>Au</u>V and <u>Au</u>Fe that it must be

in the order of 1 eV or smaller. For CrAu it is easier to estimate U^{eff}, which is about 4 eV. Using Tables 1 and 5 we find $F^0 \simeq 0.3$ eV. For the MnAu case we assume similar values as in AgMn (Chapter 6 of this thesis [47]), so that $F^0 \simeq 1.0$ eV. In copper metal $F^0 = 5.9$ eV from Auger analysis [49]. In nickel metal Fuggle et al. [50] arrived at $F^0 = 2.8$ eV from Auger analysis. The situation in nickel is, however, complicated due to the interconfigurational mixing of d^{10} and $d^9(sp)^1$ in initial and final states. Fuggle et al. did their analysis assuming the d^{10} ground state configuration and interpreted the nickel d band as d^9 final states. F^0 was derived from the reaction $2(3d^9 4s) \rightarrow 3d^{10} + 3d^8 4s^2$, using 1.4 eV (the d band centroid) for the one particle binding energy. Suppose now that d^9 and d^{10} are in fact exactly degenerate [40]. The d band observed in photoemission is now a mixture of d^{10} and $d^9 s$ states, the lowest state of which coincides with the ground state of the metal. The d^8 states observed in Auger spectroscopy are at an energy $2\varepsilon_d + U^{eff} + \delta_g$ above the ground state of the system, where $\varepsilon_d = E(d^9 k_F^1) - E(d^{10}) \simeq 0$ (k_F is a conduction state at E_F) and δ_g is the hybridization energy gain of the ground state minus the d^8 hybridization energy (approximately half the d band centroid = 0.7 eV). Fuggle et al. assumed $\delta_g = 0$ and $\varepsilon_d = 1.4$ eV, and they subtracted two times 1.4 eV = 2.8 eV from the experimental two hole binding energies in order to obtain U_{eff}, hence F^0. We assume $\delta_g \simeq 0.7$ eV and $\varepsilon_d = 0$ eV, so that we have to subtract 0.7 eV from the experimental two hole binding energies in order to obtain U_{eff}. Consequently we arrive at an F^0 that is 2.1 eV larger, i.e. $F^0 = 4.9$ eV. This value is too high as we will see; there seems to be a discrepancy between the two hole binding energies used in Ref. 50 and those of Haak et al. [51]. For the d^0, d^7 and d^8 lowest states we would find with these parameters and Tables 2.5 and 2.1

$$E(d^8\ {}^3F) = \varepsilon_d + F^0 - J - C + \delta_g = 4.0 \text{ eV}$$

$$E(d^7\ {}^4F) = 2\varepsilon_d + 3F^0 - 3J - C + \delta_g = 11.7 \text{ eV}$$

$$E(d^6\ {}^5D) = 3\varepsilon_d + 6F^0 - 6J + \delta_g = 23.8 \text{ eV}$$

The experimental peak positions are [51,52] 3.0 (eV), 9.8 (eV) and ca. 22.5 (eV) respectively, indicating an overestimation of F^0 of ca. 1 eV. So $F^0 = 3.9$ eV is

a better value giving good agreement for the d^7 and d^8 peak positions and an underestimation of 0.7 eV of the d^6 peak position, which is quite reasonable in view of the fact that the screening of a Ni d^6 state has to be with p electrons instead of the more localized s electrons. The way of treating the s-d hybridization in the above discussion is a bit crude, but the basic principles agree with a more refined many-body approach [53].

Another way of determining F^0 is by using optical data of the gas phase neutral atoms as outlined in the introduction. In Table 2.6 we collect the values of U^{eff}. The corresponding values of F^0 were found by subtracting the J's and C's using Table 2.1. We also give the gas phase Hartree Fock values of F^0 from Mann's tables [32] and the F^0 values of Cr in gold, Mn in silver, Ni in nickel metal and Cu in coppper metal from the discussion. We see that the agreement for Mn is quite bad, but note that the valency in the optical process is different from the valency that

Table 2.6. U^{eff} using optical data for the indicated reactions and the resulting F^0 value, the F^0 values in the solid as discussed in the text and the unscreened Hartree Fock value from Mann's tables.

element	reaction	U^{eff} [48]	F^0 atomic	F^0 in solid	F^0 unscreened HF [32]
Sc	$2(d^2s) \rightarrow ds^2 + d^3$	1.05	1.27	-	15.10
Ti	$2(d^3s) \rightarrow d^2s^2 + d^4$	1.93	2.21	-	17.0
V	$2(d^4s) \rightarrow d^3s^2 + d^5$	1.34	2.36	-	18.7
Cr	$2(d^5s) \rightarrow d^4s^2 + d^6$	4.62	0.94	0.3	18.4
Mn	$2(d^6s) \rightarrow d^5s^2 + d^7$	1.31	2.75	1.0	21.9
Fe	$2(d^7s) \rightarrow d^6s^2 + d^8$	1.83	2.35	-	22.4
Co	$2(d^8s) \rightarrow d^7s^2 + d^9$	2.22	2.68	-	24.8
Ni	$2(d^9s) \rightarrow d^8s^2 + d^{10}$	1.61	3.21	3.9	26.3
Cu	-	-	-	5.9	26.0

manganese has in the solid. The degree of agreement for Cr and Ni is comparable to what we found in the lanthanides. The Hartree Fock values are 15 to 20 eV higher in energy than the screened values. The optical values for F^0 of Sc, Ti and V are quite high (1 à 2 eV), but as in the case of Mn the valence of these elements is different in the solid from that in the gas phase. As they are probably divalent or even trivalent, the screening can be somewhat larger than in, for example, monovalent Cr, so that the screened F^0 value is probably between zero and one eV. If so, this will lead to negative values for U^{eff} as has been mentioned earlier by de Boer et al. in connection with their Auger analysis [54].

To show what will happen in such cases, we have drawn energy level diagrams in Fig. 2.8 of the Hund's Rule ground states and first excited states as a function of occupation for some values of F^0 and I. We used J = 0.6 (eV) and C = 0.31 (eV) everywhere. Fig. 2.8a corresponds roughly to Cr impurities. The d^4 state is close to the d^5 state, so that the ground state is of mixed d^5d^4 character. In view of this fact, it is surprising that no clear features are observed close to the Fermi level, as one would expect if the ground state were purely d^4 (see Fig. 2.5) or if a many-body resonance would build up at the Fermi level [2]. This paradox strongly resembles the paradox in AgMn (Chapter 6 of this thesis [47]), where we found a minority peak at 2.1 eV from E_F having a half-width of 1.2 eV. Andrews et al. [44] found the majority peak of Cr in Au at 0.87 eV binding energy having a halfwidth of 0.28 eV. In both cases, the ratio halfwidth to peak position is in the range of ½ indicating strong fluctuations between d^5 and d^6 in the case of AgMn and between d^4 and d^5 in the case of AuCr. Nevertheless the spectral features are those of a pure d^5 state.

Fig. 2.8b corresponds to Ti. Note that, although the one particle potential I is repulsive, a d^2 state can still be favoured due to the multiplet splitting. If F^0 gets smaller than J we get a situation like in Fig. 2.8f, where charge fluctuations take place involving more than two electrons. We must not forget, however, that the screening mechanism, though apparently more or less linear for nickel, becomes very nonlinear if an atom has already lost all its screening electrons. Addition of an extra negative charge can no longer be compensated within the same unit cell and the corresponding polarity state will be several eV higher in energy than what is to be expected from linear response theory. For Ti this

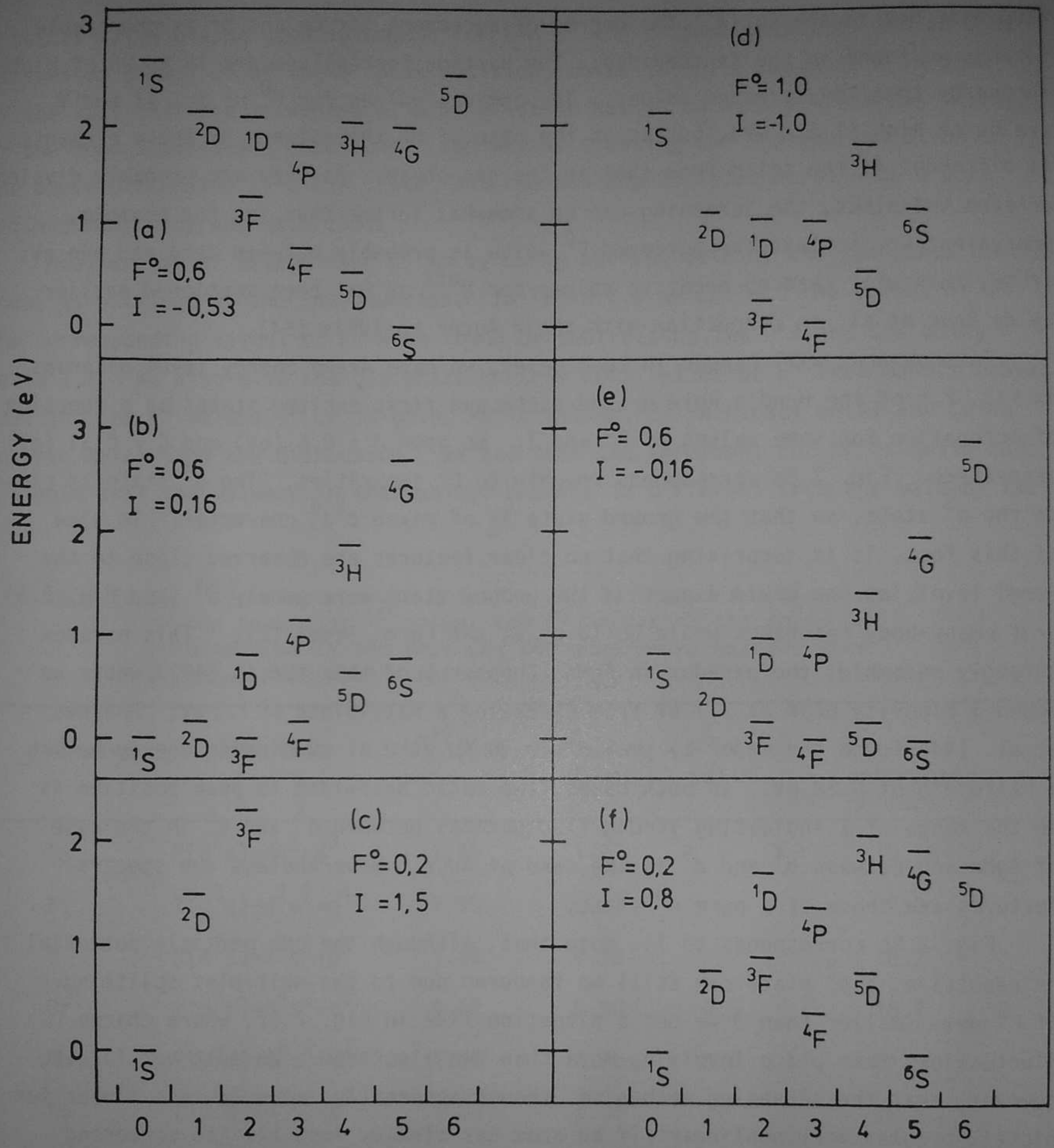

Fig. 2.8. Calculated energy positions of lowest and first excited states as a function of d-occupation for indicated parameters values of F^0 and I and using F^2 = 5.2 (eV) and F^4 = 3.2 (eV).

would mean that states having more than four d electrons are no longer fully screened. In V the d^5 state is still possible and this means that the quite extreme situation of Fig. 2.8f could in principle occur in certain V alloys. Fig. 2.8d or 2.8e are probably closer to AuV.

2.4. The 4d and 5d elements

From Mann's tables [32] we have for the 4d series

$$C = 0.50\ J$$

$$J(Z) = 0.59 + 0.056\ (Z-39)\ (eV) \qquad (2.16)$$

and for the 5d elements

$$C = 0.52\ J$$

$$J(Z) = 0.60 + 0.053\ (Z-71)\ (eV) \qquad (2.17)$$

The F^0 integrals are about 65% of the values in the chemically equivalent 3d elements. In Table 2.7 we collect the U^{eff} values from the optical data [48]. We also indicated "F^0" estimates, using J's and C's that were taken 80% of the values of Eqs. (2.16) and (2.17), however without incorporating spin orbit coupling. We see that, although the Hartree Fock values of F^0 are several eV lower than in the 3d series, the screened F^0 values remain at a lower limit of 1 à 2 eV, with the exception of Ta, which has a negative Hubbard gap. Nevertheless, the F^0 values could be still smaller in a metallic host due to the higher density of the conduction electrons. With the exception of Mo, Tc, Re and W we expect small Hubbard gaps. The possibility of a negative U^{eff} is intriguing and we expect this to occur for elements having a d^1, d^4, d^6 or d^9 configuration, as we already discussed for the 3d elements.

Table 2.7. U^{eff} from the indicated reactions using optical data [48], the resulting F^0 and F^0 from Mann's tables [32].

element	reaction	U^{eff}	"F^0"	F^0(Mann)
Y	$2d^2s \rightarrow d^1s^2 + d^3$	0.8	1.0	10.23
Zr	$2d^3s \rightarrow d^2s^2 + d^4$	1.5	1.8	11.64
Nb	$2d^4s \rightarrow d^3s^2 + d^5$	1.5	2.3	11.96
Mo	$2d^5s \rightarrow d^4s^2 + d^6$	4.6	2.2	13.14
Ru	$2d^7s \rightarrow d^6s^2 + d^8$	2.0	2.4	15.26
Rh	$2d^8s \rightarrow d^7s^2 + d^9$	2.0	2.4	16.26
Pd	$2d^9s \rightarrow d^8s^2 + d^{10}$	1.5	2.6	16.36
Ta	$2d^4s \rightarrow d^3s^2 + d^5$	-1.0	-0.2	12.10
Ir	$2d^8s \rightarrow d^7s^2 + d^9$	1.6	2.0	15.22
Pt	$2d^9s \rightarrow d^8s^2 + d^{10}$	0.9	2.0	15.36

2.5. The actinides

In the compounds of U, Np, Pu and Am the actinide atoms possess magnetic moments of 1 to 3 Bohr magnetons [55]. These moments are of mixed spin-orbital nature, the orbitular part not being quenched completely in the crystal fields. Well developed moments exist especially in systems having inter actinidic spacings of more than 3.5 Å [56]. Pure U, Np and Pu form rather wide f bands and do not show magnetic ordering. Their effective intra-atomic interactions are known to be small due to screening [16,17,19,29], although the exchange splittings of the atoms are comparable to those of the 3d metals. The f bands become very narrow, however, in compounds with large interactinidic distances [57].

The J and C values translated from the Racah parameters E_1, E_2 and E_3 fitted to optical data [58,59] and photoemission of the actinide-oxydes [60,61,62] are:

$$C = 0.41\ J$$

$$J = 0.33 + 0.070\ (Z-89)\ (eV) \tag{2.18}$$

from Mann's tables

$$C = 0.41\ J$$

$$J = 0.66 + 0.035\ (Z-89)\ (eV) \tag{2.19}$$

We see that the reduction from the Hartree-Fock values is quite significant now. The empirical C and J values of the actinides lie some 30% below those of the lanthanides. The spin orbit parameter ranges from 0.23 to 0.40 eV from uranium to berkelium [60], which is some 65% larger than the corresponding parameter in the

Table 2.8. Energies in (eV) of the indicated configurations using optical data [37].

element	f^0	f^1	f^2	f^3	f^4	f^5	f^6	f^7
Th	0.00 (d^2s^2)	0.97 (ds^2)	3.47 (f^2s^2)	-	-	-	-	-
Pa	2.73 (d^4s)	0.25 (fd^2s^2)	0.00 (f^2ds^2)	1.42 (f^3s^2)	-	-	-	-
U	3.47 (d^5s)	2.73 (fd^4s)	1.43 ($f^2d^2s^2$)	0.00 (f^3ds^2)	0.87 (f^4s^2)	-	-	-
Np	-	-	4.34 (f^2d^4s)	2.42 ($f^3d^2s^2$)	0.00 (f^4ds^2)	0.12 (f^5s^2)	-	-
Pu	-	-	-	-	4.47 ($f^4d^2s^2$)	0.78 (f^5ds^2)	0.00 (f^6s^2)	-
Am	-	-	-	-	-	6.94 ($f^5d^2s^2$)	2.11 (f^6ds^2)	0.00 (f^7s^2)

chemically equivalent lanthanides [9,63]. In Table 2.8 we list the levels of the different f occupations of the neutral gas phase actinides determined from optical data, always taking the lowest levels. In parenthesis we give the assignments of the levels [37]. From this table we can derive Hubbard gaps, as in the preceding sections. Very significant are the many different crossing levels in U, Pa and Np. As a consequence we can define three different U^{eff} values for uranium dependent on its valence. Johansson arrived at a U^{eff} of 2.3 eV for uranium, which was based on the trivalent configuration [17], but he did not mention the other valencies. As uranium metal has two f electrons the tetra valent U_{eff} is probably more important. In Table 2.9 we list the U^{eff} values derived from Table 2.8 for the various valencies that are possible.

As the one electron potentials in the solid may differ significantly from those in the gas phase the valency of the atoms can be different as well.

Table 2.9. U^{eff} in (eV) for the actinides for several valencies and corresponding reactions using optical data [37].

element	valency	reaction	U^{eff} (eV)
Th	III	$2fds^2 \rightarrow f^2s^2 + d^2s^2$	1.53
Pa	III	$2f^2ds^2 \rightarrow f^3s^2 + fd^2s^2$	1.67
Pa	IV	$2fd^2s^2 \rightarrow f^2ds^2 + d^4s$	2.23
U	III	$2f^3ds^2 \rightarrow f^4s^2 + f^2d^2s^2$	2.30
U	IV	$2f^2d^2s^2 \rightarrow f^3ds^2 + fd^4s$	-0.13
U	V	$2fd^4s \rightarrow f^2d^2s^2 + d^5s$	-0.56
Np	III	$2f^4ds^2 \rightarrow f^5s^2 + f^3d^2s^2$	2.64
Np	IV	$2f^3d^2s^2 \rightarrow f^4ds^2 + f^2d^4s$	-0.50
Pu	III	$2f^5ds^2 \rightarrow f^6s^2 + f^4d^2s^2$	2.91
Am	III	$2f^6ds^2 \rightarrow f^7s^2 + f^5d^2s^2$	2.72

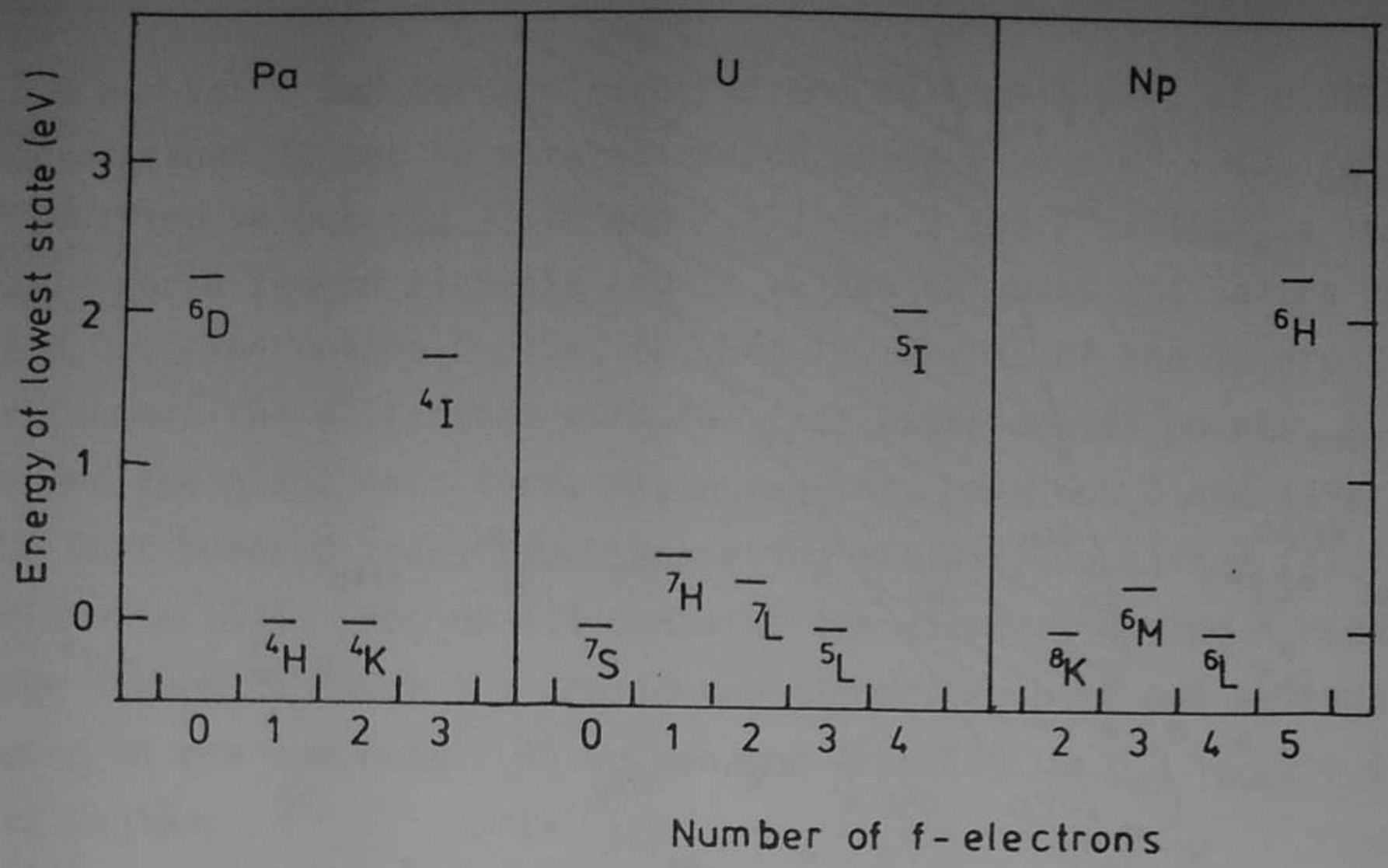

Fig. 2.9. Energy positions of lowest states as a function of f occupancy of U, Pa and Np, using Table 2.8 and adding an extra one-particle potential.

To make clear what this implies in the light actinides, we have plotted in Fig. 2.9 the values of Table 2.8 for the different f occupations, but added a one-electron potential to them, i.e. an energy that depends linearly on the f occupation. This potential was chosen such, that uranium ends up with having ~ 2 electrons on the average, Np ~ 3 and Pa ~ 1.5. Of course, such choices are arbitrary and the value of the one electron potential will depend on the electronegativity of the element(s) the actinide atom is alloyed with. Fig. 2.9 and Table 2.9 show a feature that is probably crucial in the physics and chemistry of the light actinides: the negative U^{eff} causes non-statistical charge fluctuations of two or even three electrons in the f shell. Especially if the f bands are narrow, this must give rise to peculiar and new phenomena. It might even be the basis of heavy fermion properties in some actinide compounds discovered in the last few years [64].

2.6. Conclusions

Finally, we will discuss the d and f transition metals using a plot of their Hubbard gaps against a parameter that is sensitive to the degree of spatial confine-

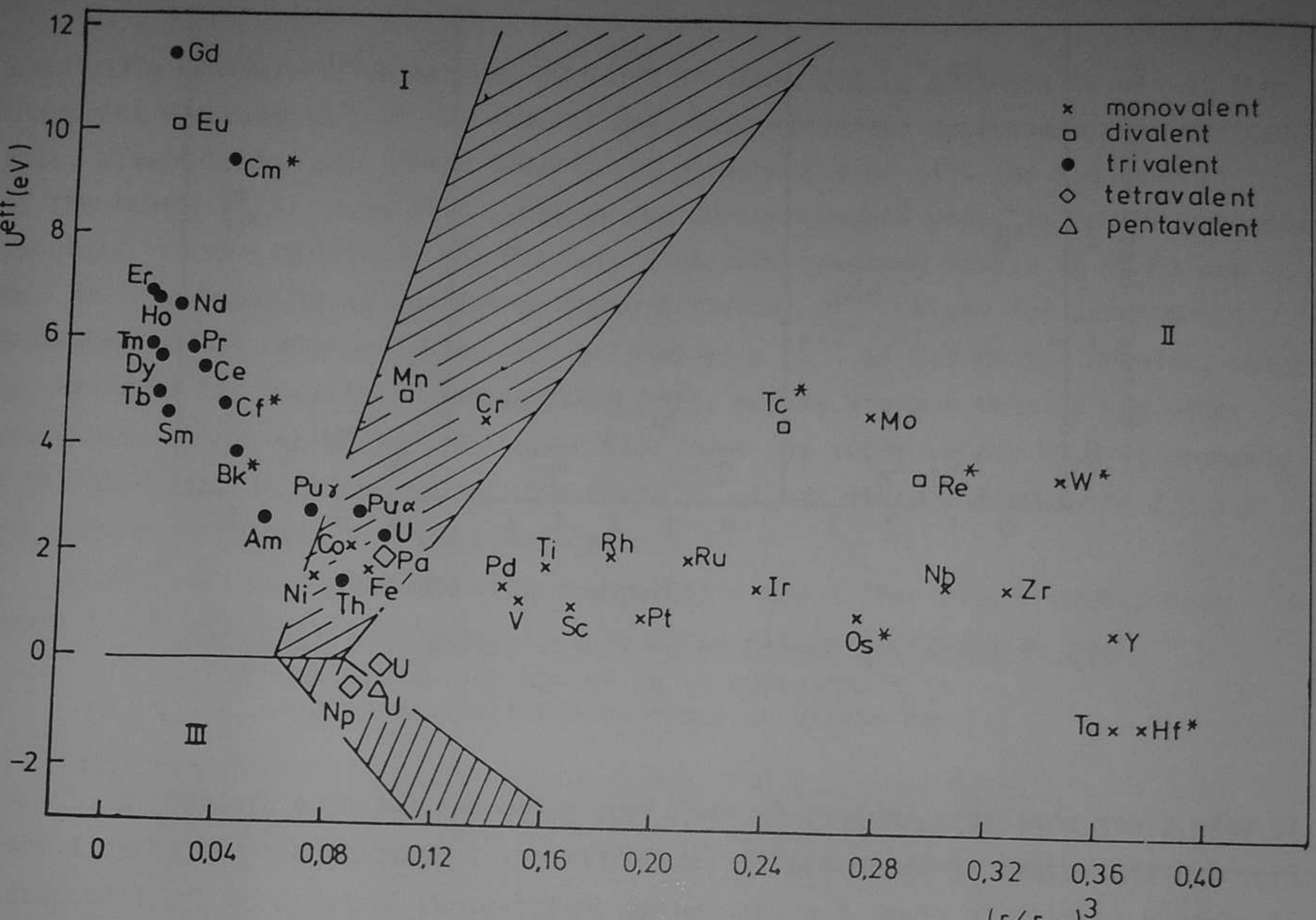

Fig. 2.10. Plot of U^{eff} against $(r_l/r_{ws})^3$ for the d and f transition metals in their elemental form, assuming valencies as discussed in the text.

ment: the $(r_l/r_{ws})^3$ values of Fig. 2.2. We could have chosen the reciprocal band-mass parameter $\mu^{-1} = \frac{1}{2} r_{ws}^3 |\phi_l(r_{ws})|^2$ instead, where ϕ is the radial d or f wave function at the Wigner Seitz radius [65], but both parameters happen to be practically proportional to each other for the materials that we discuss here.

In Fig. 2.10 we display the positions of the pure metallic elements in such a plot. The U^{eff} values are the gas phase spectroscopy values of Tables 2.3, 2.6, 2.7 and 2.9. The valencies for which U^{eff} was determined are also indicated. The values for trivalent Cm, Bk and Cf were extrapolated from the value for Am, assuming a Z independent difference between Mann's tables and the screened F^0's,

using Eq. 2.8 and Table 2.2 for the exchange and multipole part of U(Hubbard). The U^{eff} for divalent Tc and Re were estimated using $U^{eff} = F^0 + 4J$, taking 80% of Mann's tabulated values (Eq. 2.16 and 2.17) for J and $F^0 = 1(eV)$. The U^{eff} were available for a few 5d elements and so we had to guess its values for monovalent Hf and Os. The points for Cm, Bk, Cf, Tc, Re, W, Hf and Os are indicated with a star to mark the difference with the true experimental points.

We divided the plane into three major regions. Regions I and II are both sides of the Mott-Hubbard transition separating the very localized (I) from the itinerant elements [54]. Region III contains the elements having a negative U^{eff} that is large enough to cause the considered element to have two valencies differing by two or more in one compound. As we can see from Fig. 2.10, no pure elements fall in this region.

In region I polarity fluctuations are strongly suppressed and magnetic moments are formed according to Hund's Rule. Although the large U_{eff} prohibits reactions of the type $2f^n(sd)^m \rightarrow f^{n+1}(sd)^{m-1} + f^{n-1}(sd)^{m+1}$, the reactions $f^n{}_s{}^m \rightarrow f^{n+1}{}_s{}^{m-1}$ *exclusive* or $f^n{}_s{}^m \rightarrow f^{n-1}{}_s{}^{m+1}$ are still possible dependent on the one particle potential, i.e. on the compound the atom is built in. All lanthanides and the heavy actinides belong to class I.

The shaded area between regions I and II contains the heavy 3d elements and some of the light actinides. Whether a material containing such an element belongs to class I or class II depends strongly on the type of alloy or compound it is built in. For example, alloying with aluminium, which has a high density of states that couples to the d(f) orbitals increases s-d hyrbidization and effectively moves the element to the right, i.e. to region II. Alloying with a noble metal will reduce the direct d-d or f-f hybridization of the transition metal. On the other hand, the impurity-host d-d or f-d hybridization may still be significant. This will mainly affect states that fall in the host d band region, but has little influence on states above the Fermi level. The net result will be an effective shift to the left side of the shaded area. Pu is a nice example of element that can be moved from left to right just by changing the temperature. Uranium, on the other hand, is an element that can be moved up and down in the diagram, by changing the one particle potential of the f electrons. Its average number of f electrons will depend on the electronegativity of the element(s) it is alloyed

with, and the f occupation influences U^{eff} as can be seen in Fig. 2.10.

Class II contains the elements that form wide d bands in their elemental form. If diluted in the appropriate alloy, they can still form relatively narrow virtual bound states, and may carry a local moment in some cases. In view of their relatively high U^{eff}, one might expect Re and Tc (if divalent) and Mo and W (if monovalent) to have suppressed charge fluctuations. If alloyed with an appropriate host material, we expect a local moment for those elements, possibly coupled to the conduction electrons with a high Kondo temperature. As far as we know, this has not been investigated yet, apart from indications for a magnetic moment of Re and Tc in Gd [66].

The values of U^{eff} could of course differ from the atomic values, especially if the valency is different than for the gas phase atom. We have already discussed this for V and Ti, where we expect low or negative values in some cases, hence some of their compounds could belong to class III or at least be in the transition region separating class II and III.

Tantalum has a negative U in the gas phase. On the other hand, its 5d orbital is quite diffuse and it is questionable whether a negative U centre would still exist if the d electrons are strongly itinerant. Tetravalent uranium and neptunium and pentavalent uranium are in an area of narrow f bands and negative U^{eff}. In chapter 7 [67], we discuss the possibility of triplet pairing of conduction electrons induced by the negative U^{eff} of the localized f electrons of the uranium atoms in alloys. Quite interesting is, that the charge fluctuation propagator $C^0(q,\omega)$ is *enhanced* with a factor $(1 + U^{eff}\ C^0(q,\omega))^{-1}$, for negative U^{eff} materials in region II. If the condition $U^{eff} = -(C^0(q,\omega))^{-1}$ is satisfied a transition takes place to a new state where valence fluctuations with two or more electrons occur. Although we do not know where to draw this transition region precisely, we have tentatively drawn an area that contains N_p and U. It is interesting in this context, that two independent types of atoms have recently been claimed in α-uranium [68].

If compounds would exist in the far left of region III, they would show quite extraordinary behaviour, as the hybridization with the conduction states becomes small there. One would expect thermal, or pressure induced, valence fluctuations by two or more f(d) electrons.

References

1. M.D. Daybell and W.A. Steyert, Rev. Mod. Phys. 40, 380 (1968).
2. G. Grüner and A. Zawadowsky, Rep. Progr. Phys. 37, 1497 (1974).
3. N. Andrei, K. Furuya and J.H. Löwenstein, Rev. Mod. Phys. 55, 331 (1981).
4. C. Herring in "Magnetism, Vol. IV", edited by T. Rado and H. Suhl, (Academic, New York, 1964).
5. A.J. Heeger, in "Solid State Physics", edited by F. Seitz and D. Turnbull (Academic, New York, 1969), 23, 283 (1969).
6. "Valence instabilities and related narrow-band phenomena", edited by R.D. Parks, (Plenum, New York, 1977).
7. "Structure and bonding 59/60", edited by L. Manes, (Springer-Verlag, Berlin Heidelberg, 1985).
8. "The Actinides, electronic structure and related properties", part I and II, edited by A.J. Freeman and J.B. Darby, (Academic, New York, 1974).
9. G.H. Dieke, "Spectra and Energy Levels of Rare Earth Ions in Crystals", edited by H.M. Crosswhite, John Wiley and Sons, New York, 1968.
10. N.W. Ashcroft, N.D. Mermin, "Solid State Physics", (Holt, Rinehart and Winston, New York, 1976), p.1.
11. "The Handbook of Chemistry and Physics 56", edited by C. Weast, CRC Press Inc., Cleveland, 1975, p. B-237.
12. L. Manes and U. Benedict in Ref. 7, p.80-89.
13. D.C. Koskenmaki and K.A. Gschneidner in "Handbook on the Physics and Chemistry of the Rare Earths", edited by K.A. Gschneidner and L. Eyring (North-Holland, Amsterdam, 1978), Vol. 1, Chap. 4.
14. C.M. Varma, Rev. Med. Phys. 48, 219 (1976).
15. T. Penney and F. Holzberg, Phys. Rev. Lett. 34, 322 (1975).
16. B. Johansson in Ref. 6, p. 435 (1977).
17. B. Johansson, Phys. Rev. B 11, 2740 (1975).
18. J.M. Fournier and L. Manes in Ref. 7, p.3 (1985).
19. B. Johansson, Phil. Mag. 30, 469 (1974).
20. J.W. Allen and R.M. Martin, Phys. Rev. Lett. 49, 1106 (1982).
21. C.F. Fischer, "The Hartree-Fock Method for Atoms", John Wiley and Sons, New York, 1977 .

22. D. Liberman, J.T. Waber and D.T. Cromer, Phys. Rev. A 137, 27 (1965).
23. J.P. Desclaux, "Atomic and Nuclear Data Tables, Vol. 12", 310 (1973).
24. J.C. Slater, "Quantum Theory of Atomic Structure" (McGraw-Hill, New York, 1960), part I and II.
25. C.W. Nielson and G.F. Koster, "Spectroscopic Coëfficients for p^n, d^n, and f^n Configurations (MIT Press, Cambridge, Mass., 1963).
26. J.F. Herbst, R.E. Watson and J.W. Wilkins, Phys. Rev. B 13, 1439 (1976).
27. J.F. Herbst, D.N. Lowy and R.E. Watson, Phys. Rev. B 6, 1913 (1972).
28. J.F. Herbst, R.E. Watson and J.W. Wilkins, Phys. Rev. B 17, 3089 (1978).
29. J.F. Herbst and R.E. Watson, Phys. Rev. Lett. 34, 1395 (1975).
30. P.H. Dederichs, S. Blügel, R. Zeller and H. Akai, Phys. Rev. Lett. 53, 2512 (1984).
31. J. Friedel, Nuovo Cimento 7, 287 (1958).
32. J.B. Mann, Los Alamos Scientific Laboratory Report No. LASL-3690 (1967) (unpublished).
33. J.K. Lang, Y. Baer and P.A. Cox, J. Phys. F 11, 121 (1981).
34. P.A. Cox, J.K. Lang and Y. Baer, J. Phys. F 11, 113 (1981).
35. L.J. Nugent and K.L. van der Sluis, J. Opt. Soc. Am. 61, 1112 (1971).
36. D. Günnarsson and K. Schönhammer, Phys. Rev. B 28, 4315 (1983).
37. L. Brewer, J. Opt. Soc. Am. 61, 1101 (1971).
38. S. Hüfner and G.K. Wertheim, Phys. Lett. 51A, 301 (1975).
39. D. Penn, Phys. Rev. Lett. 42, 921 (1979).
40. A. Bosch, H. Feil, G.A. Sawatzky and N. Mårtensson, Solid State Commun. 41, 355 (1982).
41. J.C. Fuggle, F.U. Hillebrecht, R. Zeller, Z. Zolnierek, P.A. Bennet, and Ch. Freiburg, Phys. Rev. B 27, 2145 (1983).
42. D. van der Marel, G.A. Sawatzky, R. Zeller, F.U. Hillebrecht and J.C. Fuggle, Solid State Commun. 50, 47 (1984).
43. P.W. Anderson, Phys. Rev. 124, 41 (1961).
44. P.J. Braspennig, R. Zeller, A. Lodder and P.H. Dederichs, Phys. Rev. B 29, 703 (1984).
45. P.T. Andrews and L.T. Brown, Inst. Phys. Conf. Ser. No. 55, chapter 3, 141 (1981); H.S. Reehal and P.T. Andrews, J. Phys. F. 10, 1631 (1980).

46. W. Folkers, R. Coehoorn, D. van der Marel, unpublished.
47. D. van der Marel, G.A. Sawatzky and F.U. Hillebrecht, Phys. Rev. Lett. 53, 206 (1984); Phys. Rev. B 31, 1936 (1985).
48. C.E. Moore, "Atomic Energy Levels", part I, II and III, circular of the National Bureau of Standards, 467 (1958).
49. E. Antonides and G.A. Sawatzky, Phys. Rev. B 15, 1669 (1977).
50. J.C. Fuggle, P. Bennet, F.U. Hillebrecht, A. Lenselink and G.A. Sawatkzy, Phys. Rev. Lett. 49, 1787 (1982).
51. H.W. Haak, Thesis, 1983; H.W. Haak, J. Zaanen and G.A. Sawatkzy, to be published.
52. N. Martensson, R. Nyholm and B. Johansson, Phys. Rev. B 30, 2245 (1984).
53. J. Zaanen, to be published.
54. D.K.G. de Boer, C. Haas and G.A. Sawatzky, J. Phys. F 14, 2769 (1984).
55. D.J. Lam and A.T. Aldred in Ref. 8.
56. H.H. Hill in "Plutonium 1970", edited by W.N. Miner, Met. Soc. AIME, 1970.
57. J. Sticht and J. Kübler, Solid State Commun. 54, 389 (1985); A.M. Boring, R.C. Albers, G.R. Stewart and D.D. Koeling, Phys. Rev. B 31, 3251 (1985).
58. Y. Baer and G. Busch, J. Electron Spectrosc. Related Phenom. 5, 611 (1974).
59. M. Campagna, E. Bucher, G.K. Wertheim and L.D. Longinotti, Phys. Rev. Lett. 33, 165 (1974); 32, 885 (1974).
60. B.W. Veal, D.J. Lam, H. Diamond and H.R. Hoekstra, Phys. Rev. B 15, 2929 (1977).
61. Y. Baer, J. Schoenes, Solid State Commun. 33, 885 (1980).
62. J.R. Naegele, L. Manes, J.C. Spirlet and W. Müller, Phys. Rev. Lett. 52, 1834 (1984).
63. B.T. Thole, G. van der Laan, J.C. Fuggle, G.A. Sawatzky, R.C. Karnatak and J.M. Esteva, to be published.
64. G.R. Stewart, Rev. Mod. Phys. 56, 755 (1984).
65. M.S.S. Brooks in Ref. 7, p. 267.
66. W.D. Brewer and E. Wehmeier, Phys. Rev. B 12, 4608 (1975).
67. D. van der Marel and G.A. Sawatzky, Solid State Commun., in press (1985).
68. S. van Smaalen and C. Haas, Solid State Commun., in press (1985).

CHAPTER III

SINGLE PARTICLE THEORY FOR THE PHOTOEMISSION SPECTRA AND ELECTRONIC STRUCTURE OF (HALF)-FILLED d-SHELL IMPURITIES IN NOBLE METALS.

We derive expressions for the T-matrix, the local densities of states, the total densities of states and the photoemission spectrum for the general problem of a distortion of the host material bands by a single local impurity potential.

Explicit expressions are obtained for the limiting cases of a non-degenerate "d"-state coupled to a two band host matrix and for the five-fold degenerate d-state coupled site-diagonally to the host d-bands.

3.1. The general form of the Transition matrix

To describe the photo electron spectra and relate them to scattering properties of the impurities, we use a model hamiltonian that bears some resemblance to the Riedinger approach [1], but is different in that we include spin orbit interactions in the host material and at the impurity site. No attempts are made to use pseudo-potentials here [2,3] as we will treat the potentials as adjustable parameters in our approach.

The introduction of an impurity potential in a substitutional way generally results in:

1. an energy shift of the tightly bound impurity d levels,
2. a change in their coupling to the host bands,
3. a change in the scattering matrix of the non-resonant s and p waves incident at the impurity.

Spherical waves of f and higher orbital quantum number are less affected, as they have only a small amplitude at the impurity site, due to the relatively high centrifugal barrier compared to the kinetic energies of the particles near E_F.
A formal transformation of the hamiltonian to the cubic double point-group repres-

entations separates the s and p block from the d block of the hamiltonian. We will concentrate mainly on the latter here, as the UPS spectra of transition metals are dominated by the d part of the denstiy of states.

The hamiltonian that we will solve is:

$$H = H_{host} + \frac{1}{\sqrt{N}} \sum_{k} \sum_{\mu,\nu} \left(V^{\nu}_{k\mu} \left(C^{\dagger}_{k\mu} C_{0\nu} + C^{\dagger}_{0\nu} C_{k\mu} \right) \right) =$$

$$= H_{host} + \frac{1}{N} \sum_{k,q} \sum_{\mu,\nu} \left(\left(V^{\nu}_{k\mu} + V^{\mu}_{q\nu} \right) C^{\dagger}_{k\mu} C_{q\nu} \right) \qquad (3.1)$$

where ν and μ refer to double-point-group representations, k and q refer to momentum quantum numbers and 0 refers to the impurity site.

We will first derive a general expression for the transition matrix of such a system, using the T-matrix Dyson equation $\mathbf{T} = \mathbf{V} + \mathbf{T}\,\mathbf{g}\,\mathbf{V}$ which reads in its explicit form

$$T^{k\nu}_{k\mu} = \frac{1}{N} V^{\nu}_{k\mu} + \frac{1}{N} V^{\mu}_{q\nu} + \frac{1}{N} \sum_{q'} \sum_{\nu'\nu''} \left(T^{q'\nu'}_{k\mu} \; g^{q'\nu''}_{q'\nu'} \; (V^{\nu''}_{q\nu} + V^{\nu}_{q'\nu''}) \right) \qquad (3.2)$$

where $g^{k\nu}_{k\mu}$ is the host metal Green's function. In matrix notation, i.e. omitting the point group indices and treating all quantities as operators, Eq. (3.2) reads:

$$T^{q}_{k} = \frac{1}{N} V_{k} + \frac{1}{N} V^{T}_{q} + \frac{1}{N} \left(\sum_{q'} T^{q'}_{k} g^{q'}_{q'} \right) V^{T}_{q} + \frac{1}{N} \left(\sum_{q'} T^{q'}_{k} g^{q'}_{q'} V_{q'} \right) \qquad (3.3)$$

We solve this equation in terms of the known matrices:

$$L \equiv \frac{1}{N} \sum_{q} \left(V^{T}_{q} \; g^{q}_{q} \right); L^{T} \equiv \frac{1}{N} \sum_{q} \left(g^{q}_{q} \; V_{q} \right) \qquad (3.4)$$

$$M \equiv \frac{1}{N} \sum_{q} \left(V^{T}_{q} \; g^{q}_{q} \; V_{q} \right); \; g \equiv \frac{1}{N} \sum_{q} g^{q}_{q} \qquad (3.5)$$

and the sought for matrices:

$$Y_k \equiv 1 + \sum_q \left(T_k^q \; g_q^q \right) \tag{3.6}$$

$$X_k \equiv V_k + \sum_q \left(T_k^q \; g_q^q \; V_q \right) \tag{3.7}$$

Equation (3.3) becomes with these definitions:

$$T_k^q = \frac{1}{N} \left(Y_k \; V_q^T + X_k \right) \tag{3.8}$$

and can be solved using the resulting coupled equations:

$$Y_k = 1 + X_k g + Y_k L \tag{3.9}$$

$$X_k = V_k + Y_k M + X_k L^T \tag{3.10}$$

which are easily solved, resulting in:

$$Y_k = \left(V_k (L^T - 1)^{-1} g - 1 \right) N^{-1} \tag{3.11}$$

$$X_k = \left((L-1)^{-1} \; M - V_k \right) (N^T)^{-1} \tag{3.12}$$

with

$$N \equiv (L-1) - M(L^T - 1)^{-1} g \tag{3.13}$$

Inserting Eq. (3.11) to (3.13) in Eq. (3.8), we finally find:

$$T_k^q = \frac{1}{N}\Big((L-1)^{-1}M - V_k\Big)(N^T)^{-1} + \frac{1}{N}\Big(V_k(L^T-1)^{-1}g - 1\Big)N^{-1}V_q^T \qquad (3.14)$$

This equation only involves inversions of matrices of the rank of the number of bands taken into account. This becomes a trivial procedure in the one-band limit. We will discuss two limits next. First, where we neglect the degeneracy in the d bands, so that the problem reduces to the two-band limit, i.e. a "d"-band and an "sp"-band. Second, where we include the full d-band degeneracy but where we assume a special form of the impurity potential.

3.2. First limit: non-degenerate "d" bands.

The impurity part of the two band Hamiltonian reads:

$$H_{imp} = \frac{1}{N}\sum_{kq}\Big(\Delta_k(d_k^\dagger d_q + d_q^\dagger d_k) + V_k(c_k^\dagger d_q + d_q^\dagger c_k)\Big) \qquad (3.15)$$

where $d^\dagger$ and $c^\dagger$ refer to d-band and s-p-band creation operators respectively. We use (3.4) and (3.5) to find the matrices L and M:

$$L = \begin{pmatrix} l_d & l_s \\ o & o \end{pmatrix} \qquad (3.16)$$

$$M = \begin{pmatrix} \sigma_d + \sigma_s & o \\ o & o \end{pmatrix} \qquad (3.17)$$

where the first rows and columns refer to the d index and the second rows and columns refer to the "sp" index of the matrices and where l_d, l_s, σ_d and σ_s are defined as:

$$l_d \equiv \frac{1}{N}\sum_q \left(\Delta_q\ g_{dq}^{dq}\right)\ ;\ l_s \equiv \frac{1}{N}\sum_q \left(V_q\ g_{sq}^{sq}\right) \qquad (3.18)$$

$$\sigma_d \equiv \frac{1}{N}\sum_q \left((\Delta_q)^2\ g_{dq}^{dq}\right);\ \sigma_s \equiv \frac{1}{N}\sum_q\Big((V_q)^2\ g_{sq}^{sq}\Big) \qquad (3.19)$$

Using Eqs. (3.13), (3.16) and (3.17) we find

$$N^{-1} = D^{-1} \begin{pmatrix} 1_d^{-1} & (1_d^{-1})1_s \\ o & -D \end{pmatrix} \tag{3.20}$$

where

$$D = (1_d-1)^2 - (\sigma_s + \sigma_d)g_d^d \tag{3.21}$$

And, using Eqs. (3.14), (3.16), (3.17) and (3.20) we find the transition matrix:

$$T_k^q = \frac{1}{ND} \begin{pmatrix} \Delta_k\, g_{do}^{do}\Delta_q + (1-1_d)(\Delta_k+\Delta_q) + \sigma_s + \sigma_d\, \Delta_k g_{do}^{do} V_q + (1-1_d)V_q \\ V_k\, g_{do}^{do}\Delta_k + V_k(1-1_d) \qquad\qquad\qquad\qquad V_k\, g_{do}^{do} V_q \end{pmatrix} \tag{3.22}$$

The Green's functions can be calculated easily using the relation

$$G = g + gTg \tag{3.23}$$

so that the local impurity Green's function is:

$$G_{do}^{do} = D^{-1}\, g_{do}^{do} \tag{3.24}$$

and the change in the total Green's function:

$$Tr(G-g) = D^{-1}\left(\left(\frac{-\partial}{\partial\varepsilon}\sigma_d\right)g_d^d + 2(1-1_d)\left(\frac{-\partial}{\partial\varepsilon}1_d\right) + (\sigma_s+\sigma_d)\left(\frac{-\partial}{\partial\varepsilon}g_d^d\right) + \left(\frac{-\partial}{\partial\varepsilon}\sigma_s\right)g_d^d\right) =$$

$$= \frac{\partial}{\partial\varepsilon}(\ln D) \tag{3.25}$$

where we used the property

$$\left(g^{k\mu}_{k\mu}(\varepsilon)\right)^2 = -\frac{\partial}{\partial\varepsilon}\, g^{k\mu}_{k\mu}(\varepsilon) \tag{3.26}$$

From the definitions of l_d and σ_d we see that generally knowledge of the details of the host Green's functions is required to obtain the important denominator $D(\varepsilon)$. We will show that such detailed information is not necessary in the limit of nearest-neighbor-coupling-only between d orbitals in the alloy and pure host metal. In this case, the coupling parameter Δ_k occurring in Eq. (3.15) reads in direct space representation:

$$\Delta^o_o = \frac{1}{2}\Delta,\ \Delta^1_o = T,\ \text{all other } \Delta^j_i = 0 \tag{3.27}$$

where Δ is the energy shift of the impurity d state energy relative to the host d band centroid and T is the change in coupling to nearest neighbor d-states at the impurity site: $T = T^{imp}_{host} - T^{host}_{host}$. Now let z be the nearest neighbor coordination number so that with Eqs. (3.18) and (3.19):

$$l_d = \frac{1}{2}\Delta\, g^{d0}_{d0} + zTg^{d1}_{d0} \tag{3.28}$$

and:

$$\sigma_d = \frac{1}{4}\Delta^2\, g^{d0}_{d0} + zT\Delta\, g^{d1}_{d0} + z^2T^2\, g^{d1\pm1}_{d0} \tag{3.29}$$

where g^{d1}_{d0} is the off-diagonal Green's function:

$$g^{d1}_{d0} = \frac{1}{N}\sum_k\left(g^{dk}_{dk}\, e^{ikR}\right) \tag{3.30}$$

and R is in the first shell. In the case of nearest-neighbour-coupling-only g^{d1}_{d0} is related to g^{d0}_{d0} through the Dyson equation [4]:

$$(E - \bar{E}_d)\, g^{d0}_{d0} = 1 + T^{host}_{host}\sum_R g^{d0}_{dR} = 1 + z\, T^{host}_{host}\, g^{d1}_{d0} \tag{3.31}$$

The function

$$g_{d0}^{d1\pm1} = \frac{1}{z^2} \sum_{R\,R'} \left(g_{d0}^{dR+R'} \right) \tag{3.32}$$

where R and R' are in the first shell. The summation goes over z^2 values of R+R' that are in the zeroth, first, second or higher shells dependent on the topology of the host matrix. It is related to g_{d0}^{dR}, with R in the first shell, through the Dyson equation:

$$(E - \bar{E}_d)\, g_{d0}^{dR} = T_{host}^{host} \sum_{R'} \left(g_{dR'}^{dR} \right) = z T_{host}^{host}\, g_{d0}^{d1\pm1} \tag{3.33}$$

where R' is in the first shell. Insertion of Eqs. (3.31) and (3.33) in (3.21), (3.28) and (3.29), and writing $t = T/T_{host}^{host}$, gives:

$$D = (1+t)^2 - \left([(1+t)^2-1][E-\bar{E}_d] + \Delta+\sigma_s \right) g_{do}^{do} \tag{3.34}$$

and for the impurity local Green's function:

$$G_{do}^{do} = \frac{g_{do}^{do}}{(1+t)^2 - \left([(1+t)^2-1][E-\bar{E}_d] + \Delta + \sigma_s \right) g_{do}^{do}} \tag{3.35}$$

This expression has two rather familiar limits:

1. $t = -1$, where $\mathrm{Im}G_{do}^{do}$ is simply a lifetime broadened single line. Usually one replaces $\Delta+\sigma_s$ with an energy independent complex energy, the imaginary part of which is the inverse decay time due to the "s-d" coupling.
2. $t = 0$, where we recognize the Clogston-Wolff formula for the impurity DOS [5,6].

3.3. Second limit: local shift of the d states.

The impurity Hamiltonian is:

$$H_{imp} = \sum_{\mu\nu} \left(\Delta_{\mu}^{\nu} \, d_{o\mu}^{\dagger} \, d_{o\nu} \right) + \frac{1}{\sqrt{N}} \sum_{k\mu} \left(V_{k\mu} \, (c_{k\mu}^{\dagger} \, d_{o\mu} + d_{o\mu}^{\dagger} \, c_{k\mu}) \right) \tag{3.36}$$

With Eqs. (3.4) and (3.5) and once again turning to matrix notation, we have:

$$L = \begin{pmatrix} 1/2\Delta g_d^d & I_s \\ 0 & 0 \end{pmatrix} \tag{3.37}$$

$$M = \begin{pmatrix} 1/4\Delta g_d^d \Delta & 0 \\ 0 & 0 \end{pmatrix} \tag{3.38}$$

where the first row and column again refer to the "d" index and the second row and column to the "sp" index, but now contain block matrices of rank 10. Using Eqs. (3.13), (3.37) and (3.38), we find:

$$N^{-1} = \begin{pmatrix} (1/2\Delta g_d^d - 1)D^{-1} & (\Delta g_d^d - 1)D^{-1} I_s \\ 0 & -1 \end{pmatrix} \tag{3.39}$$

with

$$D = 1 - (\Delta + \sigma_s) g_d^d \tag{3.40}$$

And with Eqs. (3.14), (3.37), (3.38) and (3.39) we find:

$$T_k^q = \frac{1}{N} \begin{pmatrix} D^{-1}(\Delta + \sigma_s) & D^{-1} V_q \\ V_k (D^T)^{-1} & V_k g_d^d D^{-1} V_q \end{pmatrix} \tag{3.41}$$

The local impurity Green's function can be found with a little algebra:

$$G_{do\mu}^{do\mu'} = g_{do\mu}^{do\mu'} + \sum_{qq'} \sum_{\nu\nu'} \left(g_{do\mu}^{q\nu} T_{q\nu}^{q'\nu'} \, g_{q'\nu'}^{do\mu} \right) = \sum_{\mu''} \left(g_{do\mu}^{do\mu''} (D^{-1})_{\mu''}^{\mu'} \right) \tag{3.42}$$

And the change in the total Green's function:

$$\mathrm{Tr}(G-g) =$$

$$= \sum_{\substack{\mu\mu' \\ \nu\nu'}} \sum_{k} \left(g^{dk\mu'}_{dk\mu} (D^{-1})^{\nu}_{\mu'} (\Delta+\sigma_s)^{\nu'}_{\nu} g^{dk\mu}_{dk\nu'} \right) + \sum_{\mu\mu'} \sum_{k} \left(g^{sk\mu}_{sk\mu} V_{k\mu} g^{do\mu'}_{do\mu} (D^{-1})^{\mu}_{\mu'} V_{k\mu} g^{sk\mu}_{sk\mu} \right) =$$

$$= -\sum_{\substack{\mu\mu' \\ \nu}} \left((D^{-1})^{\nu}_{\mu} \frac{\partial}{\partial\varepsilon} \left(g^{do\mu}_{do\mu'} (\Delta+\sigma_s)^{\mu'}_{\nu} \right) \right) =$$

$$= \frac{\partial}{\partial\varepsilon} \mathrm{Tr}(\ln D) \qquad (3.43)$$

The change in the UPS spectrum is found as explained in section 3.5 by replacing the Green's function in the numerator with the *experimental* one:

$$J_{alloy} - J_{host} = -\pi^{-1} \, \mathrm{Im} \, D^{-1} \frac{\partial}{\partial\varepsilon} (g_{exp}) \, (\Delta + \sigma_s) \qquad (3.44)$$

3.4. Scattering phase shifts.

There exists a useful relation between the difference in the total DOS and the transition-matrix, often employed in the Friedel sum rule in the context of free electron scattering. Because the T-matrix satisfies the optical theorem:

$$\mathrm{Im}T = T^{\dagger}(\mathrm{Im}g)T \qquad (3.45)$$

the S-matrix defined as

$$S = 1 + 2i(\mathrm{Im}g)T \qquad (3.46)$$

is unitary: Here Img ensures energy conservation, or on energy shell scattering. Near the Fermi-level the d band DOS is zero, so that only scattering between s-p-states occur. In that case the S-matrix has a particular transparent form, namely:

$$S_\mu = e^{2i\eta_\mu} \tag{3.47}$$

where the basis μ has been chosen such, as to diagonalize S. In the absence of spin-orbit symmetry mixing, these are just the cubic harmonics e_g and t_{2g}. Spin orbit splitting splits the basis in the representations Γ_7, Γ_8' and Γ_8'', where Γ_8' and Γ_8'' mix as a function of energy. Still one can choose the basis such, that S is diagonal near E_F, which is useful only if the symmetry mixing does not vary too much near E_F. So we have:

$$(\text{Im } g^{s\mu}_{s\mu}(E))\ T^{k\mu}_{k\mu}(E) = (\sin \eta_\mu) e^{i\eta_\mu} \tag{3.48}$$

or, with Eq. (3.22) or (3.41)

$$\eta_\mu(E) = \text{Arg}(T^{k\mu}_{k\mu}(E)) = \text{Im}(\ln D^\mu_\mu) \tag{3.49}$$

so that, with Eq. (3.25) or (3.43)

$$\frac{\partial \eta_\mu(E)}{\partial E} = \text{Im}(G^\mu_\mu - g^\mu_\mu) \tag{3.50}$$

In other words: the energy derivatives of the scattering phase shifts equal the changes in the total density of states in the energy regions outside the host d-band.

3.5. The photo emission spectrum

In general, the photoemission current can be written as

$$J(E,\Omega) = \sum_{k_f}' \sum_{k,g} \sum_{\mu,\nu} \{M_{k_f,q,\mu} M^*_{k_f,k,\nu} \text{Im}[G^{k\nu}_{q\mu}(E-\Omega)]\}, \tag{3.51}$$

where Ω is the photon energy, E the energy of the outgoing electron, and $M_{k_f,q,\mu}$

the transition matrix element to a state k_f from a state in band μ with wave vector q. The summation over k_f is limited to the constant-energy surface E. $G^{k\nu}_{q\mu}$ is the Green's function for the alloy.

Following Shevchik [7], we write

$$M_{k_f,q,\nu} = \frac{1}{N} \sum_n e^{i(k_f-q)\cdot R_n} \sigma_n(k_f,\nu), \tag{3.52}$$

with the summation running over the atomic positions R_n, and

$$\sigma_n(k_f,\nu) = \sqrt{N} \langle \Psi_{k_f} | \mathbf{A}\cdot\mathbf{p} | \Psi_{\nu n} \rangle. \tag{3.53}$$

In this expression we have used a Wannier representation of the initial-state wave functions and have assumed that the Wannier functions are wave-vector independent as, for example, in a tight-binding model. The cross section σ_n will depend only on the kind of atom on site n, the initial-state symmetry ν, and the final-state wave function. In the case of a pure material, σ is site independent, so that

$$M_{k_f,q,\nu} = \sigma(k_f,\nu) S(k_f-q) \tag{3.54}$$

where S(k) is the form factor given by

$$S(\mathbf{k}) = \frac{1}{N} \sum_n e^{i\mathbf{k}\cdot\mathbf{R}_n} = \sum_Q \delta_{k,Q}, \tag{3.55}$$

where Q is a reciprocal-lattice vector.

For a single impurity at site $R_n = 0$, we define

$$\gamma = (\sigma_{imp} - \sigma_{host})/\sigma_{host}, \tag{3.56}$$

and we will assume that γ is independent of k_f, and that the final-state wave function is not changed by the presence of the impurity. We then obtain

$$M_{k_f,q,\nu} = \sigma(k_f,\nu)[S(k_f-q) + \gamma/N], \tag{3.57}$$

and, from Eq. (3.51)

$$J(E,\Omega) = \mathrm{Im}\left[\sum_{k_f}{}' \sum_{\mu,\nu} \sigma(k_f,\mu)\sigma^*(k_f,\nu)\left[G^{k_r}_{k_r}(E-\Omega)+2(\mathrm{Re}\gamma_\nu)\frac{1}{\sqrt{N}}\, G^{0\nu}_{k_r\mu}(E-\Omega) + \right.\right.$$

$$\left.\left. + \gamma_\mu\gamma^*_\nu \frac{1}{N}\, G^{0\nu}_{0\mu}(E-\Omega)\right]\right], \tag{3.58}$$

where k_r is k_f minus a reciprocal-lattice vector, and it lies in the first Brillouin zone. G^0_0 refers to the impurity Green's function.

We first consider the case studied by Shevchik, namely that the initial-state wave functions are unchanged by the impurity and only the cross sections are different for impurity and host. This is equivalent to

$$G^k_k = g^k_k,\ G^0_k = (1/\sqrt{N})g^k_k,\ \text{and}\ G^0_0 = (1/N)\sum_k g^k_k\ , \tag{3.59}$$

and

$$J(E,\Omega) = \mathrm{Im}\left[\sum_k{}' |\sigma|^2[g^k_k + 2(\mathrm{Re}\gamma)cg^k_k + |\gamma|^2 cg^0_0]\right]$$

$$= \mathrm{Im}\left[|\bar{\sigma}|^2\left[\sum_k{}' g^k_k(E-\Omega)\right] + \langle|\Delta\sigma|^2\rangle\sum_k g^k_k(E-\Omega)\right], \tag{3.60}$$

with $C = 1/N$, g^k_k the pure-host Green's function, and

$$|\bar{\sigma}|^2 = \left|\frac{1}{N}\sum_i \sigma_i\right|^2 = |\sigma_h|^2(1+2\gamma c) + O(1/N^2),$$

$$\langle|\Delta\sigma|^2\rangle = \frac{1}{N}\sum_i|\sigma_i - \bar{\sigma}|^2 = |\sigma_h|^2\gamma^2 c + O(1/N^2), \tag{3.61}$$

which is the same result as obtianed by Shevchik. We substitute into Eq. (3.58) the expressions for the Green's functions based on the Clogston-Wolff model (the non-degenerate version of Eq. (3.42) and (3.43))

$$J(E,\Omega) = \mathrm{Im}\Sigma'_{k_f}\left[|\sigma(k_f)|^2\left[g^{k_r}_{k_r}(E-\Omega) + \frac{1}{N}\frac{(\Delta+\sigma_s)[g^{k_r}_{k_r}(E-\Omega)]^2}{1-(\Delta+\sigma_s)g^0_0(E-\Omega)} + \right.\right.$$

$$\left.\left. + \frac{2}{N}(\mathrm{Re}\gamma)\frac{g^{k_r}_{k_r}(E-\Omega)}{1-(\Delta+\sigma_s)g^0_0(E-\Omega)} + \frac{1}{N}|\gamma|^2\frac{g^0_0(E-\Omega)}{1-(\Delta+\sigma_s)g^0_0(E-\Omega)}\right]\right] \qquad (3.62)$$

Taking $\gamma = 0$ we obtain

$$J_{diff}(E,\Omega) = \mathrm{Im}\Sigma'_{k_f}\left[|\sigma(k_f)|^2\frac{(\Delta+\sigma_s)[g^{k_r}_{k_r}(E-\Omega)]^2}{1-(\Delta+\sigma_s)g^0_0(E-\Omega)}\right], \qquad (3.63)$$

or

$$J_{diff}(E,\Omega) = -\mathrm{Im}\frac{(\Delta+\sigma_s)(\partial/\partial\Omega)g_{exp}(E-\Omega)}{1-(\Delta+\sigma_s)g^0_0(E-\Omega)}, \qquad (3.64)$$

where

$$\pi^{-1}\,\mathrm{Im}[g_{exp}(E,\Omega)] = J_{host}(E,\Omega) = \Sigma'_{k_f}|\sigma(k_f)|^2\delta(E-\Omega-\varepsilon_{k_r}),$$

and the real part is determined by the Kramers-Kronig transformation over Ω. In order to do this transformation, we assumed $J_{host}(E,\Omega) = J_{host}(E-\Omega)$.

References

1. R. Riedinger, J. Phys. F 1, 392 (1971).
2. F. Gautier, J. Phys. F 1, 382 (1971).
3. P.V. Smith, J. Phys. F 11, 1207 (1981).
4. This relation holds for tight-binding Hamiltonians where only nearest neighbors are coupled. The reader can check this from Eqs. 5.15 and 5.21 in Chapter 5 of E.N. Economou, "Green's Functions in Quantum Physics", Edited by M. Cardona, (Springer, Berlin, 1983).
5. A.M. Clogston, B.T. Matthias, M. Peter, H.J. Williams, E. Corenzwit and R.J. Sherwood, Phys. Rev. 125, 541 (1962).
6. P.A. Wolff, Phys. Rev. 124, 1030 (1961).
7. N.V. Shevchik, Phys. Rev. B 16, 3428 (1977).

CHAPTER IV

UNOCCUPIED BAND CRITICAL POINT ENERGIES OF NOBLE METALS DETERMINED WITH BREMSSTRAHLUNG ISOCHROMAT SPECTROSCOPY

We show that Bremsstrahlung Isochromat Spectroscopy (BIS) is a powerful and simple tool to determine unoccupied band critical point energies of solids. We determine some critical point energies of the noble metals and compare these to band structure calculations. We also determine the energy dependent lifetime broadening providing information about the imaginary part of the self energy corrections.

4.1. Introduction

One particle energy band dispersion relations and the influence of many body effects are of fundamental importance for the understanding of physical properties of solids. Modern computational methods have facilitated complete band structure calculations, the accuracy of which, as well as the validity of the one electron approximations made, have been a subject of intense investigation.

Experimental tools for studying band structures are Bremsstrahlung Isochromat Spectroscopy (BIS) and K Resolved Inverse Photoelectron Spectroscopy (KRIPES) for the unoccupied states and X-ray Photoelectron Spectroscopy (XPS) and Angle Resolved Photoelectron Spectroscopy (ARPES) for the occupied states.

In the high energy spectroscopies (BIS and XPS) the information obtained is more directly related to the density of states because of averaging over the whole Brillouin zone. In KRIPES and ARPES additional information concerning the energy dispersion relations can be obtained. However, because these experiments must be carried out at low energies both initial and final states are sensitive to the crystal potentials and many body effects. To separate the contributions to the spectra from initial and final states one must resort to elaborate measurements.

BIS spectra of the noble metals are known to exhibit sharp features in the

energy range up to 10 eV above the Fermi level [14, 15]. In this paper we present new data for polycrystalline Cu, Ag and Au and use the intimate connection between the observed features and calculated energy band critical points to determine the real and imaginary parts of the one particle self energies.

4.2. Experimental

The BIS spectrometer is part of an XPS apparatus equipped with a large solid angle monochromator for AlKα radiation ($\hbar\omega$ = 1486.7 eV) [1]. The BIS electron gun is a cylindrical Pierce gun [2], producing a wedge shaped beam with a rectangular cross section of 5 x 1.3 mm^2 at the sample [3]. The polycrystalline Ag, Au and Cu samples were cleaned in ultra high vacuum by either scraping or argon ion etching. XPS was used to check for surface contamination.

The BIS spectra of Cu, Ag and Au are shown in Fig.4.1. The spectra of the 3 metals are qualitatively similar as expected because of similar electronic and crystal structures [4]. The most prominent features are a plateau just above the Fermi energy followed by a sharp rise which occurs at different energies for the three metals. At even higher energies more structure is visible although the spectrum seems to gradually evolve into a structureless mononically increasing curve.

4.3. Discussion

The sharp rise occurring between 3 and 4 eV above E_F is most probably a result of crossing the $L_1(L_4^+)$ critical point often referred to as the L(7) point. At this critical point a rather flat band in the L-W direction begins with a corresponding high density of states. An accurate determination of the critical point energy can be made by comparing to band structure density of states calculations. Since the high energy density of states for Cu and Ag with a sufficiently small energy grid could not be found in the literature, we calculated these with the KKR method using 5 and 3 phase shifts for Cu and Ag respectively. In the calculations we use the self-consistent potentials of Moruzzi et al. [21] which are obtained by the application of the local density approximation in density functional

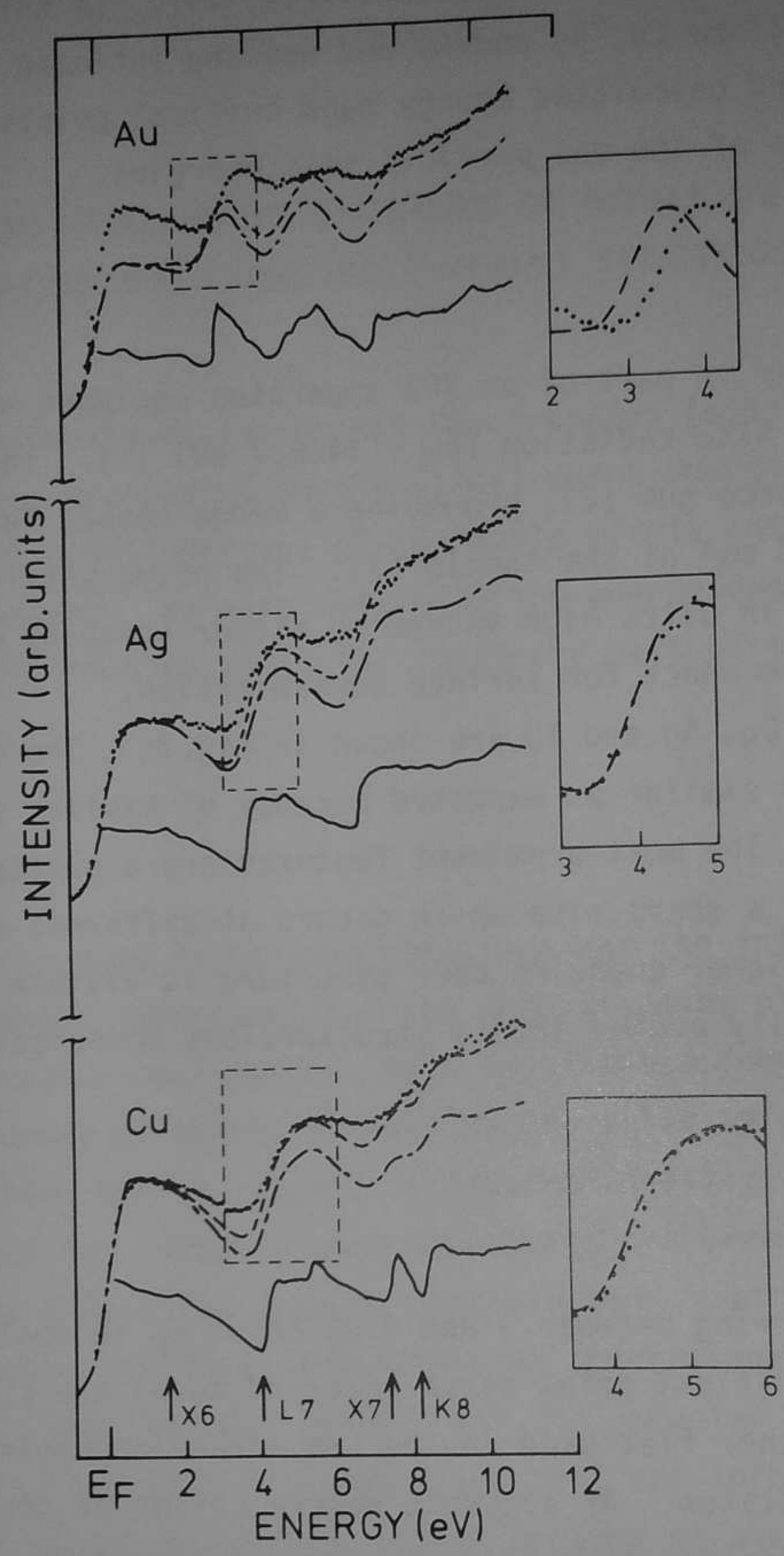

Fig. 4.1. Experimental and theoretical spectra of the unoccupied bands. Solid: theoretical DOS's, dash-dotted: theoretical DOS's convoluted with a Gaussian of 0.85 eV FWHM, dashed: theoretical DOS's convoluted with experimental ELS curves and an additional Gaussian broadening of 0.4 eV, dotted: the experimental spectra. The inserts are discussed in the text.

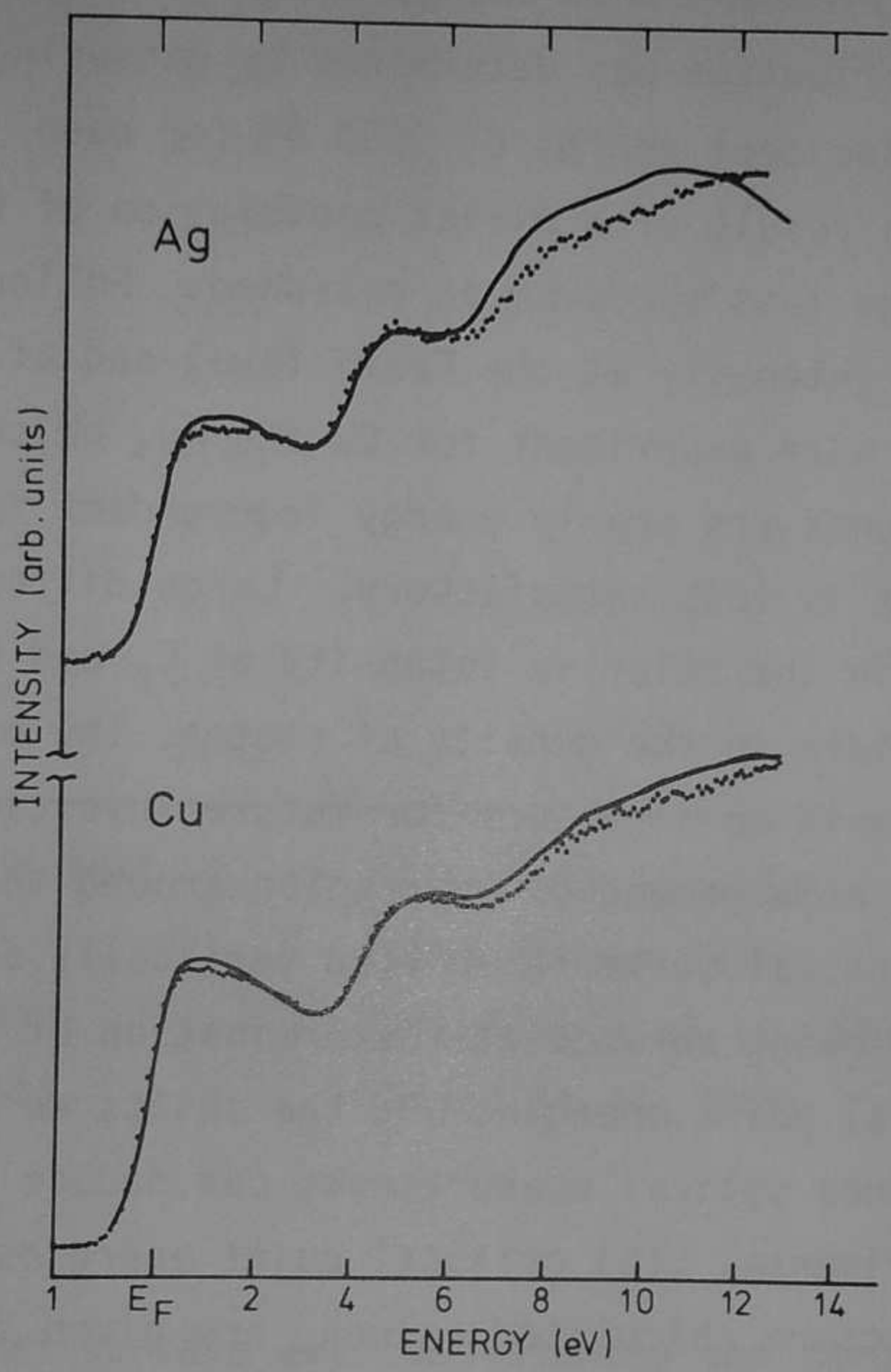

Fig. 4.2. Experimental and theoretical BIS spectra. Dotted: experimental, solid: theoretical spectra convoluted with an energy dependent Lorentzian discussed in the text.

theory. The Au density of states was taken from Cristensen [5]. These are shown as solid lines in Fig. 4.1.

The experimental resolution was incorporated by convoluting the theoretical density of states with a Gaussian of width 0.85 eV. The width was chosen to best fit the shape of the Fermi level onset of the spectrum. The resulting theoretical curves are also shown in Fig.4.1. In addition to the experimental broadening the measurements also contain a contribution from energy loss, suffered by the incident electron. This energy loss contribution was determined by measuring the energy loss spectrum at an incident energy of 1500 eV for each metal [6]. The dashed line is a result of a direct convolution of the theoretical density of states with the energy loss spectrum as measured. Following this procedure we see that the relative intensity at the Fermi level and at about 10 eV are in extremely good agreement with experiment for Cu and Ag, which indicates that the transition matrix elements are nearly energy independent for these materials. For Au the agreement is less satisfactory. Large differences between experiment and theory are seen in the relative intensity at E_F and high energies as well as in the overall structure in the density of states. The origin of this discrepancy is not known and should be a subject for future investigations.

In the insets of Fig.4.1 an enlargement of the region around the L(7) critical point is shown. Here the theoretical curve is shifted vertically and scaled to match the experimental curve allowing an accurate determination of the energy shifts. Using the tabulated L(7) critical point energies and the shifts we determine experimental L(7) energies. Since optical measurements can deduce the L(6)-L(7) gap we can also determine experimental L(6) critical point energies. These, together with various band structure calculated values, are given in Table 4.1.

The best overall agreement for Cu is the calculation of Janak et al. [7] but we should note that these authors include a linear energy dependent shift in the final calculation. The agreement with our calculation is surprisingly good for the L(7) critical points for both Cu and Ag and reasonable for the L(6) critical point. For Au the relativistic calculations of Christensen result in critical point energies which are 0.4 eV too high for L(6) and 0.4 eV too low for L(7) resulting in a large error in the L(6)-L(7) gap.

It is interesting to note that the values for the L(6) critical points as calculated by Jepsen et al. [7] are all too low which could explain why their L neck

Table 4.1. List of theoretical and experimental L(6) and L(7) critical point energies for Cu, Ag and Au. All values are in eV.

	L_6(th)	L_7(th)	L_7(exp)	L_7-L_6(exp)	L_6("exp")
Cu	-1.15	4.10[a]	4.2(0.1)[k]	5.05(0.1)[g]	-0.85(0.1)[a]
	-0.61	3.94[b]			-0.9(0.2)[j]
	-0.90	4.26[c]			
	-1.22	4.44[d]			
	-1.10	3.79[e]			
Ag	-0.48	3.82[a]	3.8(0.1)[k]	4.2[h]	-0.4(0.1)[a]
	-0.16	3.33[f]			
	-0.62	3.55[d]			
	-0.58	3.79[e]			
Au	-0.72	3.01[f]	3.4(0.1)[k]	4.5[i]	-1.1(0.1)[a]
	-1.27	3.68[d]			
	-1.35	3.18[e]			

[a]Discussed in the text
[b]Burdick, [10]
[c]Janak et al. [9]
[d]Lässer et al. [4]
[e]Jepsen et al. [7]
[f]Christensen [5]
[g]Beaglehole et al. [11]
[h]Rosei et al. [12]
[i]Chen et al. [13]
[j]Knapp et al. [8]
[k]Present work

radii in the Fermi surface are consistently too large.

In addition to the L(7) critical point there are several other critical points in the energy region from the Fermi level to 10 eV, the calculated positions of which are shown in Fig. 4.1 for Cu. However, the experimental broadening washes out these structures preventing an accurate determination of their energies.

In comparing theory with experiment as in Fig. 4.1 another problem is evident. Even after the experimental broadening we see that the theoretical features are still much too sharp. There must be an additional broadening which increases with energy above the Fermi level. We attribute this to lifetime broadening caused by

the imaginary part of the self energy corrections to the calculated band structure. In Fig. 4.2 we show results of convoluting the theoretical curve for Cu and Ag (solid lines in Fig. 4.1) with a Lorentzian with an energy dependent width (Γ)Γ = 0.09 ($E-E_F$) to simulate the lifetime broadening. This results in an almost embarrassingly good agreement with experiment for both Cu and Ag. The largest discrepancies remaining are a shift of about 0.3 and 0.4 eV to higher energies of the step at about 8 and 7 eV for Cu and Ag respectively. This suggests that the theoretical X7 and K8 critical point energies are about 0.3 - 0.4 eV too low. The lifetime broadening as introduced above results in a width of 0.9 eV at 10 eV above E_F in good agreement with the photoemission measurement of Knapp et al. [8].

The good agreement up to about 5 eV might be accidental and is in any case surprising for several reasons. First of all the real part of the self-energy corrections due to many body effects is expected to be at least several tenths of an eV [16-18]. In fact the calculation of Janak et al. [9] for Cu includes a self-energy correction amounting to 0.32 eV at 4 eV above E_F whereas our calculation does not include any such correction. Secondly it is difficult to understand why the real part of the self-energy correction could be so small with a fairly strongly energy dependent imaginary part. Thirdly it should be noted that the agreement is only good up to about 4 or 5 eV above E_F. There is a considerable discrepancy for the L_6 energy below E_F and also the d band edge (the X_5 point) is found at -1.63 and -3.24 eV for Cu and Ag respectively in our calculation whereas the experimental values are -2.0 [19] and -3.8 eV [20] respectively. Also a shift due to relativistic effects (not included in our calculation) in the L_7 energies of several tenths of an eV are expected for Ag [5].

4.4. Conclusions

All of this shows that more theoretical work should be done on the definition of the real part of the self energy correction and its relation to the various types of band structure calculations. In conclusion we have shown that BIS provides a powerful tool for locating critical point energies of solids. The technique is simple compared to other methods used up to now and can be applied to polycrystalline samples. In addition to the determination of the critical

point energies also the energy dependent lifetime broadening can be obtained providing the necessary information for determining both the real and imaginary parts of the self energy corrections to band structure calculations.

Efforts should be concentrated on improving the energy resolution of BIS so that more critical points can be located providing a detailed determination of the self energy corrections. Obviously theoretical work on both the real and imaginary part of the self-energy correction is necessary. The large discrepancies found with the band structure calculation of Au suggest that improvements in relativistic calculations are required.

References

1. J.C. Fuggle, J. Keppels, H. Hanning and Z. Zolnierek, (to be published).
2. J.R. Pierce, J. Appl. Phys. 11, 548 (1941).
3. F.U. Hillebrecht, (to be published).
4. R. Lässer, N.V. Smith and R.L. Benbow, Phys. Rev. B 24, 1895 (1980).
5. N.E. Christensen, J. Phys. F 8, L51 (1978).
6. A good approximation to the energy loss contribution for the noble metals is a straight line with a slope of approximately 3% of the threshold intensity per eV.
7. D. Jepsen, D. Glötzel and A.R. Mackintosh, Phys. Rev. B 23, 2684 (1981).
8. J.A. Knapp, F.J. Himpsel and D.E. Eastman, Phys. Rev. B 19, 4952 (1979).
9. J.F. Janak, A.R. Williams and V.L. Moruzzi, Phys. Rev. B 11, 1522 (1975).
10. G.A. Burdick, Phys. Rev. 129, 138 (1963).
11. D. Beaglehole, M. de Creszensi, M.L. Thèye and G. Vuye, Phys. Rev. B 19, 6306 (1979).
12. R. Rosei, C.H. Culp and J.H. Weaver, Phys. Rev. B 10, 484 (1974).
13. A.B. Chen and B. Segal, Solid State Commun. 18, 149 (1976).
14. C.C. Chu and P.E. Best, Phys. Rev. B 12, 4575 (1975).
15. J.K. Lang, Y. Baer and P.A. Cox, J. Phys. F 11, 121 (1981).
16. L. Hedin, Phys. Rev. 139, A796 (1965).
17. L.J. Sham and W. Kohn, Phys. Rev. 145, 561 (1966).
18. L. Hedin and B.I. Lundquist, J. Phys. C 4, 2064 (1971).

19. R. Courths, V. Bachelier, B. Cords and S. Hüfner, Solid State Commun. 29, 463 (1979).
20. R. Courths, V. Bachelier and S. Hüfner, Solid State Commun. 38, 887 (1981).
21. V.L. Moruzzi, J.F. Janak and A.R. Williams, Calculated Electronic Properties of Metals, Pergamon, New York (1978).

CHAPTER V

Pd AND Pt IMPURITY-INDUCED CHANGES IN NOBLE-METAL DENSITY OF STATES: COMPARISON OF PHOTOELECTRON SPECTROSCOPY AND THEORY.

High-resolution photoemission results on dilute noble-metal Pd and Pt alloys are presented. The impurity virtual bound state widths, splittings and positions are determined. Using difference techniques we determine the impurity-induced changes in the host-metal d bands and compare these to predictions using a model Hamiltonian. We also discuss the importance of lattice relaxation and show that the neglect of this in first-principles calculations is probably the reason for poor agreement with experiment.

5.1. Introduction

Dilute alloys of transition metals dissolved in noble metals are interesting test cases for experimental and theoretical studies of scattering, localization and correlation problems in solid-state physics [1-4]. Recently a great deal of theoretical effort has been devoted to developing so-called first-principles methods [5-9] for calculating impurity-induced changes in the density of states, and the local impurity density of states for transition-metal impurities in various metallic hosts. Although these calculations, to some extent, replace the older methods based on model Hamiltonians [10-13] the latter still provide a clear physical picture for the effects observed especially in systems where local electron correlation effects are of importance. Although the theoretical efforts have been extensive there has been relatively little experimental activity using modern techniques in the area of dilute alloys. The major experimental efforts have concentrated on various forms of transport measurements which provide detailed information on the low-energy-scale (kT) properties of these systems.

Of course it is the changes in the low-energy-scale behaviour upon alloying which directly influence the physical properties of materials. On the other hand,

the low energy scale behaviour is often determined by electronic structure changes which occur on a much higher energy scale. Well known examples are the Kondo systems in which the low energy scale properties are caused by high-energy-scale local atomic Coulomb and exchange interactions. Another more simple example is the transition-metal impurity-induced scattering of electrons at the Fermi level which is often caused by impurity potentials with a d resonant energy far removed from the Fermi level. Recently we have shown [14,15] that ultraviolet photoelectron spectroscopy (UPS) and bremsstrahlung isochromat spectroscopy can provide detailed information concerning the impurity-induced changes in the density of states. Also an attempt has recently been made to interpret transport properties and UPS data of a number of alloys in a unified approach [16].

In this chapter we present and discuss the UPS spectra of Pd and Pt impurities in noble-metal hosts. We derive from the spectra the impurity-induced changes in the density of states and show that a simple model calculation can explain the data with surprising accuracy. We show that spin-orbit effects are important especially for Pt impurities and also for Au as hosts. For CuPd there is a large discrepancy between experiment and first-principles calculations whereas the simple model works well. We argue that this is due to a neglect of lattice relaxation in the former. We discuss the effects of lattice strain on the local impurity density of states using a model Hamiltonian. A direct extension of the model used permits us to predict changes in the host d band density of states and UPS spectra resulting from vacancies in the lattice. An appendix is added to this chapter, where we discuss the possibility of crystal field and spin-orbit splitting in Ag containing 2 at.% and 10 at.% Pt and the concentration dependency of the spectra.

5.2. Experimental Procedure

The UPS spectra of polycrystalline Cu, CuPd(5 at.%), CuPt(2 at.%), Ag, AgPd(3 at.%), AgPt(2 at.%), Au, AuPd(4,5 at.%) and AuPt(4.5 at.%) were collected with a double-pass cylindrical mirror analyzer [17] in an angular integrated mode. The CMA was operated at 10 eV pass energy, giving an overall resolution of the instrument of 85 meV. The base pressure was 1.10^{-10} Torr. No noticeable changes in the spectra were found during the 30 minute scans immediately following sample

cleaning. The cycles of cleaning and measuring were repeated until about 10^5 counts were accumulated in the most intense channels that were distributed in 37.5 meV intervals over the 10 eV wide valence band regions covered in the experiment. Clean surfaces were obtained by means of Argon bombardment. The possibility of compositional changes due to preferential sputtering was checked with core level XPS in a separate vacuum chamber. No such effects could be found in the alloys discussed here. We are quite confident, therefore, that our UPS spectra are representative of the dilute limit.

The light source was a He lamp adjusted such, as to optimize He I radiation. The kinetic energies of the photo emitted electrons lie in the 6 to 16 eV region, which is an energy range of relatively large escape depths (typically 10 à 15 Å [18], compared to the 2 à 3 Å thickness of the surface layer in noble metals), so that our spectra are dominated by bulk photoemission.

The Cu based samples were the same as in Ref. 8. The Au and Ag based alloys were supplied by the Leeds group [19]. All samples were obtained from melting the weighted quantities of the components in a sealed quartz tube.

5.3. Results and Discussion

In Figs. 5.1 to 5.3 the spectra for Pt and Pd in Cu, Ag and Au are shown, together with the pure noble metal spectra. These spectra were subsequently corrected for the 23.08 eV He satellite, the intensity of which was 1,7% relative to the 21.22 eV main line as determined from the echo in the Ni Fermi edge. In addition we applied a 1/E correction [20] to the intensity to account for the energy dependent transmission of our analyzer. Finally the scattered electron background was subtracted [21] which is a necessary procedure as we want to integrate the spectral intensities later. For this purpose it was assumed, that the electron energy loss spectrum can be represented with a step function. The scattered electron background then corresponds to the integral of the background-free UPS spectrum. The relative weight of the background contribution is determined iteratively by fitting the background intensity in the energy region below the bottom of the bands. As the resulting background contributions are very smooth functions of energy this procedure does not introduce artificial sharp features

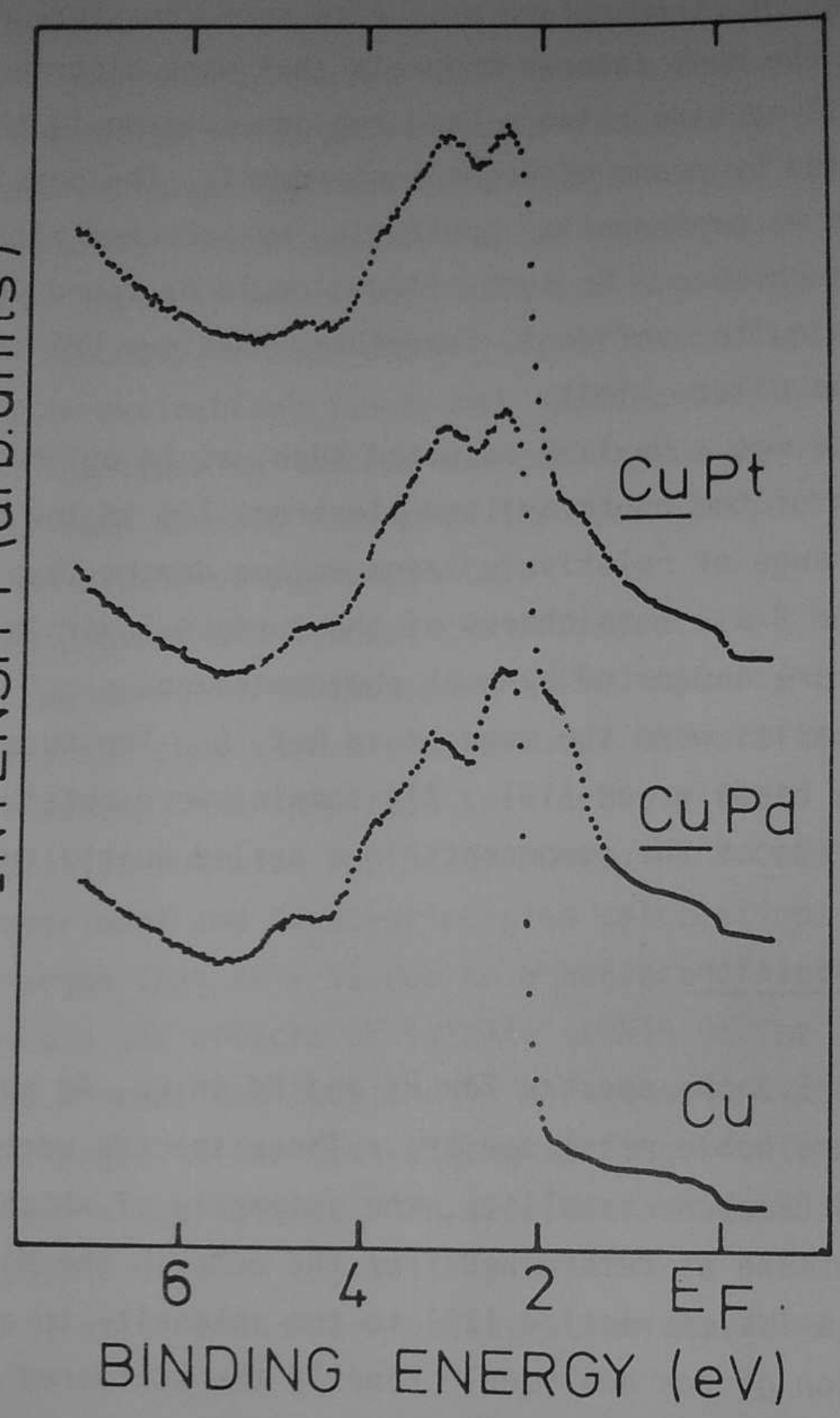

Fig. 5.1. UPS spectra of CuPd (5%), CuPt (2%) and Cu.

in the corrected spectra. The resulting spectra are shown in Figs. 5.4 to 5.6.

The spectra exhibit structure between the host metal d bands and the Fermi level due to the impurity d states. The clearest examples of cases where the impurity d state is well separated from the host d band are AgPd and AgPt shown in

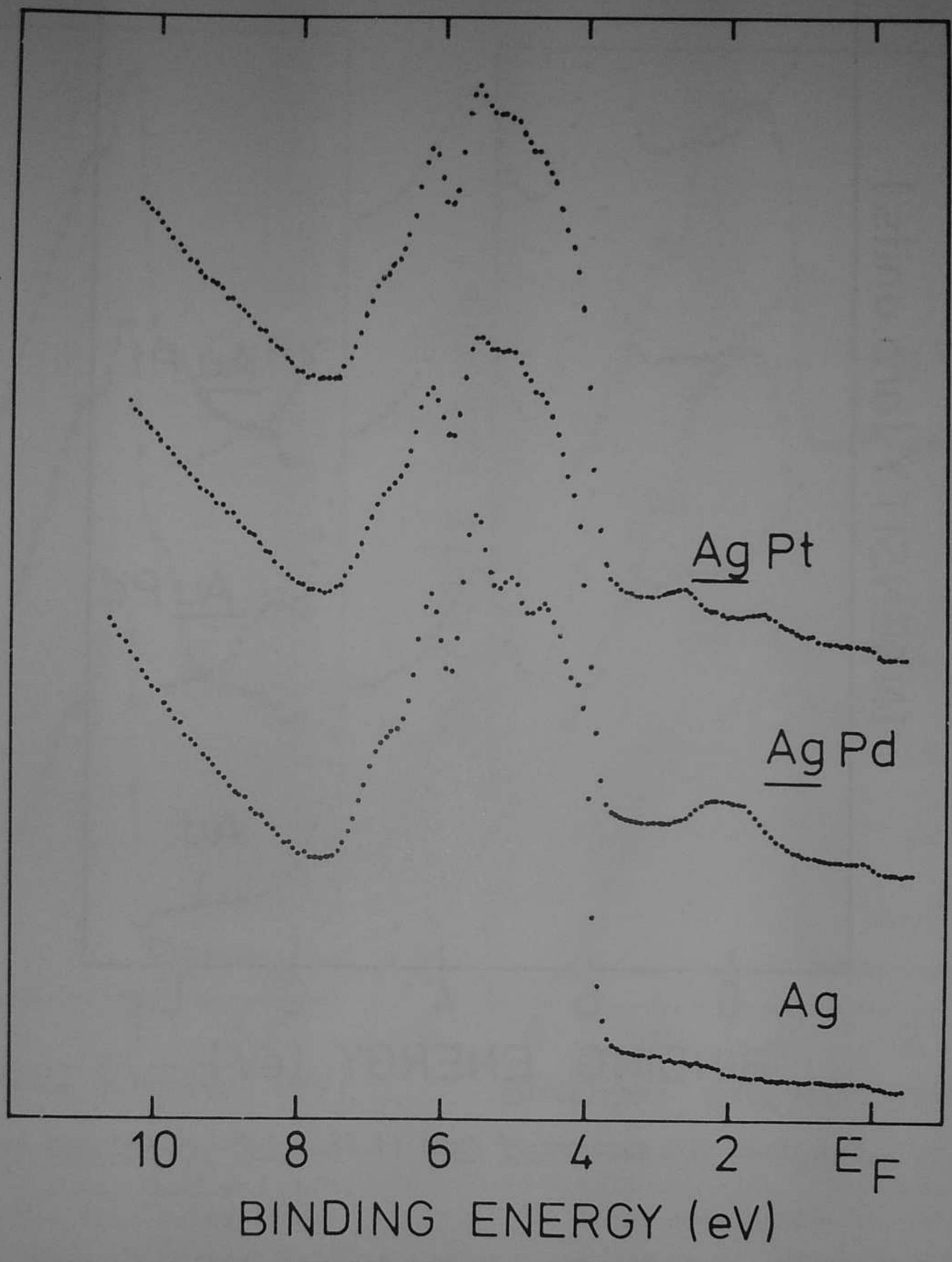

*Fig. 5.2. UPS spectra of Ag*Pd *(3%),* Ag*Pt (2%) and Ag.*

Fig. 5.5. In these cases one clearly sees the influence of the spin orbit coupling. This is most obvious for AgPt. However, we also notice that the Pt d peak closest

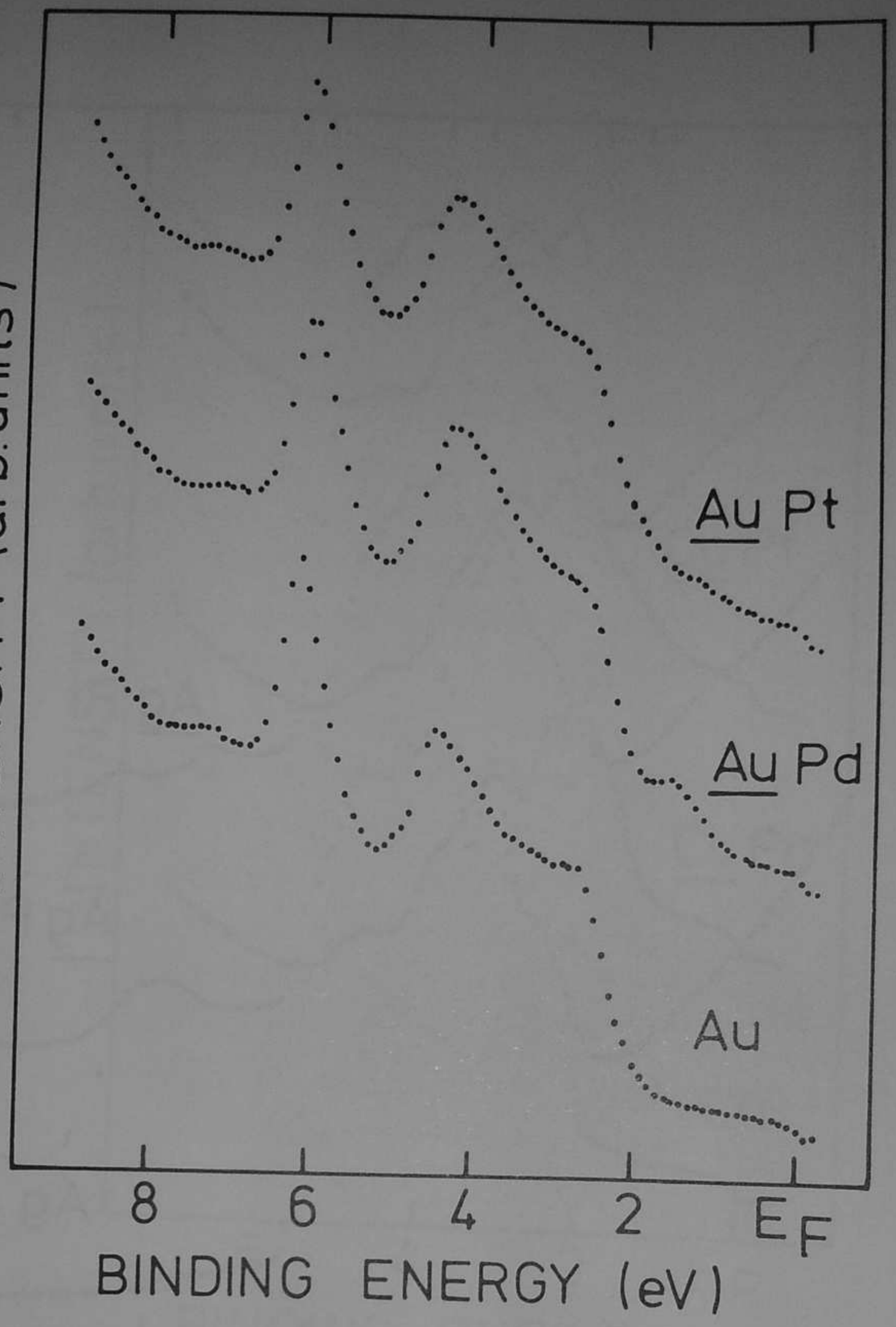

Fig. 5.3. UPS spectra of AuPd (4.5%), AuPt (4.5%) and Au.

to the Fermi level ($d_{5/2}$) is broader. In the Appendix [22] we examine this in detail and we show that the spectrum can be understood if we take into account a cubic crystal field splitting. In the O_h double group the d states span the Γ_7, Γ_8 and $\Gamma_{8'}$ irreducible representations causing (for small crystal field) the $d_{5/2}$ line to split into two components. Also in AgPd there is evidence of the spin-orbit coupling of Pd resulting in the shoulder at the high-binding-energy

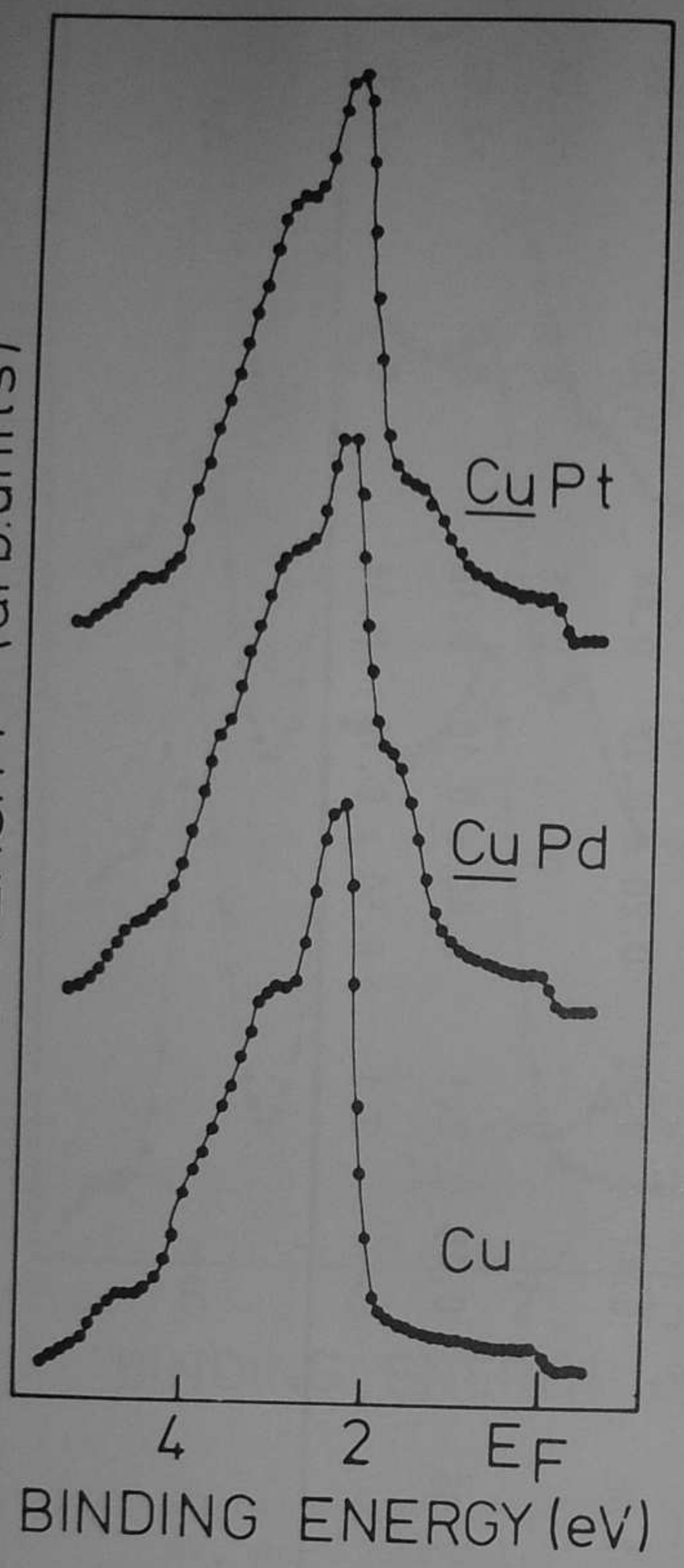

Fig. 5.4. Corrected UPS spectra for Cu, CuPd and CuPt. The thin solid lines are a guide to the eye.

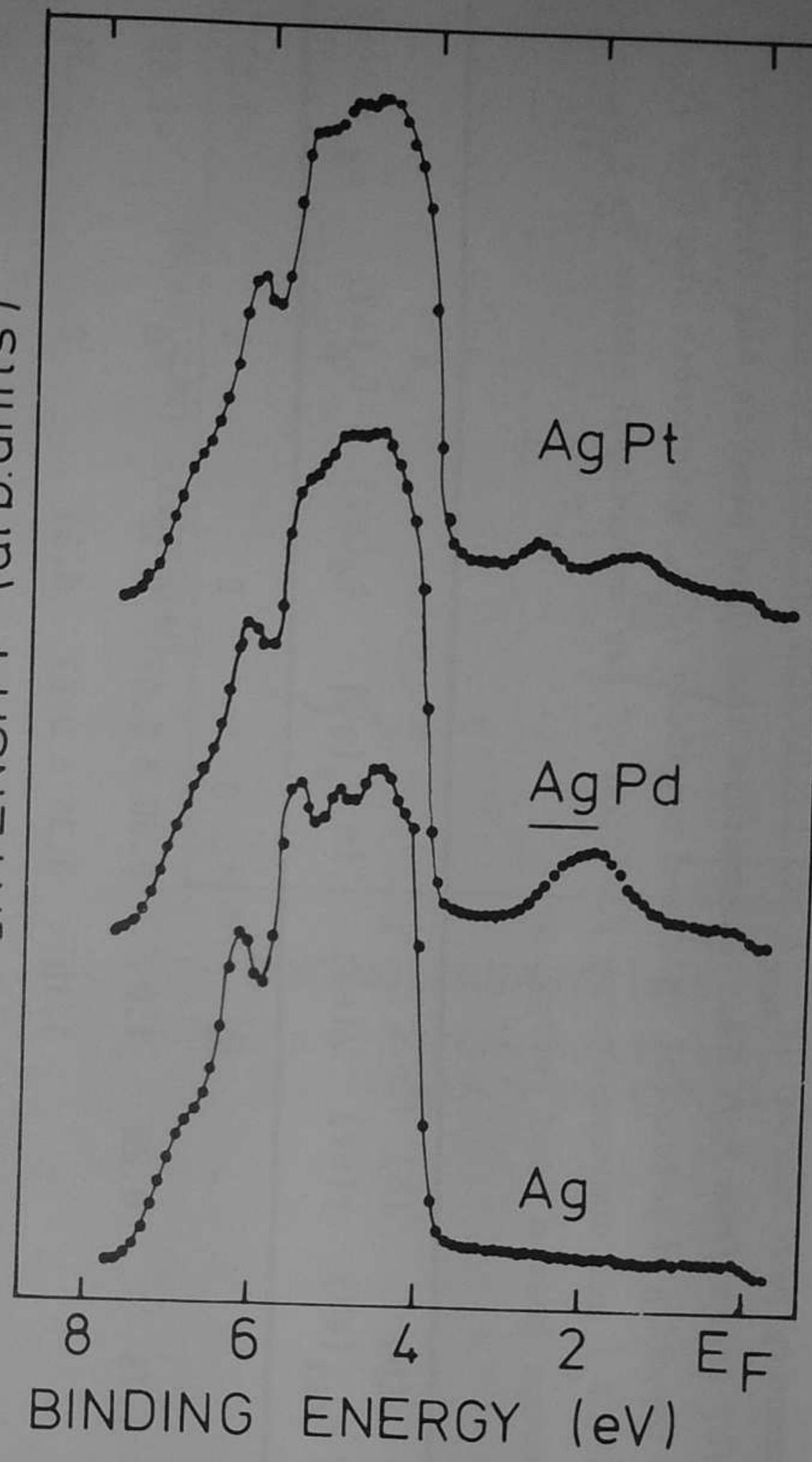

Fig. 5.5. Corrected UPS spectra of Ag, AgPd and AgPt. The thin solid lines are a guide to the eye.

side of the peak as we will see below.

For the Au and Cu hosts the impurity d structure is visible only as shoulders at the top of the host metal d bands. This is not unexpected since the top of the d band for Au and Cu lies much closer to the Fermi level than in Ag. If, as

Table 5.1. Experimental UPS impurity peak maxima (ε_{max}) and halfwidths at half maximum (Γ): (a) this work and (b) taken from Ref. 23. Parameters that were used in the theoretical spectra: change in impurity d potential (Δ), s-d coupling (σ_s), spin-orbit coupling (ξ_d), cubic crystal field (D_q) and average energy position of the impurity d states $\bar{\varepsilon}_d + \Delta$, where $\bar{\varepsilon}_d$ is the average host d band energy.

Solid	(a) ε_{max}(eV)	(a) Γ(eV)	(b) ε_{max}(eV)	(b) Γ(eV)	Δ(eV)	Im σ_s(eV)	ξ_d(eV)	D_q(eV)	$\bar{\varepsilon}_d + \Delta$(eV)
Cu	-	-	-	-	0	0	0	0	-3.52
CuPd	1.8	0.30 ± 0.07	1.75	0.28	1.0	0.30 ± 0.07	0.12	0	-2.52
CuPt	1.65/2.0	0.35 ± 0.07	-	-	1.18	0.35 ± 0.07	0.31	0	-2.34
Ag	-	-	-	-	0	0	0	0	-5.68
AgPd	1.8/2.2	0.40 ± 0.05	1.95	0.35	3.4	0.40 ± 0.05	0.18	0	-2.28
AgPt	1.5/2.6	0.28 ± 0.07	1.95	0.47	3.23	0.28 ± 0.07	0.44	0.043	-2.45
Au	-	-	-	-	0	0	0.45	0	-5.02
AuPd	1.6	0.40 ± 0.10	1.55	0.18	2.1	0.40 ± 0.10	0.18	0	-2.92
AuPt	1.3/1.9	0.50 ± 0.10	-	-	2.1	0.50 ± 0.10	0.44	0	-2.92

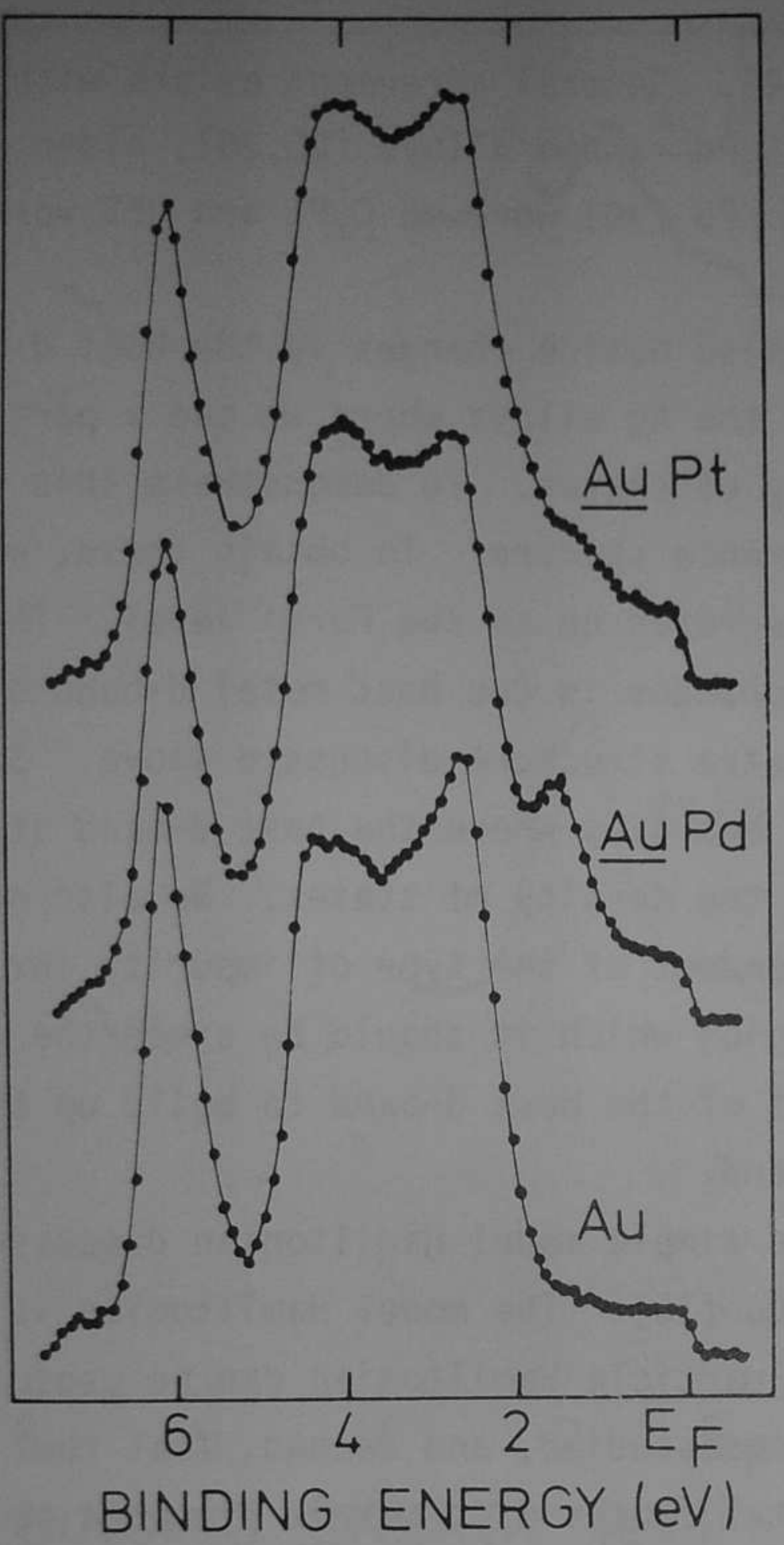

Fig. 5.6. Corrected UPS spectra of Au, AuPd and AuPt. The thin solid lines are a guide to the eye.

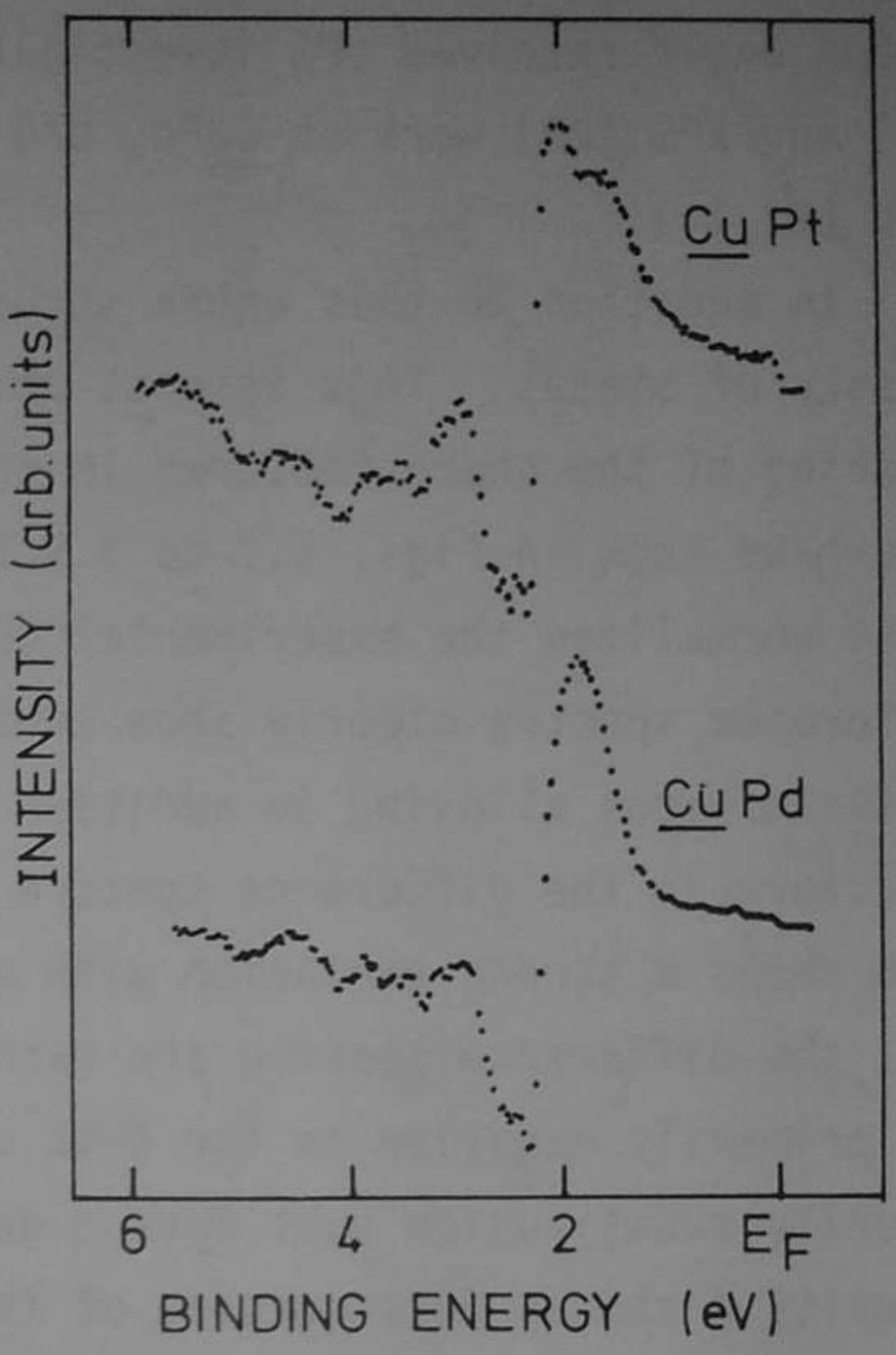

Fig. 5.7. Difference UPS spectra: CuPd-Cu and CuPt-Cu.

expected, the Pd and Pt impurity d-state energy is the same for the three noble metal hosts the impurity states will be either just in or just outside the Au and Cu host d bands. The virtual bound state peak positions and halfwidths at half maximum are given in Table 5.1 and compared to Hüfner's XPS data [23]. We see from the table that the peak positions agree quite well, but the linewidths are different, probably due to the better resolution in our measurements. A similar agreement

exists with Martensson's XPS data on CuPd [24]. General agreement exists with recent angle resolved UPS investigations on CuPd random alloys [25,26], older UPS [27] and XPS [28] work on CuPd, UPS [29] and XPS [30] work on CuPt and UPS work on AgPd [21,31].

In addition to this extra structure we also notice changes in the host d-band density of states. This is most obvious for the Ag alloys where we see a partial smearing of the sharp features in the density of states. To demonstrate this more clearly we show in Figs. 5.7 to 5.9 the difference spectra. To obtain these, we first normalized the experimental curves integrated up to the Fermi level. The difference spectra clearly show substantial changes in the host metal d-band density of states upon alloying in addition to the extra structure discussed above. Sharp structures in the difference spectra occur at energies where the host d-band structure shows a strong variation with energy in the density of states. We also notice that the difference spectra are rather independent of the type of impurity involved and primarily negative in the host d-band region which it should be since the impurity substitution must move d density out of the host d-band to build up the impurity d states just outside of the host band.

To explain these features we resort to a simple model Hamiltonian discussed in our treatment of Mn impurities in Ag and Cu [15]. The model Hamiltonian is based on two basic assumptions. First, that a one-particle Hamiltonian can be used in the description of photoemission of the systems studied, and second, that the impurity d electrons couple with the host-metal states with matrix elements equal to those determining the host-metal band structure. The only difference then, in the Hamiltonian describing the impurity system, is that the impurity d states are shifted in energy relative to those of the host. This is often referred to as the Clogston-Wolff model.

Before describing the theoretical results we make a few remarks concerning the validity of the above assumptions for the systems of interest. The d-d Coulomb and exchange interactions are known to be quite large for Pd [32] and are expected to be only slightly smaller for Pt. At first glance one might then expect correlation effects to be important especially in view of the rather narrow impurity states observed. However, we also find that the peak in the impurity density of states is well below the Fermi level so that any impurity d holes present

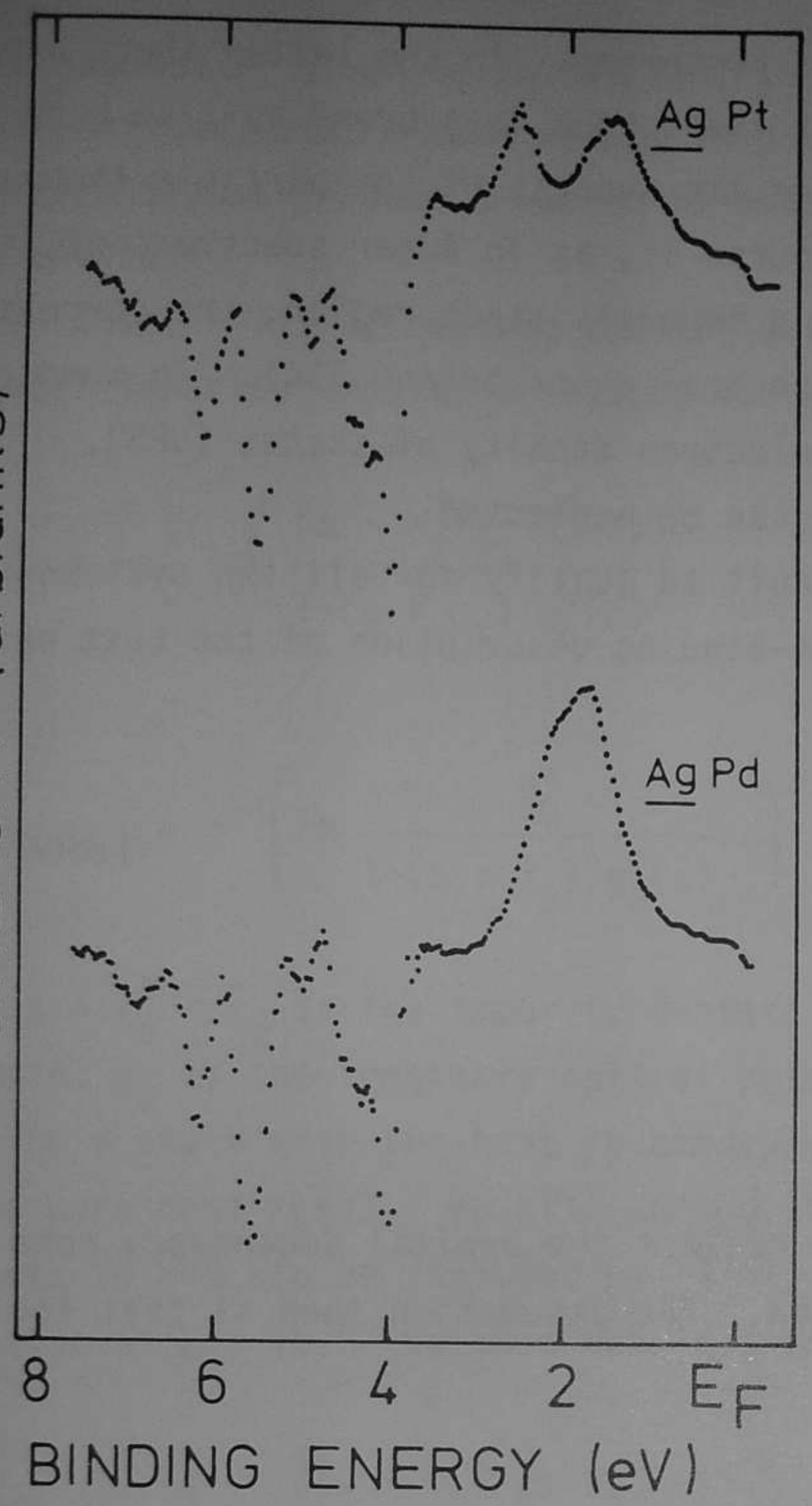

Fig. 5.8. Difference UPS spectra: AgPd-Ag and AgPt-Ag.

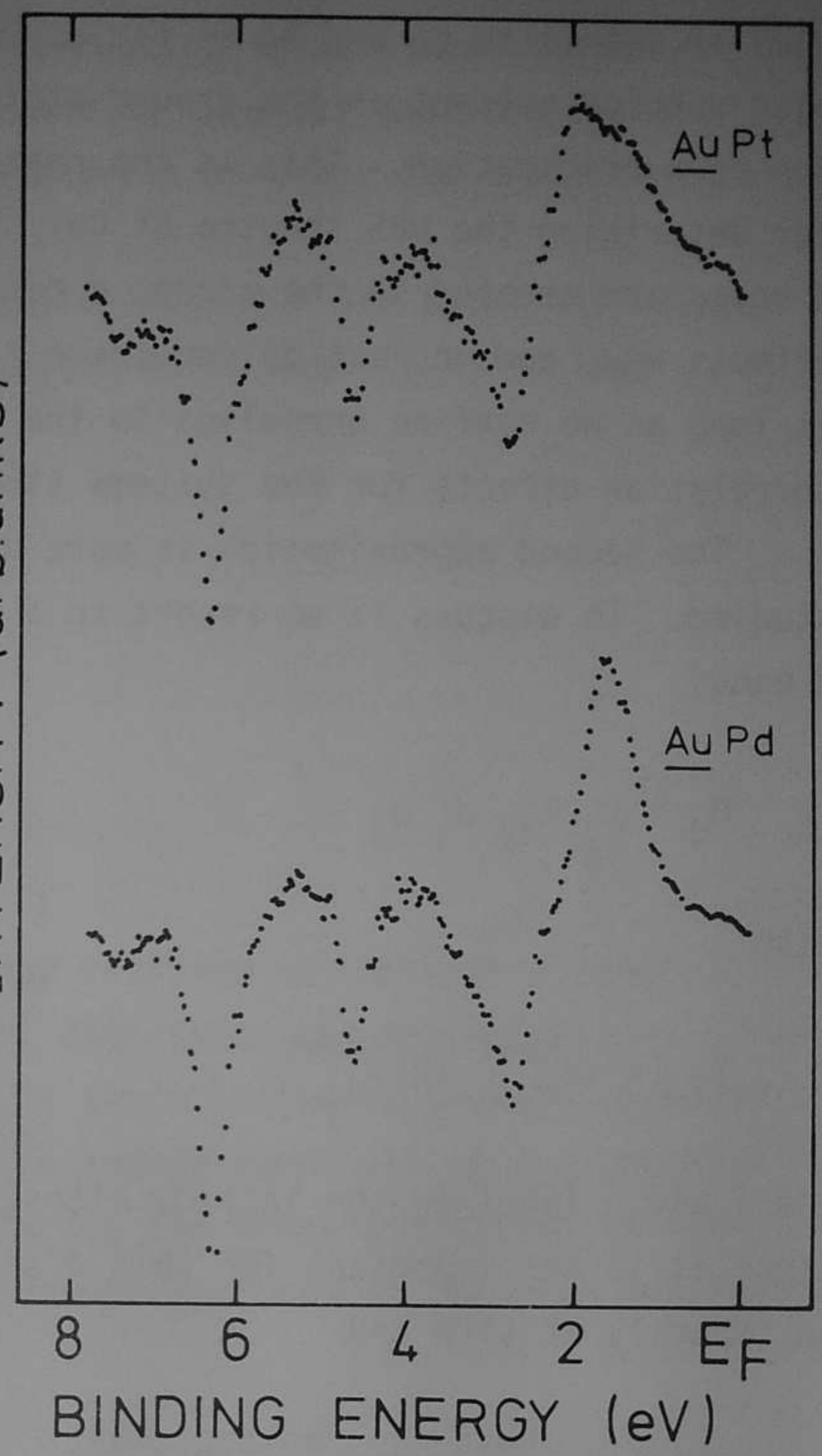

Fig. 5.9. Difference UPS spectra: AuPd-Au and AuPt-Au.

in the ground state are distributed in a large energy range above the Fermi level, in the sense of Hartree-Fock theory. We also know that correlation effects in the UPS spectra are only important if there are other d holes present with which the created d hole can correlate and if the d holes present are distributed over an energy range small or comparable to the d-d Coulomb interactions. We therefore expect correlation effects to be important in UPS only if the d holes present in the ground state are also confined to a narrow energy range as for example in Ni metal [33]. We expect Pd and Pt impurities to behave in a

similar manner to Cu and Ag as far as UPS is concerned. In the latter there are also d holes present in the ground state but they occur in a broad sp-like band due to hybridization. This is the reason for the success of one-particle theory for describing the UPS spectra of Cu. Of course if, as in Auger spectroscopy, two d holes are created in the narrow d band or d impurity state region, the correlation effects may, and in fact do, dominate the spectral distribution [34]. To summarize: as long as we confine ourselves to the N-1 electron density of states (UPS), correlation effects for the systems studied can be neglected.

The second approximation is more difficult to justify for all the systems studied. To discuss it we resort to a tight-binding description of the host metal d band:

$$H_d = \sum_{ij} T_{ij} \, d_i^\dagger \, d_j \tag{5.1}$$

with

$$T_{ij} = \langle \Psi_{d_i}^{host} | H | \Psi_{d_j}^{host} \rangle$$

and i and j labelling the lattice sites. We neglect the orbital degeneracy here since it is not important for this discussion. The assumption then is that for an impurity at site i=0

$$\langle \Psi_{d_o}^{imp} | H | \Psi_{d_j}^{host} \rangle = \langle \Psi_{d_o}^{host} | H | \Psi_{d_j}^{host} \rangle \tag{5.2}$$

which implies that if the interatomic distances are equal then also the d wave functions must have the same radial extent. We expect this to be a good approximation for AgPd, AuPt and CuNi; however, for systems like CuPt or CuPd one might expect the above approximation to be invalid especially if the Pt, Pd-Cu interatomic distances were equal to the Cu-Cu distances.

However, we certainly expect the lattice to relax upon the introduction of a large atom like Pd into Cu. In fact one expects the Pd-Cu nearest-neighbor distances to be closer to the sum of the Pd and Cu metallic atom radii than two times the Cu atomic radii. Such a lattice distortion has the tendency towards the

result assumed as given by Eq. (5.2). It is interesting to note that the near equality of the total d-band widths in pure Cu and Ag suggests that the lattice parameters adjust in such a way as to keep the nearest neighbor d-d transfer integrals constant.

In Chapter III we derived the following expressions for the total difference and local impurity density of states for a Clogston-Wolff model Hamiltonian:

$$\Delta\rho = -\pi^{-1} \mathrm{Im}\left(\frac{(\Delta + \sigma_s)\frac{\partial}{\partial\varepsilon} g_o^o(\varepsilon)}{1-(\Delta + \sigma_s)\, g_o^o(\varepsilon)} \right) \tag{5.3}$$

$$\rho_{local} = \pi^{-1}\left(\mathrm{Im} \frac{g_o^o}{1-(\Delta + \sigma_s)\, g_o^o(\varepsilon)} \right) \tag{5.4}$$

Where $\Delta = \varepsilon_d^i - \bar{\varepsilon}_d$ is the impurity d-state energy relative to the host d band centroid, σ_s is the imaginary optical potential describing the mixing of the impurity d state with the host sp bands and g_o^o is the d projected Green's function of the pure host metal. We also showed that the energy-dependent optical matrix elements in UPS can be included by simply replacing the Green's function in the numerator of Eq. (5.3) by that obtained from the UPS spectrum of the pure material:

$$\Delta\rho = -\pi^{-1}\ \mathrm{Im}\left(\frac{(\Delta + \sigma_s)\ \frac{\partial}{\partial\varepsilon}\ g_{exp}(\varepsilon)}{1\ -\ (\Delta + \sigma_s)\ g_o^o(\varepsilon)} \right) \tag{5.5}$$

In these expressions we have not taken account of spin-orbit and crystal-field effects. A full calculation taking these effects into account and also deviations from the Clogston-Wolff model are presented in Chapter III.

For the systems of interest here a suitable basis set of states to use is that determined by the irreducible representations, spanned by a d state, of the cubic double point group. These are $\Gamma_8(e_g)$, $\Gamma_8(t_{2g})$ and $\Gamma_7(t_{2g})$. In Chapter III we have derived general expressions for the change in the total density of states and impurity local density of states given by Eqs. (3.42) and (3.43). In these ex-

pressions we require knowledge of the now in matrix form $(\Delta + \sigma_s)^{\nu}_{\mu}$ and the local Green's function corresponding to the pure host $g^{o\nu}_{o\mu}(\varepsilon)$. These equations are in general quite cumbersome to work with because of the occurrence of two, in general, nondegenerate Γ_8 representations so that diagonalization of $g^{o\nu}_{o\mu}(\varepsilon)$ requires an energy-dependent transformation matrix. However, a very simple form results if we can neglect the difference in $g^{ot_{2g}}_{ot_{2g}}$ and $g^{oe_g}_{oe_g}$. In this case we can rotate the basis set and use instead $\Gamma_7(d_{5/2})$, $\Gamma_8(d_{5/2})$ and $\Gamma_8(d_{3/2})$ on which g^o_o is now diagonal

$$g^{\Gamma_7(d_{5/2})}_{\Gamma_7(d_{5/2})} = g^{\Gamma_8(d_{5/2})}_{\Gamma_8(d_{5/2})} = g^{5/2}_{5/2}$$

$$g^{\Gamma_8(d_{3/2})}_{\Gamma_8(d_{3/2})} = g^{d_{3/2}}_{d_{3/2}}$$

To demonstrate the validity of these, we show in Fig. 5.10 the Cu t_{2g} and e_g projected and total d density of states. We see that there is little difference in these and even their mean energies are equal justifying the neglect of the cubic symmetry in determining the local host density of states. For Cu and Ag the spin orbit coupling is also negligible in g^o_o so that $g^{d_{3/2}}_{d_{3/2}} = g^{d_{5/2}}_{d_{5/2}}$. For Au, however, we will find spin orbit coupling to be quite important.

In terms of the above basis the matrix elements of $(\Delta + \sigma_s)$ are given by

$$\begin{aligned}
&\langle\Gamma_7(d_{5/2})|(\Delta+\sigma_s)|\Gamma_7(d_{5/2})\rangle &&= \Delta + \delta\xi_d - 4Dq + \sigma_s \\
&\langle\Gamma_8(d_{5/2})|(\Delta+\sigma_s)|\Gamma_8(d_{5/2})\rangle &&= \Delta + \delta\xi_d + 2Dq + \sigma_s \\
&\langle\Gamma_8(d_{3/2})|(\Delta+\sigma_s)|\Gamma_8(d_{3/2})\rangle &&= \Delta - 3/2\ \delta\xi_d + \sigma_s \\
&\langle\Gamma_8(d_{5/2})|(\Delta+\sigma_s)|\Gamma_8(d_{3/2})\rangle &&= -2\sqrt{6}\ Dq
\end{aligned} \tag{5.6}$$

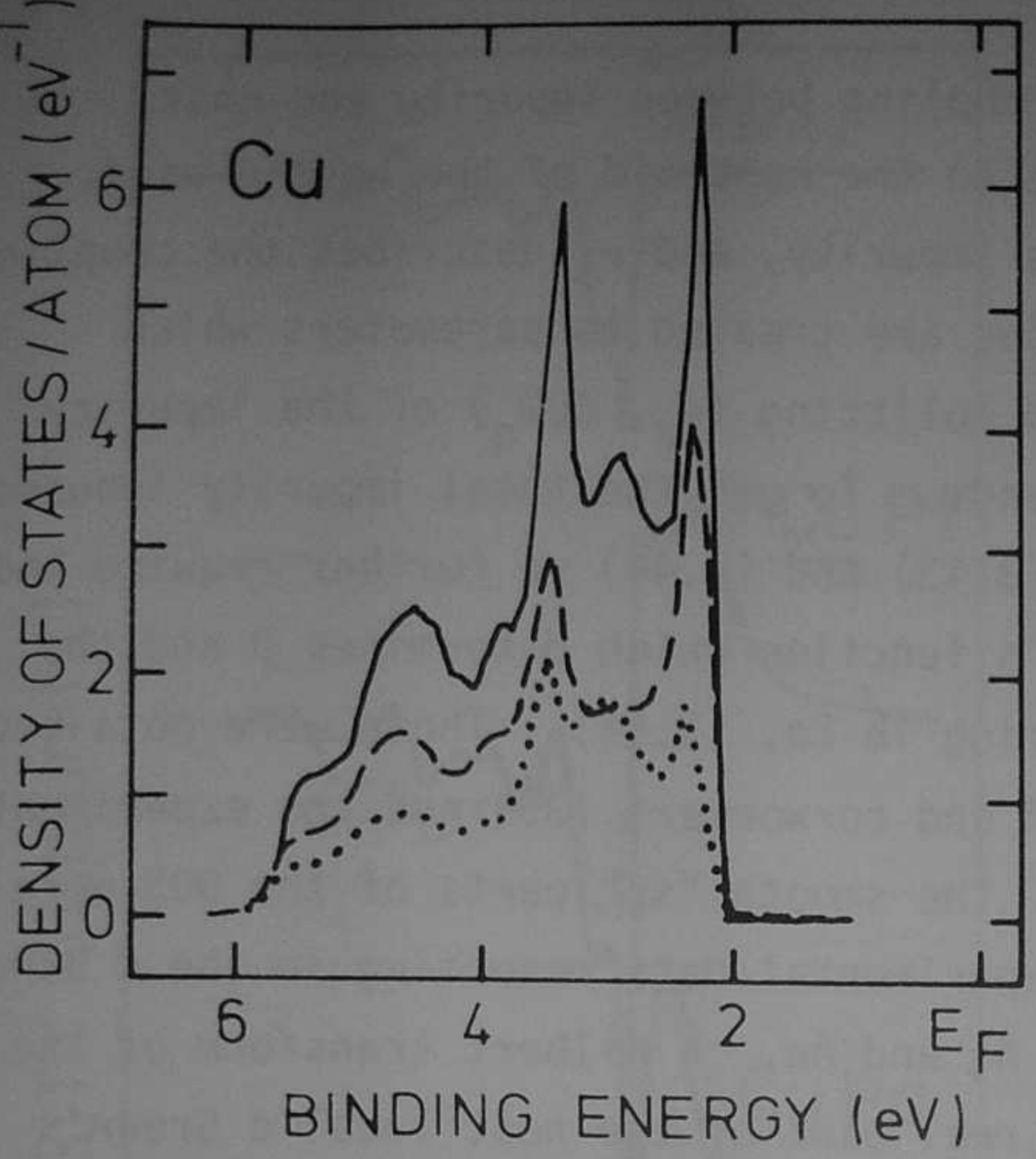

Fig. 5.10. Density of states of copper. Solid line: Total d density of states. Dashed line: t_{2g} projected DOS. Dotted line: e_g projected DOS.

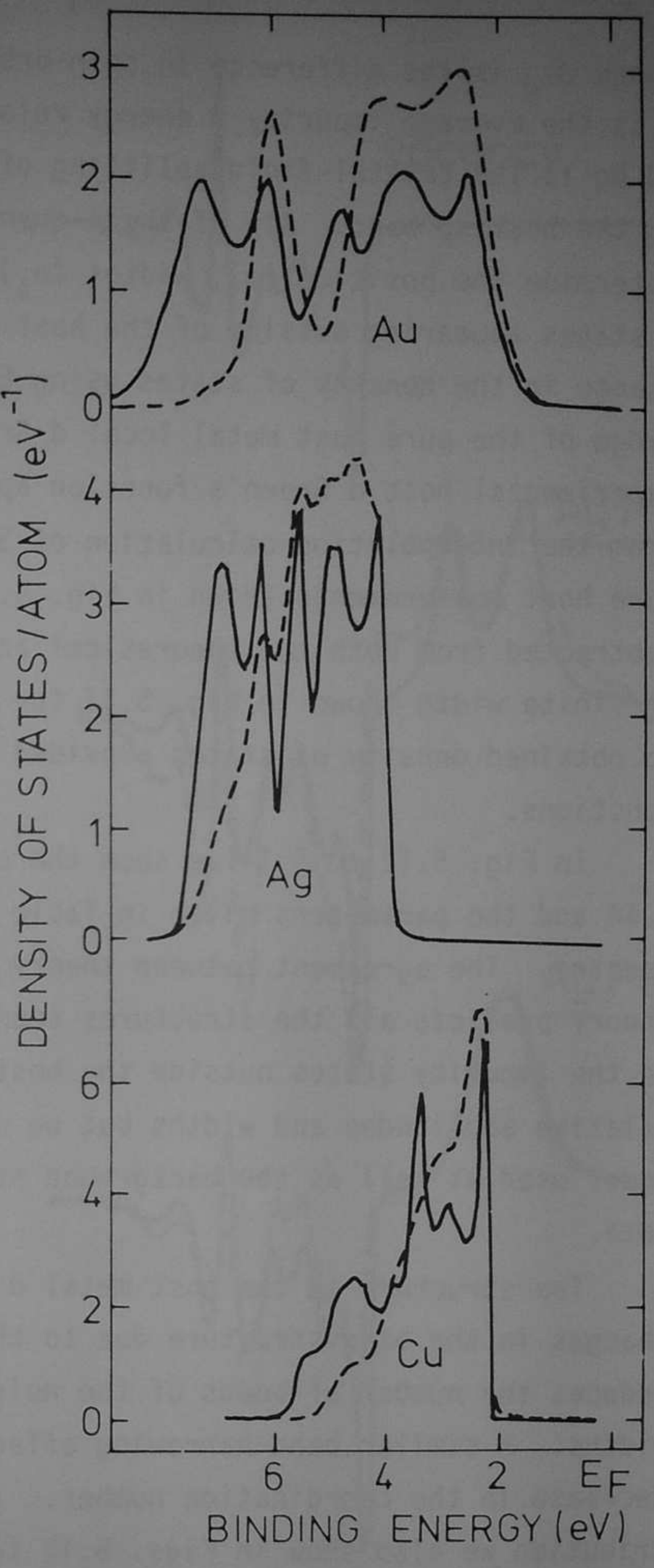

Fig. 5.11. Imaginary parts of theoretical (solid lines) and experimental (dashed lines) Green's functions of Cu, Ag and Au.

where $\delta\xi_d$ is the difference in spin-orbit coupling between impurity and host, Δ is the average impurity d energy relative to the centroid of the host d band, 10 Dq is the crystal-field splitting of the impurity, and σ_s describes the coupling to the host sp band. All of these quantities are treated as parameters which determine the position (Δ), widths (σ_s) and splitting (ξ_δ, $10D_q$) of the impurity d states appearing outside of the host d bands. To get the total impurity induced change in the density of states using Eq. (3.43) and (3.44) we further require knowledge of the pure host metal local d Green's function which determines D and the experimental host d Green's function appearing in Eq. (3.64). These were obtained from the interpolation calculation of Smith and co-workers [35] and the experimental pure host measurements shown in Fig. 5.11. The smooth "sp" parts of the DOS were subtracted from both the theoretical and experimental data resulting in the d bands of finite width shown in Fig. 5.11 for Cu, Ag and Au. A Hilbert transform of the so obtained density of states provided the real part of the host local d Green's functions.

In Fig. 5.12 to 5.14 we show the calculated difference UPS spectra using Eq. 3.44 and the parameters given in Table 5.1, together with the experimental difference spectra. The agreement between theory and experiment is surprisingly good. The theory predicts all the structures seen in the host d bands regions in addition to the impurity states outside the host d band. There are differences in the relative amplitudes and widths but we consider these as minor in view of the simple model used as well as the background subtraction techniques used in the experimental data.

The structure in the host metal d band region is primarily the result of changes in the band structure due to the removal of a noble metal atom [36]. This reduces the number of bonds of the neighbouring atoms, thereby reducing their bandwidths. A similar band-narrowing effect occurs at the surface also because of a decrease in the coordination number. To demonstrate that this is the dominant contribution we also show in Figs. 5.12 to 5.14 the calculated difference spectrum for a vacancy. This calculation was done by taking $\Delta \to \infty$ in Eq. (3.44) so that

$$\Delta\rho = \pi^{-1}\ \mathrm{Im}\left(g_o^o(\varepsilon)^{-1}\ \frac{\partial}{\partial\varepsilon}\ g_{exp}\ (\varepsilon)\right) \qquad (5.7)$$

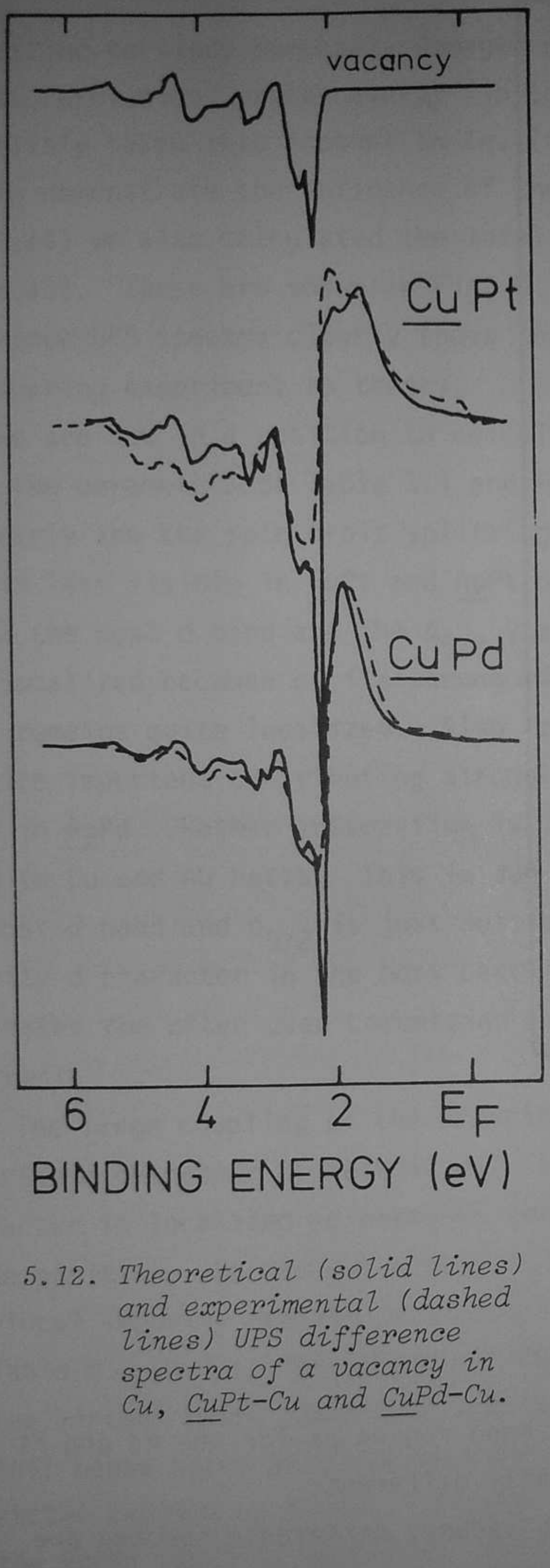

Fig. 5.12. Theoretical (solid lines) and experimental (dashed lines) UPS difference spectra of a vacancy in Cu, CuPt-Cu and CuPd-Cu.

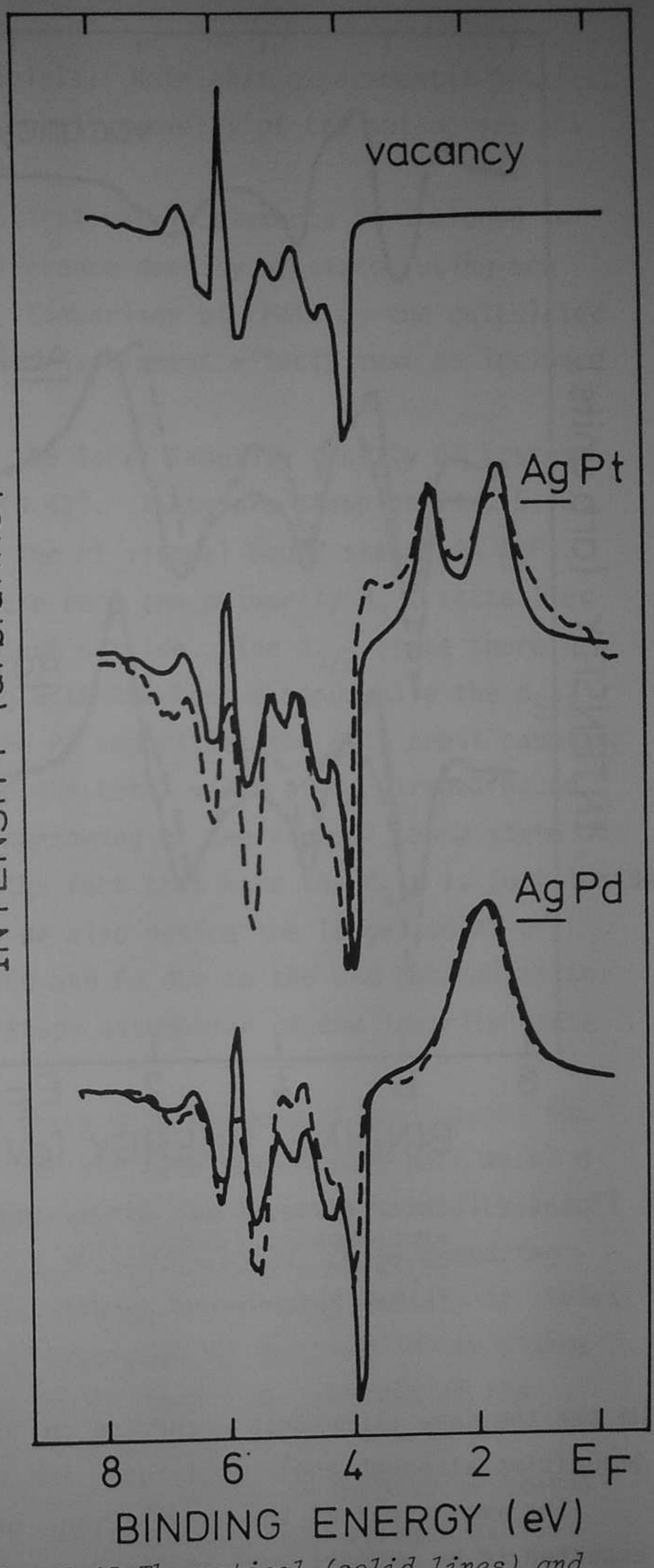

Fig. 5.13. Theoretical (solid lines) and experimental (dashed lines) UPS difference spectra of a vacancy in Ag, AgPt-Ag and AgPd-Ag.

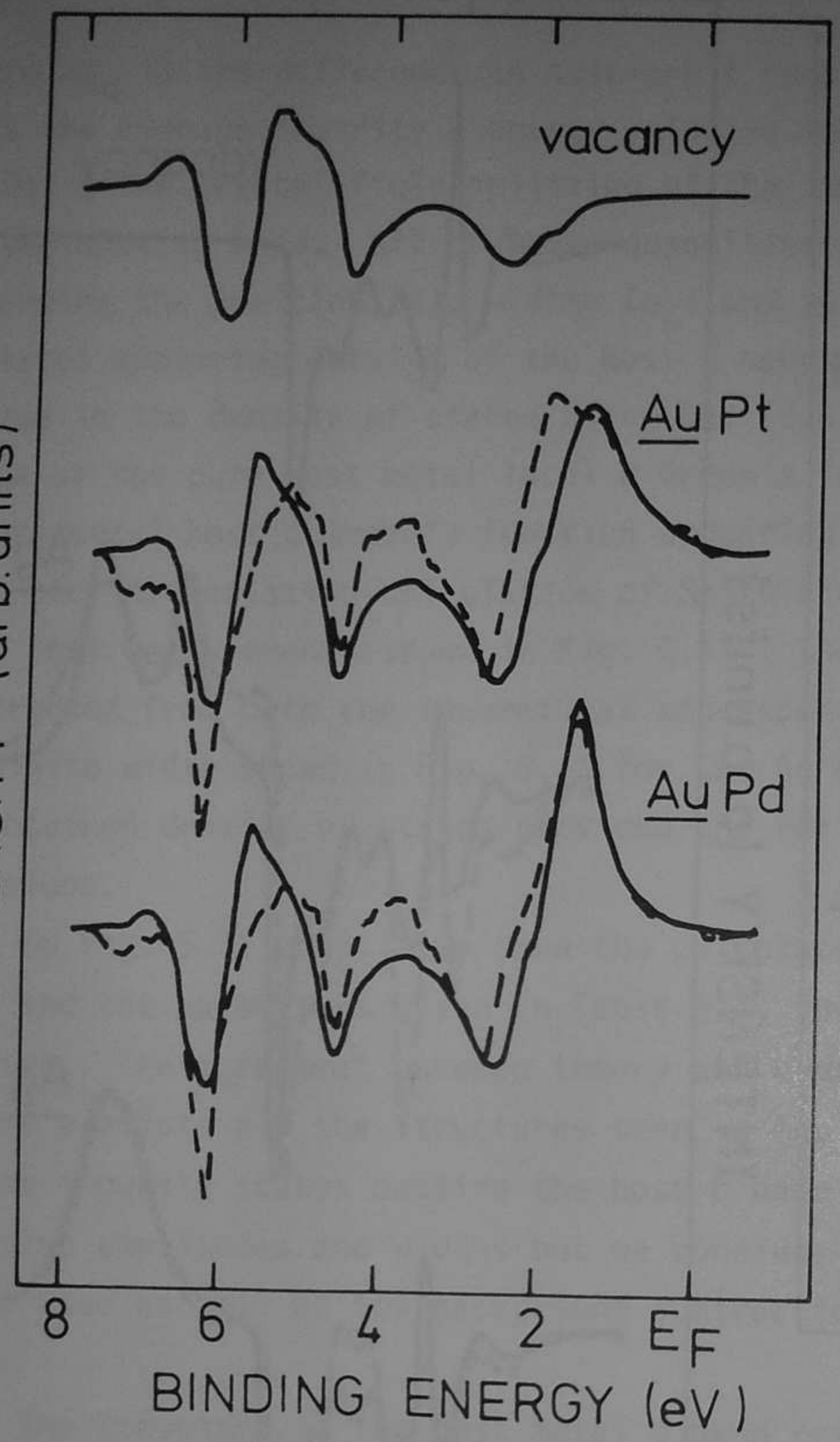

Fig. 5.14. Theoretical (solid lines) and experimental (dashed lines) UPS difference spectra of a vacancy in Au, AuPt-Au and AuPd-Au.

We see the same structures occurring in the d band region as for the Pd and Pt impurities although their amplitudes are slightly different.

The amplitudes of the oscillations in the vacancy difference spectra are expected to be proportional to the vacancy density. It would therefore be quite

interesting to study purposely damaged materials. Note that experimental details, such as resolution, photon energy (in any range), geometry of the set-up are all effectively taken into account in Eq. (5.7).

To demonstrate the influence of the optical matrix elements as included in Eq. (3.44) we also calculated the total difference density of states using now Eq. (3.43). These are shown in Fig. 5.15. Comparison of these to the calculated difference UPS spectra clearly shows that matrix element effects must be included in comparing experiment to theory.

We are now in a position to calculate the local impurity density of states using the parameters of Table 5.1 and Eq. (3.42). These are shown in Fig. 5.16. We clearly see the spin orbit splitting of the Pt virtual bound states in AgPt. This is less visible in CuPt and AuPt because here the primarily $d_{3/2}$ state lies inside the host d band and the $d_{5/2}$ state just outside. The $d_{3/2}$ state therefore is delocalized because of its strong mixing with the host d band while the $d_{5/2}$ state remains quite localized. Also for the Pd impurities the spin orbit coupling is quite important contributing strongly to the total width of Pd virtual bound state in AgPd. Rather interesting is the narrowing of the virtual bound state on going to Cu and Au hosts. This is due to the fact that here the $d_{3/2}$ is just inside the host d band and $d_{5/2}$ is just outside. We also notice the large amount of impurity d character in the host band for Cu and Au due to the d-d hybridization. This makes the often used Lorentzian line shape assumption of the impurity state incorrect.

The large coupling of the impurity d state with the host d band causes the impurity d character to delocalize. Also for the same reason some host metal d character is localized at energies corresponding to the impurity virtual bound state position. We can get a better idea of this delocalization by comparing the local impurity density of states to the change in the total density of states. In Table 5.2 we list the amount of impurity character so obtained in the states at the virtual bound state peak and at the Fermi level. We see that at the virtual bound state peak energy there is a considerable amount of host d character ranging up to 35% for CuPd. Although the change in density of states at the Fermi level is mostly of impurity d character also here as much as 15% (AgPt) is of host metal d character. It is also interesting to determine the character of the total displaced charge. This can be obtained by integrating

Table 5.2. Relative amount of impurity d character in the virtual bound state at peak maximum, at E_F and in the displaced d-charge. This is the quotient of the local DOS and difference DOS (first two columns) and of the integrated unoccupied local DOS and difference DOS (third column).

Solid	$I(E_{max})$	$I(E_F)$	I(DOS above E_F)
CuPd	65%	98%	98%
CuPt	75	98	98
AgPd	93	98	99
AgPt	87	99	99
AuPd	69	87	94
AuPt	76	86	95

the local impurity DOS and the change in the total density of states from the Fermi level to infinity. We see from Table 5.2 that the total displaced charge is again mainly of impurity character although up to 5% is located on host atoms for the Au based alloys. This implies that it is still a reasonable approximation to relate the impurity induced scattering to the local displaced charge, although it is conceptually better to think in terms of the total displaced charge. This should obey the Friedel sum rule exactly.

Of interest for the interpretation of transport measurements are the d scattering phase shifts at E_F. In Chapter III we show their relationship to the total displaced d charge (Eqs. (3.49) (3.50)). These are listed in table 5.3 together with the total change in the d density of states at the Fermi level. For comparison we also listed some experimentally determined phase shifts [22, 37, 38, 39].

Table 5.3. Change in d density of states at E_F($\Delta n_d(E_F)$) and 1=2 scattering phase shifts ($\pi^{-1}\eta_d(E_F)$) compared to experimental phase shifts. (a) Ref. 16, (b) Ref. 22, (c) Refs. 38 and 39, (d) Ref. 37.

Solid	$\Delta n_d(E_F)$ (eV^{-1})	$\pi^{-1}\eta_d(E_F)$	$\pi^{-1}\eta_d(E_F)$
CuPt	0.32 ± 0.06	-0.059 ± 0.012	-0.027 to -0.073 (a)
CuPd	0.21 ± 0.06	-0.046 ± 0.012	-0.013 to -0.055 (a)
AgPt	0.23 ± 0.05	-0.038 ± 0.010	-0.032 to -0.042 (b)
AgPd	0.31 ± 0.04	-0.062 ± 0.008	-0.036 to -0.041 (c)
AuPt	0.47 ± 0.06	-0.079 ± 0.015	-
AuPd	0.35 ± 0.06	-0.063 ± 0.015	-0.053 to 0.030 (d)

5.4. Lattice relaxation

At first glance it is rather surprising that a Clogston-Wolff-like model does so well. As mentioned above we expect it to be valid for AgPd and AuPt but the agreement with experiment for CuPd, CuPt and AgPt is somewhat surprising. This because one might have expected the Pd-Cu d-d overlap to be considerably different from the Cu-Cu d-d overlap. In this context it is interesting to compare our local density of states to that obtained from first principles calculations [5] shown in Fig. 5.17. We notice a large difference between the two calculations especially in the Cu d band region. The most obvious difference is seen at the bottom of the Cu d band where the first principles calculation shows a substantial peaking whereas our model calculation shows a small impurity contribution. The same peaking can also be seen in the CPA calculation of Rao et al. [25] and in the self consistent KKR-CPA calculation of Stocks and co-workers [40,41]. In a recent analysis of Pd Auger spectra, Davies and Weightman [42] showed that agreement with recently published impurity Auger theory [43,44] could only be obtained if the above mentioned peaking in the impurity local density of states was removed. Also our

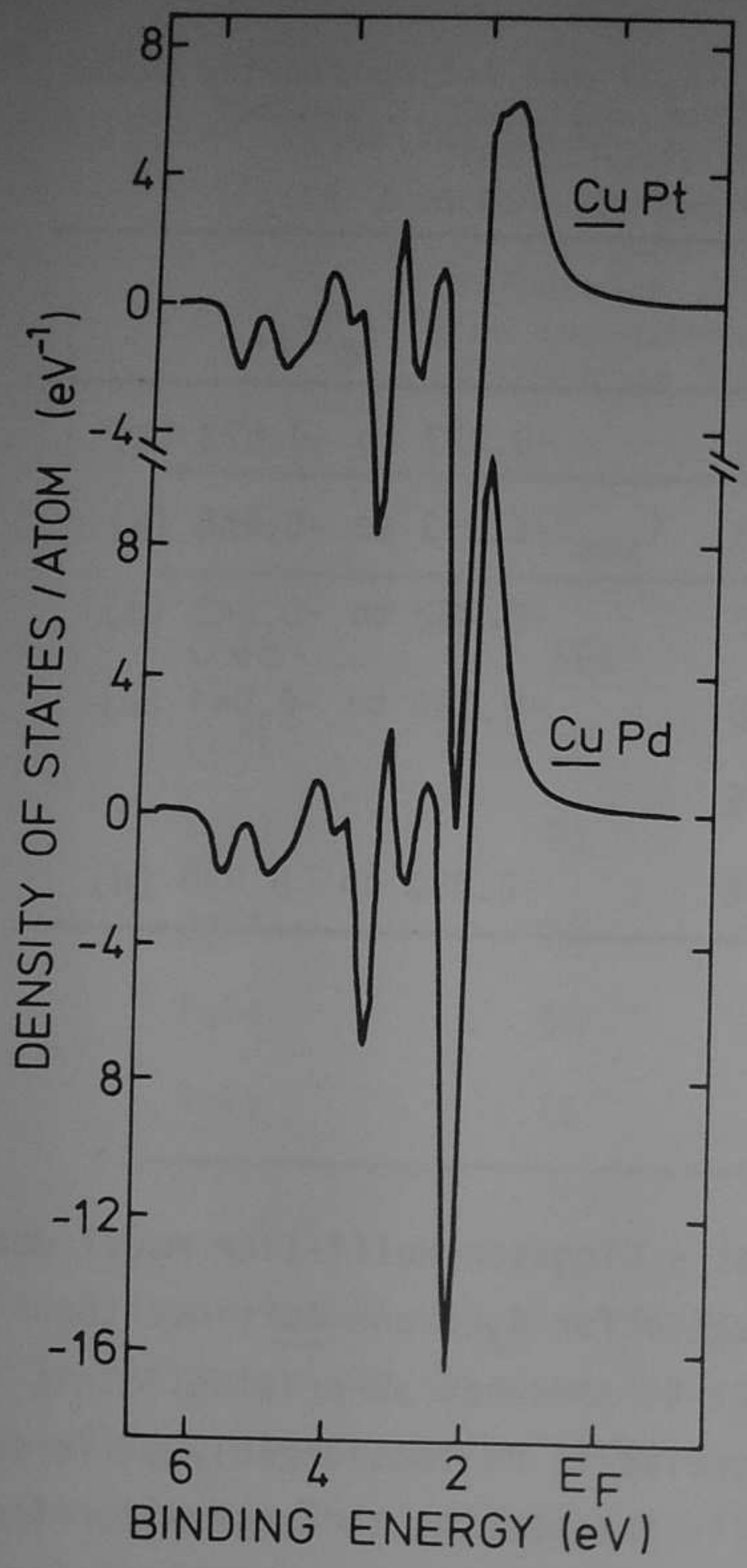

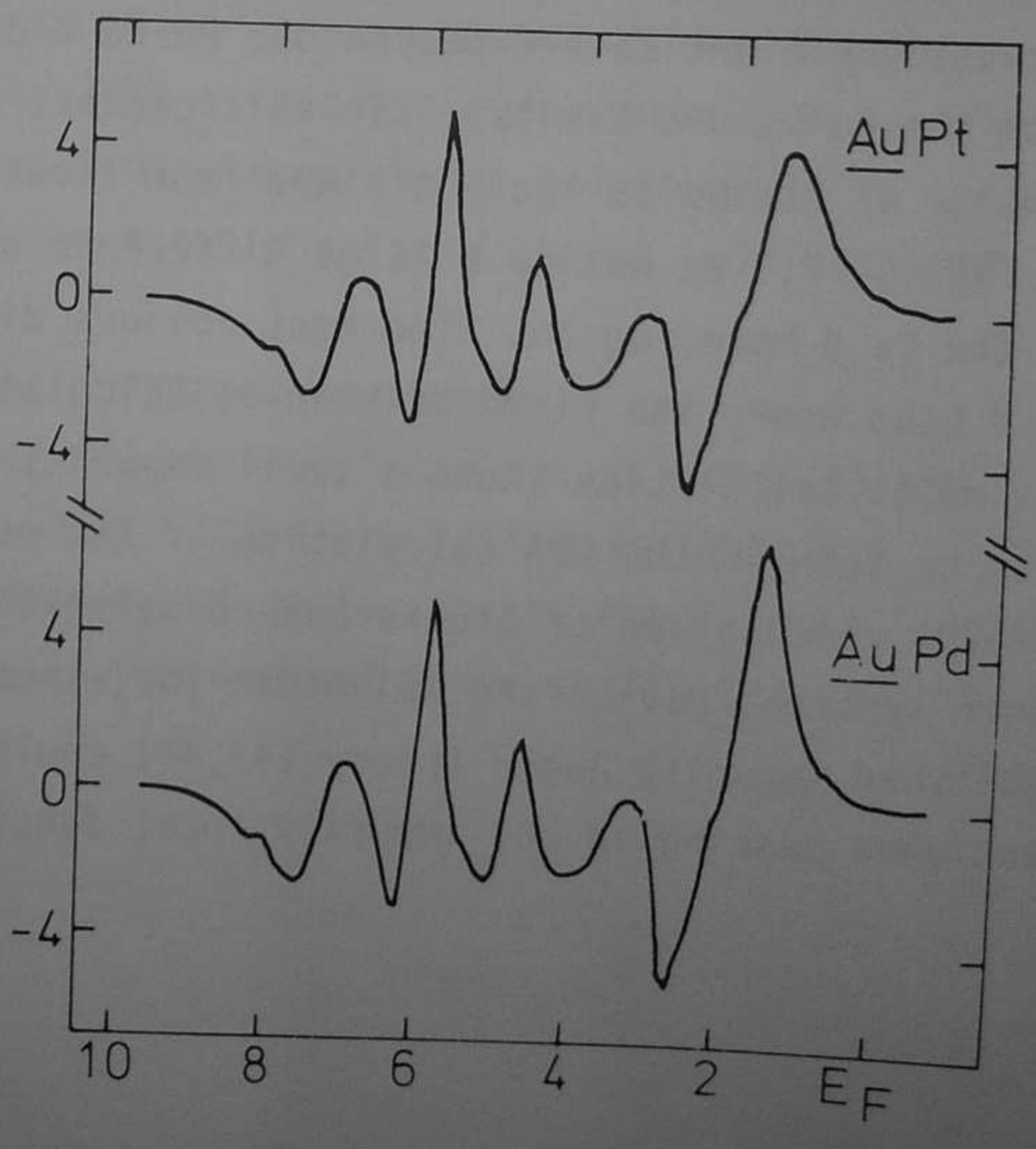

Fig. 5.15. Theoretical difference densities of states of
a: CuPt-Cu and CuPd-Cu
b: AgPt-Ag and AgPd-Ag
c: AuPt-Au and AuPd-Au.

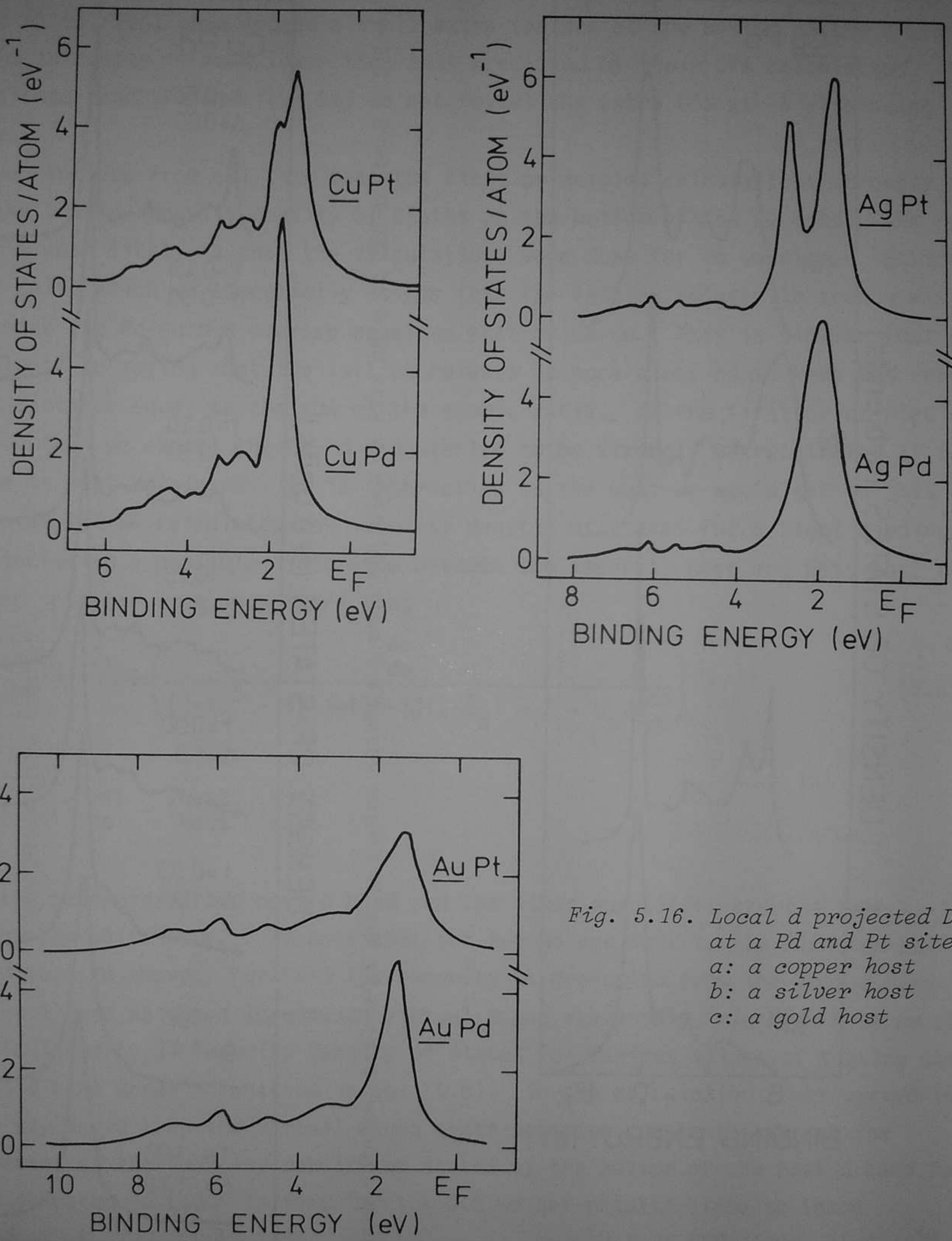

Fig. 5.16. Local d projected DOS at a Pd and Pt site in
a: a copper host
b: a silver host
c: a gold host

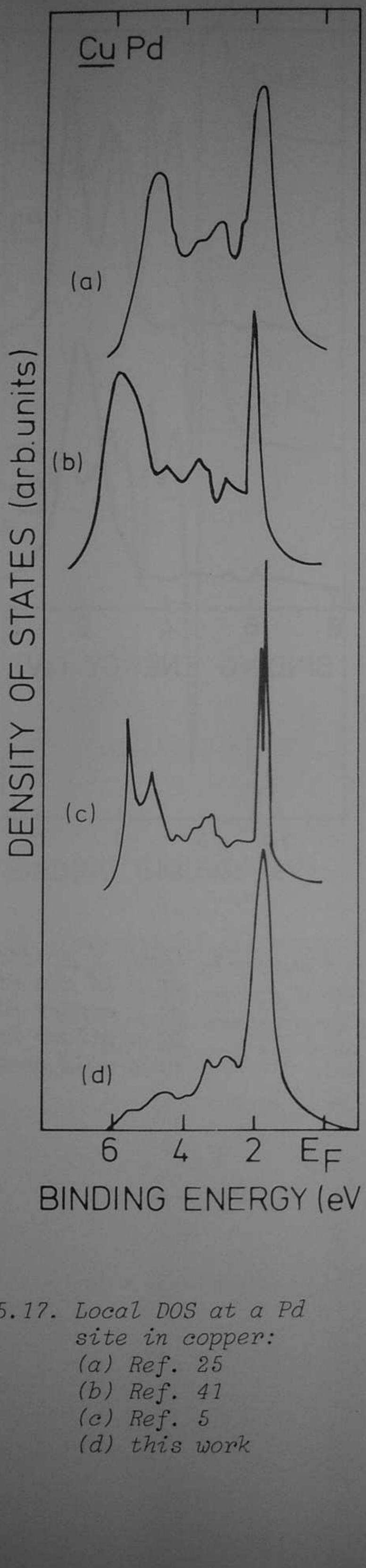

Fig. 5.17. Local DOS at a Pd site in copper:
(a) Ref. 25
(b) Ref. 41
(c) Ref. 5
(d) this work

Fig. 5.18. Local d-DOS at a Pd site in CuPd for some parameter values of the Pd-d Cu-d transfer matrix element.

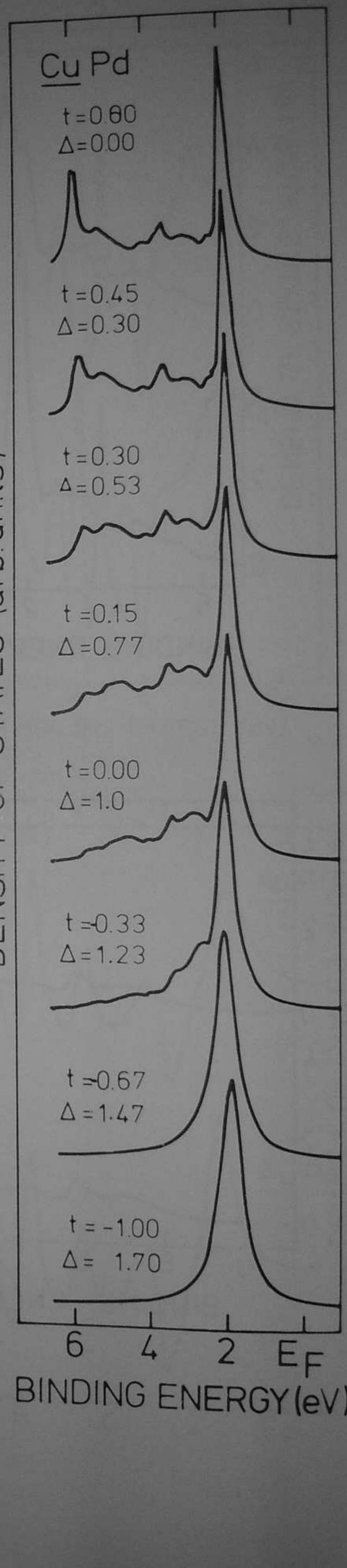

UPS data are in much better agreement with our model calculation. The UPS data of Rao et al. [25] show indeed a small extra feature at the bottom of the d band but the intensity is much lower than that predicted by their CPA calculation. Also the valence band XPS data [23,24] do not reveal the extra DOS at -6 eV binding energy.

We conclude from all this that the first principles calculations strongly overestimate the Pd impurity density of states at the bottom of the Cu band. The reason for this most likely is that the calculations were done for an unrelaxed lattice. In our calculation we essentially assume that the lattice relaxes in such a way as to make the Pd-Cu d-d overlap equal to that of Cu-Cu. This is similar (but not equivalent) to saying that the lattice relaxes in such a way as to keep the interatomic distance equal to the sum of the atomic radii. In the first principles calculation then we expect the Cu-Pd d-d overlap to be strongly overestimated if the lattice is kept unrelaxed. It is interesting to see what we would get in this case. In Chapter III we calculated the impurity denstiy of states for a tight binding model including a possible difference between the impurity-host and host-host d-d transfer integral. We show there that

$$\rho_{imp} = \pi^{-1}\ \mathrm{Im}\left(\frac{g^{do}_{do}}{(1+t)^2 - \{[(1+t)^2-1](E-\bar{E}_d) + \Delta + \sigma_s\}g^{do}_{do}}\right) \qquad (5.8)$$

where $t = (T^{host}_{imp} - T^{host}_{host})/T^{host}_{host}$

$\bar{E}_d$ is the centroid of the host d band and the other quantities are the same as in the Clogston-Wolff model. We note that for t=o we are back to the Clogston-Wolff model discussed above. For t=-1 the impurity is decoupled from the host d band ($T^{host}_{imp} = 0$) and we get a lorentzian virtual bound state only. In Fig. 5.18 we show the calculated local impurity density of states for various values of t using the Cu host d band Green's function in Eq. (5.8). In the calculation Δ was varied in such a way as to keep the virtual bound state position constant. We see the enhancement of the impurity density of states at the bottom of the host d band for t>0 as compared to t=0. In fact for $t \approx 0.6$ we get results close to those

obtained from first principles calculations and this corresponds to $T_{Pd}^{Cu} = 1.6T_{Cu}^{Cu}$. Indeed we expect T_{Pd}^{Cu} to be overestimated in the unrelaxed lattice first principles calculation because of the larger size of the Pd atom.

5.5. Degeneracy of the d bands

In order to give an idea of the relevance of taking into account the details of the degeneracy in the d bands, we calculate the local density of states at a Pt site in CuPt again, now using the e_g and t_{2g} projected DOS's [45] shown in Fig. 5.10. The centroids of the e_g and t_{2g} projected DOS's exactly coincide, which means that the average "crystal" field splitting of the bands is zero. We applied Eq. (3.42) of Chapter III to the Green's functions corresponding to these DOS's using the parameter values of Table 5.1 for CuPt. In Fig. 5.19 we compare the so obtained local density of states of CuPt to the non-degeneracy theory of Fig. 5.15a. We see that both curves coincide almost everywhere, and we conclude that incorporation of e_g - t_{2g} degeneracy is not relevant here.

A different situation, however, occurs for the Au based alloys because of the large Au spin orbit coupling. If, as indicated above, we can neglect the crystal field effects, we require only the $d_{3/2}$ and $d_{5/2}$ projected density of states to use the equations in Chapter III. In Fig. 5.20 these projections are shown [46]. The centroids of $d_{3/2}$ and $d_{5/2}$ are at 5.72 and 4.59 eV corresponding to a spin orbit coupling parameter of 0.45 eV. Applying Equation (3.42) and Equations (5.6) for the $\Delta+\sigma_s$ matrix components we obtain the projected and total impurity local density of states as shown in Figs. 5.21 and 5.22 for AuPt and AuPd. In these figures we also compare with the calculation neglecting the host spin orbit coupling. We see substantial differences in the host d band regions and also a small change (7-8%) in the density of d states at the Fermi level. This shows that for Au based alloys the host spin orbit coupling should be taken into account.

5.6. Conclusions

We have presented high resolution UPS data for dilute alloys of Pd and Pt in noble metal hosts. We have obtained the impurity induced changes in the spectra

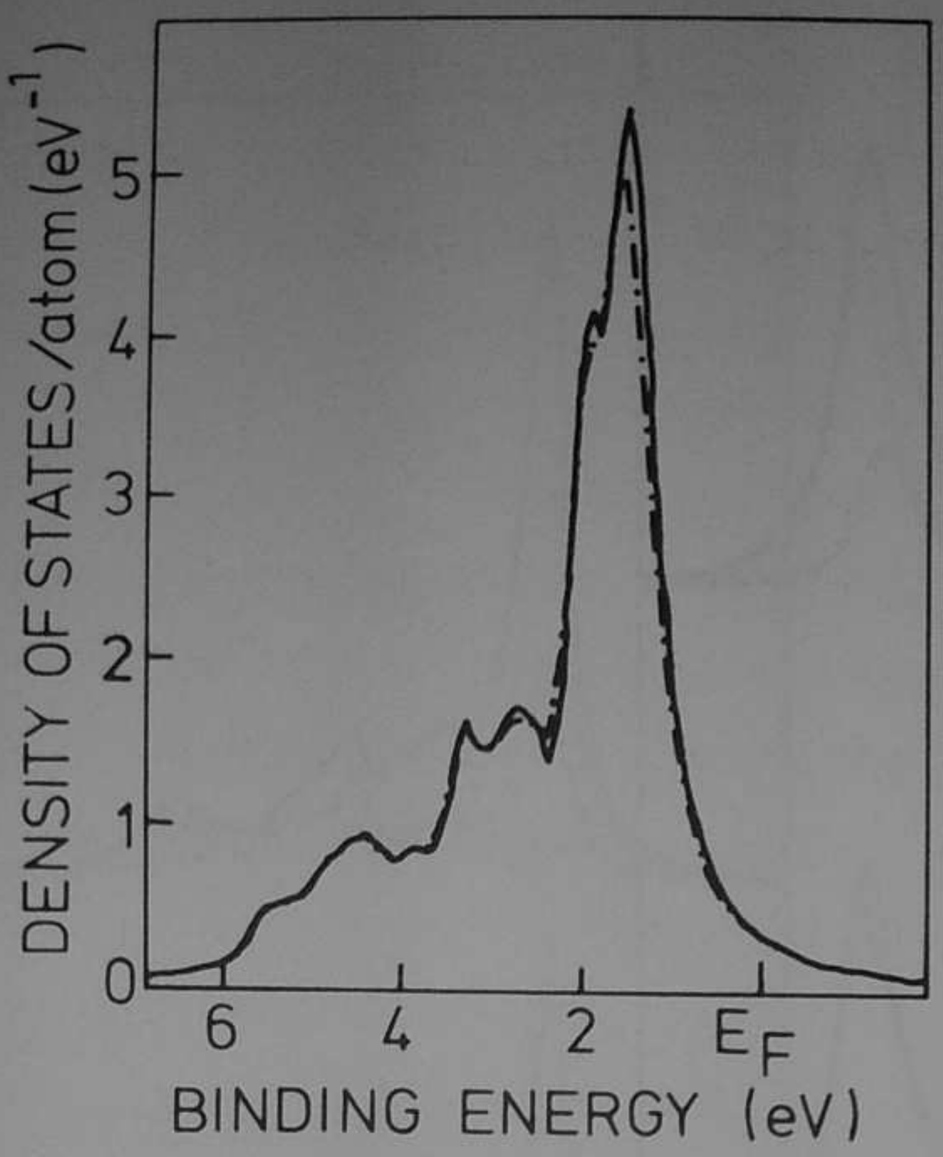

Fig. 5.19. Local d-DOS at a Pt site in CuPt using degenerate (dash-dotted) and non-degenerate (solid) theory.

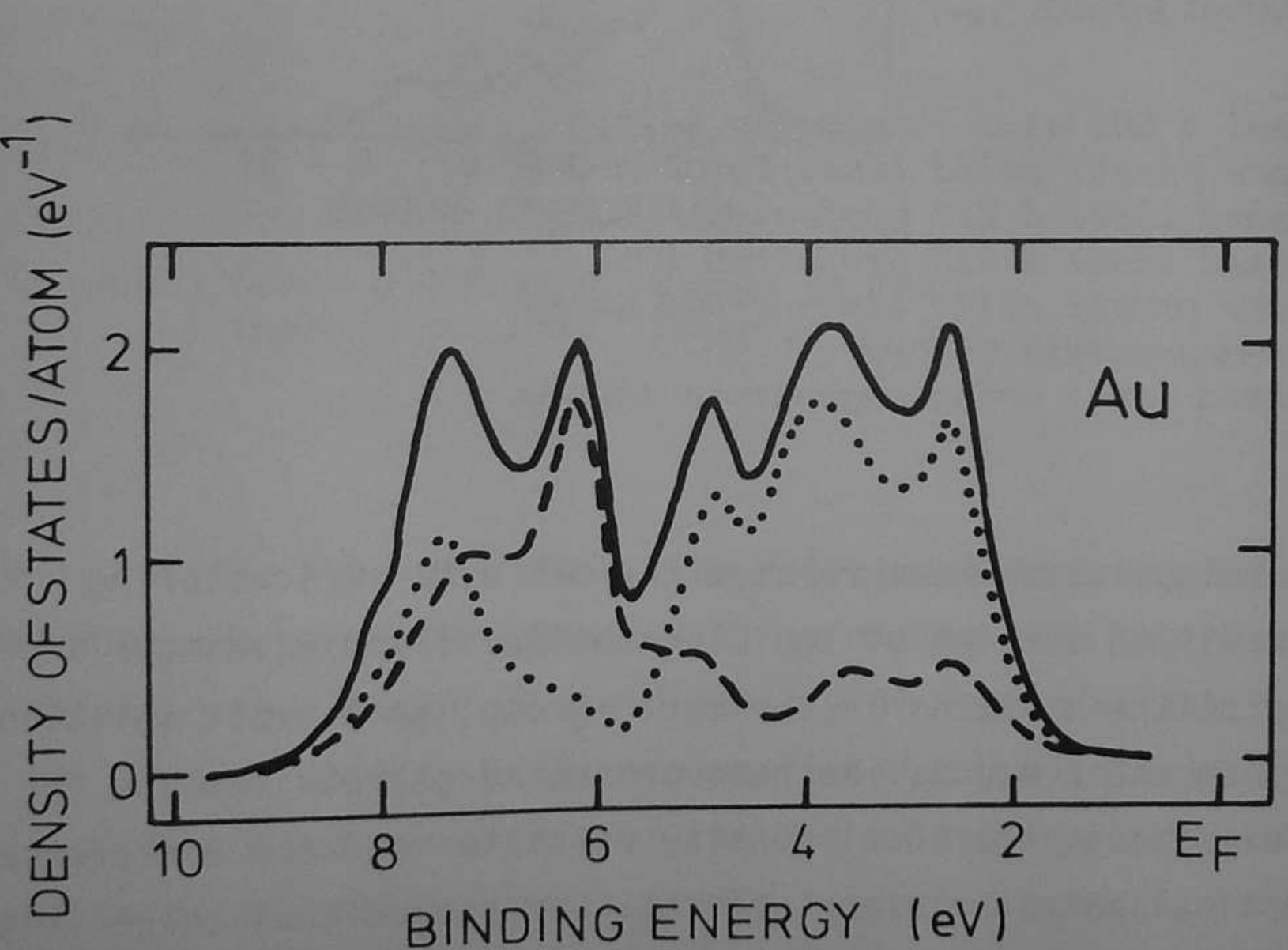

Fig. 5.20. Density of states of gold.
Solid line: Total d density of states.
Dashed line: d 3/2 projected DOS.
Dotted line: d 5/2 projected DOS.

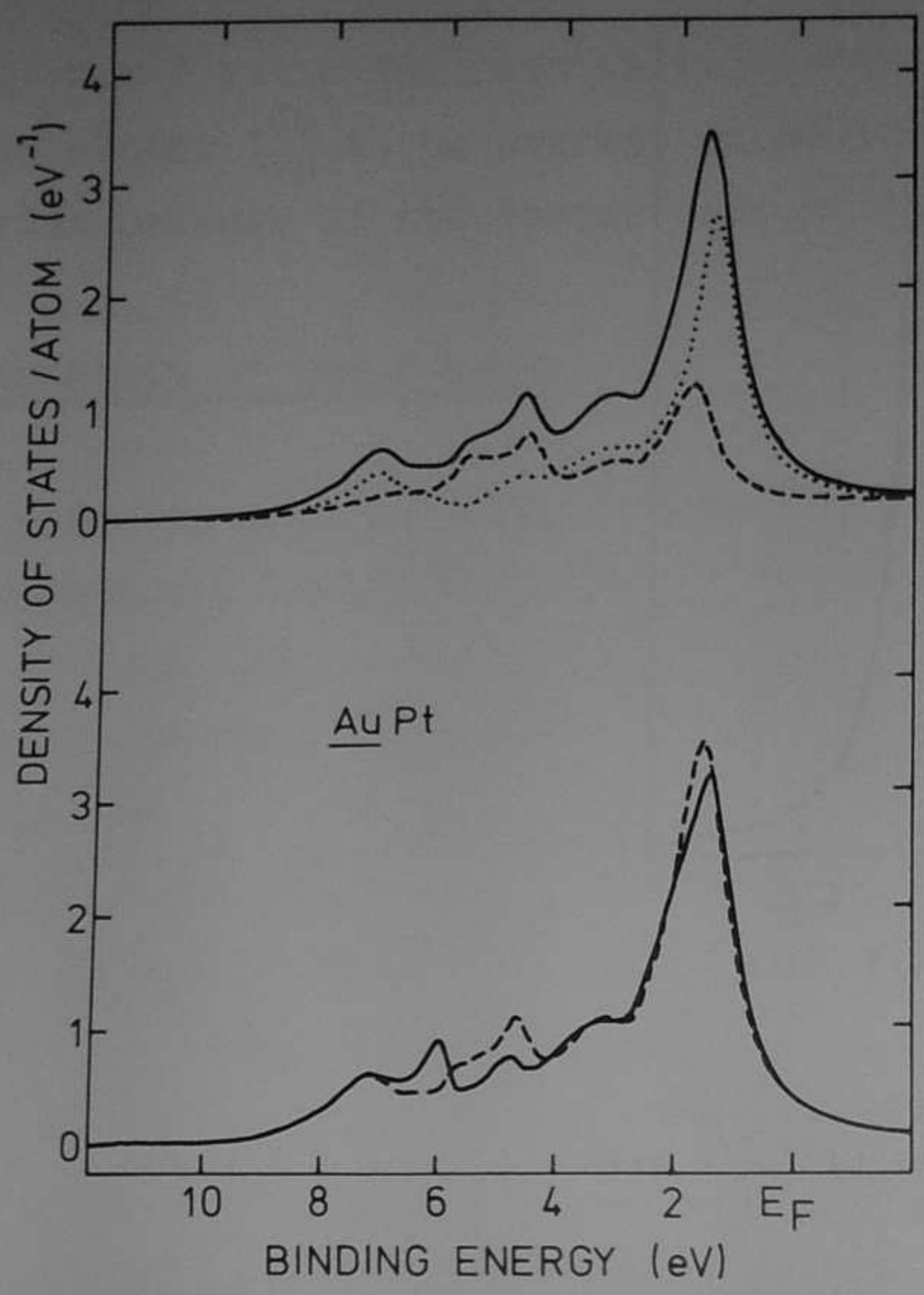

Fig. 5.21. Local d DOS at a Pt site in AuPt.
Upper panel: solid line: Total d-DOS,
dashed line: d 3/2 projected DOS,
dotted line: d 5/2 projected DOS,
Lower panel: solid line: D-DOS using non-degenerate theory.
dashed line: using degenerate theory.

using difference techniques. We have related the UPS data to scattering properties using a modified version of the Clogston-Wolff and Riedinger approaches, including degeneracy of the d states in the cubic group, spin-orbit splitting and coupling to the host sp and d bands. We have presented expressions for the difference density of states, the local density of states and the difference UPS spectra including optical matrix element effects. We showed that there is good agreement between this theory and experiment allowing us to obtain the bare impurity state energies, the spin orbit and crystal field parameters, the virtual bound state broadening due to the mixing with the sp band and the influence of the

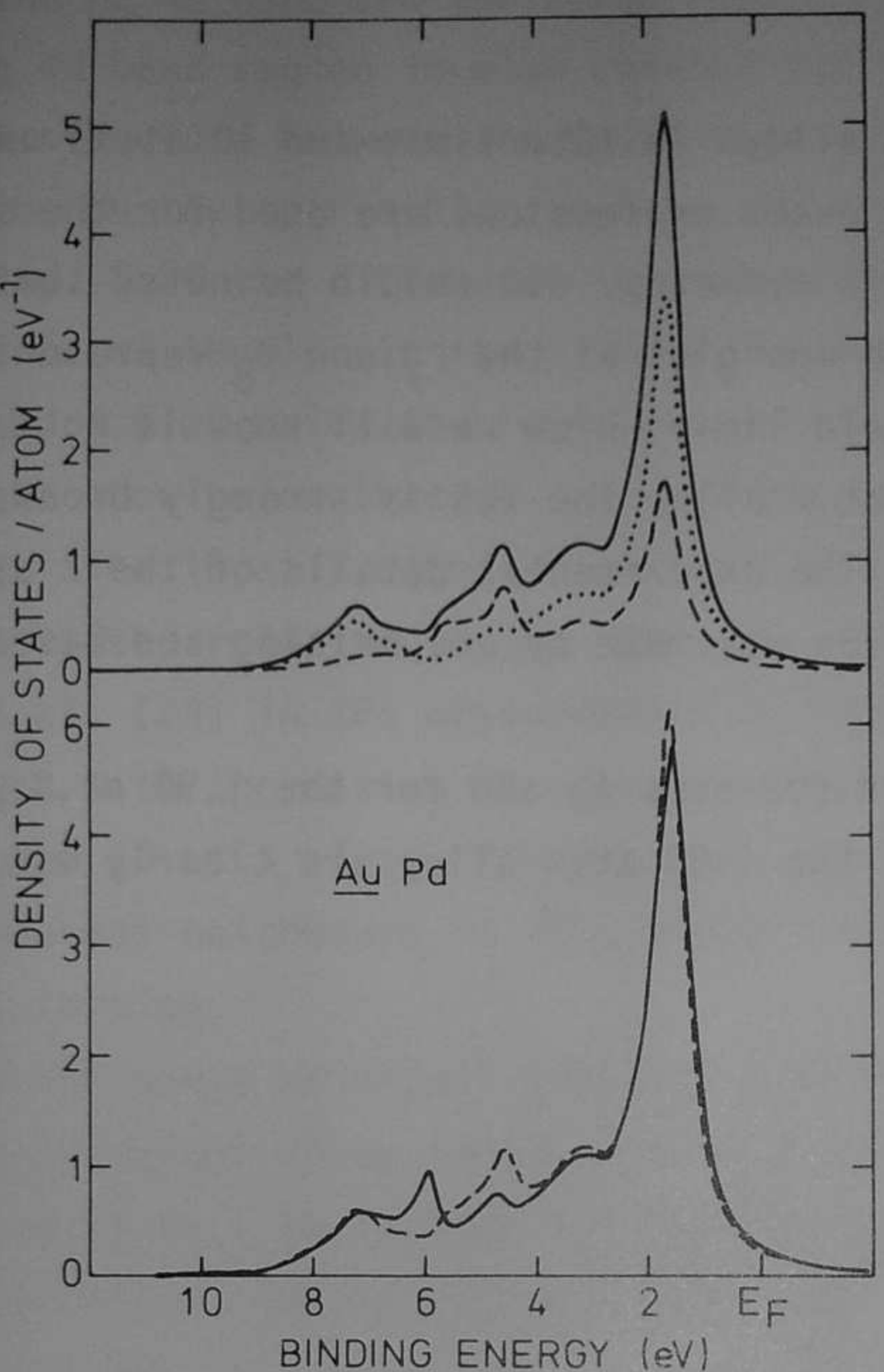

Fig. 5.22. Local d DOS at a Pd site in AuPd.
Dashed and dotted lines as in Fig. 5.21.

impurity-d host-d hybridization. The calculated impurity local density of states using the obtained parameters shows a large mixing with the host d bands. From this we obtained the change in the d density of states at the fermi level and the related 1 = 2 phase shifts which compare favourably with transport measurement.

We also discussed the effect of lattice relaxation and demonstrated that the neglect of this can lead to qualitatively incorrect predicitons of the local density of states.

Roosler
Rasler

Appendix

We present UPS data for some AgPt alloys (dilute limit and 10 at.%) and analyse them in terms of a VBS theory in which exact expressions are used for the spin-orbit and crystal-field effects in cubic symmetry. It should be noted that the expressions given by Smith [47] for the energies of the Γ_7 and Γ_8 representations are valid only in the large crystal-field limit which we will show is not applicable to AgPt. Also we show that in the 10 at.% alloy the VBS is strongly broadened, presumably due to Pt-Pt interactions. The experimental details of the 2 at.% alloy are as in section 5.2 The 10 at.% alloy was made by arc melting and was annealed for three days at 800 °C to homogenize.

In Fig. 5.23 the spectra are shown for pure Ag and for the 1.90 at.% and 10 at.% Pt alloys. The Pt 5d peaks in the 1.90 at.% alloy are clearly visible

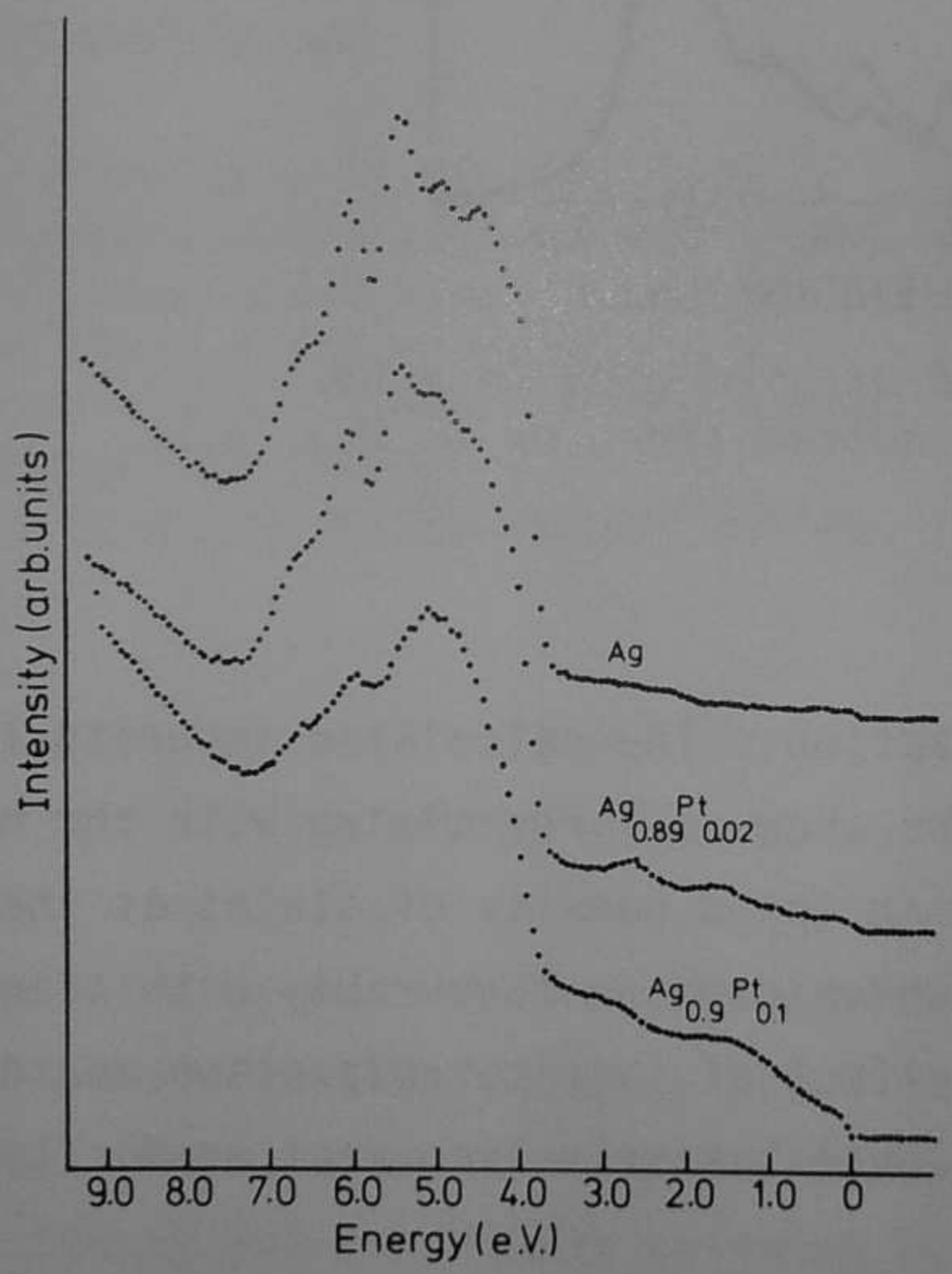

Fig. 5.23. UPS valence band spectra of pure Ag and the Ag-1.90 at.% Pt and Ag-10 at.% Pt alloys.

between the Ag 4d band and the Fermi level. In addition to these peaks, structure in the Ag 4d band region is also changed due to alloying. Here we concentrate on the extra structure between the Ag 4d band and the Fermi level, which should provide information on the spin-orbit coupling and crystal-field splitting.

In Fig. 5.24 the difference spectra are shown for an energy region up to 3.5 eV below the Fermi level. In the 1.90 at.% alloy we clearly see two peaks at about 2.65 eV and 1.6 eV below the Fermi level. The peak at about 1.6 eV is considerably broader; we show below that this is a direct consequence of the crystal-field splitting. The 10 at.% alloy also shows structure but this is strongly broadened and also shifted relative to the 'dilute' alloy. A similar shift was observed by Hüfner et al. [23] in XPS measurements of Ag-5 at.% Pt and Ag-10 at.% Pt alloys. The changes with increasing Pt concentration are probably a result of Pt-Pt contacts. For a random 10 at.% alloy, for example, the probability that a Pt atom has one or more nearest neighbours is 72%, whereas for the 1.90 at.% alloy it is only 12% for a FCC lattice.

From the above we expect that the 1.90 at.% alloy spectrum can be analyzed according to dilute alloy theory. We consider the Pt 5d states to be embedded in the sp band of Ag. We neglect for now the interactions with the Ag 4d states. This interaction is not completely negligible but in section 5.3 we have already seen that it does not strongly affect the width or splittings of the peaks.

To describe the difference spectra in terms of spin-orbit coupling, crystal-field splitting and hybridization with the Ag sp band, we assume that the difference spectrum is proportional to the Pt 5d local density of states. This is justified because the Ag sp band density of states is quite flat in this energy region, so it will hardly change upon alloying, and also the photoemission cross section for the Pt 5d electrons for He I radiation is orders of magnitude larger than that for Ag sp electrons.

We first consider the Pt 5d one-electron states including spin-orbit coupling and a cubic crystal-field splitting. In the O_h double group the irreducible representations spanned by the states of a d electron are Γ_7, Γ_8 and $\Gamma_{8'}$, which are twofold and fourfold degenerate, respectively. Neglecting first the spin-orbit coupling, the irreducible representations in crystal-field notation are then $\Gamma_7(t_{2g})$, $\Gamma_8(t_{2g})$ and $\Gamma_8(e_g)$. The spin-orbit interaction has matrix elements given by

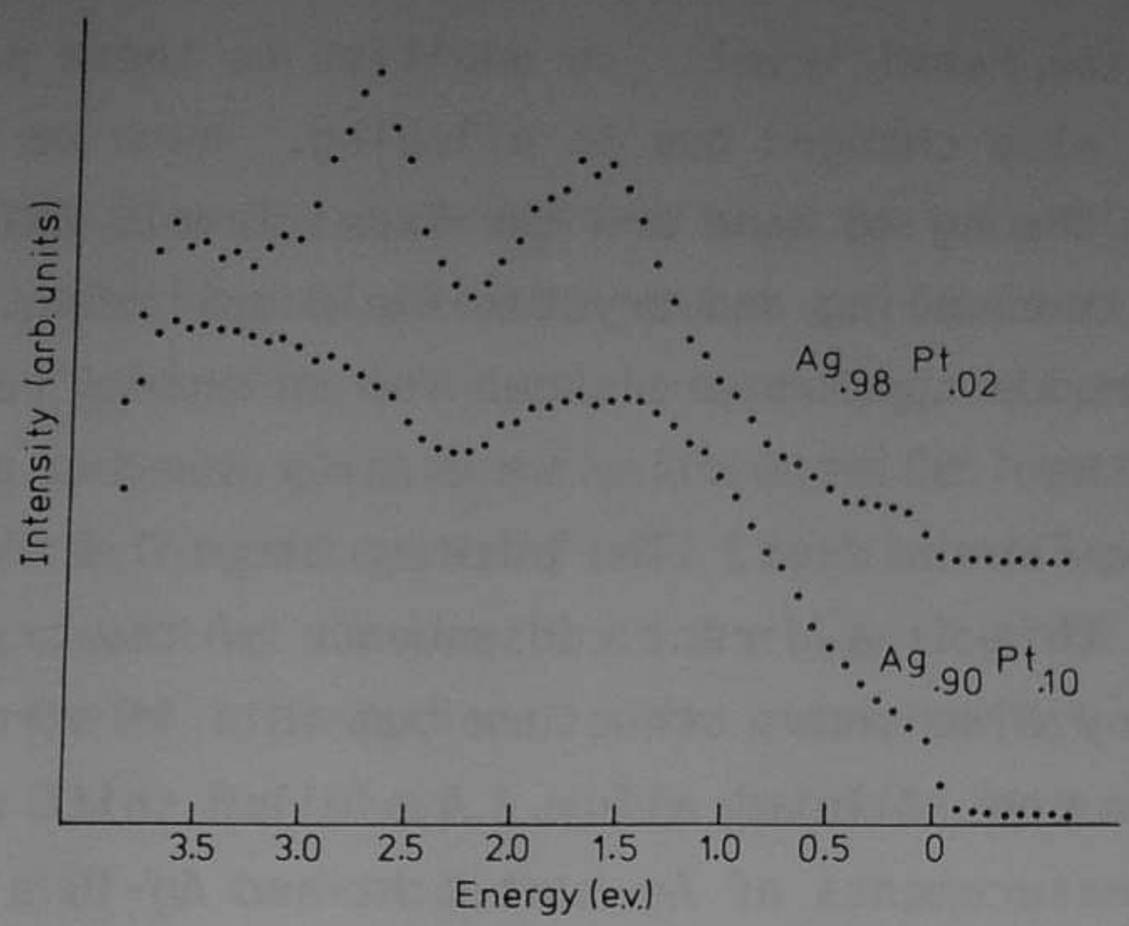

Fig. 5.24. Difference spectra (alloy - pure Ag) for the Ag-1.90 at.% Pt and Ag-10 at.% Pt alloys.

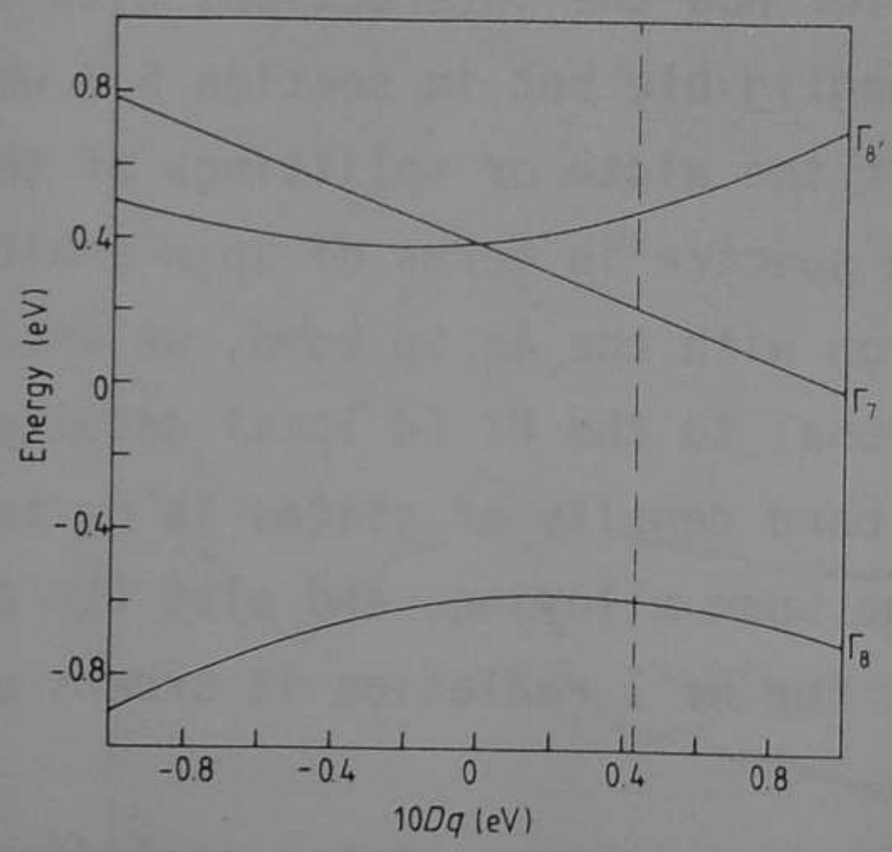

Fig. 5.25. Calcualted splitting of the Γ_7, Γ_8 and $\Gamma_{8'}$ levels with a spin-orbit coupling ξ of 0.39 eV as a function of the crystal-field splitting parameter. The broken line shows approximately the experimental value of the crystal-field splitting.

$$H_{SO}\Gamma_8^n(t_{2g}) = \frac{1}{2}\xi T_8^n(t_{2g}) + \xi\sqrt{3/2}\Gamma_8^n(e_g)$$

$$H_{SO}\Gamma_7^n(t_{2g}) = \xi T_7^n(t_{2g})$$

$$H_{SO}\Gamma_8^n(e_g) = \xi\sqrt{3/2}\Gamma_8^n(t_{2g})$$

resulting in energies

$$E(\Gamma_7) = -4Dq + \xi$$

$$E(\Gamma_8) = Dq - \frac{1}{4}\xi \pm \frac{1}{2}[(10Dq + \frac{1}{2}\xi)^2 + 6\xi^2]^{1/2}$$

where 10Dq is the crystal-field splitting parameter and ξ is the spin-orbit coupling constant. In Fig. 5.25 the energies for the three representations are shown for ξ = 0.39 eV as functions of 10Dq.

The interpretation of the experimental spectrum (which differs strongly from the theoretical spectrum of Smith [47]) now becomes clear. The broader, and in total more intense, structure at 1.6 eV must involve in total more states than the peak at 2.65 eV, suggesting an assignment to the upper Γ_7 and $\Gamma_{8'}$ states of Fig. 5.25. It should be noted that the extra broadening could not be due to a surface component shifted in energy since then the peak at 2.65 eV would have been broadened in the same way. The peak at 2.65 eV must then originate from the lower Γ_8 state of Fig. 5.25. We obtain a satisfactory fit taking 10 Dq = 0.43 eV and ξ = 0.39 eV, splitting the broader structure into two peaks at 1.50 and 1.80 eV. The screening charges obtained by integrating the Lorentzians up to ε_F are 3.89, 1.92 and 3.81 for Γ_8, Γ_7 and $\Gamma_{8'}$, respectively. Fig. 5.26 shows the theoretical curve for the above parameters assuming a Lorentzian line shape for each component with a full width at half maximum (FWHM) of 0.45 eV and intensity proportional to the degeneracy. The separate contributions of the three components are also shown. For comparison with the experimental spectrum, a linear background was added to the calculated spectrum to account for inelastically scattered electrons.

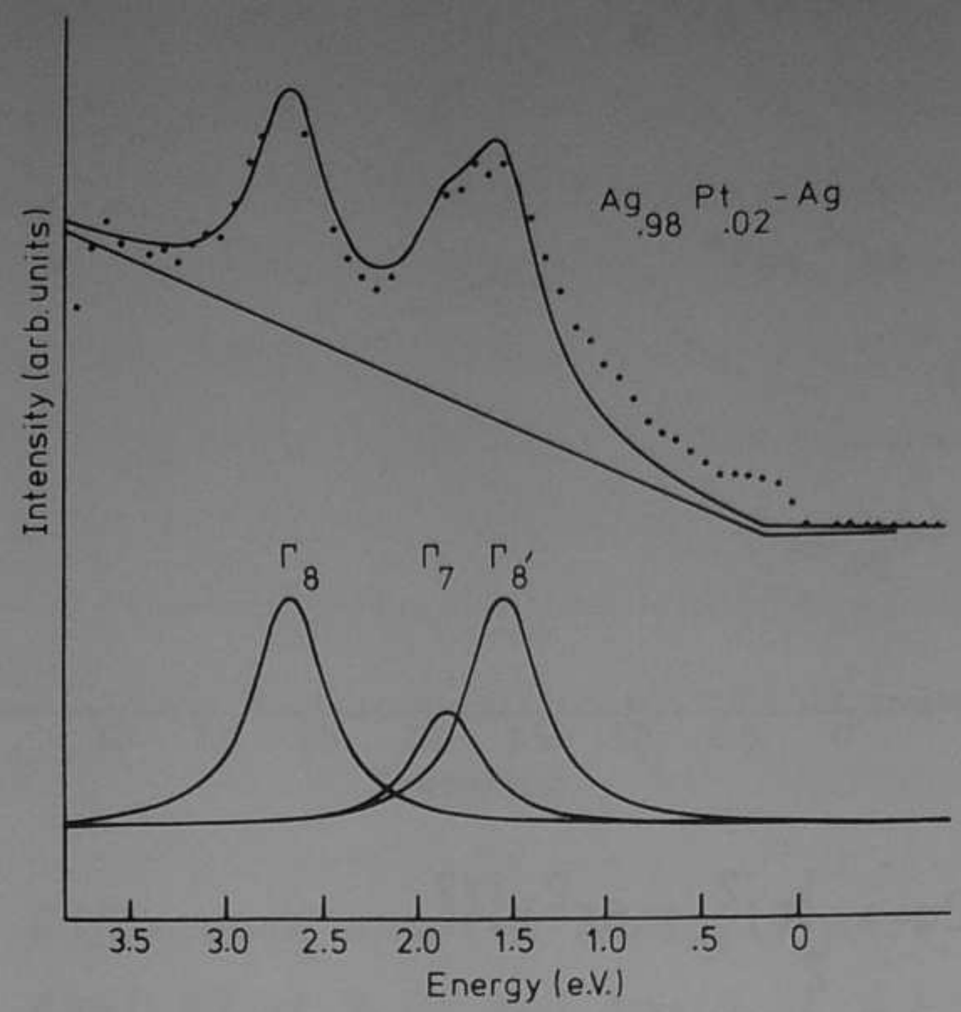

Fig. 5.26. Comparison of the experimental (dots) 1.90 at.% alloy data with the theoretically simulated spectrum (full curve). Also shown are the separate contributions of the three irreducible representations. The parameters used are ξ = 0.39 eV, 10 Dq = 0.43 eV and FWHM = 0.45 eV.

We see that the main features of the spectrum are well represented by the simple 'quasi-atomic' theory. The discrepancy observed close to the Fermi level may be due, at least in part, to Pt atoms with Pt nearest neighbours. In comparing with the 10 at.% alloy, we observe that the relative intensity close to the Fermi level increases with an increase in the number of Pt-Pt contacts.

The observed spin-orbit coupling is only slightly smaller than the spectroscopic value (0.42 eV) found for Pt [49]. A small reduction is expected because of the mixing with the Ag 4d band, which causes a larger shift towards the Fermi level of the 3/2 component than of the 5/2 component.

The crystal-field splitting is a factor of ten larger than the values Smith [35] found for Pt metal (0.023 eV) by means of interpolation. In both cases 10Dq is positive, which places the e_g levels closer to the Fermi level than the t_{2g}. It should be noted that changing the sign of 10Dq would place the twofold degenerate Γ_7

level closer to the Fermi level than the Γ_8 level and this would not fit the experimental spectrum.

References

1. J. Friedel, Nuovo Cim. Suppl. 7, 287 (1958).
2. P.W. Anderson, Phys. Rev. 124, 41 (1961).
3. Grüner and Zawadowski, Rep. Prog. Phys. 37, 1497 (1974).
4. A. Bosch, H. Feil, G.A. Sawatzky and J.A. Julianus, J. Phys. F 14, 2225 (1984).
5. P.J. Braspennig, R. Zeller, A. Lodder and P.H. Dederichs, Phys. Rev. B 29, 703 (1984).
6. J.S. Faulkner and G.M. Stocks, Phys. Rev. B 21, 3222 (1980).
7. G.M. Stocks and H. Winter, Z. Phys. B 46, 95 (1982).
8. H. Winter, P.J. Durham and G.M. Stocks, J. Phys. F 14, 1047 (1984).
9. A.J. Pindor, W.M. Temmerman, B.L. Gyorffy and G.M. Stocks, J. Phys. F 10, 2617 (1980).
10. A.M. Clogston, B.T. Matthias, M. Peter, H.J. Williams, E. Corenzwit and R.J. Sherwood, Phys. Rev. 125, 541 (1962).
11. B. Velicky, S. Kirkpatrick and M. Ehrenreich, Phys. Rev. 175, 747 (1968).
12. R. Riedigner, J. Phys. F 1, 392 (1971).
13. F. Gautier, J. Phys. F 1, 382 (1971).
14. D. van der Marel, G.A. Sawatzky, F.U. Hillebrecht, Phys. Rev. Lett. 53, 206 (1984).
15. D. van der Marel, C. Westra, G.A. Sawatzky and F.U. Hillebrecht, Phys. Rev. B 14, (1985).
16. J.A. Julianus, A. Myers, F.F. Bekker, D. van der Marel and E.F. Allen, J. J. Phys. F 15, 111 (1985).
17. A. Bosch, H. Feil and G.A. Sawatzky, J. Phys. E 17, 1187 (1984).
18. D.E. Eastman, J.A. Knapp and F.J. Himpsel, Phys. Rev. Lett. 41, 825 (1978).
19. The AuPd (4.5%), AuPt (4.5%), AgPd (3%) and AgPt (2%) samples were supplied by Dr. A. Myers and co-workers for which we want to express our gratitude.
20. J.L. Gardner and J.A.R. Samson, J. Electron Spectrosc. 6, 53 (1975).
21. A.D. McLachlan, J.G. Jenkin, R.C.G. Leckey and J. Liesegang, J. Phys. F 5,

2415 (1975).
22. D. van der Marel, G.A. Sawatzky and J.A. Julianus, J. Phys. F 14, 281 (1984).
23. S. Hüfner, G.K. Wertheim and J.H. Wernick, Solid State Commun. 17, 1585 (1975).
24. N. Mårtensson, R. Nyholm, M. Calén and J. Hedman, Phys. Rev. B 24, 1725 (1981).
25. R.S. Rao, A. Bansil, H. Asonen and M. Pessa, Phys. Rev. B 29, 1713 (1984).
26. G.S. Sohal, R.G. Jordan and P.J. Durham, Surface Science 152, 205 (1985).
27. C. Norris and L. Walldén, Solid State Commun. 7, 99 (1969).
28. V.V. Nemoshalenko, M.G. Chudinov, V.G. Aleshin, Y.N. Kucherenko, L.M. Sheludchenko, Solid State Commun. 16, 755 (1975).
29. C.R. Helms and D. Collins, Solid State Commun. 17, 459 (1975).
30. G.G. Kleiman, V.S. Sundaram and M.B. de Moraes, Phys. Rev. B 23, 3177 (1981).
31. C. Norris and P.D. Nilsson, Solid State Commun. 6, 649 (1968).
32. P. Weightman and P.T. Andrews, J. Phys. C 13, L815 (1980).
33. S. Hüfner and G.K. Wertheim, Phys. Lett. 51A, 299 (1975).
34. E. Antonides and G.A. Sawatzky, Inst. Phys. Conf. Ser. 39, 134 (1978).
35. N.V. Smith, Phys. Rev. B 3, 1862 (1971);
N.V. Smith, G.K. Wertheim, S. Hüfner and M.M. Traum, Phys. Rev. B 10, 3197 (1974).
36. R. Zeller and P.J. Braspennig, Solid State Commun. 42, 701 (1982).
37. J.A. Julianus, F.F. Bekker and P.F. de Châtel, J. Phys. F 14, 2061 (1984); ibid. 14, 2077 (1984).
38. E.F. Bekker and N. Zuiderbaan, Physica B 85, 113 (1976).
39. A.B. Callender and S.E. Schnatterly, Phys. Rev. B 7, 4385 (1973).
40. G.M. Stocks, W.M. Temmerman and B.L. Gyorffy, Phys. Rev. Lett. 41, 339 (1978).
41. P. Weightman, P.T. Andrews, G.M. Stocks and M. Winter, J. Phys. C 16, L 81 (1983).
42. M. Davies, P. Weightman, J. Phys. C 17, L 1015 (1984).
43. M. Vos, D. van der Marel and G.A. Sawatzky, Phys. Rev. B 15, 3073 (1984).
44. M. Vos, G.A. Sawatzky, P. Weightman and P.T. Andrews, Solid State Commun., 52, 159 (1984).
45. J. Stöhr, G. Apai, P.S. Wehner, F.R. McFeely, R.S. Williams and D.A. Shirley, Phys. Rev. B 14, 5144 (1976).
46. N.E. Christensen, J. Phys. F 8, L51 (1978).

47. P.V. Smith, J. Phys. F 11, 1207 (1981).
48. C.J. Ballhausen, "Introduction to Ligand Field Theory" (New York, McGraw Hill, 1962).
49. C.E. Moore, "Atomic Energy Levels", NBS Circular No. 467 (1949).

CHAPTER VI

ELECTRONIC STRUCTURE OF Mn IMPURITIES IN NOBLE METALS

Various electron-spectroscopy techniques are used to determine the electronic structure of Mn impurities in Ag and Cu. The spectral distributions of both minority- and majority-spin impurity d states are determined experimentally and compared to model calculations considering the photoemission matrix elements. The exchange and Coulomb integrals and energetic positions of the impurity d states as well as the impurity-host d-s and d-d hybridizations are determined. We find that the impurity minority-spin states are quite wide and lie close to the Fermi level, which raises questions concerning the validity of the use of a Kondo Hamiltonian to determine the low-energy scale properties. In addition, the hybridization of the majority-spin states with the host d band is larger, causing these to delocalize, whereas the magnetic moment remains localized. This large hybridization can introduce new exchange mechanisms not foreseen in conventional models. The indirect exchange processes that give rise to magnetic ordering between impurities are treated with Brillouin-Wigner theory, summing over the perturbational expansion in the spirit of $1/N_f$ theory. It is shown, that certain anti-ferromagnetic interaction terms are of comparable size relative to the RKKY interaction. This is a direct consequence of the non-applicability of the Schrieffer-Wolff transformation to the AgMn and CuMn cases.

6.1. Direct Observation of the Exchange-Split Virtual Bound State in Dilute Mn Alloys

D. van der Marel and G. A. Sawatzky
Physical Chemistry Department of the Material Science Center, University of Groningen, 9747 AG Groningen, The Netherlands

and

F. U. Hillebrecht
Institut für Festkörperforschung der Kernforschungsanlage Jülich GmbH, D-5170 Jülich, West Germany

(Received 9 January 1984)

The majority- and minority-spin states of the exchange-split virtual bound state of Mn impurities in Cu and Ag are studied with high-resolution photoemission and bremsstrahlung isochromat spectroscopy. The exchange splitting is found to be close to the atomic value. The majority-spin state is strongly hybridized with the host-metal *d* band resulting in its delocalization. The minority-spin states are localized but close to the Fermi level so that a description of the physical properties in terms of a spin Hamiltonian is not appropriate.

PACS numbers: 71.20.+c, 71.70.Gm, 75.20.Hr, 79.20.Kz

During the past decades the alloys of 3*d* transition-metal impurities dissolved in a noble-metal matrix have attracted considerable attention of theoreticians and experimentalists. Much work has been done on the Kondo[1] and spin-glass properties,[2] the latest theoretical developments[3,4] being the solution of the Kondo and Anderson[5] Hamiltonians and the development of fast-converging perturbation theories.[6] Although these theories treat the many-body effects on a high level of sophistication, they use model Hamiltonians, the validity of which depends on the relative magnitudes of the various parameters. They also lack a proper description of the band-structure details, especially the occurrence of the strong *d* resonance in the noble metals. In recent embedded-cluster[7] and coherent-potential-approximation[8] *ab initio* calculations these band-structure details are included, but exchange correlation is treated in the local density approximation.

The Mn atom is known to have an effective magnetic moment of about $5\mu_B$ even in solid solution in noble metals.[9,10] Therefore it is probably one of the most beautiful examples of a transition-metal atom with a spin-split state consisting qualitatively of a full majority- and an empty minority-spin *d* shell.

The alloys *Ag*Mn and *Cu*Mn have been investigated extensively by means of a large variety of experimental techniques. For the interpretation of the experimental results one has resorted to the use of a Kondo Hamiltonian for which one implicitly assumes that the impurity has only spin degrees of freedom. Or, in other words, one has assumed that the Schrieffer-Wolff[11] transformation of the Anderson Hamiltonian is valid. This transformation is valid if $r_\pm = \Delta_\pm/\epsilon_\pm \ll 1$, where Δ is the half-width of the virtual bound state and $\epsilon_\pm$ is its position relative to the Fermi level; $\pm$ here denote the majority- and minority-spin states.

Although several photoemission studies have been reported,[12-14] we present the first direct measurement of the unoccupied impurity-induced density of states for *Ag*Mn and *Cu*Mn as well as high-resolution photoemission data for the occupied states. We obtain values for the above-mentioned parameters and compare these to theoretical calculations. We conclude that the validity of the Schrieffer-Wolff transformation is highly questionable and that the majority states are delocalized, whereas the minority states are localized as found in Heusler alloys.[15]

The polycrystalline *Ag*Mn samples (5% and 10%) were obtained from the melt and examined metallographically for the presence of secondary phases. The polycrystalline *Cu*Mn samples (1.5%, 5%, 10%, and 15%) were supplied by the University of Leiden group.[16]

The bremsstrahlung-isochromat spectroscopy (BIS) and ultraviolet-photoelectron spectroscopy (UPS) equipment is described elsewhere[17,18] and was operated at resolutions of 0.85 eV and 90 meV, respectively. The base pressure in both chambers was less than 5×10^{-11} Torr. The samples were treated with either Ar-ion etching or scraping, and surface composition was checked with x-ray photoelectron spectroscopy and Auger-electron spectroscopy.

The UPS spectra were corrected for the He I satellite of 23.09 eV and an intensity of 0.017 relative to the main line at 21.22 eV. The energy grids were 0.02 and 0.1 eV for UPS and BIS. The UPS difference spectra were obtained by subtracting the scaled spectra.[19] The BIS difference spectra were obtained

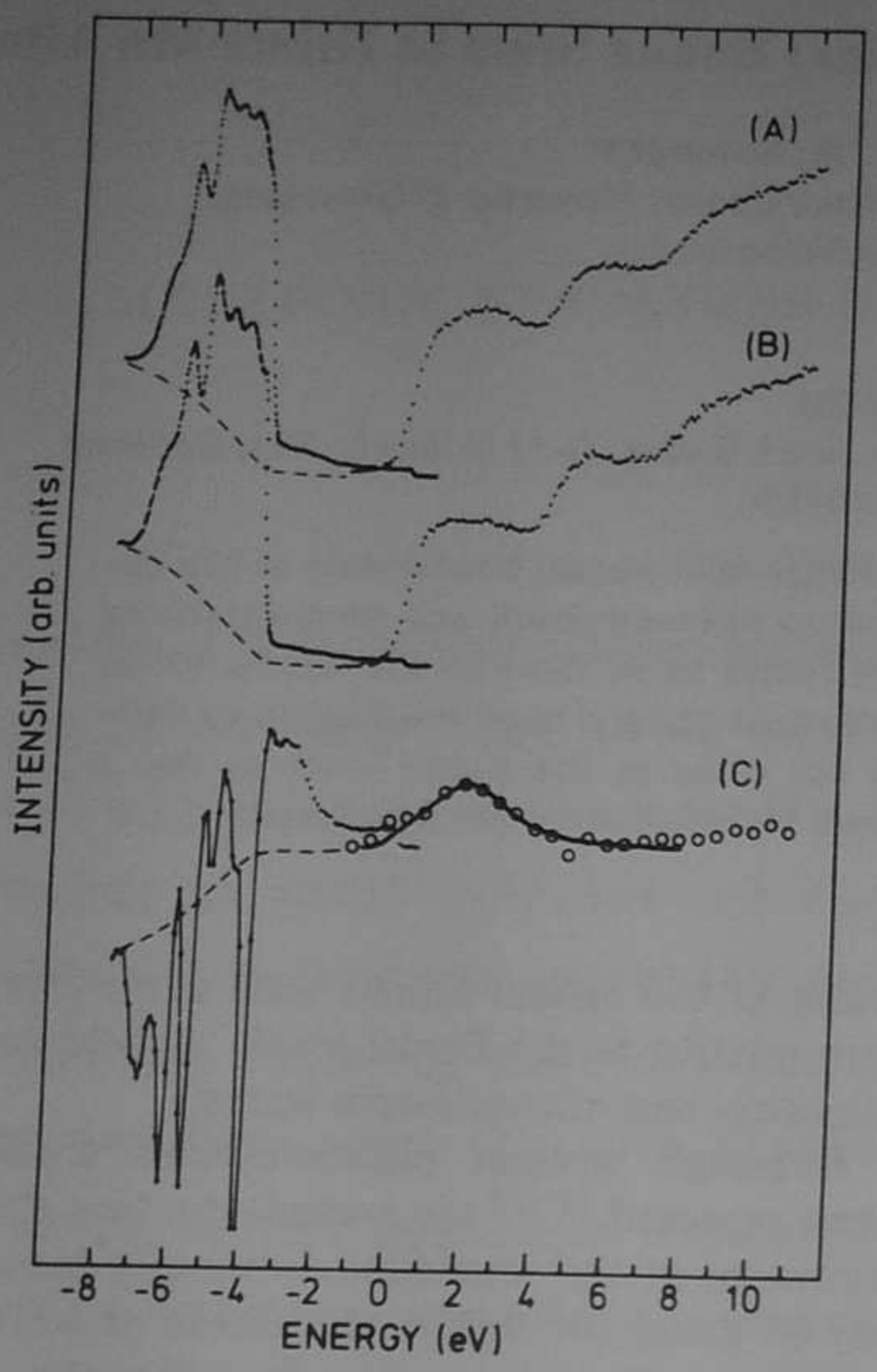

FIG. 1. Curve *A*, $Ag_{0.95}Mn_{0.05}$ UPS (left) and BIS (right). Curve *B*, Ag UPS and BIS. Curve *C*, the dots are the UPS difference spectra; for clarity only the average of five consecutive data points is shown. The thin solid line serves as a guide to the eye. The circles are the BIS difference spectra. The solid line is the fit discussed in the text. All energies are relative to E_F. The dashed lines are the secondary electron contributions to the spectra.

by scaling to equal intensity at 10 eV and subtracting.

The corrected UPS and BIS spectra of Cu, Ag, $Cu_{0.9}Mn_{0.1}$, and $Ag_{0.95}Mn_{0.05}$ are shown in Figs. 1 and 2 together with the difference spectra. The structure in the pure-metal BIS spectra has been discussed elsewhere.[20] In the alloy spectra additional structures are observed, the intensity of which is proportional to the Mn concentration.[21] We therefore interpret these structures as the Mn-impurity–induced difference in the spectral distribution. The BIS difference spectra show a Lorentzianlike peak just above the Fermi level which we interpret as the minority-spin Mn *d* states. These difference spectra were fitted with a single Lorentzian peak cut off at the Fermi level and convoluted with a 0.85-eV full width at half maximum Gaussian (solid line in Figs. 1 and 2). The Gaussian broadening is due to the experimental resolution and was determined from the Fermi-level-cutoff part of the spectrum of the pure metals. The minority-spin peak position and Lorentzian broadening are given in Table I.

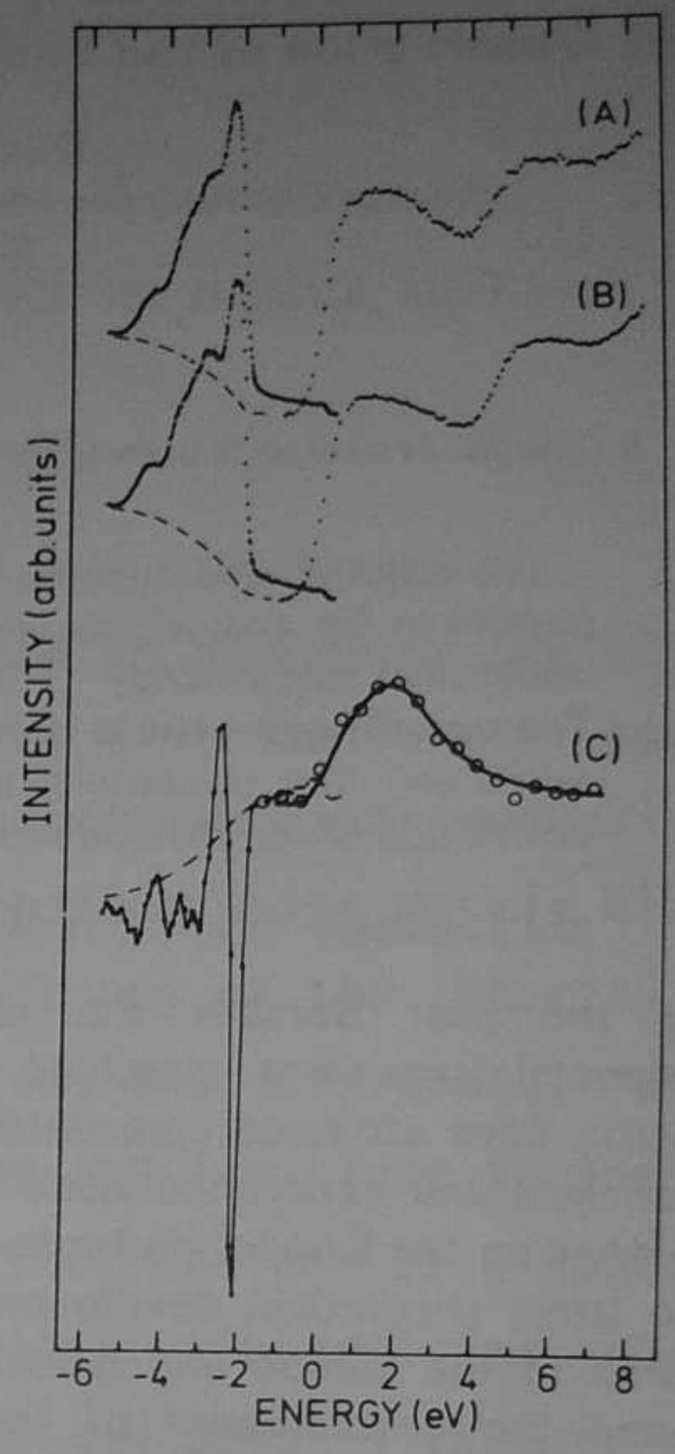

FIG. 2. Curve *A*, $Cu_{0.9}Mn_{0.1}$ UPS (left) and BIS (right). Curve *B*, Cu UPS and BIS. Curve *C*, difference spectra with dots and lines as in Fig. 1.

The UPS difference spectra show in addition to structure just below the Ag *d* band in *Ag*Mn a lot of structure within this band. The positive contribution at about −3 eV in *Ag*Mn is due to the majority-spin Mn *d* states. The strong structure in the Ag *d* band is due to two effects: firstly a dilution effect (i.e., removal of Ag)[20] and secondly the presence of Mn *d* density of states in the Ag *d* band due to hybridization. For the *Cu*Mn alloys the situation is even more complicated because no extra structure outside of the Cu *d* band is observed. The majority-spin Mn *d* state must therefore lie inside the Cu *d* band. This is not surprising since we expect the majority-spin state in Cu and Ag hosts to be at approximately the same position, which, with use of the *Ag*Mn value, would put it in the center of the Cu *d* band. This is also suggested by comparison of the positions of the minority-spin *d* states in *Cu*Mn and *Ag*Mn.

TABLE I. Most symbols are discussed in the text. $n_\pm$ is the occupancy of the impurity majority and minority states. In this work it is obtained by integrating the Lorentzian distributions up to E_F. P_{eff} is obtained with the assumption that $P_{eff}=g[S(S+1)]^{1/2}$ with $S=\frac{1}{2}(n_+-n_-)$. References (b), (d), and (f) give theoretical data. References (e) give optical data, interpreted *a posteriori*.

	ϵ_+ (eV)	Δ_+ (eV)	n_+	r_+	ϵ_- (eV)	Δ_- (eV)	n_-	r_-	$P_{eff}(\mu_B)$
*Cu*Mn[a]	. . .	. . .	~5	. . .	1.7 ±0.2	1.4 ±0.2	1.1 ±0.1	0.82	4.8
*Cu*Mn[b]	. . .	. . .	5.0	. . .	0.79[c]	0.8[c]	1.6	1.01	4.3
*Cu*Mn[d]	−3.5[c]	0.16[c]	4.9	0.05	0.8[c]	0.64[c]	1.0	0.8	4.8
*Ag*Mn[e]	−3.25	. . .	. . .	. . .	1.6	. . .	. . .	. . .	. . .
*Ag*Mn[a]	−3.1 ±0.2	0.7 ±0.1	4.65 ±0.2	0.23	2.1 ±0.2	1.2 ±0.1	0.83 ±0.1	0.57	4.7
*Ag*Mn[f]	−2.6[c]	~0.2[c]	~5.0[c]	0.07	~0.7[c]	~0.6[c]	~1.1[c]	0.86	4.80

[a]This work.
[b]Ref. 7.
[c]Estimated from the figures.
[d]Ref. 22.
[e]Refs 13 and 23.
[f]Ref. 8.

The absence of a clear peak in the UPS part of the difference spectrum of *Cu*Mn indicates that the majority-spin Mn *d* state is spread out over the whole Cu *d* band. A more detailed analysis suggesting this conclusion in terms of model calculations will be presented elsewhere.[21] Here we make the qualitative observation that the majority-spin Mn *d* state in *Cu*Mn is strongly delocalized because of hybridization with the Cu *d* band. A similar effect, but less severe, is found for *Ag*Mn. The position and half-width of the majority-spin impurity state in *Ag*Mn can be determined and are also given in Table I. The energy splitting between the majority- and minority-spin states is found to be 5.2 eV for *Ag*Mn which is considerably larger than the value obtained from first-principles calculations (3.5 eV).[7,8]

It is interesting to compare the observed energy splitting to atomic values. If we assume the ground state to be nominally $d^5\,{}^6S$, the energy splitting is

$$|E_-|+|E_+|=E(d^4\,{}^5D)+E(d^6\,{}^5D)-2E(d^5\,{}^6S)$$
$$=F^0+\tfrac{4}{14}(F^2+F^4)$$

according to Slater's atomic table.[24] This is, in a more commonly used notation for magnetic impurities, identical to $U+4J$. From Auger spectra we can also determine the energy of a $d^3({}^4F\,{}^4P)$ state,[25] from which we find $F^0\simeq\frac{1}{14}(F^2+F^4)$ or $U\simeq J$. Using the values of Table I for ϵ_- and ϵ_+ we get $F^0\simeq 1$ eV and $\frac{1}{14}(F^2+F^4)\simeq 1$ eV. The free-atom values are[26] $F^0\simeq 22$ eV and $\frac{1}{14}(F^2+F^4)\simeq 1.2$ eV showing again[27-29] that F^0 or U is strongly reduced from the free-atom value but the term splittings remain atomiclike.

As mentioned in the introduction a very important quantity to check the validity of the Schrieffer-Wolff transformation and the use of a spin Hamiltonain to treat the problem is $r_\pm$. This quantity is also listed in Table I. We see that the condition $r\ll 1$ is not really fulfilled for either *Cu*Mn or *Ag*Mn. This is mainly because the minority-spin state is so close to the Fermi energy. The consequence of this could only be determined by investigating the higher-order terms in the Schrieffer-Wolff transformation.

Using a Lorentzian fit to the spectra we can determine the occupation of the majority- and minority-spin bands as given in Table I. The average magnetic moment is found to be $4.72\mu_B$ for *Ag*Mn which agrees well with measured values ranging from $4.73\mu_B$ (Ref. 10) to $5.4\mu_B$.[30]

In conclusion we have shown the existence of the spin-split virtual bound state in *Cu*Mn and *Ag*Mn. The splitting is considerably larger than that given by first-principles calculations with an exchange interaction close to atomic values. The close proximity of the minority-spin state to the Fermi level suggests that the use of a spin Hamiltonian for these systems is not appropriate. The absence of a clear peak in the UPS spectrum of *Cu*Mn confirms the theoretical idea[7] that the Mn majority *d* state is strongly hybridized with the Cu *d* band. The full noble-metal *d* bands can therefore mediate a superexchange interaction between Mn impurities and may for first and second neighbors even dominate over the usually assumed Ruderman-Kittle-Kasuya-Yosida[31] mechanism.

We are grateful to Professor M. Campagna, Professor J. C. Fuggle, and J. Zaanen for stimulating discussions and to J. Keppels and A. Heeres for technical assistance. Two of us (D.v.d.M. and G.A.S.) would like to thank the Kernforschungsanlage Jülich for hospitality during their stay there.

This investigation was supported in part by the Netherlands Foundation for Chemical Research (SON), with financial aid from the Netherlands Organization for the Advancement of Pure Research (ZWO), and in part by the Kernforschungsanlage Jülich.

[1]G. Grüner and A. Zawadowski, Rep. Prog. Phys. **37**, 1497 (1974).

[2]J. A. Mydosh, J. Phys. Soc. Jpn. **52**, S85 (1983).

[3]P. Schlottmann, Phys. Rev. Lett. **50**, 1697 (1983).

[4]N. Andrei, K. Furuya, and J. H. Löwenstein, Rev. Mod. Phys. **55**, 331 (1983).

[5]P. W. Anderson, Phys. Rev. **124**, 41 (1961).

[6]O. Gunnarsson and K. Schöhammer, Phys. Rev. Lett. **50**, 604 (1983).

[7]P. J. Braspennig, R. Zeller, A. Lodder, and P. H. Dederichs, Phys. Rev. B **29**, 703 (1984).

[8]M. C. Munoz, B. L. Gyorffy, and K. Verhuyk, J. Phys. F **13**, 1847 (1983).

[9]A. F. J. Morgownik and J. A. Mydosh, Solid State Commun. **47**, 321 (1983).

[10]C. M. Hurd, J. Phys. Chem. Solids **30**, 539 (1969).

[11]J. R. Schrieffer and P. A. Wolff, Phys. Rev. **149**, 491 (1966).

[12]H. Höchst, P. Steiner, and S. Hüffner, Z. Phys. B **38**, 201 (1980); P. T. Andrews and C. E. Johnson, Phys. Lett. **70A**, 140 (1979).

[13]L. Walldén, Philos. Mag. **21**, 571 (1970).

[14]R. G. Jordan and G. S. Sohal, J. Phys. C **16**, L529 (1983).

[15]J. Kübler, A. R. Williams, and C. B. Sommers, Phys. Rev. B **28**, 1745 (1983).

[16]The *Cu*Mn samples were kindly supplied by the group of Professor J. A. Mydosh, for which we want to express our gratitude.

[17]A. Bosch, to be published, and thesis, University of Groningen, 1982 (unpublished).

[18]F. U. Hillebrecht, to be published.

[19]The scattered-electron background was first subtracted. The intensities of the corrected spectra integrated up to E_F were normalized and these normalization constants were used to scale the uncorrected spectra.

[20]D. van der Marel, G. A. Sawatzky, R. Zeller, F. U. Hillebrecht, and J. C. Fuggle, Solid State Commun. **50**, 47 (1984).

[21]D. van der Marel and G. A. Sawatzky, to be published.

[22]J. D. Cohen and C. P. Slichter, Phys. Rev. Lett. **40**, 129 (1978).

[23]H. P. Meyers, L. Wallden, and A. Karlson, Philos. Mag. **18**, 725 (1968).

[24]J. C. Slater, *Quantum Theory of Atomic Structure, Vol. I* (McGraw-Hill, New York, 1960), p. 492.

[25]Unpublished results. The Auger spectra showed that $U_{\text{eff}} \simeq 0$. Assuming the $d^5{}^6S$ atomic ground state, we derive for the Auger final states $U_{\text{eff}}({}^4F) = F^0 - \frac{1}{441} \times (72F^2 + 9F^4)$ and $U_{\text{eff}}({}^4P) = F^0 + \frac{1}{441}(63F^2 - 84F^4)$. The weighted averaging yields $U_{\text{eff}} = F^0 - \frac{1}{14}(F^2 + F^4)$.

[26]J. B. Mann, Los Alamos Scientific Laboratory Report No. LASL-3690, 1967 (unpublished).

[27]H. Haak, thesis, University of Groningen, 1983 (unpublished).

[28]J. C. Fuggle, P. Bennet, F. U. Hillebrecht, A. Lenselink, and G. A. Sawatzky, Phys. Rev. Lett. **49**, 1787 (1982).

[29]E. Antonides and G. A. Sawatzky, in *Transition Metals*—1977, edited by M. J. G. Lee, J. M. Perz, and E. Fawcett, IOP Conference Proceedings No. 39 (Institute of Physics, London, 1978), p. 134.

[30]A. K. Majumdar, V. Oestreich, and D. Wechsenfelder, Solid State Commun. **45**, 907 (1983).

[31]C. Kittel, in *Solid State Physics*, edited by H. Ehrenreich, F. Seitz, and D. Turnbull (Academic New York, 1969), Vol. 22.

6.2. Experimental and Theoretical UPS, BIS and AES spectra of Mn in Cu and Ag. Changes in the partial local and total densities of states.

6.2.1. Introduction

Mn dissolved in Ag and Cu form extensively studied systems of binary alloys. In 1951 dilute CuMn and AgMn were found to exhibit a resistivity minimum [1], which, after the discovery of the now well-known Kondo divergency, led to a flurry of both experimental and theoretical activity. Later [2], the same alloy systems were found to exhibit spin-glass behavior, which stimulated research in the more concentrated alloy systems. Because of the interesting properties of these materials, virtually the whole arsenal of experimental and theoretical techniques available to the solid-state physicist has been used to study these materials. The results obtained from these studies are discussed in several reviews [3].

A very basic question, which is, up to now, still open, concerns the validity of using the Kondo Hamiltonian to describe the ground-state properties of these systems. The Kondo Hamiltonian describes the scattering of conduction electrons by a localized spin via an exchange interaction $J(k,k')$, and is of the form

$$H = -(2N)^{-1} \sum_{k,q} J_{kq}[S_z(c^{\dagger}_{q\uparrow}c_{k\uparrow} - c^{\dagger}_{q\downarrow}c_{k\downarrow}) + S_+c^{\dagger}_{q\downarrow}c_{k\uparrow} + S_-c^{\dagger}_{q\uparrow}c_{k\downarrow}] \qquad (6.2.1)$$

The Zeeman part of this Hamiltonian gives rise to the so-called Ruderman-Kittel-Kasuya-Yosida [4] (RKKY) spin-density oscillations around the magnetic impurity, which, in turn, leads to an oscillatory indirect-exchange interaction between impurities. This type of interaction is usually assumed in studies of the spin-glass behavior, and much work has been done to determine the strength of the exchange interaction. The spin-flip-scattering terms give rise to the Korringa-like linear temperature dependence of the linewidths in NMR and ESR experiments. In addition, the spin-flip-scattering parts result in a divergence in the perturbational treatment of the conduction-electron scattering at a characteristic temperature referred to as the Kondo temperature.

In using the Kondo Hamiltonian, one assumes that the impurity has no electronic degrees of freedom corresponding to energies in the vicinity of the ground state. In other words, the occupied impurity states must be far below the Fermi level and the unoccupied states must be far above the Fermi level. The only impurity degrees of freedom left then are of spin and/or orbital nature. This

condition is derived in a more elegant manner by Schrieffer and Wolff [5], who showed that the more general Anderson Hamiltonian could be transformed to a Kondo Hamiltonian provided that $r_{\pm} = \Gamma_{\pm}/|\varepsilon_{\pm}| \ll 1$, where $\Gamma_{\pm}$ and $\varepsilon_{\pm}$ are the width and energy, respectively, of the majority-spin (+) and minority-spin (-) states.

It should be noted that even if the above conditions do not hold, it may still be possible, in certain cases, to describe the system with a Kondo-like Hamiltonian. To see whether or not this is the case, one would have to study the higher-order terms of the Schrieffer-Wolff transformation.

As we will show below, it is probably inappropriate to try to describe Mn impurities with a Kondo Hamiltonian, suggesting the use of the more general Anderson Hamiltonian. The Anderson Hamiltonian [6] in its more general form reads

$$H = \sum_{k,\sigma} \eta_{k\sigma} c^{\dagger}_{k\sigma} c_{k\sigma} + \sum_{m,\sigma} \varepsilon_d d^{\dagger}_{m\sigma} d_{m\sigma} + \sum_{k,m,\sigma} V_{km}(d^{\dagger}_m c_{k\sigma} + c^{\dagger}_{k\sigma} d_m) + \\ + \sum_{\substack{i,j,\\ k,l}} U(i,j,k,l) d^{\dagger}_i d_j d^{\dagger}_k d_l \ . \tag{6.2.2}$$

The last term describes the electronic structure of the impurity atom and consists essentially of two kinds of contributions.

(1) It describes the term splittings within the atom keeping the number of d electrons fixed (Hund's-rule coupling).

(2) It describes the Coulomb contribution to the energy required to remove or add an electron for each of the terms of the n+1 or n-1 states. In other words, it provides for the difference in the ionization potential and electron affinity for the atom. This form for the Anderson Hamiltonian is often approximated by

$$H_I = \tfrac{1}{2}(U-J) \sum_{\substack{m\neq n\\ m,n}} d^{\dagger}_{m\sigma} d_{m\sigma} d^{\dagger}_{n\sigma} d_{n\sigma} + \tfrac{1}{2}U \sum_{m,n} d^{\dagger}_{m\sigma} d_{m\sigma} d^{\dagger}_{n\underline{\sigma}} d_{n\underline{\sigma}} \ . \tag{6.2.3}$$

In this approximation one neglects the orbital dependence of the Coulomb interaction, which is known, from atomic theory, to be of the same order as the spin dependence. This also is clearly demonstrated in metals by the Auger spectra of pure Cu [7] and Pd impurities in Ag [8]. If the Coulomb part of the Hamiltonian

could be approximated by Eq. (6.2.3) a d^8 configuration would consist of two states, namely a singlet and a triplet with a splitting of J, whereas the Auger spectra show that the orbital splitting of the singlets and triplets is comparable to the singlet-triplet splitting.

The term splitting of the atomic d^n states determined by U(i,j,k,l) in Eq. (6.2.2) can be expressed in terms of two Slater integrals, F^2 and F^4, while the monopole contribution to the Coulomb energy is F^0. Usually, it is assumed that the monopole contribution is the largest in metals, as it is for the free atom. It then would suppress large polarity fluctuations, stabilizing a state with a particular number of d electrons. The F^2 and F^4 integrals then contribute to the stabilization of a particular term of a d^n configuration, which, in most cases, is a magnetic state.

Upon placing such an atom in a metallic host, several things can happen. The hybridization term in Eq. (6.2.2) causes a mixing of the d^n states with $d^{n\pm1}$ states, and also, in higher orders, causes a mixing of the various terms within d^n, resulting eventually in a loss of the atomic characteristics, and leads to a nonmagnetic ground state. Another consequence of the metallic surroundings is that the atomic Coulomb interactions are screened. A large number of Auger-spectroscopy investigations of Cu, Ni, Ag, Pd and impurities such as Ni and Pd in metals have shown that the monopole term (F^0) is strongly screened, whereas the higher-multipole terms (F^2 and F^4) are reduced by at most 20% from the free-atom values [9]. This is an extremely important observation for the understanding of transition-metal impurities in solids.

In addition to the approximate forms usually used for the Coulomb interactions in the Anderson Hamiltonian, one also usually assumes that the host-metal density of states is constant in the energy region of interest. For transition-metal impurities in noble-metal hosts, the high host-metal d density of states not far from the Fermi level might play an important role if these states hybridize sufficiently with the impurity d states. In this sense the noble-metal d bands are not unlike the ligand p bands in halides and chalcogenides, which are known to be the mediators for relatively strong superexchange interactions.

In an attempt to obtain more information about the relative importance of the above-mentioned interactions, we undertook a detailed investigation of CuMn

and AgMn alloys. The aim of the investigation is to obtain information concerning
(a) the energies of the majority- and minority-spin states of Mn,
(b) the magnitude of the Mn d-host sp hybridization,
(c) the importance of the Mn d-host d hybridization, and
(d) the magnitude of the impurity d-d Coulomb interactions F^0, F^2 and F^4, which are related to U and J in frequently used approximations.

The experimental techniques used are x-ray photoelectron spectroscopy (XPS), x-ray-excited Auger spectroscopy (XAES), high-resolution ultraviolet photoelectron spectroscopy (UPS), and bremsstrahlung isochromat spectroscopy (BIS).

Before we present the results, it is useful to illustrate what we might hope to learn from these techniques. To do this, we consider the Mn impurity to be in its d^5 Hund's-rule ground state $d^5(^6S)$, as suggested by the experimentally determined magnetic moment, which is close to $5\mu_B$ [10]. By the removal of one d electron, as in UPS, we can determine the energy of the d^4 states, of which only the $d^4(^5D)$ is accessible by fractional-parentage arguments. By the addition of one d electron, as in BIS, we can determine the energy of the d^6 states, of which, again, only the ^5D state is accessible. By careful data analysis, we should be able to determine the spectral distributions of these states from which the s-d and the impurity-host d-d hybridization can be determined. With Auger spectroscopy, we remove two d electrons, ending up in a d^3 configuration, of which only the ^4F and ^4P states are accessible.

From these measurements we can obtain the majority-spin "hole" energies, the minority-spin "electron" energies, and the Coulomb interactions. For the latter we proceed as follows:

$$[E(d^6(^5D)) - E(d^5(^6S))] - [E(d^4(^5D)) - E(d^5(^6S))] = F^0 + \frac{4}{14}(F^2+F^4),$$
$$[E(d^3(^4F,^4P)) - E(d^5(^6S))] - 2[E(d^4(^5D)) - E(d^5(^6S))] = F^0 - \frac{1}{14}(F^2+F^4), \quad (6.2.4)$$

as can be found in Slater's [11] treatment of term splittings, where $E(d^3(^4F,^4P))$ is the average energy. In this way, we have enough information to obtain F^0 and $F^2 + F^4$. In the more conventional notation for magnetic impurities, F^0 is equivalent to U, and $\frac{1}{14}(F^2+F^4) = J$.

It is perhaps instructive at this point to briefly discuss the energetics of d^n configurations to remind the reader of the, in atomic physics, well-known energy-level diagram. We show in fig. 6.3 all the atomic terms for the configurations $d^1 \rightarrow d^{10}$, as calculated using Slater's expressions for the term energies in terms of the F^0, F^2 and F^4 integrals. For F^0 we used 1.04 eV, and for the F^2 and F^4 integrals, 8.94 and 5.62 eV, which are reduced by 20% from the Mn free-atom values [12]. These are values which were determined from the present study as discussed below. The energy-level diagram is drawn assuming the $d^5(^6S)$ state to be the ground state. The point we want to make here is that the term energies of a d^5 configuration are spread over an 11-eV interval, which is an order of magnitude larger than the expected hybridization widths. Another important point concerns the "gap" of 3 eV seen in Fig. 6.3 between the Hund's-rule ground-state term and the first higher-energy term. It is this large gap which strongly favors a magnetic ground state.

6.2.2. Experimental Setup

A. Instrumental details

Three different experimental setups were used for the study presented here. The XPS and XAES spectra were obtained with a modified AEI (KRATOS) ES200 spectrometer. Both Al and Mg Kα x-ray sources were used. The base vacuum in the 10^{-11}-Torr range was obtained with turbine pumps and a liquid-nitrogen-cooled Ti sublimitation pump. The sample-preparation chamber was equipped with Ar-ion-etching and sample-scraping capabilities.

The UPS measurements were done using a cylindrical mirror analyzer as described by Bosch [13]. The base pressure was in the 10^{-11}-Torr range, achieved with a combination of a diffusion pump and a liquid-nitrogen-cooled Ti sublimation pump. The samples could be argon-ion-echted and heat-treated in situ. The surface contamination was checked using electron-excited Auger spectroscopy using the same electron analyzer. The light source was a He resonance lamp operated to optimize the HeI component. The energy resolution of the instrument was 40 and 80 meV at 5 and 10 eV pass energy, respectively. In the cases presented here, we used 10 eV

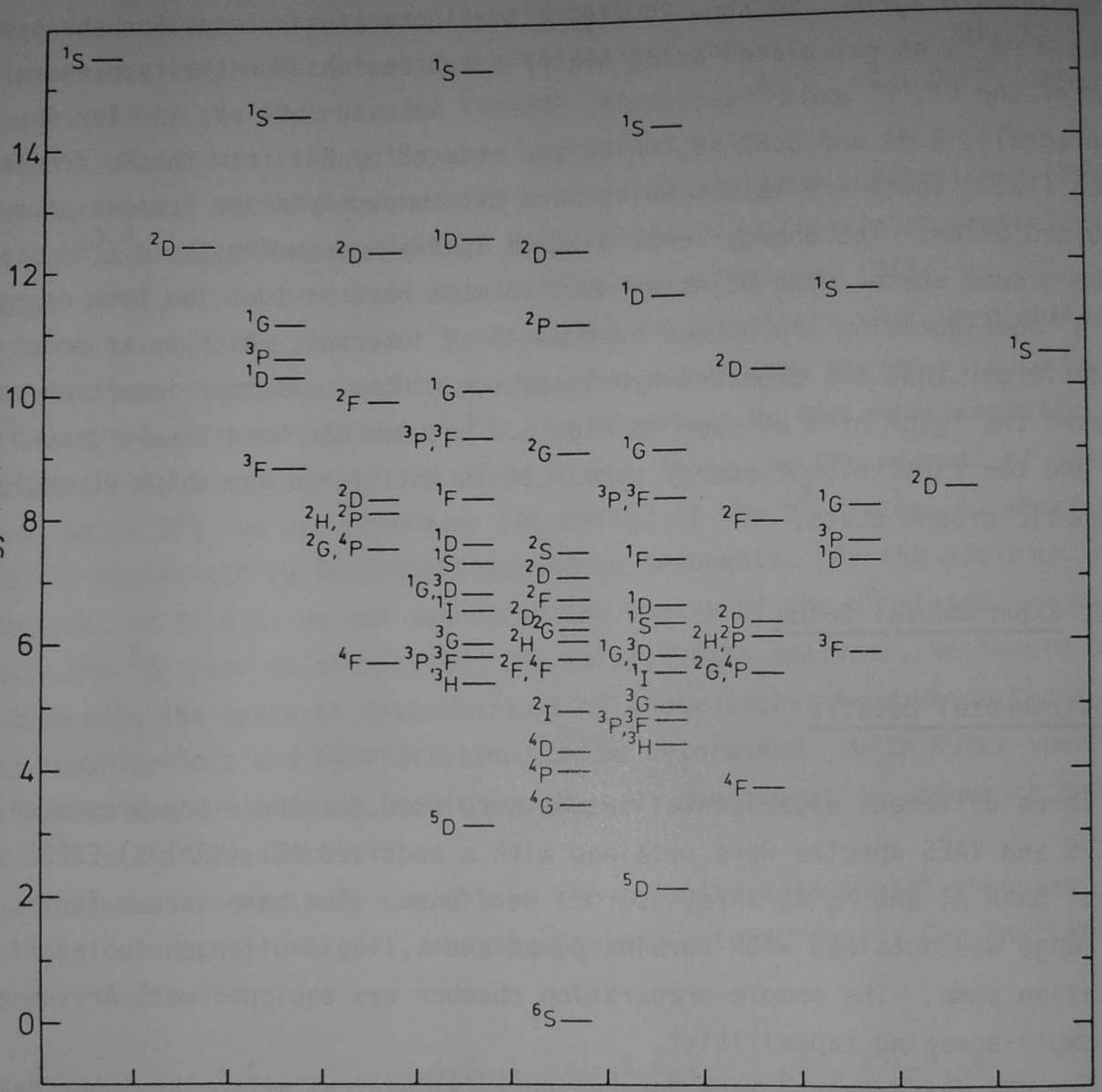

Fig. 6.3. Quasiatomic d states of a Mn atom in a Ag surrounding, calculated from Slater's atomic tables and using $I = -3.10$ eV, $F^0 = 1.04$ eV, $F^2 = 8.94$ eV, and $F^4 = 5.62$ eV.

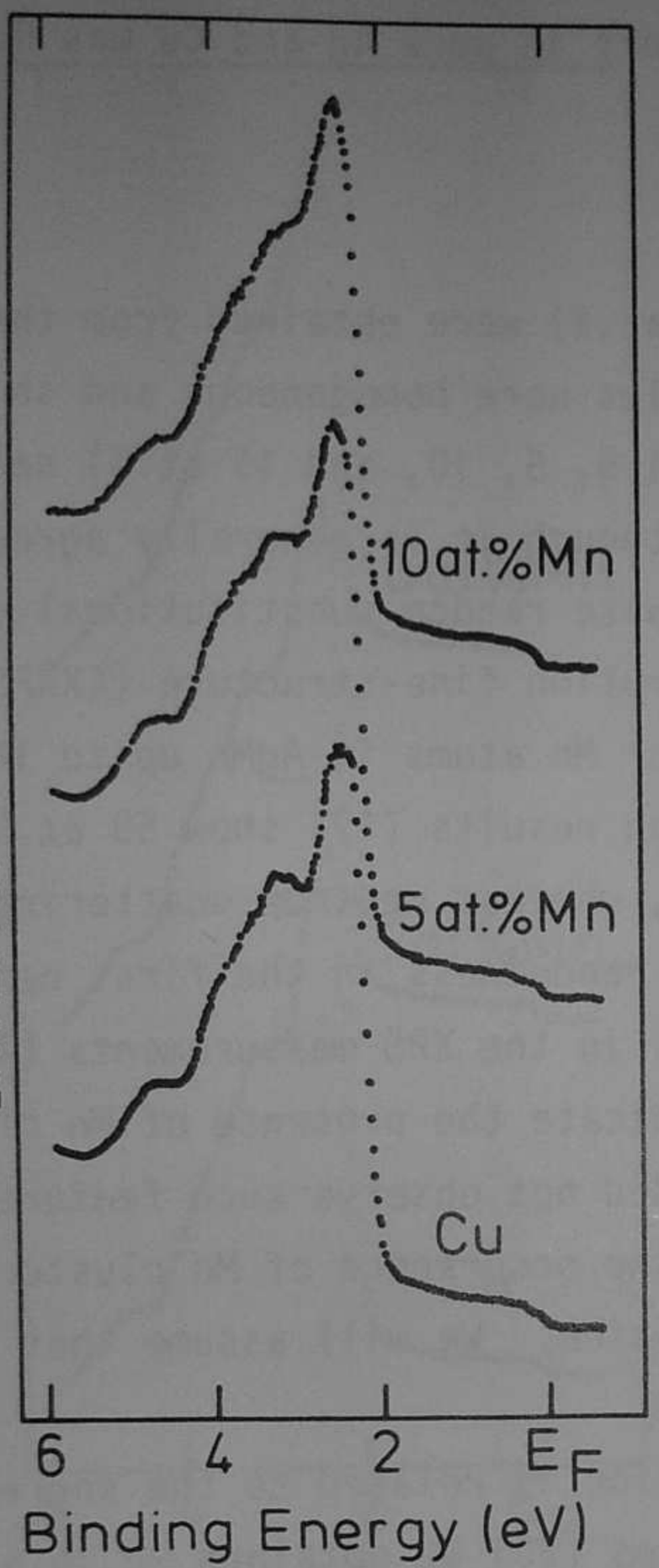

Fig. 6.4. UPS spectra of Cu, $Cu_{0.95}Mn_{0.05}$, and $Cu_{0.9}Mn_{0.1}$ dilute alloys.

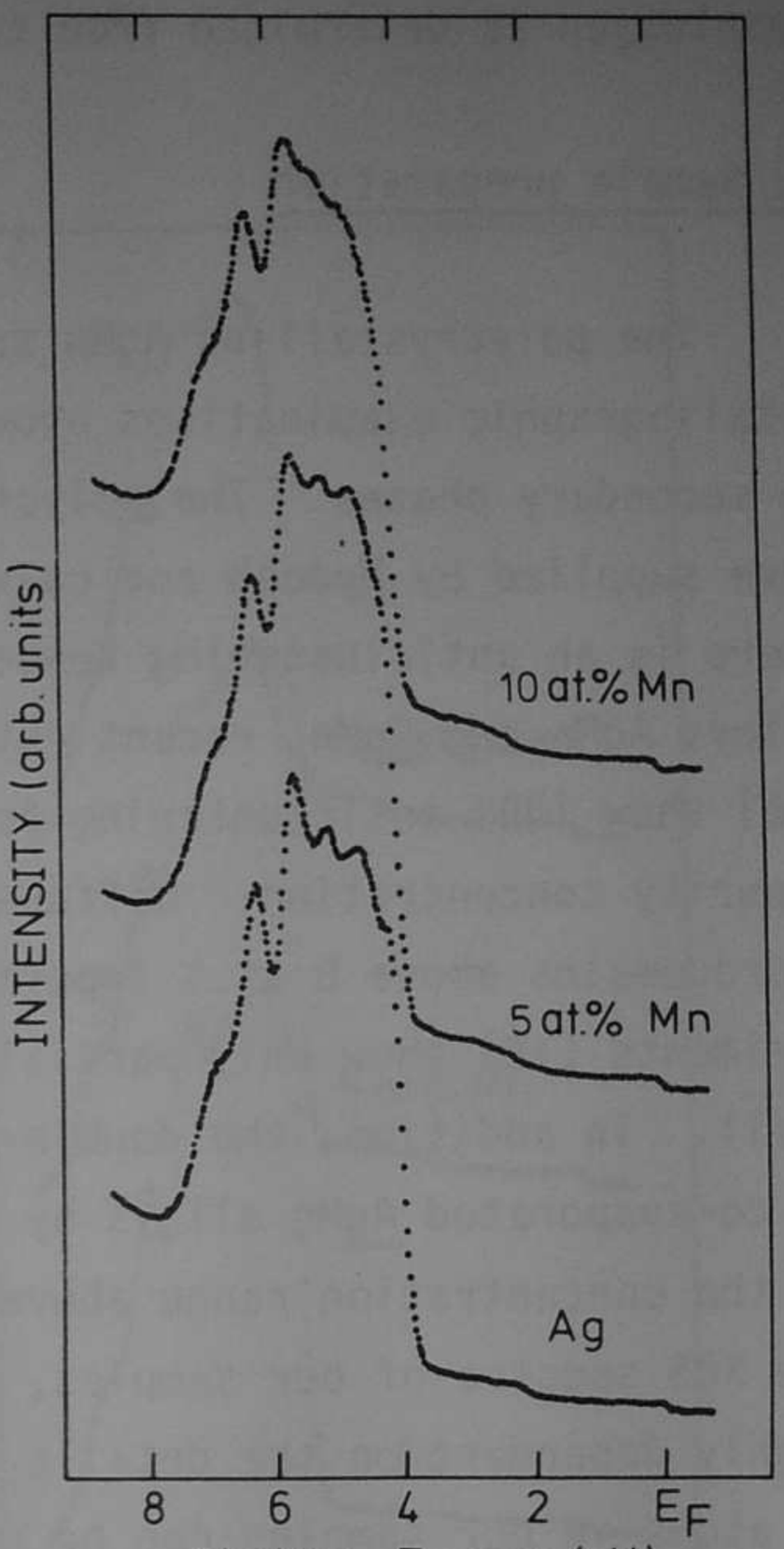

Fig. 6.5. UPS spectra of Ag, $Ag_{0.95}Mn_{0.05}$, and $Ag_{0.9}Mn_{0.1}$ dilute alloys.

pass energy. To obtain sufficient statistics, multiple scans were accumulated with intermittent surface treatments every 30 min.

The BIS results were obtained with an instrument described elsewhere [14]. The base pressure was in the 10^{-11}-Torr range but increased to 10^{-10} Torr with the electron gun operating. Surface-contamination checks were done with XPS in the same instrument. Again, multiple scans were required to obtain sufficient

statistics with intermittent sample scraping in the preparation chamber. The resolution as determined from the Fermi-edge cutoff in pure Ag and Cu was 0.85 eV.

B. Sample preparation

The polycrystalline AgMn samples (5 and 10 at.%) were obtained from the melt. Metallographic examinations showed that the samples were homogeneous and showed no secondary phases. The polycrystalline CuMn (1.5, 5, 10, and 15 at.%) samples were supplied by Mydosh and co-workers [15]. Although it is generally agreed that there is an anticlustering tendency in the otherwise random substitutional dilute alloys AgMn and CuMn, recent extended x-ray-absorption fine-structure (EXAFS) results [16] show 100% anticlustering for nearest-neighbor Mn atoms in AgMn up to 14 at.% impurity concentration. Diffuse x-ray-diffraction results [17] show 50 at.% Mn microdomains above 8 at.% impurity concentration, whereas neutron-scattering experiments [18] show only partial deviations from randomness in the first neighbor shell. In addition, the double-peaked structures in the XPS measurements [19] on co-evaporated AgMn alloys by Höchst et al. indicate the presence of Mn clusters in the concentration range above 7 at.%. As we did not observe such features in the XPS spectra of our samples, we believe that the occurrence of Mn clusters is highly dependent on the details of sample preparation. We will assume that the Mn atoms in our samples can be considered diluted.

Another problem concerning the Mn concentration is related to the segregation enthalpy of Mn in Cu and Ag. From Miedema's tables [20] we obtained -0.16 and 0.12 eV for the segregation enthalpy of Mn in Cu and Ag, respectively. This would imply that equilibrium Mn surface concentration in a CuMn alloy is almost 100 at.% at room temperature. We checked the impurity concentrations of our samples after scraping and argon-ion etching in situ with electron-excited AES and XPS.

All the results showed that the Mn surface concentration was strongly enhanced in all AgMn and CuMn alloys immediately after insertion of the polished samples, and that the surface was strongly oxidized. However, as soon as the oxygen- and carbon-free surface surface was obtained, with either scraping or argon-ion etching, the cross-section-weighted Mn 2p lines, as compared to the host-core lines, had intensities close to those expected from the chemical composition.

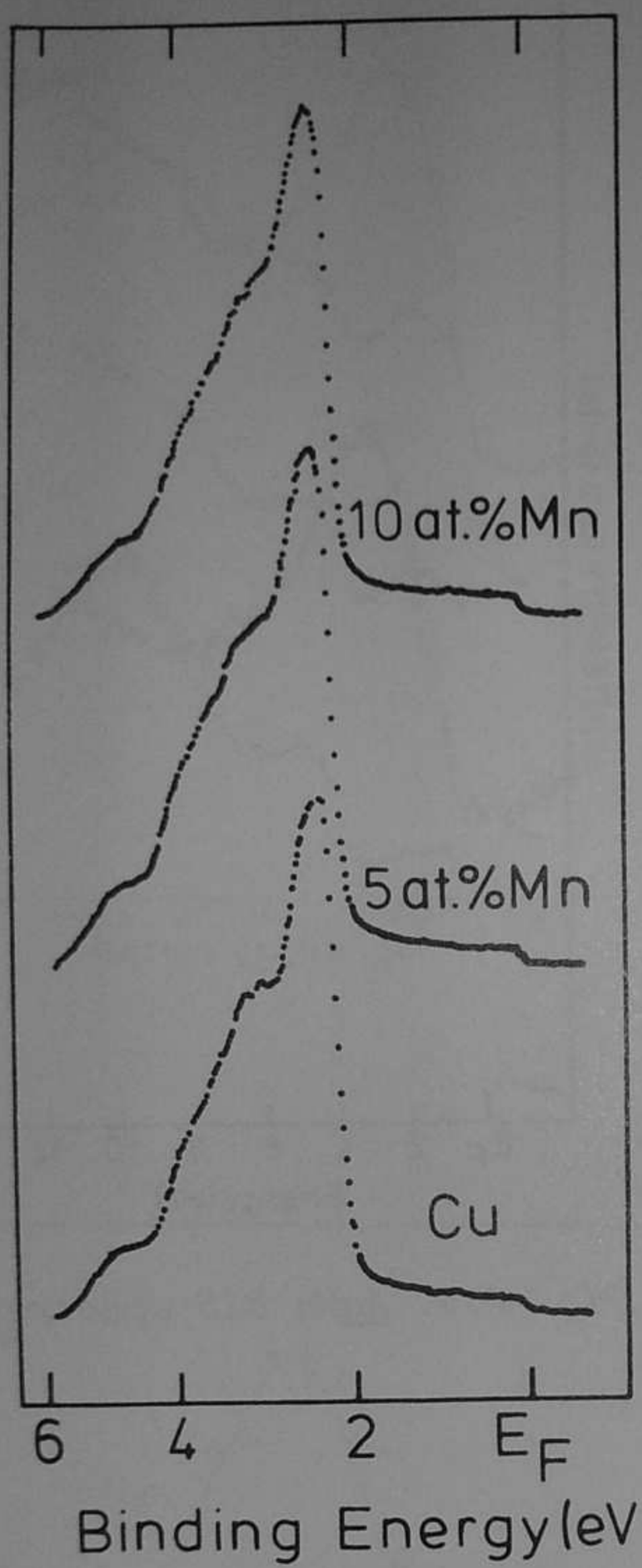

Fig. 6.6. UPS spectra of Cu, $Cu_{0.95}Mn_{0.05}$, and $Cu_{0.9}Mn_{0.1}$ dilute alloys corrected for a HeI satellite, analyzer transmission, and inelastic scattered electrons.

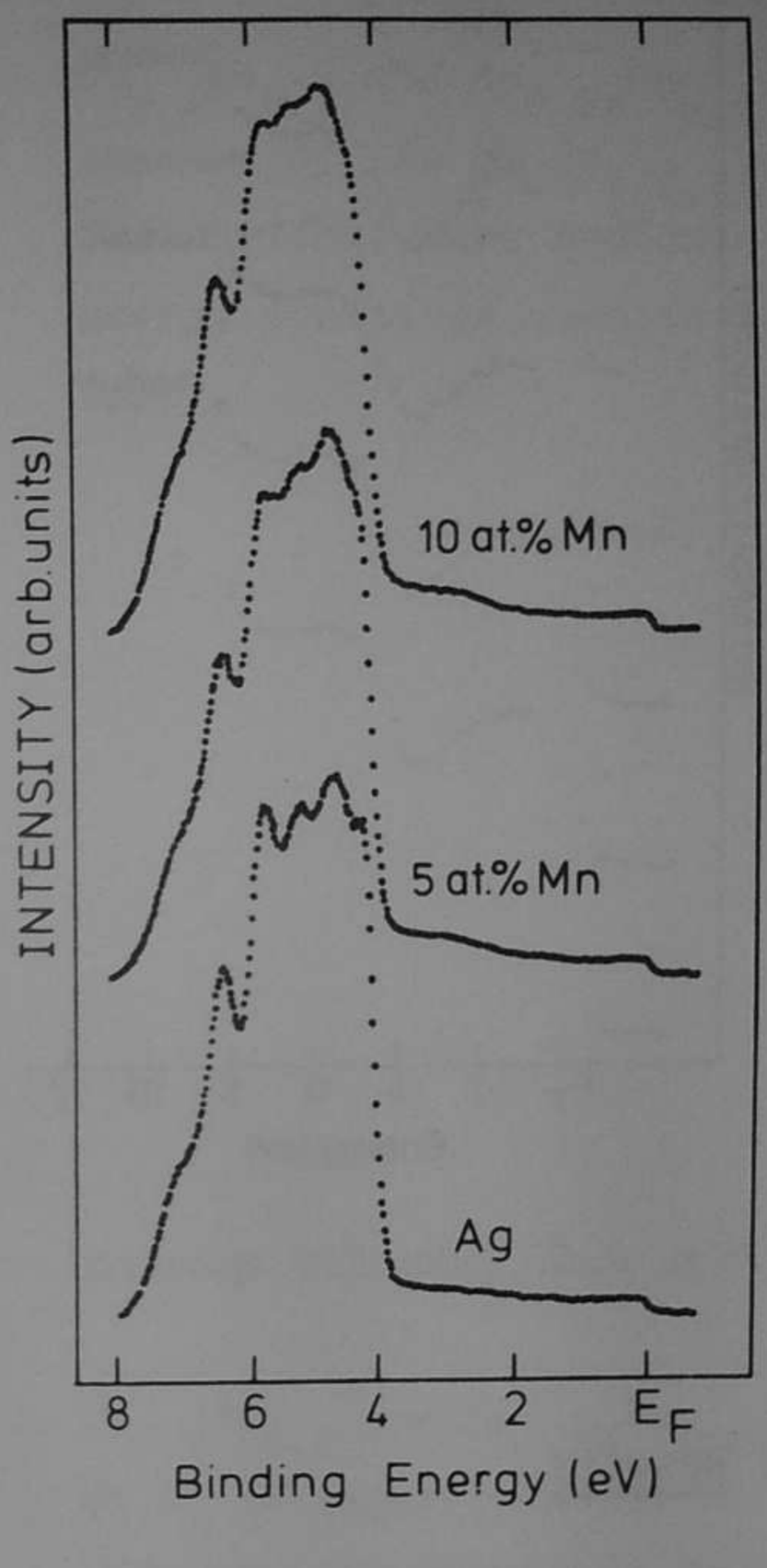

Fig. 6.7. UPS spectra of Ag, $Ag_{0.95}Mn_{0.05}$, and $Ag_{0.9}Mn_{0.1}$ dilute alloys corrected as in Fig. 6.6.

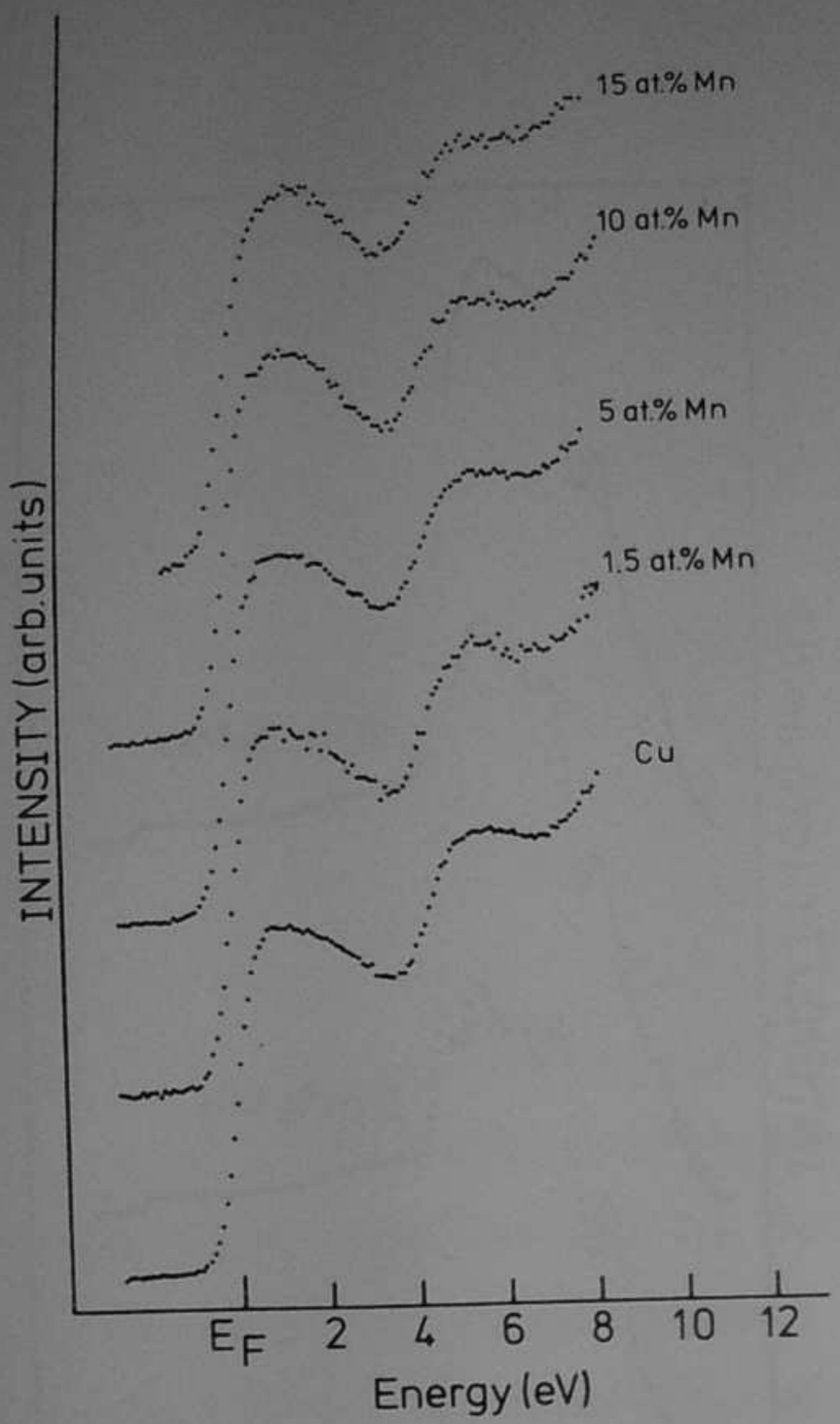

Fig. 6.8. CuMn BIS spectra

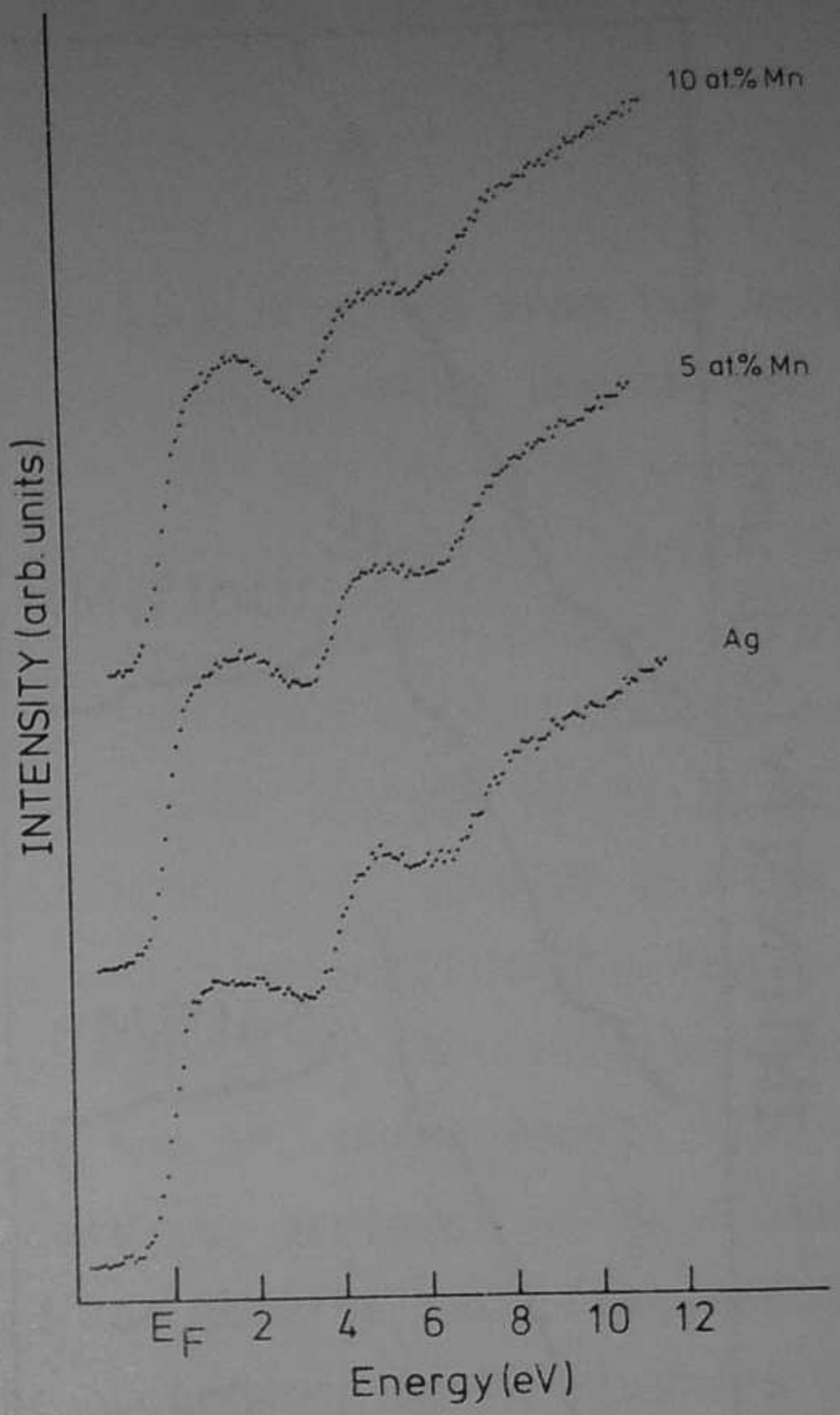

Fig. 6.9. AgMn BIS spectra

6.2.3. Results

In Figs. 6.4 and 6.5 we show the UPS spectra of the pure hosts and several concentrations of Mn in Ag and Cu. These spectra were subsequently corrected for the 23.08-eV He satellite and for a scattered-electron background. The He-satellite relative intensity was obtained from the Ni Fermi edge. The scattered-electron background was corrected for by using an iterative procedure [21]. In addition we applied a 1/E correction [22] to the intensity to account for the energy-dependent transmission of our analyzer. The so-obtained corrected spectra are shown in Figs. 6.6 and 6.7.

The BIS spectra shown in Figs. 6.8 and 6.9 have not been corrected in any way,

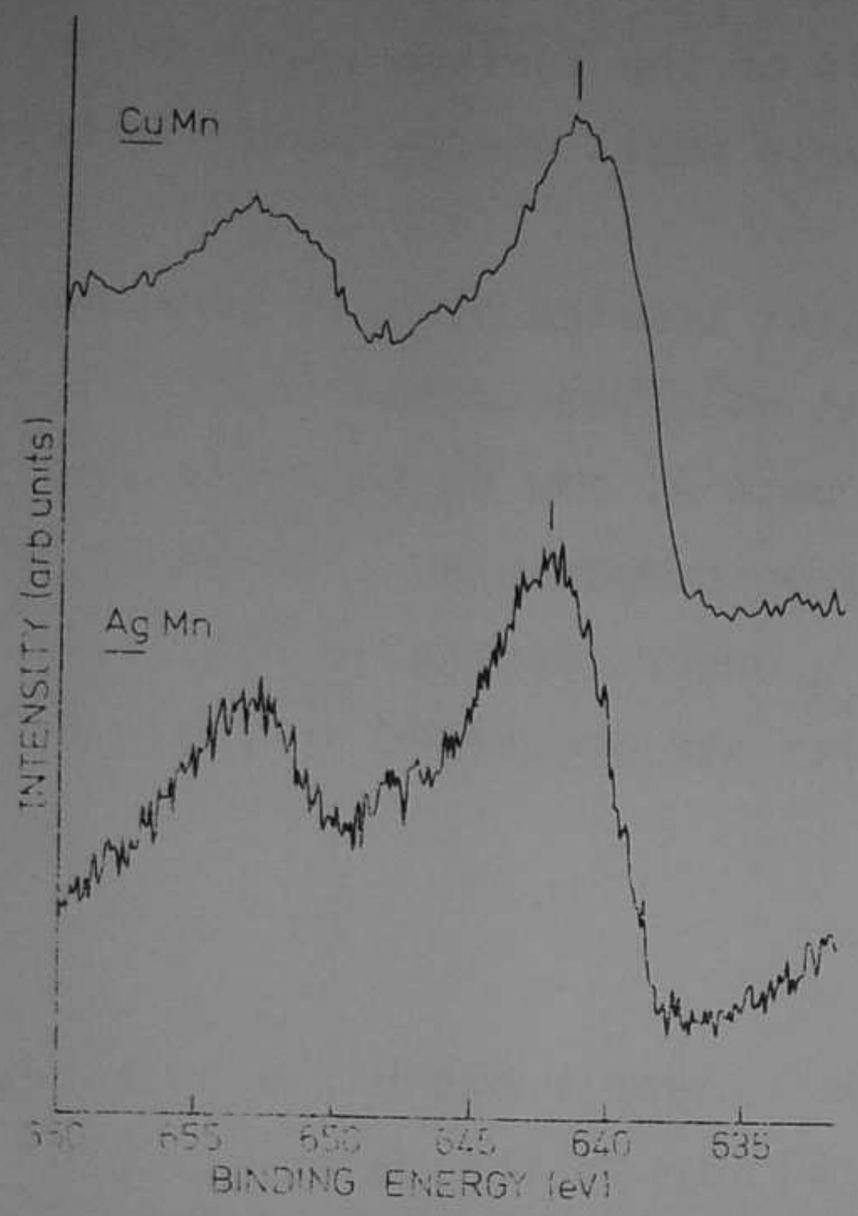

Fig. 6.10. $Cu_{0.9}Mn_{0.1}$ *and* $Ag_{0.95}Mn_{0.5}$ *XPS spectra of the Mn* $2p_{1/2,3/2}$ *lines. The vertical bars indicate the energy positions used in the text.*

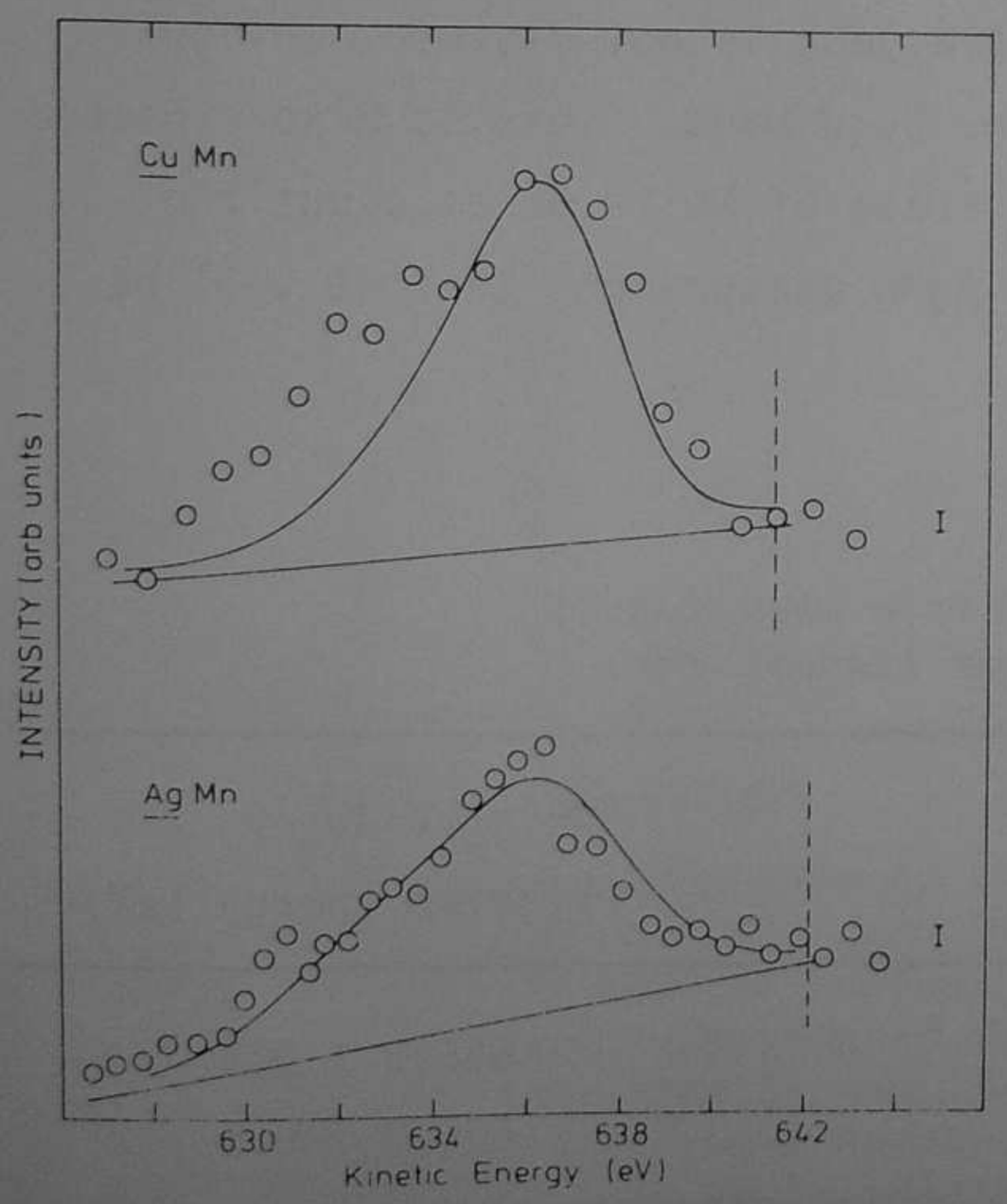

Fig. 6.11. $Cu_{0.9}Mn_{0.1}$ *and* $Ag_{0.95}Mn_{0.05}$ *Mn* L_3 *VV Auger spectra. Circles, experimental; solid lines, theoretical (see text). The vertical lines correspond to the Mn* $2p_{3/2}$ *XPS peak positions of Fig. 6.10, or, in different words, to the two-hole - excitation threshold.*

since, at the high energies used, experience shows that the inelastic scattering background is not nearly as sensitive to the details of the surface as it is in UPS. Furthermore, the transmission in this relatively small energy range is nearly energy independent.

The XPS and AES measurements were done on samples treated by both scraping and argon-ion etching. No detectable difference was observed in the spectra using these procedures. The spectra were obtained using both Al adn Mg Kα x-ray sources to avoid accidental overlap of Auger and photoelectron components. The Mn 2p XPS spectra are shown in Fig. 6.10, and the $L_{2,3}M_{4,5}M_{4,5}$ Auger spectra in Fig. 6.11. The Mn 2p binding energies and Auger kinetic energies are presented in Table 6.2.

6.2.4. Discussion

The UPS spectra of AgMn alloys shown in Fig. 6.5 clearly exhibit a peak between the Ag d band and the Fermi level which we attribute to the majority-spin virtual bound state of Mn. Assuming that the ground state is close to $d^5(^6S)$, this peak would correspond to a $d^4(^5D)$ state. We note, however, that this state is quite close in energy to the Ag d band, so that hybridization herewith could be quite important. In the CuMn spectra this extra peak is not visible, which suggests that the Mn $d^4(^5D)$ state lies inside the Cu d band. This is also expected from energetic considerations. Assuming the d^4 state of Mn to be at about the same energy in Ag and Cu hosts, we see from the AgMn measurement that it will be close to the center of the Cu d band.

Table 6.2. Binding energies and average kinetic energies of Mn $2p_{3/2}$ XPS lines and L_3VV Auger transitions.

System	Mn $2p_{3/2}$ XPS binding energy (eV)	Mn L_3VV Auger kinetic energy (eV)
AgMn	642.2 ± 0.5	635.3 ± 0.5
CuMn	641.3 ± 0.5	635.0 ± 0.5

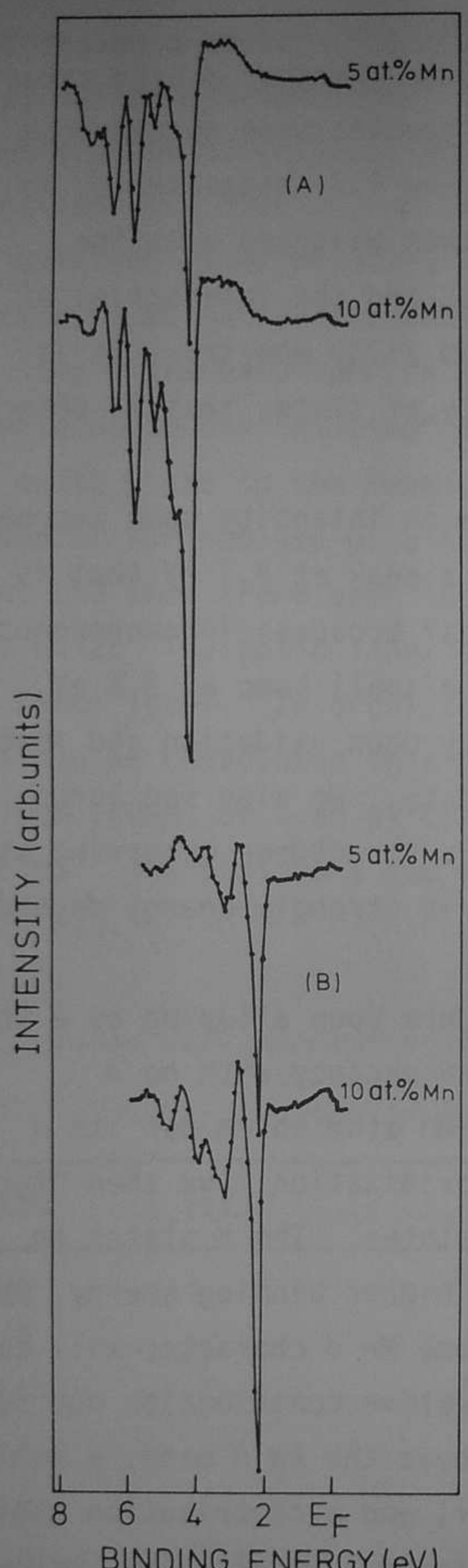

Fig. 6.12. Difference spectra of the (A) AgMn and (B) CuMn UPS spectra and the corresponding pure-metal spectra of Figs. 6.6 and 6.7. The 5- and 10-at.% alloy difference spectra are at an absolute scale relative to the pure-host - metal spectra. The solid lines serve as a guide to the eye.

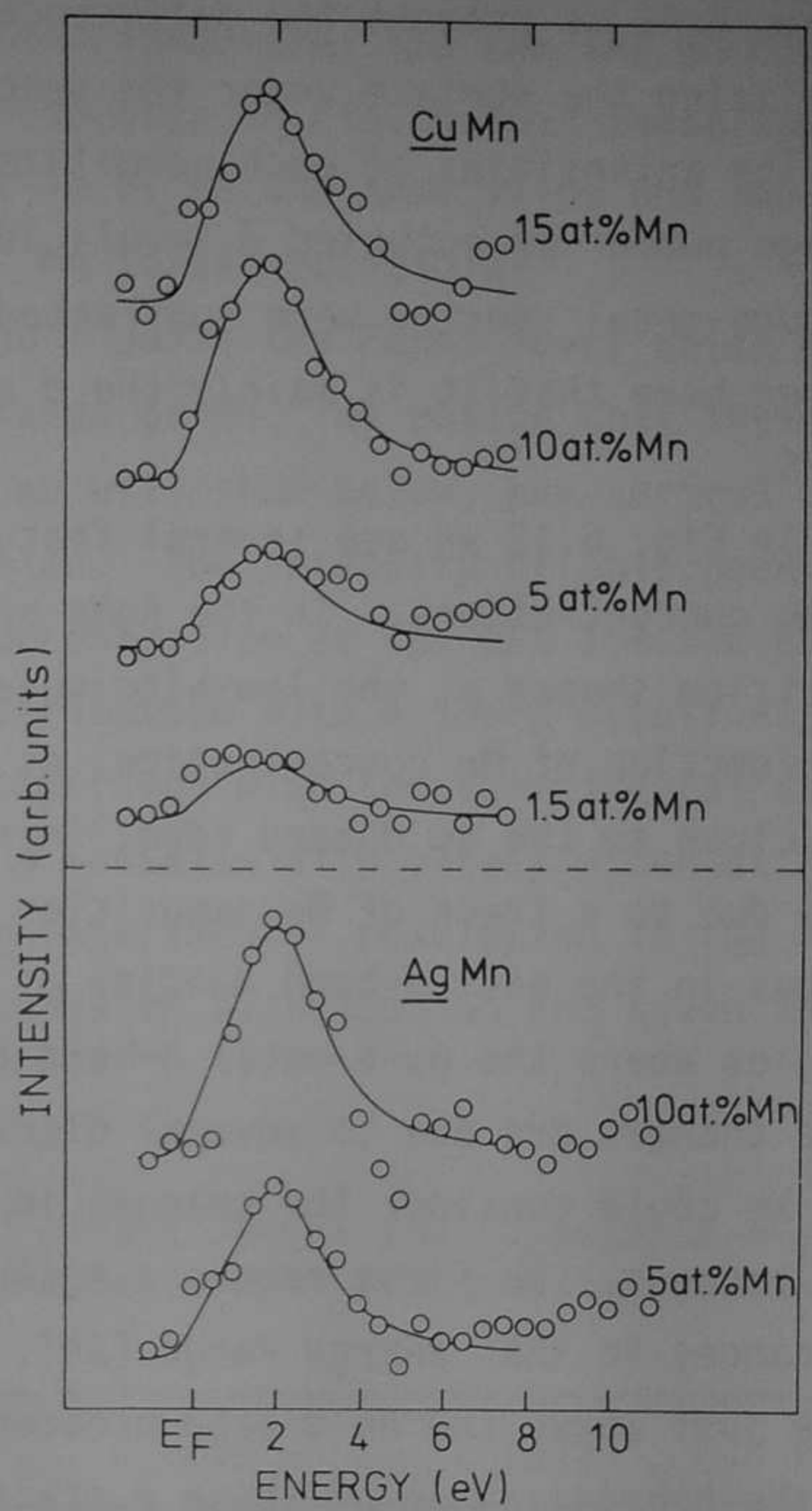

Fig. 6.13. Difference spectra of the AgMn and CuMn BIS spectra and the corresponding pure-metal spectra of Figs. 6.8 and 6.9. The intensities of the difference spectra are at an absolute scale relative to the pure-host-metal spectra.

This would result in strong mixing with the Cu d states.

In order to obtain a better picture of the changes in the host d-band structure, in Fig. 6.12 we present the difference spectra. These spectra were obtained by normalizing the surface under the spectra of Figs. 6.6 and 6.7 integrated up to E_F. The intensities of each normalized spectrum were then weighted with the average number of occupied d levels in the atomic state, and the intensities of the pure-metal spectra were subtracted from the weighted alloy spectra. It is assumed here that it is mainly the d part of the density of states that is observed in UPS.

In Fig. 6.12 we see several features that increase in intensity upon increasing the Mn concentrations. In the AgMn spectra we observe a peak at 3.1 eV that is Lorentzian shaped at the low-binding-energy side and that broadens inhomogeneously as a function of Mn concentration, as in AgPt [23]. The small hump at 3.6 eV, very close to the Ag d-band edge, increases in intensity upon oxidation and seems to be due to a trace of Mn impurities in an oxidized state. We also see large changes in the host d-band density of states, with sharp structures occurring at energies where the pure-metal d-band density of states is strongly energy dependent. These changes are due to several discernable effects.

We could consider the changes in electronic structure upon alloying as a three-step process. We first remove a Ag(Cu) atom, creating a vacancy with no d resonances in that energy range [24]. We now put in a Mn atom which has its d state just above the Ag d band broadened by the s-d hybridization. We then "turn on" the hybridization of these d states with the Ag d states. The d states on Ag atoms close to a Mn site will be pushed to somewhat higher binding energy, while those for Ag atoms far away will remain unchanged and some Mn d character will appear in the Ag d band. The net effect of this will be a negative contribution due to the removal of an Ag atom, a positive Mn d peak just above the Ag d band, a positive contribution in the Ag d band due to the Mn d character, and a contribution similar to the energy derivative of the Ag d-band density of states. We will show below that all these qualitative effects are nicely described by a more formal theory.

Since Mn has a large magnetic moment in Ag and Cu, not all the Mn d states can be full, yet we see a "gap" between the occupied d states and the Fermi level, suggesting that a subset of split-off states is full, which would correspond to a

half-filled d shell. The other remaining Mn d states are observed above the Fermi level in the BIS spectrum (Figs. 6.8 and 6.9), in addition to steplike structures which are due to critical points [25] in the band structure. To see the Mn contribution more clearly, we show the difference spectra in Fig. 6.13. These spectra are obtained by normalizing the intensities at 10 eV to the same value and subtracting. At 10 eV we expect the influence of Mn to be negligible.

The difference spectra show only a peak just above the Fermi level which must correspond to the "missing" minority-spin d states of Mn. We notice that these are quite close to the Fermi level, which, as we will show below, has serious consequences for the use of a Kondo-like Hamiltonian. The intensity of this peak shows the same trend upon increasing the Mn concentration as the UPS spectra of Fig. 6.12. The solid line is a Lorentzian distribution with a sharp cutoff at the Fermi level. In order to make a direct comparison with the experimental spectra possible we convoluted this distribution with a Gaussian with a full width at half maximum (FWHM) of 0.85 eV corresponding to the experimental resolution in the BIS spectra. The positions and widths for the Lorentzian distribution are given in Table 6.3.

*Table 6.3. Experimental (footnotes a and b) and theoretical (footnote c-e) values for the minority- and majority-spin peak positions and widths of Ag*Mn *adn Cu*Mn.

System	ε_+(eV)	Γ_+(eV)	r_+	ε_-(eV)	Γ_-(eV)	r_-
AgMn[a]	-3.1 ± 0.2	0.7 ± 0.1	0.23	2.1 ± 0.2	1.2 ± 0.1	0.57
AgMn[b]	-3.25			1.6		
AgMn[c]	-2.6[f]	0.2[f]	0.07	0.7[f]	0.6[f]	0.86
CuMn[a]				1.7 ± 0.2	1.4 ± 0.2	0.82
CuMn[d]				0.79[f]	0.8[f]	1.01
CuMn[e]	-3.5[f]	0.16[f]	0.05	0.8[f]	0.64[f]	0.8

[a] This work.
[b] Reference 30.
[c] Reference 32.
[d] Reference 29.
[e] Reference 31.
[f] Estimated from the figures.

Before going on to the other results, we would first like to analyze the UPS and BIS data in more detail in terms of a model Hamiltonian. For the model Hamiltonian we use a modified Clogston-Wolff [26] model to include the s-d hybridization and the large exchange splitting. This model treats the impurity d-host d hybridization in a simple, but in our case, realistic, manner. The majority-spin part (H_+) describes the ionization spectrum and the minority-spin part (H_-) describes the affinity spectrum, assuming the ground state to be $d^5(^6S)$. The Hamiltonian is written as

$$H = \sum_\sigma \left[\sum_k \varepsilon_k d^\dagger_{k\sigma} d_{k\sigma} + \sum_l \eta_l c^\dagger_{l\sigma} c_{l\sigma} + \Delta_{d\sigma} d^\dagger_{0\sigma} d_{0\sigma} + \sum_l V_{ld} (d^\dagger_{0\sigma} c_{l\sigma} + c^\dagger_{l\sigma} d_{0\sigma}) \right] \qquad (6.2.5)$$

Here, ε_k describes the energy dispersion of the host d band, η_k that of the s band, $\Delta_{d\sigma} = E^i_{d\sigma} - \bar{\varepsilon}_d$ the average impurity d-state energies relative to the d-band centroid, and V_{kd} the hybridization of the impurity d state with the sp band. The impurity d-host d hybridization is included implicitly, and the assumption is made that the impurity d wave function is identical to that of the host, but its energy is shifted. In this mode the d-d Coulomb interactions do not appear explicitly, but are incorporated in the energy difference $\Delta_{d+} - \Delta_{d-}$. This approximate treatment of the Coulomb interactions is reminiscent of a spin-polarized Hartree-Fock calculation. In writing the Hamiltonian in this way, we assume that H_+ commutes with H_-, which neglects all possible spin-flip processes and the influence of higher-energy terms present in the impurity atom's electronic structure (see Fig. 6.3). The spin-flip processes are, of course, of utmost importance to describe the Kondo properties. We, however, expect these to be important only very close to the Fermi level, and to have no significant influence on the larger-energy-scale properties. The above approximate manner of including Coulomb and exchange interactions will be valid only if the ground state is close to $d^5(^6S)$, which we know is true for Mn impurities in Ag and Cu.

Having made these approximations, we have reduced the problem to that of the sum of two one-particle problems, which is easily solved. Using the Dyson equation, the local-impurity density of states is given by

$$\pi^{-1} \sum_\sigma \mathrm{Im} G^{d0\sigma}_{d0\sigma} = \rho_{d0} \qquad (6.2.6)$$

where

$$G^{d0\sigma}_{d0\sigma} = g^{d0\sigma}_{d0\sigma} + g^{d0\sigma}_{d0\sigma}\Delta_{d\sigma}G^{d0\sigma}_{d0\sigma} + g^{d0\sigma}_{d0\sigma}\sum_k V_{kd}G^{d0\sigma}_{sk\sigma} \tag{6.2.7}$$

and

$$G^{d0\sigma}_{sk\sigma} = f^{k\sigma}_{k\sigma}V_{kd}G^{d0\sigma}_{d0\sigma}\ , \tag{6.2.8}$$

or

$$G^{d0\sigma}_{d0\sigma} = \frac{g^{d0\sigma}_{d0\sigma}}{1 - \left[\Delta_{d\sigma} + \sum_k (V_{kd})^2 f^{k\sigma}_{k\sigma}\right] g^{d0\sigma}_{d0\sigma}} \tag{6.2.9}$$

Furthermore,

$$g^{d0\sigma}_{d0\sigma} = \sum_k \frac{1}{\omega - \epsilon_k}$$

is the host d-band density of states, and

$$f^{k\sigma}_{k\sigma} = \frac{1}{\omega - \eta_k}$$

describes the s-band density of states. To simplify matters, we further assume that $(V_{kd})^2$ can be replaced by its average value, and that the host s-band density of states is constant in the relevant energy region so that

$$\sum_k (V_{kd})^2 f^{k\sigma}_{k\sigma} \simeq i\Gamma_\sigma, \tag{6.2.10}$$

$$G^{d0\sigma}_{d0\sigma} = \frac{g^{d0\sigma}_{d0\sigma}}{1 - (\Delta_{d\sigma} + i\Gamma_\sigma) g^{d0\sigma}_{d0\sigma}} \tag{6.2.11}$$

Obviously, our difference spectra do not correspond to the local-impurity density of states, which is positive everywhere. This is also expected since the host density of states will also be modified. We therefore also calculate the total density of states:

$$\rho_d(\text{tot}) = \pi^{-1} \text{Im} \Sigma \sum_{k,\sigma} G^{dk\sigma}_{dk\sigma}. \tag{6.2.12}$$

The Dyson equation gives

$$G^{dk\sigma}_{dq\sigma} = g^{dq\sigma}_{dq\sigma}\delta_{kq} + g^{dq\sigma}_{dq\sigma} \frac{\Delta_{d\sigma}}{N} \sum_m G^{dm\sigma}_{dm\sigma} + g^{dq\sigma}_{dq\sigma} \sum_l \frac{V_{ld}}{\sqrt{N}} G^{dk\sigma}_{sl\sigma}\ , \tag{6.2.13}$$

$$G^{dk\sigma}_{sl\sigma} = f^{l\sigma}_{l\sigma} V_{ld} \sum_m \frac{1}{\sqrt{N}} G^{dk\sigma}_{dm\sigma}, \tag{6.2.14}$$

$$G^{dk\sigma}_{dq\sigma} = g^{dq\sigma}_{dq\sigma}\delta_{qk} + g^{dq\sigma}_{dq\sigma}\left[\frac{\Delta_{d\sigma} + i\Gamma_\sigma}{N}\right] \sum_m G^{dk\sigma}_{dm\sigma}, \tag{6.2.15}$$

or

$$G^{dk\sigma}_{dk\sigma} = g^{dk\sigma}_{dk\sigma} + \frac{1}{N}\left[\frac{(\Delta_{d\sigma} + i\Gamma_\sigma)(g^{dk\sigma}_{dk\sigma})^2}{1 - \frac{\Delta_{d\sigma} + i\Gamma_\sigma}{N} \sum_k g^{dk\sigma}_{dk\sigma}}\right]\ , \tag{6.2.16}$$

$$\Delta\rho_d(\text{tot}) = -\pi^{-1} \text{Im} \sum_\sigma \frac{(\Delta_{d\sigma} + i\Gamma_\sigma) \frac{\partial}{\partial\omega} \frac{1}{N} \sum_k \frac{1}{\omega - \varepsilon_k}}{1 - (\Delta_{d\sigma} + i\Gamma_\sigma) \frac{1}{N} \sum_k \frac{1}{\omega - \varepsilon_k}} \tag{6.2.17}$$

where $\Delta\rho_d(\text{tot})$ is the change in the density of states in the dilute limit. We notice that the total change in the d density of states contains a derivative which results in the sharp structures seen in Fig. 6.12.

A difficulty with this expression is that $\Delta\rho_d(\text{tot})$ is not zero for $\Delta = 0$ as it should be, since in a calculated band structure the s-d hybridization is already included. The term remaining involving $i\Gamma$, however, introduces a negligible error

for the values of Γ which we require to give the experimental virtual-bound-state widths.

A direct comparison of experiment and theory can, however, only be made after inclusion of the photoemission matrix elements. For Ag and Cu these matrix elements are not constant over the host d band, and, in addition, the matrix element for Mn d photoemission can be considerably different from that of Ag and, to a lesser degree, Cu. In Chapter 3.3, we have derived an expression for the matrix element effects following closely the arguments of Shevchik [27], but including non-k-conservation in the initial state. From this we see that if the atomic cross sections for guest and host atoms are the same, we can write

$$\Delta\rho_d(\text{tot}) = -\pi^{-1}\,\text{Im}\left[\frac{\Delta(\partial/\partial\omega)g_{exp}(\omega)}{1 - \Delta g_0^0(\omega)}\right] \tag{6.2.18}$$

where $g_{exp}(\omega)$ is obtained from the pure-host UPS spectrum, i.e.,

$$I_d(\omega) = \pi^{-1}\,\text{Im}[g_{exp}(\omega)]. \tag{6.2.19}$$

In this way we can include, purely experimentally, the matrix-element effects within the host d bands. By including the matrix elements in this way, we should be able to make a fairly detailed comparison with experiment.

In Fig. 6.14 we compare the calculated spectrum to the experimental difference spectrum. The values of $\Delta_\pm$ and $\Gamma_\pm$ are chosen to give the correct peak positions and widths, and for $g_0^0(\omega)$ we use the semiempirical density of states as calculated by Smith [28]. The large experimental linewidth of the BIS part was included in the theory by convoluting the part above the Fermi level with a Gaussian of FWHM 0.85 eV. We see that the above-described theory follows the experimental curve surprisingly well.

To demonstrate the influence of the energy-dependent matrix-element effects, we also show, in Fig. 6.15, the calculated difference density of states (Eq. (6.2.17)) using the same parameters as for the curves of Fig. 6.14. Clearly, the theory including the matrix-element effects gives a much better representation of the spectrum. The peak positions as well as the relative intensities of the oscillations in the d band are strongly modified by matrix-element effects. In this theory

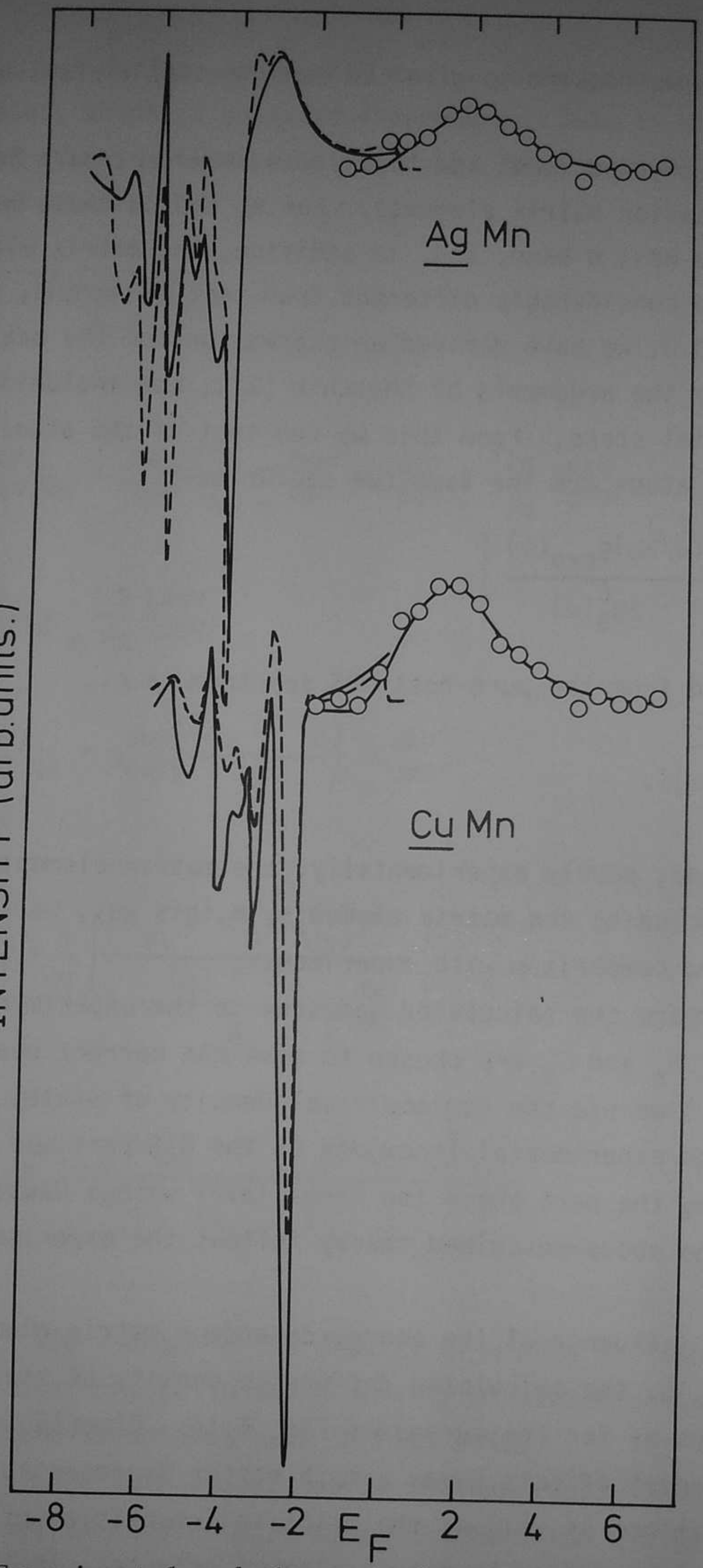

Fig. 6.14. Experimental and theoretical UPS and BIS difference spectra of $Cu_{0.9}Mn_{0.1}$ *and* $Ag_{0.95}Mn_{0.05}$. *Dashed lines and circles, experimental spectra; solid lines, theoretical spectra.*

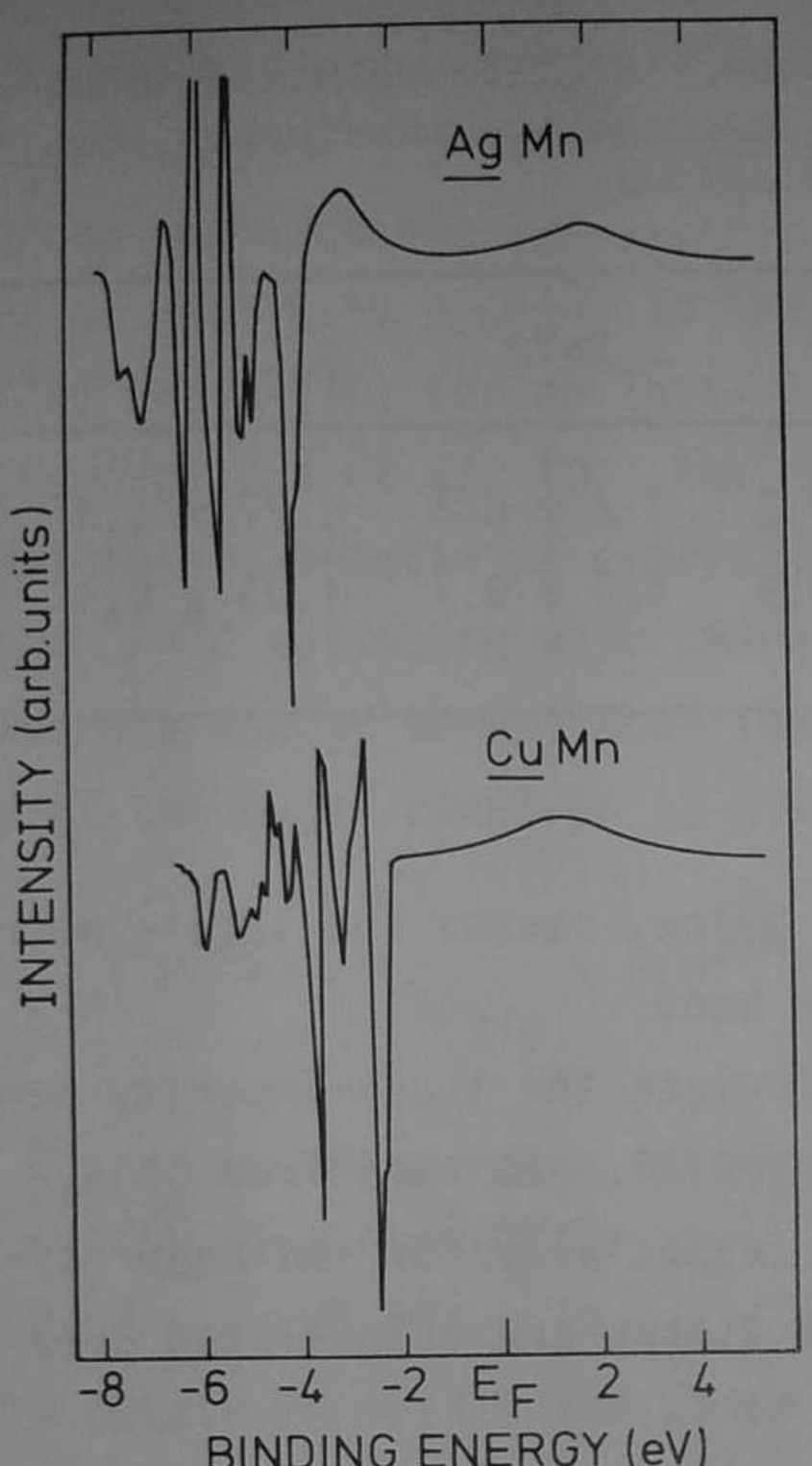

Fig. 6.15. Calculated difference density of states of AgMn minus Ag, and of CuMn minus Cu.

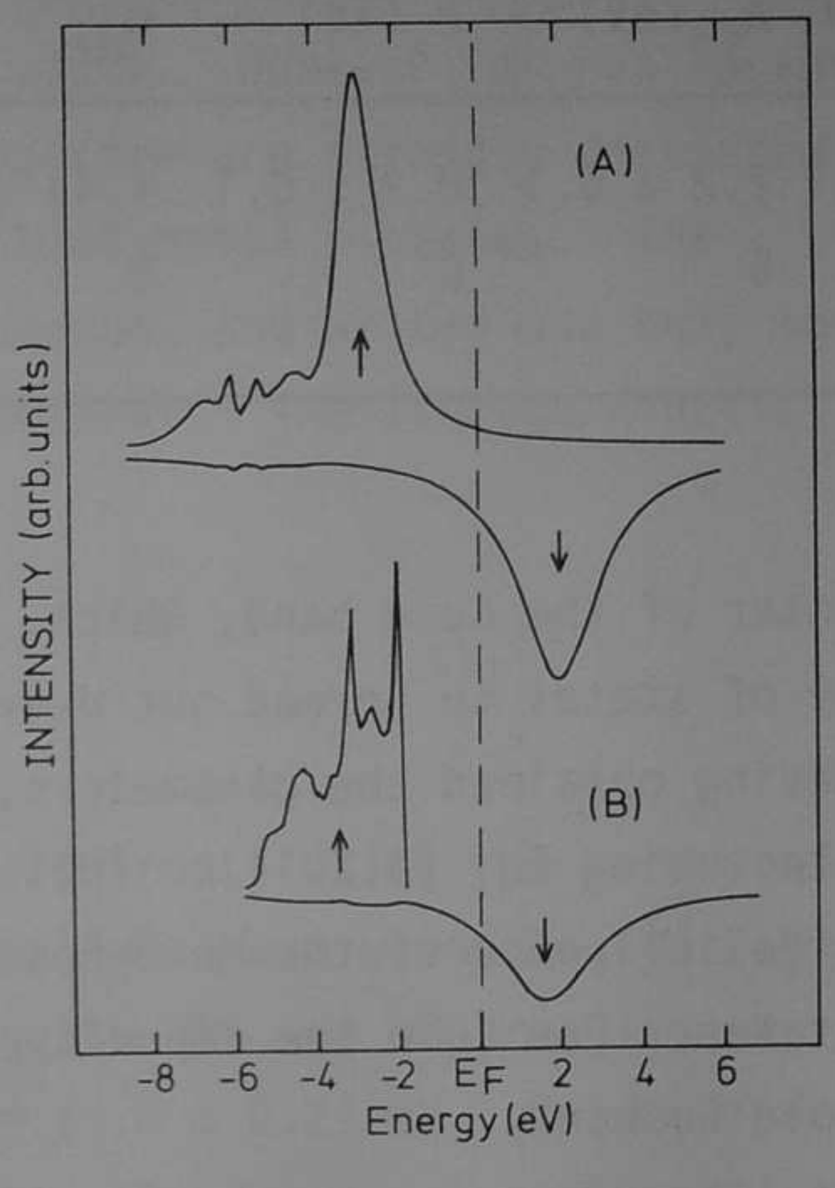

Fig. 6.16. Calculated spin-projected local d density of states at a Mn site in a (A) Ag and (B) Cu surrounding.

we have assumed equal cross sections for Mn and host d emission. This is probably not valid for AgMn, but we notice from Eq. (3.3.12) in Chapter 3.3 that the influence of a different cross section ($\gamma \neq 0$) for host and guest atoms does not effect the term involving the derivative of the density of states, and merely adds an only slowly-varying energy-dependent contribution in the host d band and a small modification of the intensity of the impurity line.

The parameters used to obtain the simulation in Fig. 6.14 are given in Table 6.4. We notice that Δ_{d+} for CuMn is zero, placing the Mn majority-spin state in

Table 6.4. Parameters used in the model calculations. P_{eff} is obtained using $P_{eff} = g\sqrt{S(S+1)}$, with $S = \frac{1}{2}(n_+ - n_-)$. $n_\pm$ are the occupancies of the majority- and minority-spin impurity $\bar{d}$ states.

System	Δ_{d+}(eV)	Γ_+(eV)	n_{d+}	Δ_{d-}(eV)	Γ_-(eV)	n_{d-}	P_{eff}
Ag<u>M</u>n	2.2 ± 0.1	0.7 ± 0.1	4.44 ± 0.1	7.3 ± 0.2	1.2 ± 0.1	0.77 ± 0.1	4.6
Cu<u>M</u>n	0	0	5	4.7 ± 0.2	1.4 ± 0.1	1.09 ± 0.1	4.8

the center of the Cu d band, which, as we will see below, causes the local-impurity density of states to spread out over the whole Cu d band.

Having obtained the parameters, we can now calculate the local-impurity density of states using Eq. (6.2.11). This is shown in Fig. 6.16. We see, from this, the large influence of the Mn d-host hybridization, especially for the majority-spin states. For Cu<u>M</u>n the impurity majority-spin d states are delocalized over the whole Cu band.

By integrating up to the Fermi level, we can also determine the occupation of the majority- and minority-spin states, as given in Table 6.4, and the magnetic moment. We find $P_{eff} = 4.8\mu_B$ and $4.7\mu_B$, respectively, for Cu<u>M</u>n and Ag<u>M</u>n, which agree well with magnetic-susceptibility measurements [10]. We also see from Fig. 6.16 that the Mn minority-spin states are quite close to the Fermi level and have a considerable width. This suggests that the use of a Kondo Hamiltonian for describing the low-energy-scale properties is not appropriate. As discussed in the Introduction, the Schrieffer-Wolff transformation is only valid for $r_\pm = \Gamma_\pm/\varepsilon_{d\pm} \ll 1$, which certainly is not the case for these systems. The values of $r_\pm$ are given in Table 6.3, from which we see that r_- is between 0.5 and 1.

In Table 6.3 we also give the experimentally determined widths and positions of the impurity states, together with values from other investigations. We notice that the splitting between the majority- and minority-spin states, as determined here (5.3 eV for Ag<u>M</u>n), is considerably larger than that obtained from first-principles calculations (3.5 eV) [29].

As described in the Introduction, we can obtain the Coulomb interactions from the minority- and majority- spin Mn d-state energies. From these, we obtain $F^0 + \frac{4}{14}(F^2 + F^4) = 5.2$ eV for Ag**Mn**. To obtain the separate contributions of $F^0 = U$ and the exchange $J = \frac{1}{14}(F^2 + F^4)$, we can use the Auger results. The Auger spectra of Fig. 6.11 should, in the atomic limit, consist of two lines corresponding to $d^3(^4F)$ and $d^3(^4P)$ for an initial $d^5(^6S)$ ground state. However, as has recently been shown by Vos et al. [8], the impurity Auger spectra are strongly distorted in nobel metals because of hybridization with the host-metal d states. The expected ^4F-^4P splitting will therefore not be observed, and we can use only the term average energy to estimate the Coulomb interactions. The average kinetic energy of the Auger electron is given by

$$E_{kin}(^4F,^4P) = E_{2p_{3/2}} - E(d^3(^4F,^4P)),$$

where $E_{2p_{3/2}}$ is the binding energy of the Mn $2p_{3/2}$ electron. Using the values of Table 6.2 we find $E(d^3(^4F,^4P)) = (6.8 \pm 0.7)$ eV for Ag**Mn**, and using Eq. (6.2.4) we find $F^0 - \frac{1}{14}(F^2+F^4) \simeq (0.0 \pm 0.7)$ eV, and using the UPS and BIS results we finally obtain $F^0 \simeq (1.0 \pm 0.7)$ eV and $\frac{1}{14}(F^2+F^4) \simeq (1.0 \pm 0.2)$ eV. We see from these estimates that F^0 is strongly reduced from the free-atom value (22 eV) [11], a result which is quite general for 3d transition metals [8]. The higher-multipole terms in the Coulomb interaction, F^2 and F^4, remain close to the atomic value, $\frac{1}{14}(F^2+F^4) = 1.2$ eV [11]. This also is a quite general result for the transition metals [8]. The solid lines in Fig. 6.11 are theoretical impurity Auger spectra obtained in the way described by Vos et al.[8], starting from the local-impurity majority-spin DOS of Fig. 6.16. For the details of the calculation, we refer to [8]. From the values for F^0, F^2. and F^4, we obtain $U_{eff}(^4P) = 1.3$ eV and $U_{eff}(^4F) =$ -0.6 eV for Mn in Ag, as can also be verified from Fig. 6.3. For Mn in Cu we took 0.7 and -1.2 eV respectively, assuming the same term splitting as in the Ag host, but a smaller F^0 value of about 0.4 eV.

Upon comparing the theoretical and experimental **Cu**Mn LVV spectra, we see that, experimentally, there is some more intensity at about 631 eV kinetic energy. We believe that this is caused by a slight oxidation of the Mn atoms during the measurement, as the intensity in this region was somewhat enhanced several hours after

initial cleaning of the sample. However, also in the higher-kinetic-energy regions of the spectrum there are differences between the experimental and the theoretical line shape which may be very well due to the presence of the Mn minority-spin states close to the Fermi level. In the presence of a core hole, these states may become partially occupied, and the implicit assumption of initially full shells in the Auger process is no longer justified. An exact theory that takes into account such effects is, however, not available at present.

The above-mentioned values of F^0, F^2 and F^4, in addition to the UPS d^4 final-state energy, were used to generate the term energy diagram in Fig. 6.3. This diagram shows that the most important excited states mixed into the ground state because of hybridization with the sp bands are the $d^6(^5D)$ and $d^4(^5D)$ states. It is interesting that these states are also both magnetic, so that the mixing will not destroy the local moment.

From the above analysis we have obtained a fairly good picture of the electronic structure of these alloys, at least for the so-called high-energy-scale region. We already pointed out that the Clogston-Wolff-like theory used is not valid to describe the low-energy-scale region and therefore cannot be expected to be correct at the Fermi level. The high-energy-scale results, however, can now be used to do a more sophisticated calculation of the low-energy-scale properties. We notice from Fig. 6.3 that the most important configurations which will mix via s-d hybridization with the $d^5(^6S)$ state are the $d^6(^5D)$ and $d^4(^5D)$ states. Of secondary importance are the $d^5(^4G,^4P,^4D)$ states which can mix in higher orders in V_{kd} via the $d^6(^5D)$ and $d^4(^5D)$ states. We also notice that the $d^6(^5D)$ and $d^4(^5D)$ states are both fivefold orbitally degenreate, which is sufficiently large to expect a fast convergence of a (1/N)-type perturbation expansion [33].

The Kondo Hamiltonian has been extensively used to describe the exchange interaction between magnetic impurities leading to the well-known RKKY oscillatory behavior thereof. The above results raise serious questions concerning the validity of such an approach for two reasons. First, the validity of the use of the Kondo Hamiltonian is questionable, and, second, the Mn d-host d hybridization, which we find to be strong, is not included in the RKKY theory. The most extreme cases are the majority-spin states in CuMn, which are apparently delocalized over the entire Cu d band. This strong delocalization is also present, to a lesser extent,

in AgMn. The minority-spin Mn states can, on the other hand, be considered to be quite localized, although even these have some density in the host-metal d band. As a result the magnetic *moments* are localized at the Mn atoms, but the d *electrons* are not. A consequence of this is that d electrons also mediate exchange interactions between local moments. We see that there are two extensions of the usual RKKY interaction [4] to be made:

(1) The Anderson Hamiltonian must be used instead of the Kondo Hamiltonian.

(2) The occupied d bands of the host material must be included.

6.2.5. Conclusions

From this study we have obtained the following:

(1) A direct determination of the energy and widths of the impurity majority- and minority-spin states in CuMn and AgMn.

(2) The host d band is strongly perturbed by the impurity, which is well described by a modified spin-polarized Clogston-Wolff mode.

(3) The majority-spin impurity states are strongly delocalized via hybridization with the host d band. The minority-spin states remain quite localized.

(4) The close proximity of the minority-spin impurity state to the Fermi level, together with its large width, indicates that the use of a Kondo-like Hamiltonian to describe these systems is not appropriate.

(5) The monopolelike impurity d-d Coulomb interaction is strongly reduced from the free-atom value, whereas the higher multipole terms are close to the atomic values.

(6) The host-metal d band could be an important mediator for superexchange-like interactions between impurity spins.

References

1. A.N. Gerritsen and J.O. Linde, Physica (Utrecht) 17, 573 (1971); 18, 877 (1951).
2. D. Jha and M.H. Jericho, Phys. Rev. B 3, 147 (1971); A. Nakamura and D. Kinoshita, J. Phys. Soc. Jpn. 27, 382 (1969); 32, 441 (1972).
3. N. Andrei, K. Furuya and J.H. Löwenstein, Rev. Mod. Phys. 55, 331 (1983);

J.S. Schilling, Adv. Phys. 28, 657 (1979); G. Grüner and A. Zawadowski, Rep. Prog. Phys. 37, 1497 (1974); J.A. Mydosh, J. Phys. Soc. Jpn. 52, 585 (1983); A.J. Heeger, in Solid State Physics, edited by F. Seitz and D. Turnbull (Academic, New York, 1969), 23, 283 (1969); F. Kondo, ibid., p. 183.

4. C. Kittel, in Solid State Physics, edited by F. Seitz and D. Turnbull (Academic, New York, 1968), 22; M.A. Ruderman and C. Kittel, Phys. Rev. 96, 99 (1954); T, Kasuya, Prog. Theor. Phys. 16, 45 (1956); K. Yosida, Phys. Rev. 106, 893 (1957).
5. J.R. Schrieffer and P.A. Wolff, Phys. Rev. 149, 491 (1966); J.R. Schrieffer, J. Appl. Phys. 38, 1143 (1967); see, however, L.L. Hirst (Z. Phys. 244, 230 (1971)) for a remark on a factor-of-2 in error in the latter reference.
6. P.W. Anderson, Phys. Rev. 124, 41 (1961).
7. E. Antonides and G.A. Sawatzky, in Transition Metals, edited by M.J.G. Lee, J.M. Perz and E. Fawcett (IOP, Bristol, 1978), p.134 (IOP Conf. Proc. No. 39).
8. M. Vos, D. van der Marel and G.A. Sawatzky, Phys. Rev. B 29, 3073 (1984).
9. D. van der Marel, G.A. Sawatzky and F.U. Hillebrecht, Phys. Rev. Lett. 53, 206 (1984); J.C. Fuggle, P. Bennett, F.U. Hillebrecht, A. Lenselink and G.A. Sawatzky, ibid. 49, 1787 (1982). Also see Ref. 7.
10. A.F.J. Morgownik and J.A. Mydosh, Solid State Commun. 47, 321 (1983); C.M. Hurd, J. Phys. Chem. Solids 30, 539 (1969); A.K. Majumdar, V. Oestreich and D. Wechsenfelder, Solid State Commun. 45, 907 (1983); M. Hanson, J. Phys. 8, 1225 (1978).
11. J.C. Slater, Quantum Theory of Atomic Structure (McGraw-Hill, New York, 1960), p.492.
12. J.B. Mann, Los Alamos Scientific Laboratory Report No. LASL-3690 (1967) (unpublished).
13. A.J. Bosch, J. Phys. E 17, 1187 (1984). Ph.D. thesis, University of Groningen, 1982.
14. F.U. Hillebrecht (unpublished).
15. The CuMn samples were kindly supplied by Professor J.A. Mydosh, for which we want to express our gratitude.
16. E. Dartyge and A. Fontaine, J. Phys. F 14, 721 (1984).
17. H. Bouchiat, Phys. Rev. B 23, 1375 (1981).

18. A.F.J. Morgownik and J.A. Mydosh, Solid State Commun. 47, 325 (1984).
19. H. Höchst, P. Steiner and S. Hüffner, Z. Phys. B. 38, 201 (1980); P.T. Andrews and C.E. Johnson, Phys. Lett. 70A, 140 (1979).
20. A.R. Miedema, Z. Metallkdn. 69, 455 (1978).
21. A.D. McLachlan, J.G. Jenkin, R.C.G. Leckey and J. Liesegang, J. Phys. F 5, 2415 (1975).
22. J.L. Gardner and J.A.R. Samson, J. Electron Spectrosc. Relat. Phenom. 6, 53 (1975).
23. D. van der Marel, G.A. Sawatzky, and J.A. Julianus, J. Phys. F 14, 281 (1984).
24. The effect of removing an atom equals the limit $\Delta\to\infty$ in Eq. 6.2.17. Thus, $\Delta\rho = \pi^{-1}\mathrm{Im}(\partial/\partial\omega)[\mathrm{lng}\ (\omega)]$.
25. D. van der Marel, G.A. Sawatzky, R. Zeller, F.U. Hillebrecht and J.C. Fuggle, Solid State Commun. 50, 47 (1984).
26. A.M. Clogston, B.T. Matthias, M. Peter, H.J. Williams, E. Corenzwit and R.J. Sherwood, Phys. Rev. 125, 541 (1962).
27. N.J. Shevchik, Phys. Rev. B 16, 3428 (1977).
28. N.V. Smith, Phys. Rev. B 3, 1862 (1971); 9, 1365 (1974).
29. P.J. Braspennig, R. Zeller, A. Lodder and P.H. Dederichs, Phys. Rev. B 29, 703 (1984).
30. H.P. Meyers, L. Wallden and A. Karlson, Philos. Magn. 18, 725 (1968).
31. J.D. Cohen and C.P. Slichter, Phys. Rev. Lett. 40, 129 (1978).
32. M.C. Muñoz, B.L. Gyorffy and K. Verhuyk, J. Phys. F 13, 1847 (1983).
33. T.V. Ramakrishan, in Valence Fluctuations in Solids, edited by L.M. Falicov, W. Hanke and M.B. Maple (North-Holland, Amsterdam, 1981), p.13; P.W. Anderson, ibid., p.451.

6.3. Rudermann Kittel oscillations, particle pair production and indirect charge transfer as mediators of magnetic ordering.

6.3.1. Introduction

An important aspect of the local moment problem is the magnetic ordering between impurities. It has been known for a long time, that the indirect exchange interaction (Eq. (6.2.1)) between the local moment and conduction electrons causes an oscillatory polarization of the electron gas surrounding the local moment [1,2,3,4]. This polarization cloud then couples to the other local moments in the system. The result is an effective interatomic exchange Hamiltonian between moments, the sign of which depends on the distance between the local moments in an oscillatory fashion.

In the preceding section [5],we have shown that the indirect exchange mechanism outlined above is insufficient in two ways for CuMn and AgMn: (1) The use of a Kondo Hamiltonian (Eq. (6.2.1)) for the impurity-electron gas coupling is overidealized, and (2) the occupied host d bands may contribute to the coupling mechanism.

In this section, we show how the use of an Anderson Hamiltonian affects the results that one would get from a Kondo-Hamiltonian, using a perturbation expansion of the ground state energy. We also briefly discuss the role of the d bands.

In the past, the Anderson Hamiltonian has been applied to this problem more often [6,7,8,9]. Usually a Hartree-Fock ground state energy calculation is done for two impurity moment alignments (parallel and antiparallel) of the two impurity model. This is different from calculating the ground state energy for the two impurities in a total spin triplet or singlet state (if each impurity carries one spin) or in a suitable set of spin states if the impurities carry more than one spin. What one would like to find is an energy expression in terms of $S_0 \cdot S_R$, where S_0 and S_R are the spin operators of both local moments at sites O and R. Recently an ab initio calculation has been done for AgMn and CuMn [10] using the local spin density approximation, also resulting in energies of parallel and antiparallel moments, for first to fourth neighbor moments. These calculations take into account the full bandstructure of the host s, p and d bands and do not rely

on approximations for the shape of the Fermi surface etc. On the other hand, their exchange splittings are too small compared to our experiments due to the use of the local density approximation.

6.3.2. Perturbation theory

We will first treat the indirect exchange interaction for two s-impurities, then generalize this to the 2l+1-fold degenerate case. We will use essentially Brillouin-Wigner perturbation theory (but sum over the different terms in the spirit of a 1/N perturbational series, where N equals the degeneracy of the ground state level of the local moment) to calculate the ground state energy for the triplet and singlet total configurations of the spin ½ impurities. The expression for the ground state ansatz is:

$$|g_s\rangle = \frac{1}{\sqrt{2}} \left(d^\dagger_{O\uparrow}\, d^\dagger_{R\downarrow} + s\, d^\dagger_{O\downarrow}\, d^\dagger_{R\uparrow}\right)|g\rangle$$

$$|g\rangle = \left(\prod_{\sigma,k<k_F} C^\dagger_{k\sigma}\right)|\Psi_{vac}\rangle \qquad (6.3.1)$$

$$s = S^{-1}\, S_O \cdot S_R + 1 - S$$

where $S = \frac{1}{2}$ is the impurity spin at sites O and R. So s is 1(-1) for the triplet (singlet) configuration.

The excited states of the impurity atoms are s^0 and s^2 with energies ϵ_d and ϵ_d+U relative to the Fermi level. The unperturbed Hamiltonian is:

$$H^{(0)} = \sum_{k,\sigma} \eta_k\, C^\dagger_{k\sigma}\, C_{k\sigma} + \sum_{R_i} \left\{ \sum_\sigma \left(\epsilon_d\, d^\dagger_{R_i\sigma}\, d_{R_i\sigma}\right) + U d^\dagger_{R_i\uparrow}\, d_{R_i\uparrow}\, d^\dagger_{R_i\downarrow}\, d_{R_i\downarrow} \right\} \qquad (6.3.2)$$

where R_i is O or R for the two impurity system. The total Hamiltonian $H = H^{(0)} + H^{(1)}$ contains the perturbation:

$$H^{(1)} = \sum_{R_i} \sum_{k,\sigma} \left\{ V_k\, e^{i\mathbf{k}\cdot\mathbf{R}_i}\, d^\dagger_{R_i\sigma}\, C_{k\sigma} + H.C. \right\} \qquad (6.3.3)$$

As $H^{(1)}$ has no diagonal matrix elements, the Brillouin-Wigner expansion for the ground state corresponds to solving [11]:

$$E_0 = S(E_0) \tag{6.3.4}$$

with

$$S(z) = \langle g_s | H^{(1)} \ (z-PH)^{-1} \ PH^{(1)} \ | g_s \rangle \tag{6.3.5}$$

where P is the projection operator

$$P = 1 - |g_s\rangle\langle g_s| \tag{6.3.6}$$

The function S(z) can be expanded in a 1/N series [12]:

$$S(z) = S_0(z) + (1/N)S_1(z) + (1/N)^2 \ S_2(z) + ... \tag{6.3.7}$$

where the S_i (z) are the functions

$$S_0(z) = \sum_m \frac{\langle g_s | H^{(1)} | m \rangle \langle m | H^{(1)} | m \rangle}{(z - E_m)} \tag{6.3.8}$$

$$(1/N)S_1(z) = \sum_{klm} \frac{\langle g_s | H^{(1)} | k \rangle \langle k | H^{(1)} | l \rangle \langle l | H^{(1)} | m \rangle \langle m | H^{(1)} | g_s \rangle}{(z-E_k)(z-E_l')(z-E_m)} \tag{6.3.9}$$

etc.

where $E_l' = E_l + S_0(z)$ if the state $|l\rangle$ is the ground state plus electron-hole pairs in the conduction bands. Otherwise we have $E_l' = E_l = \langle l | H^{(0)} | l \rangle$. The modification with $S_0(z)$ corresponds to the zeroth order (in 1/N theory) self energy insertion in the propagator $\frac{1}{z-E_l}$, and must therefore be included in *any* order of the Brillouin-Wigner expansion.

Following Zhang and Lee [12] we can also expand E_0 in 1/N and with

Eq. (6.3.4) we find

$$E_0^{(0)} = S_0(E_0^{(0)}) \tag{6.3.10}$$

$$E_0^{(1)} = \left(1 - \frac{\partial S_0}{\partial E_0^{(0)}}\right)^{-1} S_1\,(E_0^{(0)}) \tag{6.3.11}$$

Usually $\frac{\partial S_0}{\partial E_0^{(0)}}$ is small and can be neglected in the evaluation of $E_0^{(1)}$. Note, that in Eq. (6.3.11) S_1 is evaluated for $E_0^{(0)}$. This means that in those terms where the propagator correction $S_0(z)$ enters, it is exactly cancelled by z in view of Eq. (6.3.10).

Now the function $S_0(z)$ corresponds to processes where an impurity emits and reabsorbs a virtual hole or electron. As the second impurity is not involved in the process, S_0 does not depend on the relative orientation of the impurity moments. Eq. (6.3.10) leads to:

$$E_0^{(0)} = -2 \sum_k |V_k|^2 \left(\frac{1-f_k}{\eta_k - \epsilon_d - E_0^{(0)}} + \frac{f_k}{\epsilon_d + U - \eta_k - E_0^{(0)}}\right) \tag{6.3.12}$$

It may seem confusing that Eq. (6.3.12) cannot be separated in two independent terms for each impurity, but one must also take into account $S_1\,(E_0^{(0)})$, which contains lowest order contributions from each impurity independently (independent of the relative orientation). The part of S_1 that depends on $S_0 \cdot S_R$ is represented by processes where one impurity emits an electron-hole pair, that is reabsorbed by the second impurity. Such a process is visualized in Fig. 6.17. In Fig. 6.18 we use a more compact notation [13,14] for the different self-energy contributions.

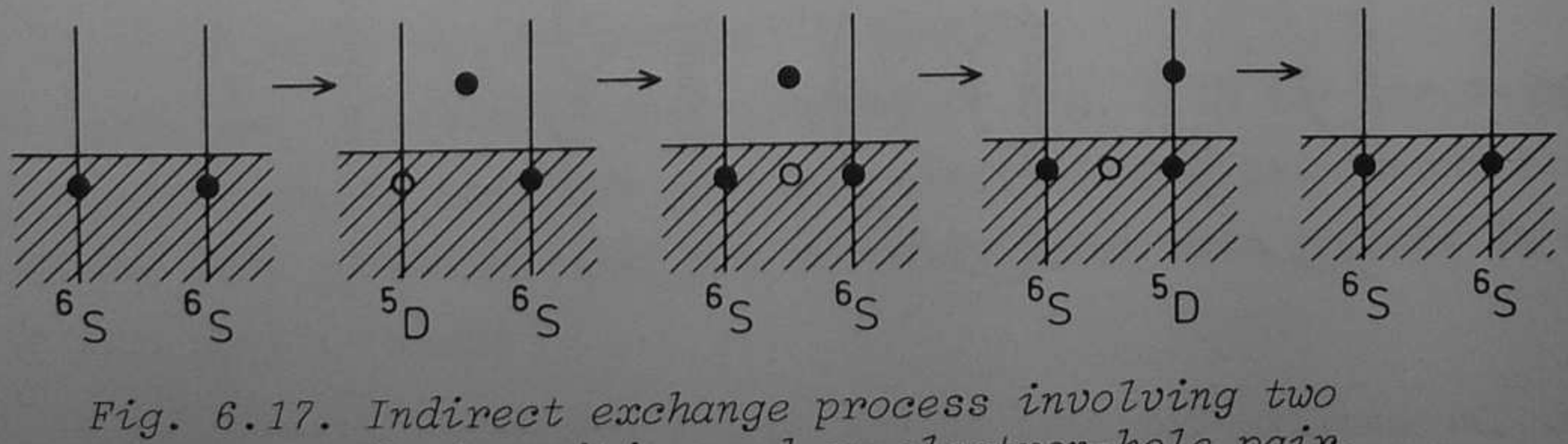

Fig. 6.17. Indirect exchange process involving two Mn impurities and an electron-hole pair.

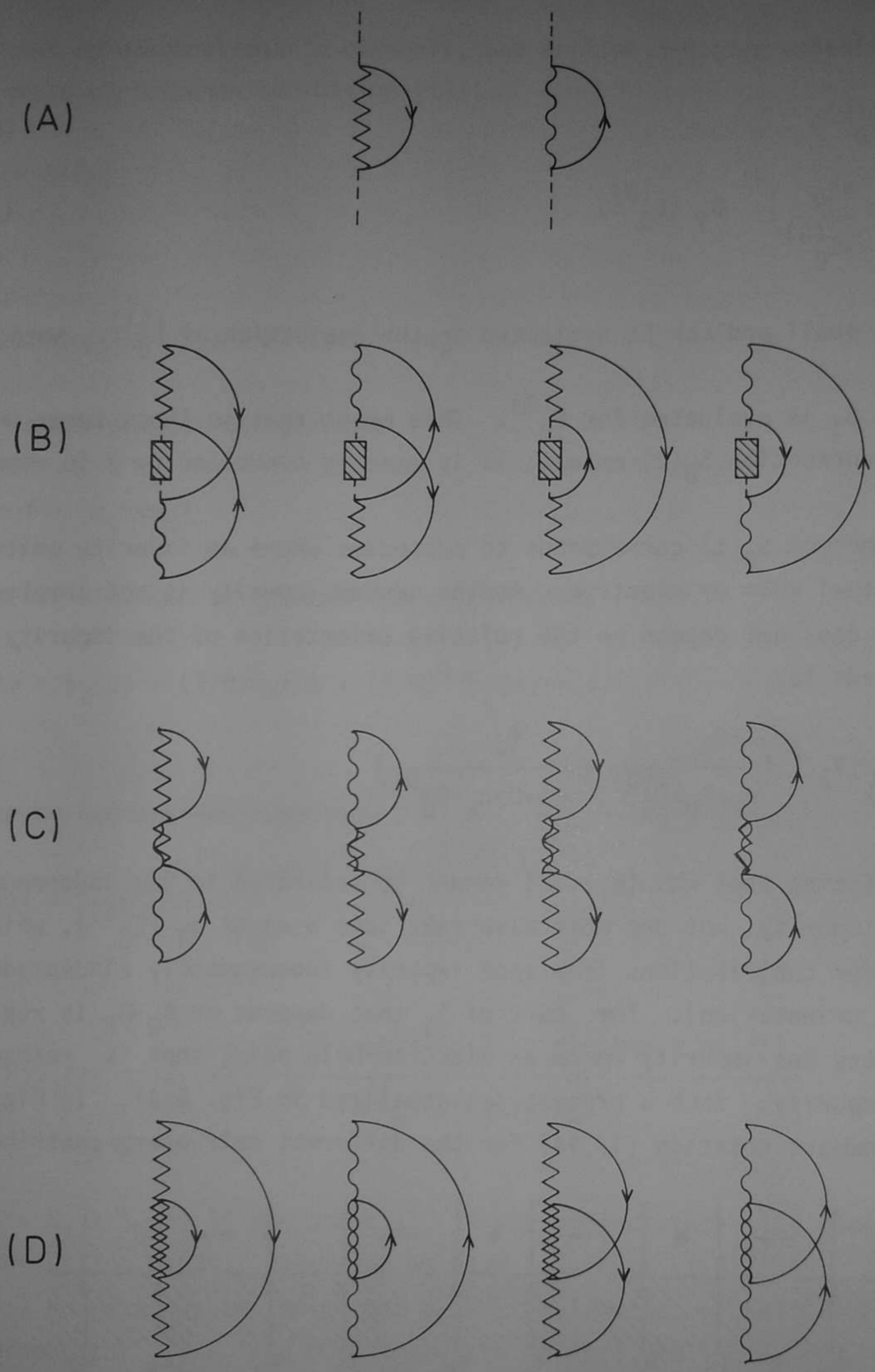

Fig. 6.18a: Irreducible diagrams of the function $S_0(z)$.
b,c and d: Irreducible diagrams of the function $S_1(z)$.

Because the intermediate states include many-body states of the impurity atoms, they do not obey ordinary anti-commutation relations. Therefore, the diagrams should be read as Goldstone diagrams instead of Feynman diagrams [13]. The dashed lines at the top and bottom of the diagrams in Fig. 6.18 and in the center of those in Fig. 6.18b correspond to the ground state propagor. In the self-energy expressions the dashed lines at the top and bottom of each graph have to be ignored. The wiggly (wavy) lines are states where one impurity has emitted (absorbed) an electron. Overlapping wiggly (wavy) lines are states where both impurities have emitted (absorbed) an electron. The hatched blocks are the self-energy insertions of Fig. 6.18a. As we are interested in indirect exchange interactions, we must write out the diagrams in such a way that electrons are exchanged between the impurities. For example, the process of the first diagram of Fig. 6.18d can be translated to: impurity A emits electron k, impurity B emits electron q, impurity A absorbs electron q and impurity B absorbs electron k (from top to bottom), which is an exchange process. The same diagram contributes to: impurity A emits electron k, impurity B emits electron q, impurity B absorbs electron q, and impurity A absorbs electron k, which are processes that involve independent virtual excitations of both impurities and therefore do not depend on relative impurity orientation. True enough, the Pauli principle forbids k and q to be of equal spin-momentum quantum number, but this exclusion only gives a vanishing contribution to the self-energy. Each of the exchange processes of Fig. 6.18 contributes twice, because the order in which both impurities are involved can be reversed.

Note, that the diagrams of Fig. 6.18b are the only ones that represent successive electron-hole pair emission and reabsorption. The other diagrams are of a more complex nature and include states, where both impurities are excited at the same time. The latter diagrams are absent if one uses the Hamiltonian of Eq. (6.2.1) instead of an Anderson Hamiltonian. We will see later that they contribute to short range antiferromagnetic coupling.

We are ready now to evaluate the diagrams of Fig. 6.18 for the s-impurity case. Fig. 6.18b contains the four possible electron-hole pair production events. As these are the only processes that are normally taken into account in RKKY theory, we will indicate them as such:

$$S_{RKKY}(z) = -2s \sum_{kq}\left[V_q^2\, V_k^2(\cos(\mathbf{k}-\mathbf{q})\cdot\mathbf{R})\left(\frac{U+\eta_k-\eta_q-2z}{(\eta_k-\epsilon_d-z)(\epsilon_d+U-\eta_q-z)}\right)^2 \frac{(1-f_k)f_q}{\eta_k-\eta_q+\{S_0(z)-z\}}\right] \tag{6.3.13}$$

Note that $S_0(z)-z$ equals zero for $z = E_0^{(0)}$. If we had not included the self-energy insertion S_0, the presence of $z(<0)$ in the denominator would have resulted in an artificial gap at the Fermi level. In Rayleigh-Schrödinger perturbation theory this "gap" term would not have appeared in the denominator. Apparently the use of a 1/N expansion removes some of the artifacts introduced by Brillouin-Wigner theory.

Fig. 6.18c forms a class of processes, where the intermediate state has an electron removed from one impurity and added to the other one. We will call this type of process "indirect charge transfer" (ICT). So Fig. 6.18c contributes:

$$S_{ICT}(z) = 2s\,\frac{1}{U-z}\left|\sum_k\left\{V_k^2\, e^{i\mathbf{k}\cdot\mathbf{R}}\left(\frac{1-f_k}{\eta_k-\epsilon_d-z} - \frac{f_k}{\epsilon_d+U-\eta_k-z}\right)\right\}\right|^2 \tag{6.3.14}$$

Fig. 6.18d forms a class of processes where the impurity pair is doubly ionized in the intermediate state, i.e., where a pair of electrons or holes is emitted and reabsorbed. We will call them particle pair production processes (PPP):

$$S_{PPP}(z) = s\sum_{kq}\left[e^{i(\mathbf{k}-\mathbf{q})\cdot\mathbf{R}}\left(\frac{1}{\epsilon_d+U-\eta_k-z}+\frac{1}{\epsilon_d+U-\eta_q-z}\right)^2 \frac{f_k f_q}{2(\epsilon_d+U)-\eta_k-\eta_q-z}\right]$$

$$+ s\sum_{kq}\left[e^{i(\mathbf{k}-\mathbf{q})R}\left(\frac{1}{\eta_k-\epsilon_d-z}+\frac{1}{\eta_q-\epsilon_d-z}\right)^2 \frac{(1-f_k)(1-f_q)}{\eta_k+\eta_q-2\epsilon_d-z}\right] \tag{6.3.15}$$

We will assume $|z|,|\eta_k| \ll |\epsilon_d|$ and $|z|,|\eta_k| \ll (\epsilon_d+U)$ in the denominators of Eqs. (6.3.13) to (6.3.14) and a three dimensional parabolic band with one electron per unit cell ($\Omega = 3\pi^2\, k_F^{-3}$). We furthermore define the range function [1]:

$$F(x) = \frac{x\cos x - \sin x}{x^4} \tag{6.3.16}$$

and the constants:

$$J_{sd} = - \frac{UV^2}{|\epsilon_d|(\epsilon_d+U)} \tag{6.3.17}$$

$$K = |J_{sd}|V^2 \left(\frac{1}{|\epsilon_d|^2} + \frac{1}{(\epsilon_d+U)^2} \right) \tag{6.3.18}$$

In terms of which

$$S_{RKKY} = 2s\, J_{sd}^2 \left(\frac{g}{4k_F{}^6}\right)\left(\frac{2m_e}{\hbar^2}\right) \int_0^{k_F} \left(\frac{\sin kR\, k^2 dk}{kR}\right) \int_{k_F}^{\infty} \left(\frac{\sin qR\, q^2\, dq}{qR(q^2-k^2)}\right) =$$

$$= \frac{9\pi}{8E_F} J_{sd}^2 F(2Rk_F)s \tag{6.3.19}$$

$$S_{ICT} = 2s \frac{V^4}{U} \left| \left\{ \frac{1}{|\epsilon_d|} \left(\frac{3}{2k_F{}^3}\right) \int_{k_F}^{\infty} \left(\frac{\sin kR}{kR} k^2 dk\right) - \right.\right.$$

$$\left.\left. - \frac{1}{\epsilon_d+U} \left(\frac{3}{2k_F{}^3}\right) \int_0^{k_F} \left(\frac{\sin kR}{kR} k^2 dk\right) \right\} \right|^2 =$$

$$= \frac{9}{2} \frac{V^4}{U} \left(\frac{1}{|\epsilon_d|} + \frac{1}{\epsilon_d+U} \right)^2 (Rk_F F(Rk_F))^2 s \tag{6.3.20}$$

$$S_{PPP} = 2s\, V^4 \left[\frac{1}{(\epsilon_d+U)^3} \left\{ \frac{3}{2k_F{}^3} \int_0^{k_F} \left(\frac{\sin kR}{kR} k^2 dk\right) \right\}^2 + \right.$$

$$\left. + \frac{1}{|\epsilon_d|^3} \left\{ \frac{3}{2k_F{}^3} \int_{k_F}^{\infty} \left(\frac{\sin kR}{kR} k^2 dk\right) \right\}^2 \right] =$$

$$= \frac{9}{2} V^4 \left(\frac{1}{|\epsilon_d|^3} + \frac{1}{(\epsilon_d+U)^3} \right) (Rk_F F(Rk_F))^2 s \tag{6.3.21}$$

Omitting $S_0 \cdot S_R$ independent terms we finally arrive at:

$$S_{RKKY} = \frac{9\pi}{8E_F} J_{sd}^2 F(2Rk_F) S^{-1} S_0 \cdot S_R \qquad (6.3.22)$$

$$S_{ICT} + S_{PPP} = \frac{9}{2} K(Rk_F F(Rk_F))^2 S^{-1} S_0 \cdot S_R \qquad (6.3.23)$$

These expressions can be extended to the five-fold degenerate case by replacing Eq. (6.3.3) with [15]:

$$H^{(1)} = \sum_{R_i} \sum_{k,m,\sigma} \left\{ V_{km} e^{ik \cdot R_i} d^{\dagger}_{R_i m\sigma} c_{k\sigma} + H.C. \right\} \qquad (6.3.24)$$

with

$$V_{km} = V_k Y_{lm} (\hat{k}) \qquad (6.3.25)$$

where the Y_{lm} are associated Legendre polynomials normalized to 4π.

The expression for the groundstate must be replaced with

$$|g_s\rangle = \frac{1}{\sqrt{2}} (D^{\dagger}_{0,5/2} D^{\dagger}_{R,3/2} + s D^{\dagger}_{0,3/2} D^{\dagger}_{R,5/2}) |g\rangle$$

$$D^{\dagger}_{R,5/2} = \prod_m d^{\dagger}_{R,M,\uparrow}$$

$$D^{\dagger}_{R,3/2} = S^- D^{\dagger}_{R,5/2} \qquad (6.3.26)$$

and S^- is the spin lowering operator. The z spin quantum number of $|g_s\rangle$ is 4 and the main spin quantum number is 5(4) for s=1 (-1), whereas the total spin of each impurity is 5/2. In other words $s = S^{-1} S_0 \cdot S_R + 1-S$. The only effect of these modifications on Eqs. (6.3.13) to (6.3.15) is to replace U with $U^{eff} = U + 4J$ and the insertion of a factor

$$\frac{1}{2l+1}\left(\sum_m Y_{lm}(\hat{k})\, Y_{lm}(\hat{q})\right)^2 = (2l+1)\,(P_l(\hat{k}\cdot\hat{q}))^2 \qquad (6.3.27)$$

which equals one for l=0 and is one on the average for any other l-values. The occurrence of the $(P_l(\cos\theta_{kq}))^2$ in the summations over k and q is a severe complication of the algebra in performing the summations. We have not tried to solve this problem, but the fact that this factor is one on the average shows that Eqs. (6.3.22) and (6.3.23) are good approximations in the degenerate case.

The V_k's of Eq. (6.3.25) are related to the H.W.H.M. of the majority and minority peaks corresponding to the half filled shell through

$$\Gamma = \frac{2l+2}{2l+1}\,\mathrm{Im}\left(\frac{1}{N}\sum_k V_{km}^2 g_{k\sigma}^{k\sigma}\right) = \pi\rho_\sigma \frac{2l+2}{2l+1} V^2 \qquad (6.3.28)$$

Here ρ_σ is the s-p band density of states at the Fermi level for one spin direction. The angular integration over V_{km}^2 results in $4\pi V_k^2$ in view of Eq. (6.3.25), and we assume V_k^2 to be energy independent in the energy region of interest. The factor $\frac{2l+2}{2l+1}$ stems from the fractional $d^5(^6S)$ parentage of the $d^6(^5D)$ and $d^4(^5D)$ states.

In Table 6.3.1 we give the J(n) values for n'th neighbor atoms according to the expression

$$E_{exch} = -J(n)\, S_o \cdot S_n \qquad (6.3.29)$$

using Eqs. (6.3.17) to (6.3.28) for the l=2 case. A negative sign means antiferromagnetic coupling. We used the experimental UPS and BIS parameters of Table 6.2.2 for Γ, ϵ_d and U^{eff}, and neglected the contribution of the majority peak for CuMn. We took the values 7.03 (eV) and 5.49 (eV) for the Fermi temperatures of Cu and Ag respectively which correspond to a parabolic band, one electron per atom and the room temperature atomic densities of these elements. The one spin density of states at E_F is then $\frac{3}{4} E_F^{-1}$.

We see that the indirect charge transfer and particle pair production processes contribute significantly to the exchange, particularly for nearest neighbor atoms. The values should not be taken too literally, however, in view of the assumptions

Table 6.3.1. Values for J(n) in Kelvin

n	Solid	ICT+PPP	RKKY
1	CuMn	-259	-21
2		-14	9
3		-40	-5
4		-11	-1
1	AgMn	-91	-13
2		-5	6
3		-14	-3
4		-4	0

made to arrive at Eqs. (6.3.20) and (6.3.21). Especially the limit $|n_k| << |\epsilon_d|$ etc. is only valid near the Fermi level and more reliable results must be expected from incorporating the k dependence of the denominators in Eqs. (6.3.13), (6.3.14) and (6.3.15). This cannot influence the sign of the ICT contributions, which is always anti-ferromagnetic. The latter is not rigorous for the PPP contributions as one can see from Eq. (6.3.15). The importance of the ICT and PPP processes is a direct consequence of the inapplicability of the Schrieffer-Wolff transformation for CuMn and AgMn as we have mentioned before. Note that in the limit $|\epsilon_d|$ $|\epsilon_d+U| >> \Gamma$ the ICT and PPP terms vanish compared to the RKKY interaction, as their contribution is proportional to $E_F/|\epsilon_{\pm}|$ relative to the RKKY term. This is the main reason why these interactions are normally neglected [17].

It is remarkable that the theoretical results [10] agree on the sign of the interaction for nearest neighbor atoms, although the spin glass-susceptibility analysis [16] indicates ferromagnetic coupling in that case.

The occupied d bands can participate in indirect exchange, mainly through the processes of Fig. 6.18b, where one d hole and one sp electron are emitted and reabsorbed. This will give rise to oscillations in the exchange interaction of a different type than the RKKY interaction. As the d-holes are removed quite far

from the Fermi level in CuMn and AgMn, the interaction decays faster than the RKKY interaction as a function of impurity distance. The strongest effect occurs for nearest neighbor atoms, where the exchange of electrons and holes occurs directly through the d-d hybridization. This gives rise to anti-ferromagnetic [18] coupling. Also the processes where one particle is transferred directly and one travels through the sp bands results in anti-ferromagnetic coupling. The reason for this is that delocalization of the d electrons into the empty d-states of the neighbor atom is easier for the antiferromagnetic alignment of the impurities. This leads to an energy-gain relative to the ferromagnetic orientation if the transfer matrix element of electron and hole are of equal sign. For half-filled d-shells the direct d-d hopping matrix elements have a positive sign on the average. The indirect hopping matrix element through the k-electrons will also be positive if the distance between the impurities is small compared to the distance between the nodes in the free electron wave function ($Rk_F << \pi$). This condition is fulfilled for nearest neighbors in the Z=1 FCC lattice. We see that any unenhanced type of indirect exchange gives anti-ferromagnetic interactions for nearest neighbors with half-filled d-shells.

The RKKY-term of Eq. (6.3.22) would become ferromagnetic if the impurity atoms could approach each other closer than the nearest neighbor distance. Vice versa, exchange enhancement of the susceptibility of the conduction electrons makes the range of ferromagnetic coupling larger [19]. This becomes important in host materials like Pd, where the d bands cross the Fermi level, but can be neglected in the sp bands of Cu and Ag.

We conclude that indirect charge transfer and particle pair production processes contribute significantly to the indirect exchange interactions in CuMn and AgMn. This is due to the inapplicability of the Schrieffer-Wolff transformation in these systems and strongly affects the often assumed RKKY interaction between impurities.

References

1. C. Kittel in Solid State Physics, edited by F. Seitz and D. Turnbull (Academic, New York, 1968), Vol. 22.
2. M.A. Ruderman and C. Kittel, Phys. Rev. 96, 99 (1954).
3. T. Kasuya, Progr. Theor. Phys. 16, 45 (1956).
4. K. Yosida, Phys. Rev. 106, 893 (1957).
5. D. van der Marel, G.A. Sawatzky and F.U. Hillebrecht, Phys. Rev. Lett. 53, 206 (1984); Phys. Rev. B 31, 1936 (1985).
6. B. Caroli, J. Phys. Chem. Solids 28, 1427 (1967).
7. J.C. Parlebas, J. Phys. F 4, 1392 (1974).
8. G. Malmström, D.J.W. Geldart and C. Blomberg, J. Phys. F 6, 233 (1976).
9. D.C. Price, J. Phys. F 8, 933 (1978).
10. A. Oswald, R. Zeller, P.J. Braspennig and P.H. Dederichs, J. Phys. F 15, 193,(1985).
11. J.M. Ziman, "Elements of Advanced Quantum Theory" (Cambridge University Press, Cambridge, 1969), p.53.
12. F.C. Zhang and T.K. Lee, Phys. Rev. 28, 33 (1983).
13. H. Keiter and J.C. Kimball, Int. J. Magn. 1, 233 (1971).
14. P. Coleman, Phys. Rev. B 28, 5255 (1983).
15. B. Caroli, J. Phys. F 5, 1399 (1975).
16. A.F.J. Morgownik and J.A. Mydosh, Solid State Commun. 47, 321 (1983).
17. M. Lavagna and M. Cyrot, Solid State Commun. 55, 555 (1985).
18. S. Alexander and P.W. Anderson, Phys. Rev. 133, 1594 (1964).
19. B. Giovanni, M. Peter and J.H. Schrieffer, Phys. Rev. Lett. 12, 736 (1964).

CHAPTER VII

MICROSCOPIC THEORY FOR TRIPLET PAIRING IN AN ANDERSON LATTICE

A microscopic mechanism for triplet pairing of conduction electrons is discussed. It is argued that the effective f-f interaction on a uranium atom in a metallic lattice may be attractive. A unitary transformation of an Anderson (empty) lattice hamiltonian results in a Fröhlich like hamiltonian with the phonons replaced by doubly (de) occupied f states.

7.1. Introduction

Recently the uranium compounds UBe_{13} and UPt_3 have attracted considerable attention, because in these solids superconductivity and "heavy fermion" properties co-exist [1,2,3,4]. It has been suggested that these systems are "triplet" superconductors for a number of reasons [5,6].

It is often assumed, that paramagnon exchange is the microscopic origin of the triplet pairing in these superconductors, like in ^3He [7,8]. Nevertheless, this point is far from being settled, as paramagnon theory predicts a positive pressure induced change in T_c [9], contrary to experimental results [10]. Strong Coulomb repulsion between uranium 5f electrons is believed to prevent the formation of conventional s-wave Cooper pairs on the one hand [6] and on the other hand, the 5f states act as a reservoir of quasi localized quenched moments close to a magnetic transition, thus having strong spin fluctuations, which may bind conduction electrons into p-wave Cooper pairs [9].

The aim of this chapter is to point out that the Coulomb repulsion at the uranium sites may be very small due to screening, and may even be exceeded by the local 5f Hund's Rule exchange interactions, resulting in a net local attraction between parallel spins in the uranium 5f shell. We show that hybridization between conduction states and 5f states then leads to a net attraction between parallel

spins in the conduction bands near E_F. We will show, that there is indeed a close relation between an Anderson lattice type hamiltonian and a triplet BCS hamiltonian.

Before turning to the actual model, we will first briefly discuss the energetics of a single 5f atom. We will do this for the case of an atom having almost unoccupied f levels. Clearly this situation is quite different from what is expected to be found in uranium compounds, but we will argue later, that our findings can be applied to the more general f^n state under certain circumstances. Restricting our discussion to the lowest Hund's Rule states of each multiplet, we can express the energy of an atom having zero, one or two f electrons as [11]:

$$E(f^0(^1S)) = 0$$

$$E(f^1(^2F)) = \varepsilon_f$$

$$E(f^2(^3H)) = 2\varepsilon_f + U - K$$

where U and K are shorthand for Coulomb monopole interactions and exchange plus multipole interactions, expressed in terms of Slater integrals as:

$$U = F^0$$

$$K = \frac{1}{9} F^2 + \frac{17}{363} F^4 + \frac{25}{14157} F^6$$

If we put such an atom into a solid, the one electron potential ε_f changes and the Coulomb interactions are screened due to the response of the electron gas to a polarity change of the 5f shell. In Mn [12], Ni [13] and Cu [14] the reduction of F^0 due to screening is about 20 eV compared to the theoretical bare atomic values of Mann's tables [15]. In the rare earths this reduction is 23 eV on the average [16,17] (Chapter II of this thesis). The multipole integrals, on the other hand, are only slightly reduced in these cases, indicating that the electron gas does not respond to the details of the charge distribution in a given polarity state. This is the reason, why atomic like multiplets are observed in valence XPS, BIS and XAS of the rare earths [18,19] and Mn impurities [12,20]. It is also the principle origin of the large Hubbard gap in systems where the d or f shell is

half occupied, such as Eu, Gd and Mn impurities, as these gaps have a lower bound of 21J, even when F^o is screened to zero.

We believe, that localized behavior and strong screening also exist in actinide compounds for a number of reasons:

(1) Bandstructure calculations of uranium compounds show that the dispersional part of the 5f bands are extremely narrow, especially in view of the fact, that part of the width is due to spin orbit splitting [21,22,23].

(2) BIS and XPS valence spectra of UO_2 and other actinide oxydes can be explained quite well with atomic multiplet theory [24,25], indicating that in the solid the F^2, F^4 and F^6 integrals are not strongly different from atomic values. Now the bare atomic theoretical value of F^o is 19.3 eV for uranium [15]. Assuming that the same mechanisms exists in the iron row elements, the lanthanides and the actinides, we expect a reduction of about 20 eV, thus reducing F^o to (almost) zero. In fact, comparison of the combined XPS and BIS valence spectra of UAl_2, UPt_3 [26] and UBe_{13} [27] with those of Pr or Nd [18] shows that the Hubbard gap must be much smaller in the former case, which we also expect from the smaller bare F^o integral. Of course, we must remember that the interpretation of the (inverse) photoemission spectra of uranium intermetallic compounds is highly non-trivial, as initial and final states are presumably of mixed valent character, like in Ce [28,29]. We see that, although the Coulomb interaction is strongly reduced, the exchange interactions are not, so that a simple band theory of uncorrelated particles is probably not applicable. In Ref.17 we use atomic values for F^2, F^4 and F^6 and a strongly screened F^o to show that the atom fluctuates between f^2, f^3 and f^o, whereas f^1 is relatively high in energy. In our model we will reverse the picture in order to avoid cumbersome mathematics: the lowest state is $f^o(^1S)$, $f^1(^2F)$ is at the energy ε_f and the energy of $f^2(^3H)$ is ε_H. We will assume that f^3 and higher polarity states, as well as the other terms of the f^2 multiplet, have high enough energies to be irrelevant to our discussion. We will also assume that there are only two f orbitals f_1 and f_2 that mix into the ground state, each one coupling to an orthogonal conduction band, also carrying the index m = 1 or 2.

7.2. Transformation to an electron-phonon-like Hamiltonian

The model hamiltonian is:

$$H = H_o + H_1 \tag{7.1}$$

$$H_o = \sum_{Rm\sigma} (\varepsilon_f \, f^+_{Rm\sigma} f_{Rm\sigma}) + \sum_{R\sigma\sigma'\sigma''\sigma'''} \Big\{ U(n_f,\sigma,\sigma',\sigma'',\sigma''') \, f^+_{R1\sigma} \, f_{R1\sigma'} \, f^+_{R2\sigma''} \, f_{R2\sigma'''} \Big\} + \sum_{km\sigma} (\eta_k c^+_{km\sigma} \, c_{km\sigma}) \tag{7.2}$$

$$H_1 = \sum_{Rkm\sigma} \left(\frac{1}{\sqrt{N}} V_{km} \, e^{ik\cdot R} \, f^+_{Rm\sigma} \, c_{km\sigma} + H.C. \right) \tag{7.3}$$

where $U(f^2(^3H)) = \varepsilon_H - 2\varepsilon_f$

and all other terms are assumed to be high in energy and are projected out with $U \to \infty$. In the case of a single impurity at site o we can apply the Schrieffer-Wolff transformation [30,31] taking f^o as the polarity of the atom and obtain a transformed hamiltonian.

$$\tilde{H} = \sum_{km\sigma} (\eta_k \, c^+_{km\sigma} c_{km\sigma}) + \sum_{kqm\sigma} \left(\frac{1}{N} W_{kq} \, c^+_{km\sigma} \, c_{qm\sigma} \right)$$

where

$$W_{kq} = -\tfrac{1}{2} V^2 \left(\frac{1}{\varepsilon_f - \eta_k} + \frac{1}{\varepsilon_f - \eta_q} \right) \tag{7.4}$$

Similarly, if the polarity is f^2, we obtain

$$\tilde{H} = \sum_{km\sigma} (\eta_k \, c^+_{km\sigma} \, c_{km\sigma}) + \sum_{qkm\sigma\sigma'} \left(\frac{1}{N} J_{kq} \langle f^2 | f^+_{m\sigma} f_{m\sigma'} | f^2 \rangle \, c^+_{km} \, c_{qm\sigma'} \right)$$

where

$$J_{kq} = -\tfrac{1}{2} V^2 \left(\frac{1}{\varepsilon_f - \varepsilon_H - \eta_k} + \frac{1}{\varepsilon_f - \varepsilon_H - \eta_q} \right) \tag{7.5}$$

which is the usual Kondo hamiltonian. The lowest order term in the Schrieffer-Wolff transformation also gives us terms corresponding to the annihilation and creation of two conduction electrons and a polarity change of two charges in the f shell. In their original paper [30], Schrieffer and Wolff recognized the occurrence of such terms, but discarded them, because polarity changes by two charges were high energy states irrelevant to the topic of the Kondo effect. In our case, however, these states become important as we want to consider the limit where their energies are low.

Let us turn to the lattice hamiltonian of Eqs. (7.1) to (7.3). We make a transformation $\tilde{H} = e^{+S} H e^{-S}$, such that the terms linear in H_1 vanish. This leads to

$$\tilde{H} = H_0 + \tilde{H}_2 + \tilde{H}_3 + \tilde{H}_4 + \ldots \tag{7.6}$$

where

$$\langle \alpha | S | \beta \rangle = \frac{\langle \alpha | H_1 | \beta \rangle}{E_\beta - E_\alpha} \tag{7.7a}$$

$$\langle \alpha | \tilde{H}_2 | \beta \rangle = \langle \alpha | \tfrac{1}{2} [H_1, S] | \beta \rangle = \tfrac{1}{2} \sum_\gamma \left\{ \left(\frac{1}{E_\beta - E_\gamma} + \frac{1}{E_\alpha - E_\gamma} \right) \langle \alpha | H_1 | \gamma \rangle \langle \gamma | H_1 | \beta \rangle \right\} \tag{7.7b}$$

$$H_n = \frac{n-1}{n(n-2)} [\tilde{H}_{n-1}, S] \tag{7.7c}$$

The terms quadratic in H_1 are provided by $\tilde{H}_2$ and for our discussion there are three relevant types of matrix elements $\langle \alpha | H_2 | \beta \rangle$:

(1) α and β correspond to f^0 at all lattice sites.

(2) idem., except at site **R**, where α corresponds to f^0 and β to f^2. Terms connecting f^0 to f^1 at two different sites have zero amplitude.

(3) idem., except at site **R**, where α and β correspond to f^2.

These terms are readily obtained and read:

$$\tilde{H}_{2,1} = \frac{1}{N} \sum_{Rkqm\sigma} \left\{ e^{iR\cdot(k-q)} W_{kq} C^{\dagger}_{km\sigma} c_{qm\sigma} \right\} \tag{7.8a}$$

$$\tilde{H}_{2,2} = \frac{1}{N} \sum_{RR'kk'm_s} \left\{ T_{kk'} e^{i(k\cdot R + k'\cdot R')} \right.$$

$$\left. \sum'_{\sigma\sigma'} (c^{\dagger}_{k1\sigma} c^{\dagger}_{k'2\sigma} f_{R1\sigma} f_{R'2\sigma'} + H.C.) \right\} \tag{7.8b}$$

$$\tilde{H}_{2,3} = \frac{1}{N} \sum_{Rkqm\sigma\sigma'} \left\{ e^{iR(k-q)} J_{kq} \langle f^2_R | f^{\dagger}_{Rm\sigma} f_{Rm\sigma'} | f^2_R \rangle c^{\dagger}_{km\sigma} c_{qm\sigma'} \right\} \tag{7.8c}$$

where the summation over σ and σ' in Eq. (7.8b) is subject to the conditions that the total spin is one and the z component is m_s and:

$$T_{kk'} = -\tfrac{1}{2} V_k V_{k'} \left\{ \frac{1}{\varepsilon_f - \eta_k} + \frac{1}{\varepsilon_f - \eta_{k'}} + \frac{1}{\varepsilon_f - \varepsilon_H + \eta_k} + \frac{1}{\varepsilon_f - \varepsilon_H + \eta_{k'}} \right\} \qquad (R = R')$$

$$= 0 \qquad (R \neq R') \tag{7.9}$$

and W_{kq} and J_{kq} are already defined in Eqs. (7.4) and (7.5). $\tilde{H}_{2,1}$ is a renormalization of the conduction electron energies due to hybridization with the f^1 states. This term can be included in H_0 without affecting the physics. $\tilde{H}_{2,3}$ describes the spin flip scattering of the conduction electrons from the $f^2(^3H)$ local moments. These terms are extremely important if f^2 is lower in energy than f^0 and may result in Kondo compensation of the magnetic moment at low temperatures. They also cause a renormalization of the $f^2(^3H)$ energies, which we symbolically indicate by replacing ε_H in H_0 with $\tilde{\varepsilon}_H$. $\tilde{H}_{2,2}$ describes simultaneous hops of two conduction electrons to a 5f site. We can use formal exciton notation for the f^2 states, where the electrons are separated with a spatial vector Δ:

$$B^{\dagger}_{q\uparrow\uparrow\Delta} = \frac{1}{\sqrt{N}} \sum_R \left\{ e^{iq\cdot R} f^{\dagger}_{R+\frac{1}{2}\Delta\ 1\uparrow} f^{\dagger}_{R-\frac{1}{2}\Delta\ 2\uparrow} \right\}$$

and similar expressions for the other two spin functions. These states have energies $2\varepsilon_f$ for $\Delta \neq 0$ and ε_H for $\Delta = 0$. Now Eq. (7.8) becomes:

$$\tilde{H}_2 = \frac{1}{\sqrt{N}} \sum_{kqm_s} \left(\sum_{\sigma\sigma'}{}' , \left\{ T_{kq} c^{\dagger}_{k1\sigma} c^{\dagger}_{q2\sigma'} , B_{k+qm_s0} + \text{H.C.} \right\} \right) \tag{7.10}$$

which is quite similar to a Fröhlich interaction [32], except that the role of phonons is taken over by f^2 states and that pairs of creation operators occur instead of pairs consisting of one creation and one annihilation operator.

7.3. Further transformations to triplet pairing interaction

Now there are two ways that two conduction electrons are coupled in fourth order of H_1:

(1) The simultaneous (de)occupation of f^2 states quadratic in $\tilde{H}_2$.

(2) Through the fourth order term in the Schrieffer-Wolff transformation $\tilde{H}_4$ of Eqs. (7.6) and (7.7).

The first possibility is easily accomplished by a second transformation, similar to the treatment of electron-phonon interactions. One simply looks for a generator S that removes all terms linear in $\tilde{H}_2$, as in Eqs. (7.6) and (7.7). Such a transformation also modifies $\tilde{H}_3$, $\tilde{H}_4$ etc. by adding fifth and sixth order terms in H_1 to them. As we won't consider terms of fifth and higher order, this is no point of concern. The lowest order term in our new hamiltonian $\tilde{\tilde{H}}$ is quadratic in $\tilde{H}_2$ and we will indicate it with $\tilde{\tilde{H}}_4$:

$$\tilde{\tilde{H}}_4 = \frac{1}{N} \sum_{kk'qq'm_s} \sum_{\sigma\sigma'}{}' \left(V(k,k',q,q') \delta(k+k'-q-q') \; c^{\dagger}_{q1\sigma} c^{\dagger}_{q'2\sigma'} c_{k'2\sigma'} c_{k1\sigma} \right) \tag{7.11}$$

where

$$V(k,k',q,q') = -\tfrac{1}{2} T_{kk'} T_{qq'} \left(\frac{1}{\varepsilon_H - \eta_k - \eta_{k'}} + \frac{1}{\varepsilon_H - \eta_q - \eta_{q'}} \right) \langle [B_{k+k'm_s0}, B^{\dagger}_{q+q'm_s0}] \rangle \tag{7.12}$$

As the two particle states $B^{\dagger}_{qm_s0}|\Psi>$ are no real bosons, we expect some difficulties with this expression as soon as the f^2 states become thermally occupied. As long as $|\Psi>$ contains no f^2 character, the commutator in Eq. (7.12) conserves momentum:

$$<f^0|[B_{km_s0}\ ,\ B^{\dagger}_{qm_s0}]|f^0> = \delta_{kq} \tag{7.13}$$

The mixing in of f^2 states through thermal fluctuations will destroy momentum conservation and decrease the coherent part of the interaction. In Fig. 7.1 we see, that our interaction is attractive and increases as ε_H approaches zero. For $\varepsilon_H = 2\varepsilon_f$ we have $T_{kk'} = 0$ resulting in no coupling, as expected. However, if $\varepsilon_H > 2\varepsilon_f$ we get again an attractive interaction, which is rather unphysical, as the f electrons repel each other in this limit. Another unphysical behaviour is near $\varepsilon_H = \varepsilon_f$, where $T_{kk'}$ has a pole.

Both problems are solved, if we add $\tilde{H}_4$ to the interaction, so that we add up all quartic terms contributing to the electron-electron interaction. The expressions for $\tilde{H}_3$ and $\tilde{H}_4$ are:

$$\tilde{H}_3 = \frac{1}{3}\,[[H_1,S],S] \text{ and } \tilde{H}_4 = \frac{1}{8}[[[H_1,S],S],S] \tag{7.14}$$

$\tilde{H}_3$ does not contribute to electron-electron coupling in fourth order, as it changes the f occupation by one or three. In $\tilde{H}_4$ there are two different channels that contribute: (1) $|k>$ scatters to $|f_{R1}>$ and then to $|k'>$ followed by a similar process involving $|q>, |R>$ and $|q'>$. (2) A simultaneous hop of k and q to f^2 and back to k' and q'. Terms where k and q are scattered to different sites R and R' cancel in the summation over both channels. The matrix elements of $\tilde{H}_4$ are:

$$<\beta|\tilde{H}_4|\alpha> = \frac{1}{8\mu\gamma\rho}\sum\Bigg(<\beta|H_1|\gamma><\gamma|H_1|\mu><\mu|H_1|\rho><\rho|H_1|\alpha>$$

$$\left\{\frac{3}{(E_\beta-E_\gamma)(E_\alpha-E_\rho)}\left[\frac{1}{E_\rho-E_\mu}+\frac{1}{E_\gamma-E_\mu}\right]+\frac{1}{(E_\rho-E_\mu)(E_\mu-E_\gamma)}\left[\frac{1}{E_\alpha-E_\rho}+\frac{1}{E_\beta-E_\gamma}\right]\right\}\Bigg) \tag{7.15}$$

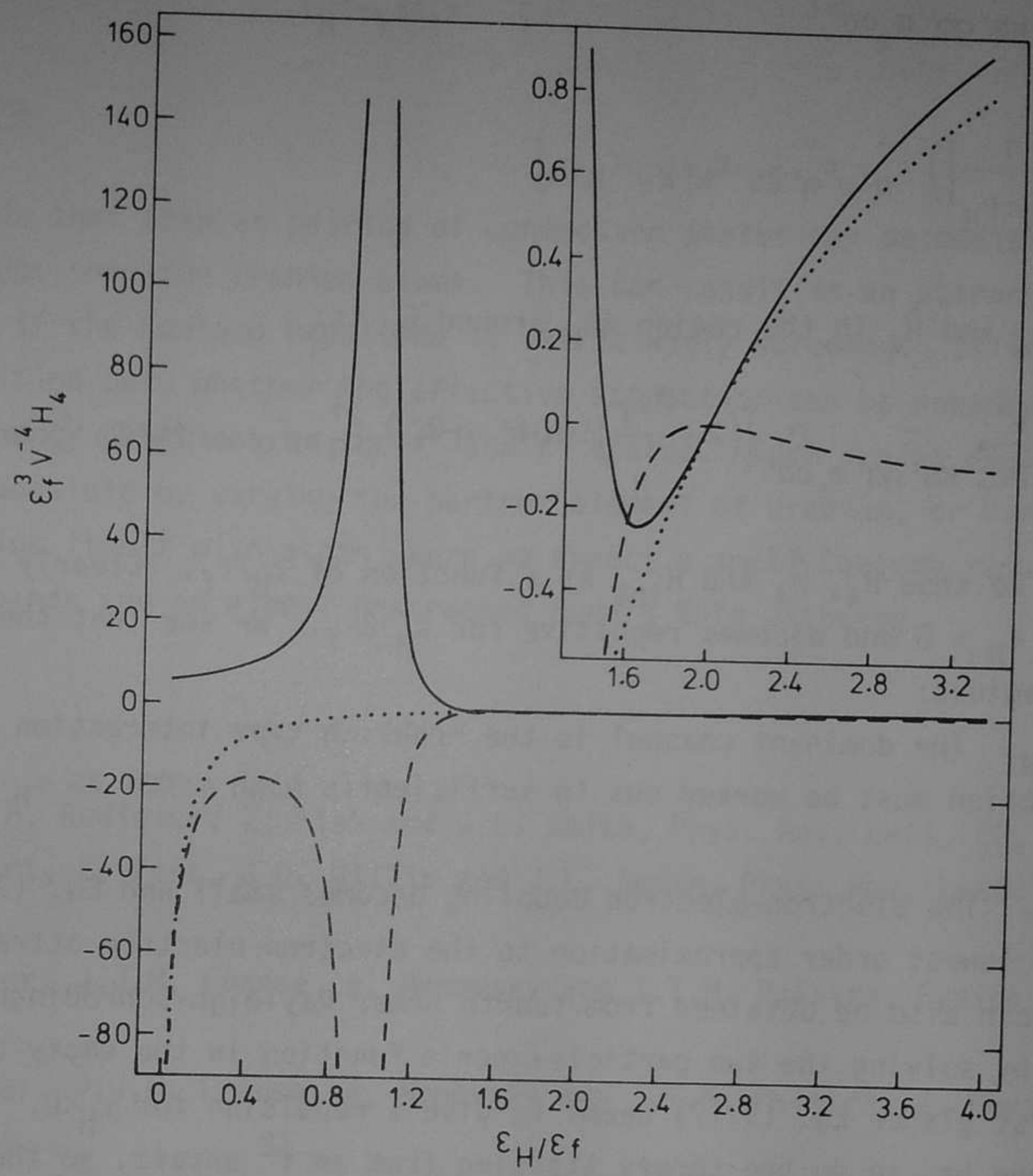

Fig. 7.1. Effective conduction electron interactions $\tilde{H}_4$ *(solid curve),* $\tilde{\tilde{H}}_4$ *(broken) and* H_{int} *(dotted) as a function of* $\varepsilon_H/\varepsilon_f$. *The insert shows an expanded view of the region around* $\varepsilon_H/\varepsilon_f = 2$.

In the case that $|\alpha\rangle$ and $|\beta\rangle$ refer to f^0 states, this expression can be worked out for conduction states near E_F:

$$\tilde{H}_4 = \frac{1}{N} V^4 \sum_{kk'qq'} \sum_{m_s\sigma\sigma'}' \left\{ \delta(k+k'-q-q') \left(\frac{2}{\varepsilon_f^3} + \frac{1}{\varepsilon_f(\varepsilon_f-\varepsilon_H)} \right) \right.$$

$$\left. \left[\frac{3}{\varepsilon_f} + \frac{1}{\varepsilon_f-\varepsilon_H} \right] \right) c^\dagger_{q1\sigma} c^\dagger_{q'2\sigma'} c_{k'2\sigma'} c_{k1\sigma} \Big\} \qquad (7.16)$$

The sum of $\tilde{H}_4$ and $\tilde{\tilde{H}}_4$ in the region $\pm\varepsilon_H$ around E_F is:

$$H_{int} = \frac{V^4}{N\varepsilon_f^3} \sum_{kk'qq'} \sum_{m_s\sigma\sigma'}' \left\{ \left(2 - \frac{4\varepsilon_f}{\varepsilon_H} \right) \delta(k+k'-q-q') \; c^\dagger_{q1\sigma} c^\dagger_{q'2\sigma'} c_{k'2\sigma'} c_{k1\sigma} \right\} \qquad (7.17)$$

In Fig. 7.1 we show $\tilde{H}_4$, $\tilde{\tilde{H}}_4$ and H_{int} as a function of $\varepsilon_H/\varepsilon_f$. Clearly H_{int} behaves regular for $\varepsilon_H > 0$ and becomes repulsive for $\varepsilon_H > 2\varepsilon_f$. We see that there are two important regions:

(1) Small ε_H. The dominant channel is the Fröhlich type interaction of Eq. (7.10). This interaction must be worked out to sufficiently high order as ε_H approaches zero.

(2) $\varepsilon_H \gtrsim \varepsilon_f$. The electron-electron coupling becomes small and Eq. (7.17) is a fairly good lowest order approximation to the electron-electron attraction. Eq. (7.17) can also be obtained from fourth order Rayleigh-Schrödinger perturbation theory, or by solving the two particle Green's function in the empty band limit.

At first glance Eq. (7.17) seems to give a repulsion for $\varepsilon_H < 0$. However, in this case one has to do the theory starting from an f^2 ansatz, so that the commutator of Eq. (7.12) reverses sign. The net result is again an attractive interaction. There are a few problems in this case, related to the fact that $f^2(^3H)$ are three-fold spin degenerate. If, for example, all moments point in the same direction, triplet pairing will occur for one spin direction only. A similar problem exists if the moments are ordered anti-ferromagnetically. If, on the other hand, the local moments are compensated by the spin-flip terms of Eq. (7.8c) to form a Kondo singlet, each of the three spin states is equally occupied and the commutator of Eq. (7.12) obtains the value -1/3. This seems to be reasonable in UBe_{13} and UPt_3 which have Kondo resp. spin fluctuation temperatures of ca. 10 K

[1,2,3,4], which is much larger than the temperatures where superconductivity sets in.

7.4. Conclusions

We conclude that triplet pairing of conduction states may be mediated by simultaneous hops into the uranium atoms. This can result in an attraction between parallel spins if the Coulomb repulsion is sufficiently screened. It looks like a challenge to find out, whether the effective attraction can be enhanced by tuning the relative energy positions of the f^0 and f^2 states. Such tuning could, in principle, be possible by varying the partner element of uranium, or even by replacing uranium itself with atoms where we expect a small Coulomb repulsion, narrow f or d bands and an almost unscreened Hund's Rule exchange.

References

1. H.R. Ott, H. Rudigier, Z. Fisk and J.L. Smith, Phys. Rev. Lett. 50, 1595 (1983).
2. G.R. Stewart, Z. Fisk, J.O. Willis and J.L. Smith, Phys. Rev. Lett. 52, 679 (1984).
3. A. de Visser, J.J.M. Franse, A. Menovsky and T.T.M. Palstra, Fysica 127b, 442 (1984).
4. A. de Visser, J.J.M. Franse, A. Menovsky and T.T.M. Palstra, J. Phys. F14, L191 (1984).
5. H.R. Ott, H. Rudigier, T.M. Rice, K. Ueda, Z. Fisk and J.L. Smith, Phys. Rev. Lett. 52, 1915 (1984).
6. C.M. Varma, Bull. Am. Phys. Soc. 29, 857 (1984); 29, 404 (1984).
7. P.W. Anderson, Phys. Rev. B 30, 1549 (1984).
8. P.W. Anderson, Phys. Rev. B 30, 4000 (1984).
9. O.T. Valls and Z. Tešanović, Phys. Rev. Lett. 53, 1497 (1984).
10. J.O. Willis, J.D. Thompson, Z. Fisk, A. de Visser, J.J.M. Franse and A. Menovsky, Phys. Rev. B 31, 1654 (1985).
11. C.W. Nielson and George F. Koster, "Spectroscopic coefficients for the p^n, d^n and f^n configurations", The MIT Press, Massachusetts Institute of

Technology (1963).
12. D. van der Marel, G.A. Sawatzky and F.U. Hillebrecht, Phys. Rev. Lett. 53, 206 (1984); Phys. Rev. B 31, 1936 (1985).
13. J.C. Fuggle, P. Bennet, F.U. Hillebrecht, A. Lenselink and G.A. Sawatzky, Phys. Rev. Lett. 49, 1787 (1982).
14. E. Antonides and G.A. Sawatzky in "Transition Metals-1977", edited by M.G. Lee, IOP Conference Proceedings No. 39 (Institute of Physics, London, 1978), 134.
15. J.B. Mann, Los Alamos Scientific Laboratory Report No. LASL-3690 (1967).
16. J.F. Herbst, P.N. Lowy and R.E. Watson, Phys. Rev. B 6, 1913 (1972).
17. D. van der Marel and G.A. Sawatzky (unpublished).
18. J.K. Lang, Y. Bear and P.A. Cox, J. Phys. F 11, 121 (1981).
19. J.M. Esteva, R.C. Karnatak, J.C. Fuggle and G.A. Sawatzky, Phys. Rev. Lett. 50, 910 (1983); B.T. Thole, G. van der Laan, J.C. Fuggle, G.A. Sawatzky, R.C. Karnatak and J.M. Esteva, in press, Phys. Rev. B (1985).
20. B.T. Thole, R.D. Cowan, G.A. Sawatzky, J. Fink and J.C. Fuggle, Phys. Rev. B 31, 6856 (1985).
21. J. Sticht and J. Kübler, Solid State Commun. 54, 389 (1985).
22. A.M. Boring, R.C. Albers, G.R. Stewart and D.D. Koelling, Phys. Rev. B 31, 3251 (1985).
23. P. Strange and B.L. Gyorffy, "Proceedings of the Conference on Electronic Structure and Properties of Rare Earth and Actinide Intermetallics", St. Pölten, Austria, Sept. 3-6 (1984).
24. Y. Bear and J. Schoenes, Solid State Commun. 33, 885 (1980).
25. B.W. Veal, D.J. Lam, H. Diamond and H.R. Hoekstra, Phys. Rev. B 15, 2929 (1976).
26. J.W. Allen, S.J. Oh, L.E. Cox, W.P. Ellis, M. Wire, Z. Fisk, J.L. Smith, B.B. Pate, I. Lindau and A.J. Arko, to be published.
27. E. Wuilloud, Y. Bear, H.R. Ott, Z. Fisk and J.L. Smith, Phys. Rev. B 29, 5228 (1984).
28. F.U. Hillebrecht, J.C. Fuggle, G.A. Sawatzky, M. Campagna, O. Günnarsson and K. Schönhammer, Phys. Rev. B 30, 1777 (1984).
29. O. Günnarsson and K. Schönhammer, Phys. Rev. Lett. 50, 604 (1983).
30. J.R. Schrieffer and P.A. Wolff, Phys. Rev. 149, 491 (1966).
31. J.R. Schrieffer, J. Appl. Phys. 38, 1143 (1967).
32. H. Fröhlich, Proc. Phys. Soc. A 215, 291 (1952).

SAMENVATTING

In de beschrijving van de toestandsdichtheid van metalen wordt meestal gebruik gemaakt van het onafhankelijke electronen model, waarbij men aanneemt dat de bewegingen van de electronen in de vaste stof niet gecorreleerd zijn en ieder electron slechts de gemiddelde potentiaal van de overige deeltjes voelt. In theorieën, waarbij men iets verder gaat en een complexe zelf-energie toevoegt aan de één-deeltjes energieën, beschouwt men de zogenaamde exchange-correlatie als een storingsterm, die tot eindige orde in een reeks ontwikkeling meegenomen wordt. Dit beeld is correct in het geval van één gat in een volle band of schil, één electron in een lege band of schil of in het geval van een electron of gat in een precies half-gevulde schil. Ook kan men dit model toepassen indien de wisselwerkingen verwaarloosbaar zijn ten opzichte van de bandbreedte voor een gedeeltelijk gevulde band. In het omgekeerde geval, waar de wisselwerkingen tussen de electronen juist groot zijn ten opzichte van de bandbreedte, is het beter de hybridizatie op te vatten als storingsparameter, terwijl men de electron-electron interacties "exact" meeneemt. Systemen waar dit het geval is hebben vaak interessante eigenschappen, zoals magnetisme, het Kondo effect, gemengde valentie en zware fermion eigenschappen.

In dit proefschrift worden (inverse) foto electron spectroscopische- en Auger experimenten beschreven aan systemen bestaande uit een overgangsmetaal atoom met een sterk gecorreleerde d-schil ingebed in een gastheer met een ongecorreleerde sp band en een gevulde d band. Het één gaten foto electron spectrum van de gastheer banden kan dus beschreven worden met behulp van het onafhankelijke electronen model. Als ingebed atoom werden eerst Pd en Pt onderzocht (hoofdstuk V), waar men een vrijwel gevulde d schil verwacht, zodat ook daar het onafhankelijke deeltjes model gebruikt kan worden voor de foto electron spectra. Deze spectra zijn nauw verwant aan de toestandsdichtheid, maar zijn gemoduleerd door optische matrix elementen. Door gebruik te maken van de foto electron spectroscopische informatie over het gastheer materiaal kan men de spectra van de verdunde legeringen precies berekenen (hoofdstuk III). De experimentele resultaten geven, via de theorie, informatie over sommige transport eigenschappen van de legeringen.

De volgende stap is atomen met halfgevulde d schillen te onderzoeken (Mn,

hoofdstuk VI). Het foto electron spectrum weerspiegelt nu de meerderheids spins en het inverse fotoelectron spectrum de minderheids spins. Ook nu kan men de theorie van hoofdstuk III gebruiken voor de interpretatie. De experimentele gegevens worden gebruikt om uitspraken te doen over de fysische grootheden met betrekking tot de Kondo- en spinglas eigenschappen. De combinatie van AES, UPS en BIS stelt ons tevens in staat om de Coulomb en exchange parameters binnen de d-schil van Mn te bepalen. Een belangrijke conclusie is, dat de exchange interactie zijn atomaire karakter niet verliest in de vaste stof. De electrostatische Coulomb interactie, daarentegen, is in de vaste stof veel kleiner dan in het atoom t.g.v. afscherming. In hoofdstuk II wordt dit gegeven uitgediept voor de d en f overgangsmetalen. Wij komen daar tot de opmerkelijke conclusie, dat de combinatie van afscherming en exchange in een aantal gevallen tot een attractieve wisselwerking tussen parallele spins kan leiden. Dit plaatst het "heavy fermion" probleem in een nieuw daglicht. Met behulp van kanonieke transformaties wordt in hoofstuk VII aangetoond, dat een dergelijke interactie tussen gelocaliseerde electronen doorwerkt in de geleidings-electronen en kan leiden tot de vorming van triplet paren.

DANKWOORD

Met genoegen denk ik terug aan de samenwerking gedurende mijn promotieonderzoek met mensen binnen en buiten Groningen. Mijn dank is groot.

Rosemarie van Gelder heeft bijna al mijn huishoudelijke taken op zich genomen en heel wat uurtjes besteed aan het corrigeren. Ook heeft zij mij op ongeëvenaarde wijze altijd weer op weten te beuren als de druk eens niet beneden de 10^{-9} Torr wilde komen.

Ook George Sawatzky sprong op momenten van mentale en vacuümtechnische ineenstorting bij met woord en daad. De wetenschappelijke discussies die ik met hem gevoerd heb waren uiterst leerzaam en inspirerend.

Willem Zevenberg, Bert van Dammen en Henk Bruinenberg hebben heel wat hand en spandiensten verricht en het feitelijke werk gedaan aan de uitbreiding van de apparatuur met een MBE kamer.

Jan Julianus heeft vele preparaten en discussiemateriaal aangedragen en een deel van de UPS experimenten hebben wij gezamenlijk uitgevoerd.

Uli Hillebrecht danke ich sehr für die viele interessante Diskussionen während meinem Aufenthalt in Jülich und für die Experimentelle Unterstützung des Untersuches.

Jupp Keppels bin ich erkenntlich für die technische Assistenz während dem Arbeit an die CuMn und AgMn legierungen.

Arend Heeres heeft veel geholpen bij het oplossen van problemen met de electronica en bij de ESCA metingen.

Dr. R. Zeller machte seine KKR Bandstructur Berechnungen verfügbar für Kapitel IV.

I greatly appreciate the style in which John Fuggle contributed to chapter two; both by encouraging the research and by supplying the liquids.

Cor Westra heeft door middel van ESCA metingen bijgedragen aan het tot stand komen van hoofdstuk VI.

Anita Severijnse heeft het gehele proefschrift getypt. Ook heeft zij, samen met Greetje Lap, de publikaties en andere geschriften getypt. Daardoor kent zij de inhoud van dit boekje beter dan menigeen.

Dave van der Beek heeft met grote nauwgezetheid en buitengewoon vlot al het tekenwerk verzorgd.

Het treft dan ook dat Klaas Gilissen deze kunstwerkjes met zijn gevoelige platen en puntbron camera's haarscherp heeft vastgelegd.

Bernard van Meurs heeft vele nuttige adviezen gegeven op het gebied van electronica, o.a. bij het bouwen van het Baffingly Rapid Anolog INStrument (BRAINS) en heeft mij vaak versteld doen staan met zijn verrassend simpele electronische creaties. Vooral het teletype interface, bestaande uit zegge en schrijve één transistor van een kwartje deed de deur dicht.

Berend Kwant heeft menigmaal een zonnetje doen schijnen door op het juiste moment de juiste chemicalie te voorschijn te toveren.

De discussies met Maarten Vos, Reinder Coehoorn, Gerrit van der Laan, Kees Flipse, Piet van der Ploeg, Jan-Rens Reitsma en Jan Zaanen waren talrijk en divers. De interacties met laatstgenoemde hebben geleid tot meer correlatie in het onderzoek en een verdieping van het inzicht in de theorie van de vaste stof.

Anne de Visser ben ik zeer erkentelijk voor het leveren van de Uranium verbindingen en voor het doorsturen van (p)reprints op het gebied van heavy fermion systemen.

RECEPTIE NA AFLOOP VAN DE PROMOTIE

IN HET ACADEMIEGEBOUW

BROERSTRAAT 5, GRONINGEN